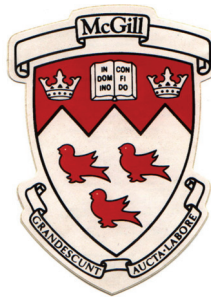


**MATRIX PROTEIN-MINERAL INTERACTIONS
IN AVIAN EGGSHELL AND DURING CALCIUM
CARBONATE AND CALCIUM OXALATE
CRYSTAL GROWTH IN VITRO**

by

Yung-Ching Chien, Ph.D.

Faculty of Dentistry
McGill University
Montreal, Quebec, Canada
August 2009



A thesis submitted to McGill University, Faculty of Graduate and Postdoctoral Studies, in partial fulfillment of the requirements of the degree of doctor of philosophy

Copyright © Yung-Ching Chien 2009

**Dedicated in loving memory to my grandmother,
Chien Hsu Nian.**

ABSTRACT

In many normal and pathologic calcified tissues, osteopontin (OPN) is a prominent protein intimately associated with biominerals. This work aims to elucidate how OPN regulates crystal growth in two biosystems: calcitic avian eggshell during growth and resorption, and *in vitro* calcium oxalate dihydrate (COD) growth related to pathologic urolithiasis (kidney stones).

To understand how OPN and other proteins participate in calcite growth and organization in avian eggshell, ultrastructural matrix-mineral relationships of unfertilized, unincubated chicken eggshell were examined using scanning and transmission electron microscopy (SEM and TEM). OPN was localized *in situ* in eggshell with high resolution colloidal-gold immunolabeling, and the effects of this protein on calcite growth were assessed *in vitro*. The detailed ultrastructures described here reconcile, for the first time, how an extensive organic matrix coexists with the calcitic mineral phase in eggshell. OPN preferentially binds to the {104} crystallographic face and subsequently occludes into the mineral, and thus directs calcite orientation by influencing crystal growth and morphology in eggshell. Moreover, OPN accumulates at interfacial boundaries between various eggshell compartments, maintaining the structure of eggshell compartments and the patency of eggshell pores by inhibition of mineralization at these interfaces.

Once constructed, the eggshell can serve as a calcium source for skeletal mineralization in the growing embryonic chick. Ultrastructural changes within the eggshell mammillae during shell resorption by chick embryo were examined systematically by SEM. The results suggest that the extensive mineral-occluded matrix network in mammillae may regulate dissolution of shell mineral by providing channels facilitating calcium release.

To investigate OPN related to COD formation common in urolithiasis, the effects of full-length OPN, and a poly-aspartic acid-rich peptide of OPN (DDLDDDDD, poly-Asp₈₆₋₉₃),

were examined in COD crystal growth studies. By combining SEM, light and confocal microscopy using fluorescently tagged poly-Asp₈₆₋₉₃, together with computational modeling, it was observed that OPN and poly-Asp₈₆₋₉₃ similarly inhibit (and thus enhance) the {110} faces of COD, and that the peptide is occluded into the COD crystals – this identifies an important motif involved in OPN binding to COD.

Collectively, these data provide new insights into how OPN and its peptides (and likely other proteins) bind to, and are occluded within, various biominerals to regulate crystal growth, and in some cases, to facilitate mineral dissolution.

RESUME

Dans beaucoup de tissus calcifiés normaux et pathologiques, l'ostéopontine est une protéine de premier plan qui est intimement associée aux biominéraux. Cette étude vise à déterminer comment l'ostéopontine régule la croissance cristalline dans deux biosystèmes : la calcite de coquilles d'œuf aviaire durant sa croissance et sa résorption, et la formation *in vitro* d'oxalate de calcium dihydraté associé à l'urolithiase (calculs rénaux) pathologique.

Pour comprendre comment l'ostéopontine et d'autres protéines participent à la croissance et à l'organisation de la calcite dans la coquille d'œuf aviaire, on a étudié, à l'aide d'un microscope électronique à balayage (MEB) et d'un microscope électronique à transmission (MET), les relations ultrastructuralles entre les matrices organique et minérale de coquilles d'œuf de poule non fertilisé et non incubé. L'ostéopontine a été localisée *in situ* dans la coquille d'œuf par immunomarquage à haute résolution à l'aide d'or colloïdal et les effets de cette protéine sur la croissance de la calcite ont été évalués *in vitro*.

Les ultrastructures détaillées décrites ici montrent pour la première fois la coexistence d'une matrice organique étendue et de la phase calcitique minérale dans la coquille d'œuf. L'ostéopontine se lie de préférence à la face cristallographique $\{104\}$, pour ensuite s'occlure dans le minéral et diriger ainsi l'orientation des cristaux de calcite en influençant la croissance et la morphologie cristalline dans la coquille d'œuf. Qui plus est, l'ostéopontine s'accumule au niveau des joints interfaciaux entre les différents compartiments de la coquille d'œuf, maintenant la structure de ces compartiments et la perméabilité des pores de la coquille en inhibant la minéralisation sur ces joints interfaciaux.

Une fois construite, la coquille d'œuf peut servir de source de calcium pour la minéralisation du squelette de l'embryon lors de son développement. Les changements

ultrastructuraux dans les mamelons qui se forment sur la coquille lors de sa résorption par l'embryon ont été systématiquement examinés au microscope électronique à balayage. Les résultats permettent de penser que l'important réseau matriciel minéral occlus présent dans ces mamelons pourrait réguler la dissolution des minéraux de la coquille en fournissant des voies favorisant la libération du calcium.

Pour étudier l'ostéopontine associée à la formation d'oxalate de calcium dihydraté lors de l'urolithiase, on s'est penché sur les effets de l'ostéopontine pleine longueur et d'un peptide d'ostéopontine riche en acide polyaspartique (DDLDDDDD, poly-Asp₈₆₋₉₃) dans des études de la croissance de cristaux d'oxalate de calcium dihydraté. En combinant la microscopie électronique à balayage, la microscopie optique et la microscopie confocale utilisant du poly-Asp₈₆₋₉₃ marqué par fluorescence, ainsi que la modélisation assistée par ordinateur, on a observé que l'ostéopontine et le poly-Asp₈₆₋₉₃ inhibent de façon similaire (et donc renforcent) les faces {110} de l'oxalate de calcium dihydraté et que le peptide est occlus dans les cristaux de ce dernier – ce qui identifie un important motif impliqué dans la liaison de l'ostéopontine à l'oxalate de calcium dihydraté.

Collectivement, ces résultats donnent un nouvel aperçu de la façon dont se lient l'ostéopontine et ses peptides (de même que d'autres protéines, probablement) et leur occlusion de divers biominéraux afin de réguler la croissance cristalline et, dans certains cas, de faciliter la dissolution minérale.

ACKNOWLEDGEMENTS

I am grateful to all those who helped me in the pursuit and achievement of my education at the Ph.D. level, and I extend my appreciation to the following individuals:

Professor Marc D. McKee, who patiently supervised, supported and guided me through the completion of my thesis and introduced me to the disciplines of biology and biomineralization, and, who encouraged me to be independent and gave me the freedom to pursue my own goals, and without whom, this thesis would never have been completed.

Professor Hojatollah Vali, co-supervisor, who generously shared his knowledge and expertise in the field of transmission electron microscopy, for contributing constructive criticisms and valuable comments for improving my research and being a supportive friend during a difficult time in my life.

Special and sincere thanks to Ms. Lydia Malynowsky, Senior Technician of Professor McKee's Laboratories, Faculty of Dentistry, for all her help, favors and friendship. Ms. Sandra Lally and Ms. Glenna Keating, Senior Technician of the Geochemical Laboratories for training me to carry out atomic absorption analyses. Ms. Archana Srivastava, Technician of the Department of Anatomy and Cell Biology, for training me on Laser Confocal Microscopy.

The staff and support personnel of the McGill Facility for Electron Microscopy Research for their technical and professional assistance, friendship, encouragement and enthusiasm, particularly, Dr. S. Kelly Sears (Manager, FEMR), a colleague and friend, who cheerfully helped out with the proofreading of the thesis; Ms. Line Mongeon (Technician), who is always kind and friendly, for training and many technical helps on SEM. Ms. Jeannie Mui (Senior Technician) and Lee Ann Monaghan (Technician), for their technical help on TEM, for their insightful advice on sample preparation, and for

their kindness and long-term friendship. Ms. Lenora Naimark (Administrative Assistant), for her sincere advice and friendship.

Dr. Claudio Pedraza and Mr. William Addison, for their friendship, insightful discussions and encouragement.

I am deeply grateful to my family for their support, especially my parents, my wife, my sister and brothers, and my son and daughter for their enduring love, patience, and encouragement.

Table of Contents

Abstract	i
Resume	iii
Acknowledgements	v
Table of Contents	vii
List of Figures	x
List of Tables	xiii
Contribution of authors	xiv
1 Introduction	
1.1 Biomineralization	1
1.2 Crystal Growth	6
1.3 Protein effects on crystal growth	10
1.4 Examples of acidic, mineral-binding proteins in vertebrate biological systems	13
1.5 Osteopontin	20
1.6 Avian eggshell structure, composition, formation	27
2 Colloidal-gold immunocytochemical localization of osteopontin in avian eggshell gland and eggshell	
2.1 Preface	39
2.2 Abstract	40
2.3 Introduction	41
2.4 Materials and methods	43
2.5 Results	45
2.6 Discussion	47
2.7 Acknowledgements	49
3 Ultrastructural matrix-mineral relationships in avian eggshell, and effects of osteopontin on calcite growth <i>in vitro</i>	

3.1	Preface	57
3.2	Abstract	58
3.3	Introduction	59
3.4	Materials and methods	62
3.5	Results	68
3.6	Discussion	75
3.7	Conclusions	84
3.8	Acknowledgements	84
4	Avian eggshell structure and osteopontin	
4.1	Preface	103
4.2	Abstract	104
4.3	Introduction	104
4.4	Materials and methods	105
4.5	Results and discussions	106
4.6	Acknowledgements	109
5	Ultrastructure of avian eggshell during resorption following egg fertilization	
5.1	Preface	113
5.2	Abstract	114
5.3	Introduction	115
5.4	Materials and methods	118
5.5	Results	120
5.6	Discussion	126
5.7	Acknowledgements	133
6	Modulation of calcium oxalate dihydrate growth by selective crystal-face binding of phosphorylated osteopontin and poly-aspartate peptide showing occlusion by sectoral (compositional) zoning	

6.1	Preface	145
6.2	Abstract	146
6.3	Introduction	147
6.4	Materials and methods	150
6.5	Results	156
6.6	Discussion	159
6.7	Conclusions	166
6.8	Acknowledgements	166
6.9	Supporting data	167
7	Conclusions	176
8	Bibliography	179
9	Appendix	228

List of Figures

Figure	Title	Page
1.1	Schematic illustration of the growing surface of a crystal.....	9
1.2	Structural model of osteopontin.....	25
1.3	The reproductive system of domestic chicken.....	28
1.4	The ectodermal epithelium of chorioallantoic membrane of avian egg.	37
2.1	Western blotting of osteopontin extracted from eggshell and bone matrix.....	50
2.2	Shell gland mucosal histology by light and electron microscopy.....	51
2.3	Scanning electron micrographs of calcified eggshell structure	52
2.4	Matrix architecture in eggshell. Micrographs of a chemically fixed, fully decalcified eggshell preparation sectioned for histology.....	53
2.5	Immunogold labeling for OPN, followed by transmission electron microscopy of the eggshell matrix in the palisades region in a decalcified eggshell sample.....	54-55
2.6	Scanning electron micrographs of OPN on the surface of the cleaved calcite along the {104} crystallographic faces of fractured eggshell....	56
3.1	Cross-sectional profile of avian eggshell.....	86
3.2	Ultrastructure of mammillary bodies in eggshell observed by SEM....	87-88
3.3	Scanning electron micrographs of an eggshell fractured to provide an <i>en face</i> view of the internal structure of the mamillary bodies.....	89
3.4	Colloidal-gold immunolabeling for OPN of eggshell mammillary structure viewed by SEM and TEM.....	90-91
3.5	Ultrastructure of the palisade layer in eggshell by SEM.....	92-93
3.6	Colloidal-gold immunolabeling for OPN in eggshell palisade structure viewed by SEM and TEM.....	94-95
3.7	SEM imaging of typical calcite crystallographic cleavage faces from cross-fractured eggshell in the palisades region, and immunolocalization of OPN.....	96-97

3.8	Ultrastructure of the vertical crystal layer and cuticle in eggshell, and immunolocalization of OPN.....	98-99
3.9	Ultrastructure by SEM secondary electron imaging (SEI) and OPN immunolocalization in the pore system of the eggshell.....	100-101
3.10	Effect of OPN on calcite growth <i>in vitro</i>	102
4.1	Scanning electron micrographs of fractured avian eggshell and eggshell membranes.....	110
4.2	Scanning and transmission electron micrographs of undecalcified and decalcified eggshell and epithelial cells of the shell gland.....	111-112
5.1	Cross-sectional profiles by light microscopy of ground sections of eggshell and by SEM of fractured eggshell from an unfertilized egg and from eggshells of fertilized eggs incubated for various periods of time.	134-135
5.2	SEM of a calcium reserve body (CRB) sac and its contents in a fertilized eggshell at day 12 of incubation corresponding to the onset of eggshell resorption.....	136
5.3	Energy dispersive x-ray spectroscopy (EDS) obtained by SEM on the contents and periphery of the CRB sac.....	137-138
5.4	Morphological changes in the peripheral regions of the CRB sac attributable to mineral dissolution in 12-day incubated fertilized eggs viewed by SEM.....	139-140
5.5	Dissolution of mineral in the shell mammillary bodies of fertilized eggs incubated for 12 days, and exposure of organic matrix by this process, as viewed by SEM.....	141-142
5.6	SEM of resorbed eggshell mammillae and the CRB from fertilized eggs incubated for 16 days.....	143
5.7	SEM of resorbed eggshell mammillae and the CRB from fertilized eggs incubated for 19 days.....	144
6.1	Immunohistochemical localization, colloidal-gold immunolabeling for OPN in human kidney stone; COD crystals precipitated from normal male human urine; Western blots for OPN of normal human	168

	urine and the protein extract of COD crystals.....	
6.2	Scanning electron micrographs of COD grown in solution in the presence of full-length, phosphorylated OPN at the indicated concentrations.....	169
6.3	Scanning electron micrographs of COD grown in solution in the presence of synthetic aspartic-acid rich peptides at the indicated concentrations.....	170
6.4	Conventional fluorescence micrographs, and laser confocal micrographs, of COD crystals grown in the presence of fluorescently-tagged poly-Asp ₈₆₋₉₃ at the indicated concentrations.....	171
6.5	Summary of data using SHAPE software renditions of effects of full-length OPN and poly-Asp ₈₆₋₉₃ peptide on COD crystal growth morphology.....	172-173
6.6	Molecular modeling of poly-Asp ₈₆₋₉₃ peptide binding to {110} and {101} crystallographic faces of COD.....	174-175

List of Tables

Table	Title	Page
6.1	Adsorption energies of Poly-Asp ₈₆₋₉₃ peptide-COD interaction in kcal/mol (estimated by RosettaSurface).....	167

CONTRIBUTIONS OF AUTHORS

The thesis is a collection of manuscripts written by the candidate as primary author with the collaboration of the co-authors. Copyright waivers from the publishers are included in the appendix.

1. Maxwell T. Hincke, Yung-Ching Chien, Louis C. Gerstenfeld and Marc D. McKee; Colloidal-gold immunocytochemical localization of osteopontin in avian eggshell gland and eggshell; *Journal of Histochemistry and Cytochemistry*, (2008), 56(5):467-76

The ultrastructure of avian eggshell imaged by SEM and the immunogold labeling for OPN in avian eggshell were contributed by YCC (Figures 3-6 in the manuscript; this represents the majority of the data presented in this paper). Western blotting of eggshell extract for OPN was provided by MTH (Figure 1). Shell gland mucosal histology by light and electron microscopy were contributed by MDM (Figure 2). The polyclonal antibody against avian OPN was provided by LCG. MTH, YCC, and MDM discussed and interpreted the experimental data. The manuscript was written by MDM, and to some extent by YCC, and edited by MTH. All authors reviewed and agreed on the content of the manuscript.

2. Yung-Ching Chien, Maxwell T. Hincke, Hojatollah Vali, Marc D. McKee; Ultrastructural matrix-mineral relationships in avian eggshell, and effects of osteopontin on calcite growth in vitro; *Journal of Structural Biology*, (2008), 163(1):84-99.

All experiments were designed and performed by YCC, under the supervision of MDM and the advice of MTH and HV. Preparation and organization of experimental data were done following discussions between YCC and MDM. The writing of manuscript draft was done by YCC, and corrected by MDM. MTH and HV were involved in manuscript editing and data interpretation. All authors reviewed the manuscript and agreed on the content.

3. Yung-Ching Chien, Maxwell T. Hincke, and Marc D. McKee; Avian eggshell structure and osteopontin; *Cells, Tissues, Organs*, (2009), 189(1-4):38-43.

YCC designed and carried out all the experiments, except the immuno-gold labeling for OPN of the epithelial cells of shell gland (Figure 2c in manuscript), which was provided by MDM. As a brief review manuscript of avian eggshell ultrastructure, the manuscript was written by MDM and YCC, and all authors reviewed and agreed to its content.

4. Yung-Ching Chien, Maxwell T. Hincke, and Marc D. McKee; Ultrastructure of avian eggshell during resorption following egg fertilization; *J. Struct. Biol.* [July 10; DOI: 10.1016/j.jsb.2009.07.005. Epub ahead of print].

All experiments were designed by MDM and YCC, and carried out by YCC. MTH was involved in discussion and interpretation. The manuscript was written by YCC, corrected by MDM, and edited by MTH. All authors reviewed and agreed on its content.

5. Yung-Ching Chien, David L. Masica, Jeffrey J. Gray, Sarah Nguyen, Hojatollah Vali, and Marc D. McKee; Modulation of calcium oxalate dihydrate growth by selective crystal-face binding of phosphorylated osteopontin and poly-aspartate peptide showing occlusion by sectoral (compositional) zoning; *J. Biol. Chem.* [July 6; DOI: 10.1074/jbc.M109.021899. Epub ahead of print].

YCC designed and performed most of the crystal growth experiments and the microscopic observations (SEM of crystal morphology and fluorescent light and confocal microscope observations), except the calcium oxalate precipitated from normal human urine and the in vitro crystal growth with the addition of commercial poly-aspartic acids, which were performed by SN. Immunohistochemical localization of OPN in human kidney stones and Western blotting of normal human urine for OPN were performed by SN. DLM carried out the computational modeling to simulate the OPN peptide-calcium oxalate mineral surface interactions. JJG and HV were involved in discussion and interpretation of data. The manuscript was written by YCC, with sections contributed by DLM. The whole project was conducted and supervised by MDM.

Chapter 2

Manuscript 1

2.1 Preface

This chapter presents new data about osteopontin secreted from the avian eggshell gland and its ultrastructural localization in the eggshell. Substantial new information on the architecture of the proteinaceous shell matrix is provided. In addition, osteopontin is localized within this matrix and at a specific crystallographic face of calcite – the mineral phase of eggshell.

Reproduced with permission from *J. Histochem. Cytochem.* (2008), 56(5):467-76

Colloidal-gold immunocytochemical localization of osteopontin in avian eggshell gland and eggshell

Maxwell T. Hincke¹, Yung-Ching Chien², Louis C. Gerstenfeld³ and Marc D. McKee^{2,4}

¹Department of Cellular and Molecular Medicine, University of Ottawa, Ottawa, Ontario, Canada, ²Faculty of Dentistry, McGill University, Montreal, Quebec, Canada,

³Department of Orthopaedic Surgery, Boston University, Boston, MA, USA,

⁴Department of Anatomy and Cell Biology, McGill University, Montreal, Quebec, Canada

2.2 Abstract

During mineralization of the avian eggshell there is a sequential and orderly deposition of both matrix and mineral phases. Therefore, the eggshell is an excellent model for studying matrix-mineral relationships and the regulation of mineralization. Osteopontin, as an inhibitor of crystal growth, potently influences the formation of calcium phosphate and calcium carbonate biominerals. The purpose of this study was to characterize matrix-mineral relationships, specifically for osteopontin, in the avian eggshell using high-resolution transmission (TEM) and scanning (SEM) electron microscopy in order to gain insight into how calcite crystal growth is structured and compartmentalized during eggshell mineralization. Osteopontin was localized at the ultrastructural level by colloidal-gold immunocytochemistry. In EDTA-decalcified eggshell, an extensive matrix network was observed by TEM and SEM throughout all regions and included interconnected fibrous sheets, irregularly shaped aggregates, vesicular structures, protein films and isolated protein fibres. Osteopontin was associated with protein sheets in the highly mineralized palisades region; some of these features defined boundaries which compartmentalized different eggshell structural units. In fractured and undecalcified eggshell, osteopontin was immunolocalized on the {104} crystallographic faces of

calcite – its natural cleavage plane. The specific occlusion of osteopontin into calcite during mineralization may influence eggshell structure to modify its fracture resistance.

Keywords: Osteopontin, calcite, biomineralization, eggshell, eggshell matrix, chicken.

2.3 Introduction

Mineralized (calcified) matrices in most biological systems typically contain collagenous and noncollagenous proteins, and proteoglycans, in intimate contact with mineral (Robey, 1996). The avian eggshell is an example where these matrix-mineral relationships produce a complex and highly structured calcitic bioceramic where there is a spatial separation between its collagenous and mineralized compartments (Arias et al. 1992, Dennis et al. 1996, Nys et al. 2004). Thus, the eggshell represents an attractive model for studying the principles by which noncollagenous proteins regulate mineralization. The avian egg sequentially acquires all of its components as it traverses specialized regions of the oviduct. The innermost structure associated with the eggshell is a meshwork of interwoven fibres known as the shell membranes. This structure, organized into inner and outer layers of differing fibre sizes, contains collagens (type I, V and X) which are deposited on the surface of the forming egg as it enters the proximal (white) isthmus (Wong et al. 1984; Arias et al. 1991; Fernandez et al. 1997). Eggshell mineralization is subsequently initiated in the distal (red) isthmus where organic aggregates are deposited on the surface of the outer eggshell membranes at quasi-periodic, but seemingly randomly located sites; nucleation of polycrystalline aggregates of calcium carbonate occur at these positions. The egg, now with its membranes and initial mineral deposits, then enters the uterus (shell gland) where calcium carbonate deposition continues outward to give rise to the inner mammillary (cone) layer and the outer palisade (calcitic prism) layer during approximately 15 hours of shell formation (Parsons, 1982; Hamilton, 1986; Burley and Vadehra, 1989; Nys et al. 2004). Mineralization occurs while the egg is bathed in uterine fluid – an acellular milieu containing high levels of ionized calcium and bicarbonate greatly in excess of the solubility product of calcite (Nys et al. 1991). Lastly, a hydroxyapatite-containing cuticle is deposited upon the outermost surface of the shell (Dennis et al. 1996).

The eggshell is approximately 96% calcium carbonate mineral, while the remaining organic material is distributed throughout the shell as a proteinaceous matrix (3.5%, with the remainder as water) of which approximately half can be readily solubilized by decalcification of the shell. The native and soluble precursors of the eggshell matrix are present in the uterine fluid, where the protein composition varies during the initial, calcification and terminal phases of eggshell deposition (Gautron et al. 1997). Proteomic analysis has identified more than 500 eggshell matrix proteins (Mann et al. 2006), with the most abundant corresponding to those previously identified and categorized as follows. *Eggshell-specific proteins*, such as the ovocleidins and ovocalyxins, were originally identified by N-terminal amino acid sequencing and immunochemistry. One of these, ovocleidin-116, has been cloned and found to correspond to the protein core of a novel dermatan sulfate proteoglycan (Hincke et al. 1999). Another ovocleidin, ovocleidin-17, is a C-type lectin-like phosphoprotein related to pancreatic stone protein which occurs in glycosylated and nonglycosylated forms in the shell matrix (Hincke et al. 1995; Mann, 1999; Mann and Siedler, 1999). Ovocalyxin-32 is a 32 kDa protein with similarity to the mammalian carboxypeptidase inhibitor latexin and the human skin protein RAR-TIG1 (retinoic acid receptor-responsive, tazarotene-induced gene 1)(Gautron et al. 2001a). The sequence of another ovocalyxin, ovocalyxin-36, has homology to proteins associated with the innate immune response, such as lipopolysaccharide-binding proteins (LBP), bactericidal permeability-increasing proteins (BPI) and palate, lung and nasal epithelium clone (Plunc) family proteins (Gautron et al., 2007). The *egg white proteins* – ovalbumin, lysozyme and ovotransferrin – are also present in the uterine fluid, and are primarily localized in the shell membranes and in the mammillary cone layer of the eggshell (Hincke 1995; Hincke et al. 2000; Gautron et al. 2000b). Lastly, osteopontin, a *mineralized tissue protein* found in bone, teeth and cartilage, is also a prominent phosphoprotein of the eggshell matrix (Pines et al. 1994; Fernandez et al. 2003; Mann et al. 2007). Sequential incorporation of matrix proteins into the mineralizing eggshell results in their differential localization between the inner (mammillary) and outer (palisade) layers of the mineralized shell (Hincke et al. 1992).

We hypothesize that the incorporation of shell matrix proteins into specific eggshell compartments regulates calcite mineral growth and provides eggshell with its requisite

structure and functional properties to afford protection to the embryo from potentially harmful environmental factors. The soluble proteins of calcitic matrices modify crystal growth, and thus regulate the macroscopic structure and biomechanical properties of the resulting bioceramic. In mollusk shells, specific proteins control mineral phase switching between the calcite and aragonite forms (Belcher et al. 1996). Partially purified eggshell matrix proteins inhibit calcium carbonate precipitation and alter patterns of calcite crystal growth; however, the role of individual matrix proteins is unknown (reviewed in Nys et al. 2004).

Osteopontin is associated with mineralization in all mammalian hard tissues (McKee and Nanci, 1996). In the chicken, uterine expression of the osteopontin gene is temporally associated with eggshell mineralization via a coupling of physical distension of the uterus with osteopontin gene expression (Lavelin et al. 1998). Partially purified chicken eggshell osteopontin strongly inhibits calcium carbonate precipitation in a phosphorylation-dependent manner (Hincke and St. Maurice, 2000), suggesting that it could potentially have significant influence over eggshell mineralization *in vivo*. In order to learn more about how eggshell osteopontin affects mineralization in biological systems, we have investigated its ultrastructural localization pattern in the shell gland and within the eggshell matrix of the domestic chicken.

2.4 Materials and methods

Gel electrophoresis and Western blotting. White Leghorn hens were individually caged and maintained under conditions approved by the animal care committee of the Animal Research Centre, Agriculture Canada, Ottawa Canada, as previously described (Tsang et al. 1990). Unfertilized eggs laid by white leghorn hens were obtained from commercial sources. Powdered tibial bone (from 18-day chicken embryos), eggshell and uterine tissue from the mid-uterus of domestic White Leghorn chickens (*Gallus gallus*) were selectively extracted with 4 M guanidine HCl, 0.3 M HCl, 0.5 M NaCl at pH 7, and 4 M guanidine HCl, pH 7.4 (Gotoh et al. 1995). Preferential solubilization of osteopontin under these conditions was examined by SDS-PAGE and Western blotting. Lyophilized protein was solubilized in Laemmli sample buffer for separation by SDS-PAGE on 15% gels. Protein concentration of such samples was determined by a microplate

modification of the Micro BCA™ protein assay kit (Pierce, Rockford, IL) using bovine serum albumin (BSA) as a standard (Hincke and Nairn 1992). Western blotting was performed following electrotransfer to PVDF membranes (Bio-Rad Laboratories Canada Ltd., Mississauga, Canada). Membranes were blocked with 3% BSA and probed with primary antibodies to osteopontin (1/2000 dilution), which were raised to chicken bone osteopontin as described previously (Gerstenfeld et al. 1990). Following incubation with secondary antibody-HRP conjugate (1/5000) (Amersham, GE Healthcare, Baie d'Urfe, Canada), immunoreactive bands were visualized with the enhanced chemiluminescence procedure using Enhanced Luminol reagent (Perkin-Elmer, Boston, MA).

Light microscopy, transmission electron microscopy and immunocytochemistry. Eggshell (as above) and shell gland (uterus) taken from a laying hen with an egg in mid-calcification within the shell gland were fixed and processed in LR White acrylic resin (London Resin Company, Berkshire, UK) as previously described (McKee and Nanci, 1995). Survey sections (0.5 µm) of embedded tissue cut with a diamond knife on an ultramicrotome (model Reichert Ultracut E, Leica, Wetzlar, Germany) were stained with toluidine blue and coverslipped. Light micrographs were obtained using a Sony DXC-950 3-CCD camera (Sony, Tokyo, Japan) mounted on an optical microscope (model Leitz DMRBE, Leica, Wetzlar, Germany). For transmission electron microscopy (TEM), selected regions were trimmed, and ultrathin sections (80 nm) were placed on Formvar™- and carbon-coated nickel grids. Grid-mounted tissue sections were processed for colloidal-gold immunocytochemistry by incubation of the sections with primary antibody (1/10 dilution), after which immunolabeling patterns were visualized by incubation with protein A-colloidal gold complex (14 nm gold particles; Dr. G. Posthuma, University of Utrecht, The Netherlands) followed by conventional staining with uranyl acetate and lead citrate, as described previously (McKee and Nanci, 1995). Incubated grids were examined in a JEOL JEM 2000FXII transmission electron microscope (JEOL Ltd, Tokyo, Japan) operated at 80 kV.

Scanning electron microscopy and immunocytochemistry. For morphological imaging of undecalcified eggshell, freshly fractured eggshell fragments were dried in air and mounted with conductive carbon cement onto metallic SEM stubs to provide a transverse cross-section view of eggshell/membrane. Fractured eggshell fragments were

also decalcified in an 8% EDTA solution with 1% glutaraldehyde, and then sequentially dehydrated with ethyl alcohol and hexamethyldisilazane, or dehydrated by critical-point drying for imaging of eggshell matrix organization. Samples were then sputter-coated with a 20-25 nm thick Au-Pd thin film and imaged using a Hitachi field-emission gun scanning electron microscope (FE-SEM) operating at an accelerating voltage of 5 kV (model S-4700, Hitachi High Technologies America, Pleasanton, CA). To localize osteopontin in eggshell matrix and to investigate eggshell ultrastructure and matrix-mineral relationships, we used SEM coupled with immunogold labeling for osteopontin. Briefly, undecalcified and aldehyde-fixed, or EDTA-decalcified and fixed, eggshell fragments were incubated with primary antibody against osteopontin and protein A-colloidal gold complex as above. The samples were coated with a 40-60 nm-thick carbon layer and examined by FE-SEM using both secondary and backscattered electron imaging modes while operating at an accelerating voltage of 9 kV.

2.5 Results

In these studies we utilized a well-characterized antibody raised against chicken bone osteopontin (Gotoh et al. 1995). Powdered eggshell and chicken bone were sequentially extracted to obtain i) extra-mineral proteins soluble in 4 M guanidine HCl, ii) mineral-bound proteins soluble in dilute acid, iii) mineral-bound proteins that are acid insoluble but soluble in neutral high salt conditions, and iv) mineral-bound proteins that are finally solubilized in 4 M guanidine HCl. Western blotting of these extracts revealed that eggshell osteopontin is only present in the dilute acid mineral-bound extract; the majority of bone osteopontin was extractable under the same conditions. Osteopontin exists as 2-3 predominant forms in both eggshell and bone, with an apparent size ranging between 46-54 kDa (Fig. 1). Slight differences in molecular weight and proportions of each form indicate that bone and eggshell osteopontin differ in their post-translational modifications. We have previously demonstrated, by microsequencing of partially purified eggshell osteopontin, that serine residues 12, 14 and 15 are phosphorylated (Hincke and St. Maurice, 2000). Metabolic ³²P labeling studies on osteopontin secreted by cultured chicken osteoblasts also identified the same phosphorylated residues (Salih et al. 1997). In addition to phosphorylation, mammalian osteopontins have been found to

exhibit various degrees of glycosylation, glycanation and/or sulfation (Prince et al. 1987, Nagata et al. 1989, Sodek et al. 1995, Masuda et al. 2000). These post-translational modifications alter the apparent molecular weight of osteopontin as determined by SDS-PAGE (Kazanecki et al. 2007).

The cellular source of eggshell osteopontin was investigated within the uterine mucous membrane by immunogold labeling and TEM. Ciliated (clear) and granular (non-ciliated) cells constitute the surface epithelium which lines the lumen, as demonstrated in Figure 2A by light microscopy. Colloidal-gold immunocytochemistry revealed that secretion granules in the granular cells were intensely immunopositive (Figs. 2B,C). Ciliated cells and cells of the subjacent tubular glands of the shell gland mucosa were not immunolabeled (data not shown). These results indicate that osteopontin is synthesized and secreted by the granular epithelial cells of the shell gland, a finding in agreement with conclusions previously drawn from *in situ* hybridization and immunohistochemical studies performed at the light microscopic level (Pines et al. 1994; Fernandez et al. 2003). The granular cells also synthesize and secrete the novel dermatan sulfate proteoglycan of the eggshell matrix, ovocleidin-116 (Hincke et al. 1999), suggesting that this epithelial cell type is a key player in the secretion of the eggshell matrix.

Examination of cross-fractured eggshell by SEM demonstrated the overall structure of the calcified eggshell which forms upon the shell membranes (Fig. 3A). The mammillary layer is composed of a regular array of cones or knobs; at higher magnification the individual fibres of the outer eggshell membrane are seen to penetrate the tips of these structures (see also Hincke et al. 2000). The palisade layer consists of groups of aligned calcitic columns (or prisms) that are perpendicular to the eggshell surface and extend outwards from the mammillary cones. This layer ends at the vertical crystal layer having a mineral texture differing from that of the palisade region. At higher magnification, the palisades show extensive planes of cleaved calcite and abundant spherical voids (Figs. 3B,C). The overall architecture of the strikingly abundant matrix that co-exists with the mineral phase in all regions of the eggshell was revealed in decalcified shell prepared for histology (Fig. 4A). At higher magnification of the palisades region, SEM reveals details of the matrix presenting as an extensive

network of protein sheets and fibres, and also as small spherical granules/vesicles dispersed within this matrix (Fig. 4B).

Osteopontin immunogold labeling and TEM of thin sections of decalcified eggshell was performed in order to determine its localization within the organic matrix. This approach revealed a prominent concentration of osteopontin in the palisades region (Fig. 5), where osteopontin immunolabeling was associated with flocculent and diffuse sheets of organic material (Figs. 5A-C). Gold particles were predominantly associated with the planar sheets of matrix that aligned generally parallel or slightly angled to the eggshell surface (Figs. 5A-C). Unlabeled spherical granules ranging in size from 200-300 nm, and having electron-lucent centres, were dispersed between and along the sheets of matrix. These structural features of the matrix architecture were also readily apparent by SEM (Fig. 4B). SEM performed in the secondary (Fig. 5D) or backscattered (Fig. 5E) electron imaging mode, for morphology and enhanced gold particle detection respectively, confirmed osteopontin immunogold labeling along the sheets of matrix. Osteopontin imaging in the palisades of cross-fractured eggshell that was not decalcified was obtained by SEM analysis in both secondary and backscattered electron imaging modes (Figs. 6A,B), and showed specific gold-particle labeling for osteopontin at the surface of the cleaved calcite along the {104} crystallographic faces.

2.6 Discussion

In this study, we have characterized matrix-mineral relationships in avian eggshell using ultrastructural approaches that included TEM, SEM and high-resolution immunogold labeling that associated osteopontin with specific structures of the eggshell matrix, and with specific crystallographic faces of the calcitic mineral. We have also identified the granular epithelial cells of the shell gland mucosa as the source of this osteopontin.

Following decalcification and processing of the eggshell for TEM and SEM, the organic matrix of the palisades region of the avian eggshell exhibited two structural features; vesicular structures with electron-lucent cores dispersed along and between flocculent sheets of organic material that aligned generally parallel, or slightly angled, to the eggshell surface. Previous observations on this matrix have led to the proposal that

its properties and organization might inhibit crack propagation and add to the overall strength of the shell (Simons and Wiertz, 1963; Silyn-Roberts and Sharp, 1986; Nys et al. 2004). We observed that osteopontin immunoreactivity was concentrated in the palisades region, where it was almost exclusively associated with the planar sheets of matrix, while being absent from the dispersed spherical vesicles. Notably, in other mineralized tissues there is likewise a striking accumulation of osteopontin at planar matrix-matrix / mineral interfaces in bones and teeth where osteopontin accumulates at cement lines (reversal and resting lines, actually planes in three dimensions) and is thought to serve in matrix adhesion at these sites, or in limiting micro-crack propagation (McKee and Nanci, 1996). Alternatively, layered osteopontin-containing matrix sheets may reflect a self-assembly mechanism by which calcite growth rates are periodically limited (regulated) in this rapidly mineralizing system – one of the fastest known in biology. Cyclical variations in osteopontin secretion into the uterine fluid, or cyclical phases of accelerated calcite growth, might each contribute to this layered matrix structure. In contrast to the localization of osteopontin in these planar matrix accumulations, previously we have shown that the eggshell-specific matrix protein ovocleidin-116 immunolocalizes to the vesicular structures in the palisades region (Hincke et al. 1999).

The relationship of osteopontin to the calcitic mineral phase was determined by immunolabeling of undecalcified shell followed by visualization of colloidal-gold detection sites using the secondary and backscattered electron imaging modes of SEM. These imaging modalities revealed that occluded osteopontin is present on the surface of cleaved calcite along the {104} crystallographic faces. The elongated calcite crystals in the palisades region tend to be preferentially orientated with their (001) planes parallel (*c*-axis perpendicular) to the shell surface, which would orient the {104} plane at 44 degrees from a plane tangential to the surface (Silyn-Roberts and Sharp, 1986; Rodriguez-Navarro et al. 2002). The {104} calcite face is the natural cleavage plane and specific osteopontin binding to this growing crystal face during mineralization could modify the resistance of the shell to fracture along this plane. In support of this hypothesis, we note that in sea urchin calcitic adult exoskeletons (test plates, spines) and larval endoskeletal spicules, occluded acidic glycoproteins are specifically adsorbed on

the {110} planes and improve the fracture properties of calcite crystals by interfering with the {104} natural cleavage planes (Emlet, 1982; Berman et al. 1988; Seto et al. 2004). While the primary function of osteopontin may be to regulate crystal growth patterns and speed by binding to mineral in the eggshell, its incorporation into calcite as an occluded crystal protein might serve the secondary function of also providing some resistance to {104} cleavage.

The relationship of occluded osteopontin observed in undecalcified preparations, to that found in the matrix sheets of fully decalcified samples, has yet to be determined, although experiments are currently underway using gentle mineral- and protein-etching procedures to decipher their respective contributions. While it is generally difficult to simultaneously observe both matrix and mineral, we have made some progress in this regard as reported in the present study. Further work using etching approaches should provide insight into the co-existence of these phases in eggshell. Likewise, it will be important to study the interaction of osteopontin and other purified eggshell matrix proteins with growing calcite crystals, and to investigate binding partners of osteopontin and self-assembly into a matrix, in order to fully understand these interactions. Finally, we are currently examining whether osteopontin incorporation into the eggshell may also serve some role in the dissolution of the shell to provide calcium to the skeleton of the growing embryo.

2.7 Acknowledgements

Funding for this research was provided by the NSERC CRO program (MTH, MDM), the Poultry Industry Council (MTH), the CIHR (MDM) and the FQRNT (MDM). MDM thanks Isabelle Turgeon, Lydia Malynowsky and Line Mongeon for their expert technical assistance with this project. MDM is a scholar of the FRSQ, and a member of McGill's Centre for Bone and Periodontal Research (Jamson T.N. Wong Laboratories), Centre for Biorecognition and Biosensors, and Institute for Advanced Materials.

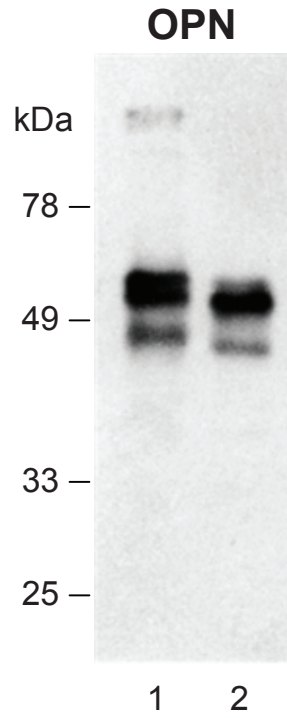


Figure 1. Western blotting of osteopontin extracted from eggshell and bone matrix. Acid extract of mineral-bound proteins from tibial bone (lane 1) and eggshell (lane 2), prepared as described in Materials and Methods. Bone extract, 25 μ g; Shell extract, 25 μ g.

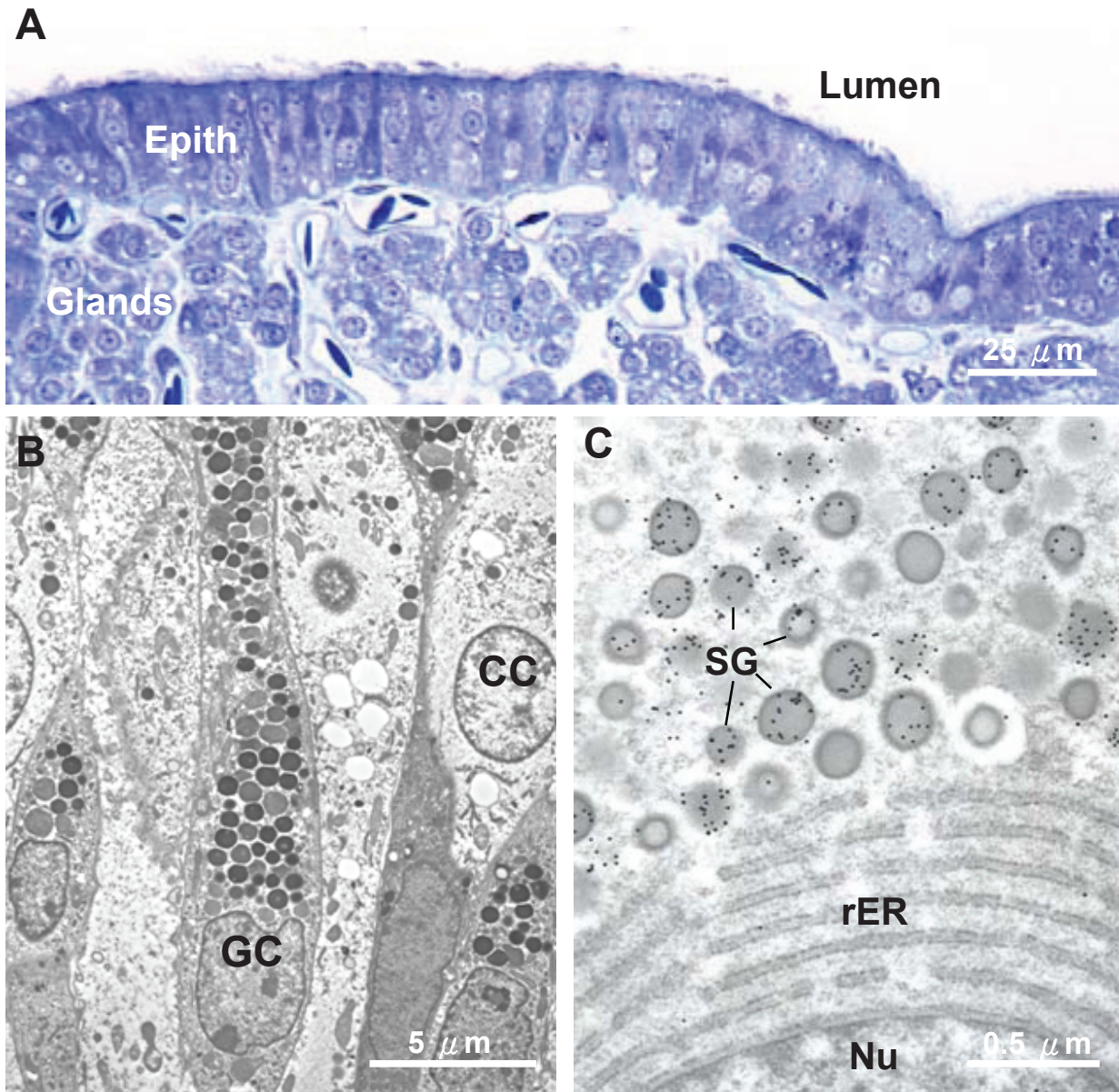


Figure 2. Shell gland mucosal histology by light and electron microscopy. (A) In the avian shell gland, epithelial cells (Epith) line the lumen through which the egg and forming eggshell pass. Coiled tubular glands are located in the mucosa just below the epithelium, and both the surface epithelial cells and the cells of the mucosal glands secrete directly into the uterine fluid. (B) By transmission electron microscopy, two major cell types can be distinguished in the epithelium of the shell gland – granular cells (GC) and ciliated cells (CC). (C) Granular cells show numerous supranuclear secretory granules (SG), just distal to abundant rough endoplasmic reticulum (rER), that label intensely after immunogold staining for osteopontin. Nu, nucleus.

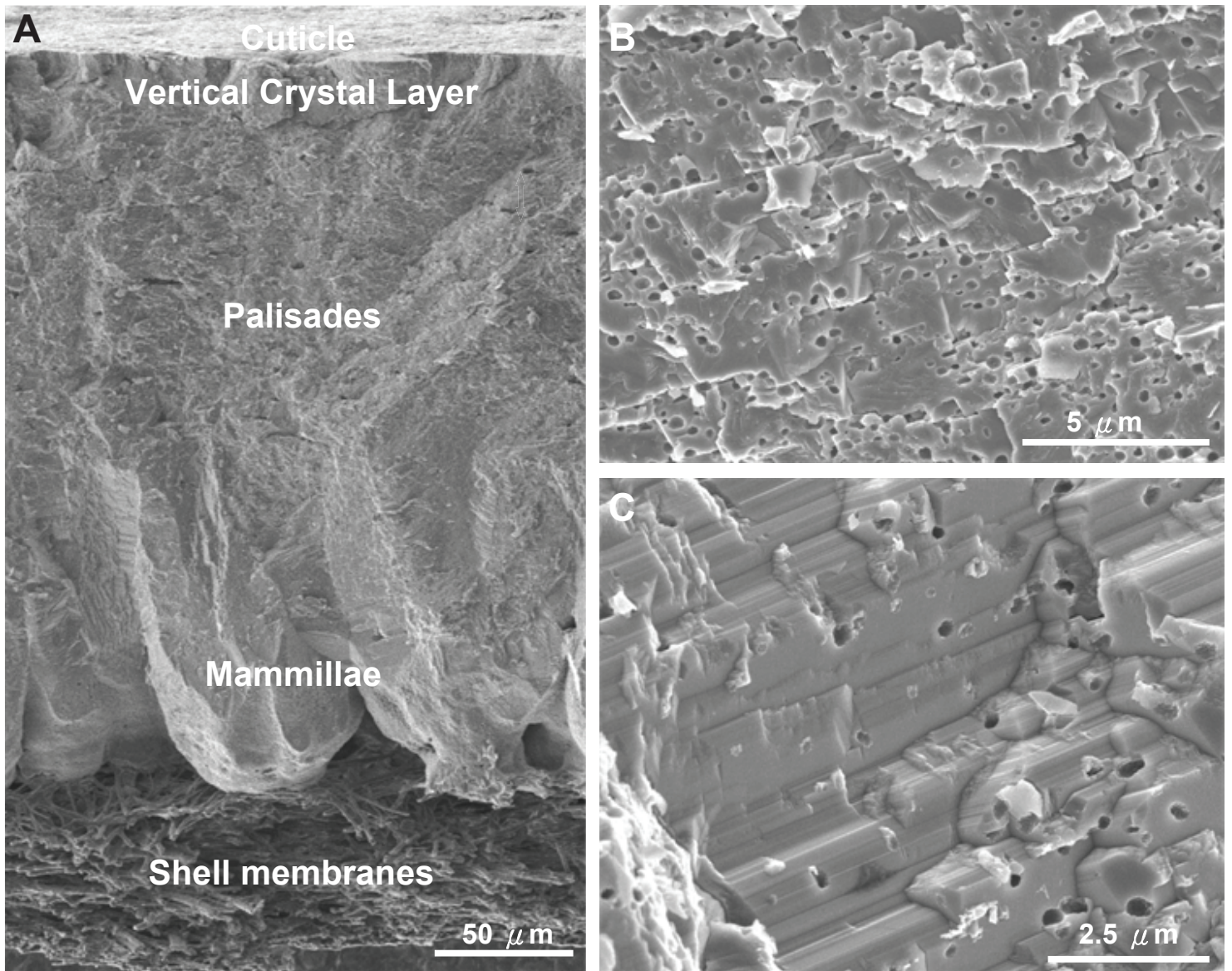


Figure 3. Calcified eggshell structure. (A) Scanning electron micrographs of avian eggshell showing overall structure and regions of the calcified eggshell which form on the shell membranes during the egg-laying cycle. At this low magnification, and starting adjacent to the shell membranes, eggshell consists of mammillae, palisades, vertical crystal layer and cuticle. (B,C) Higher magnification of the palisades region shows extensive planes of cleaved calcite, and numerous small, spherical voids.

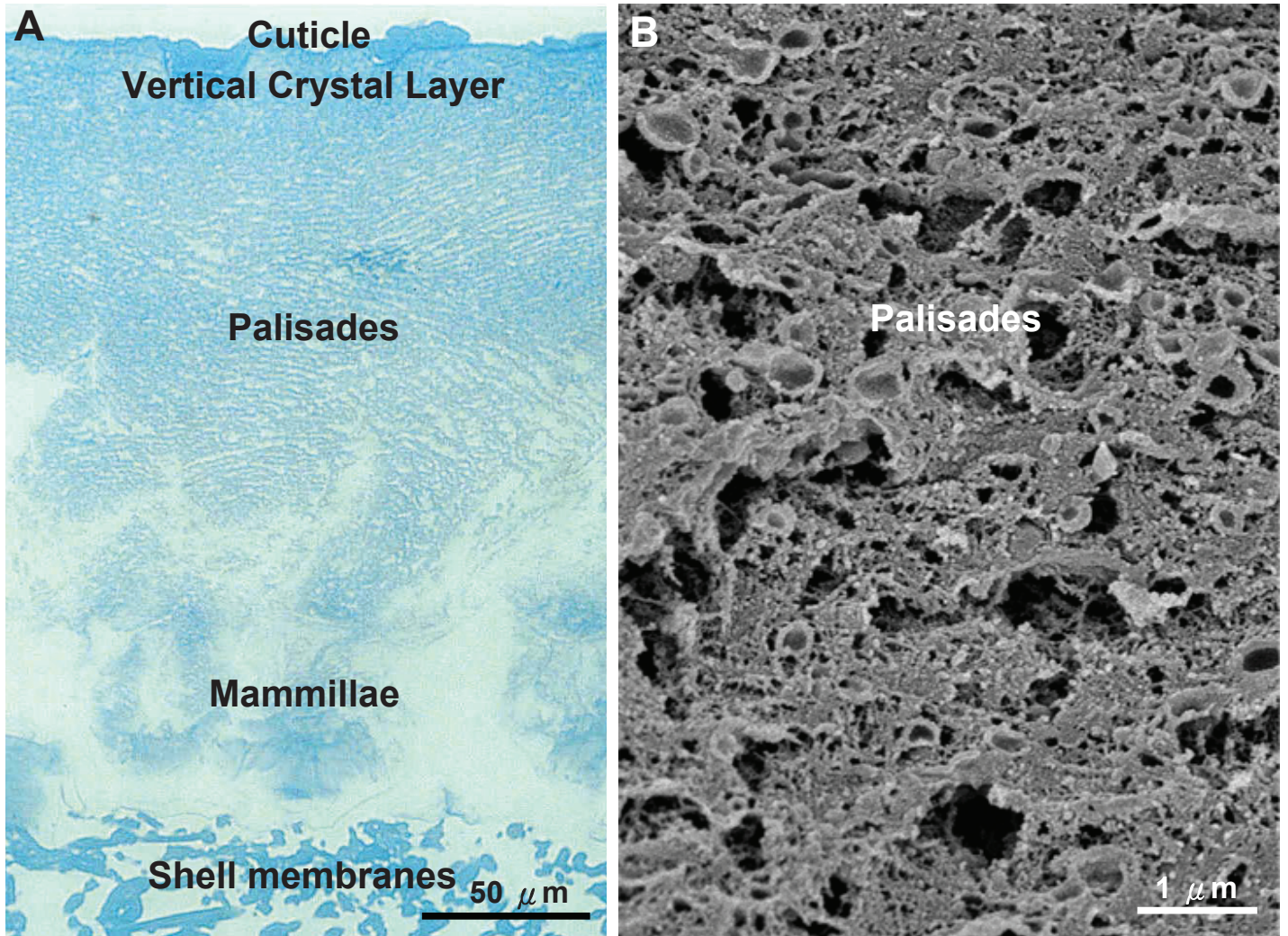


Figure 4. Matrix architecture in eggshell. Micrographs of a chemically fixed, fully decalcified eggshell preparation sectioned for histology (A), or viewed by scanning electron microscopy (B), to visualize the organic matrix of the eggshell. Abundant matrix coexists with calcitic mineral as an extensive network of protein sheets and fibres, and also with small spherical vesicles dispersed within this matrix.

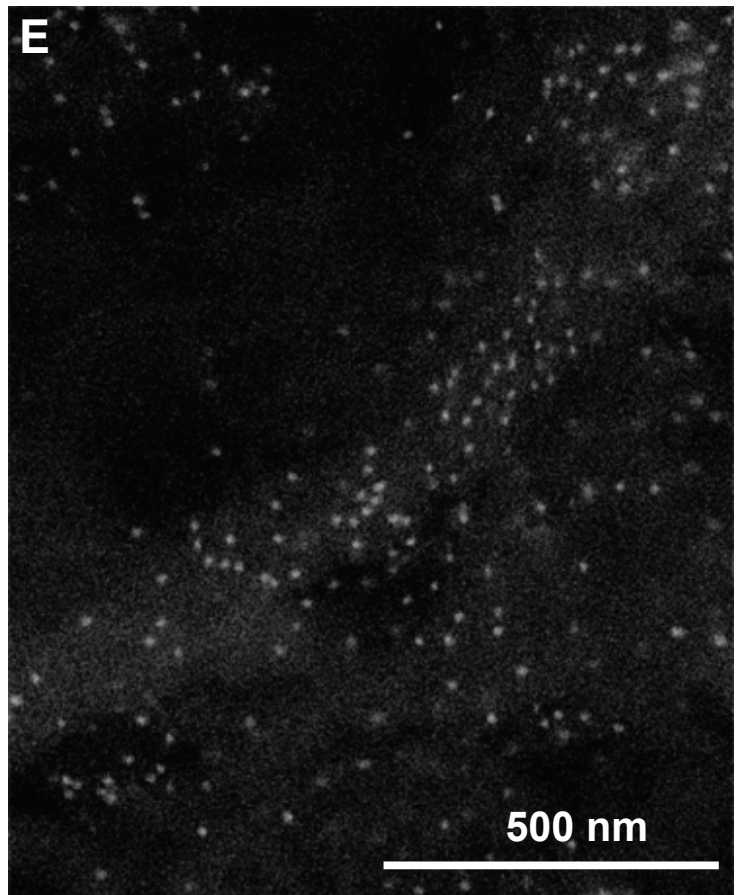
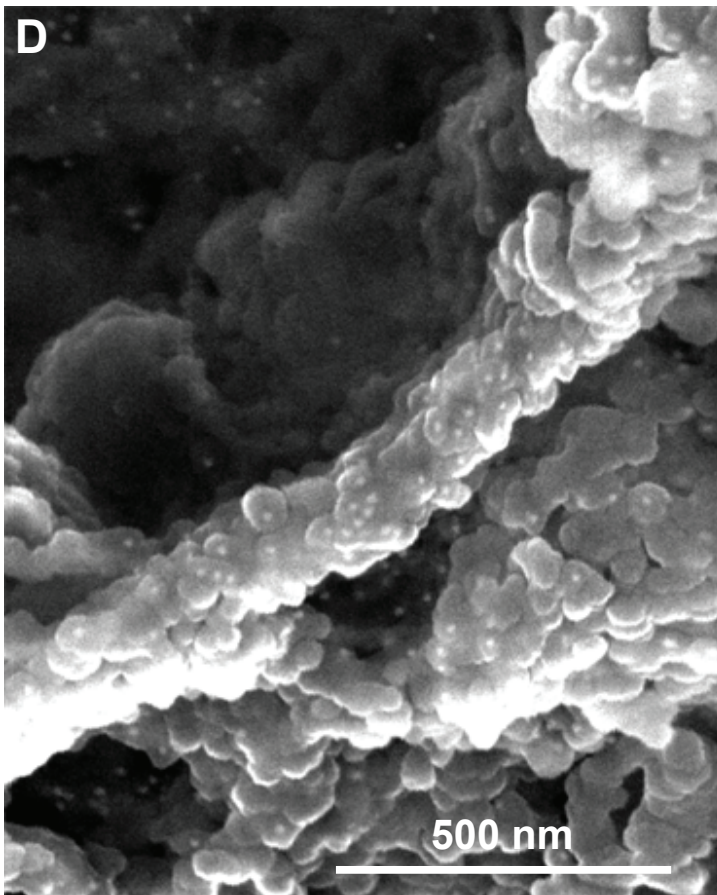
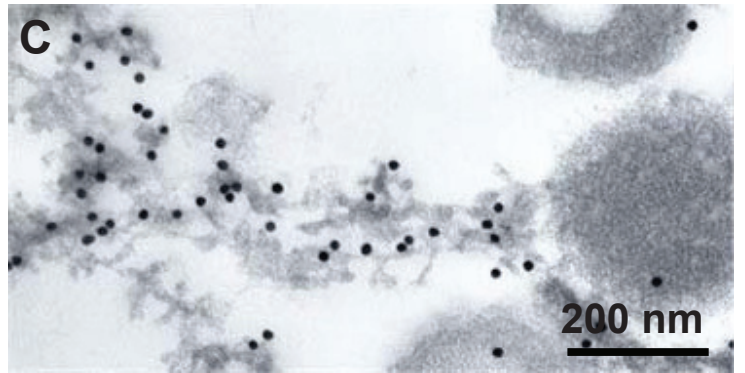
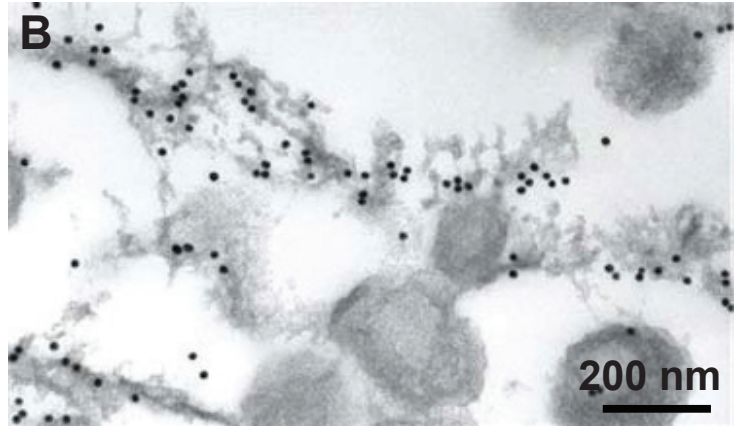
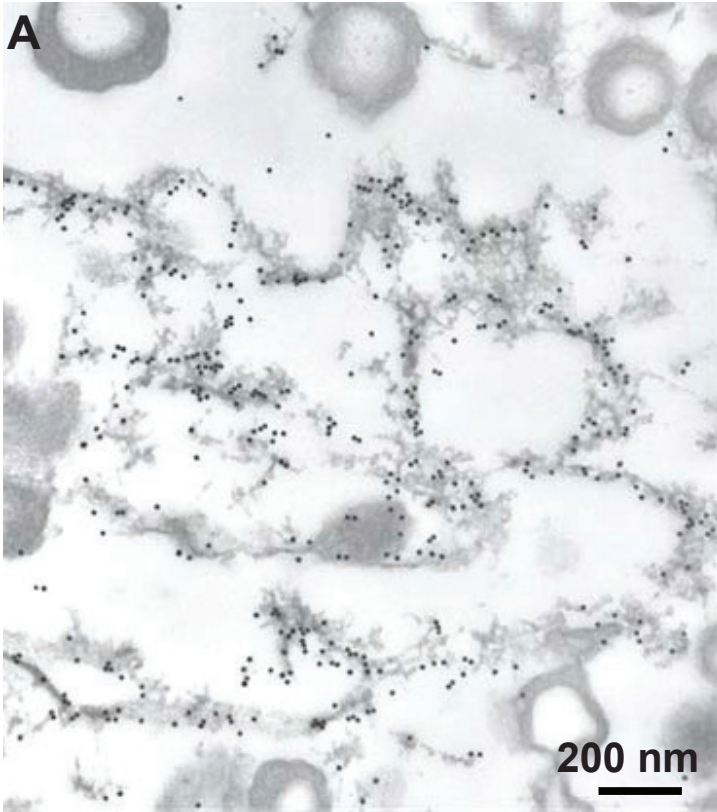


Figure 5. Osteopontin as a constituent of the eggshell matrix in the palisades region in a decalcified eggshell sample. (A-C) Immunogold labeling for osteopontin, followed by transmission electron microscopy, revealed a prominent concentration of this protein in the palisades region. Gold particles were predominantly associated with planar sheets of matrix that aligned generally parallel to the eggshell surface or at an angle (see also Fig. 2B). Spherical vesicles ranging in size from 200-300 nm and having electron-lucent centres were dispersed between and along the sheets of matrix (see also Fig. 2B). By scanning electron microscopy performed in the secondary (D) or backscattered (E) electron imaging mode, for morphology and enhanced gold particle detection respectively, immunogold labeling for osteopontin appears along the sheets of matrix. Roughly globular structures associated with the gold particles represent the totality of the probe structure which includes the gold particle, its shell of protein A, and the primary anti-osteopontin antibody.

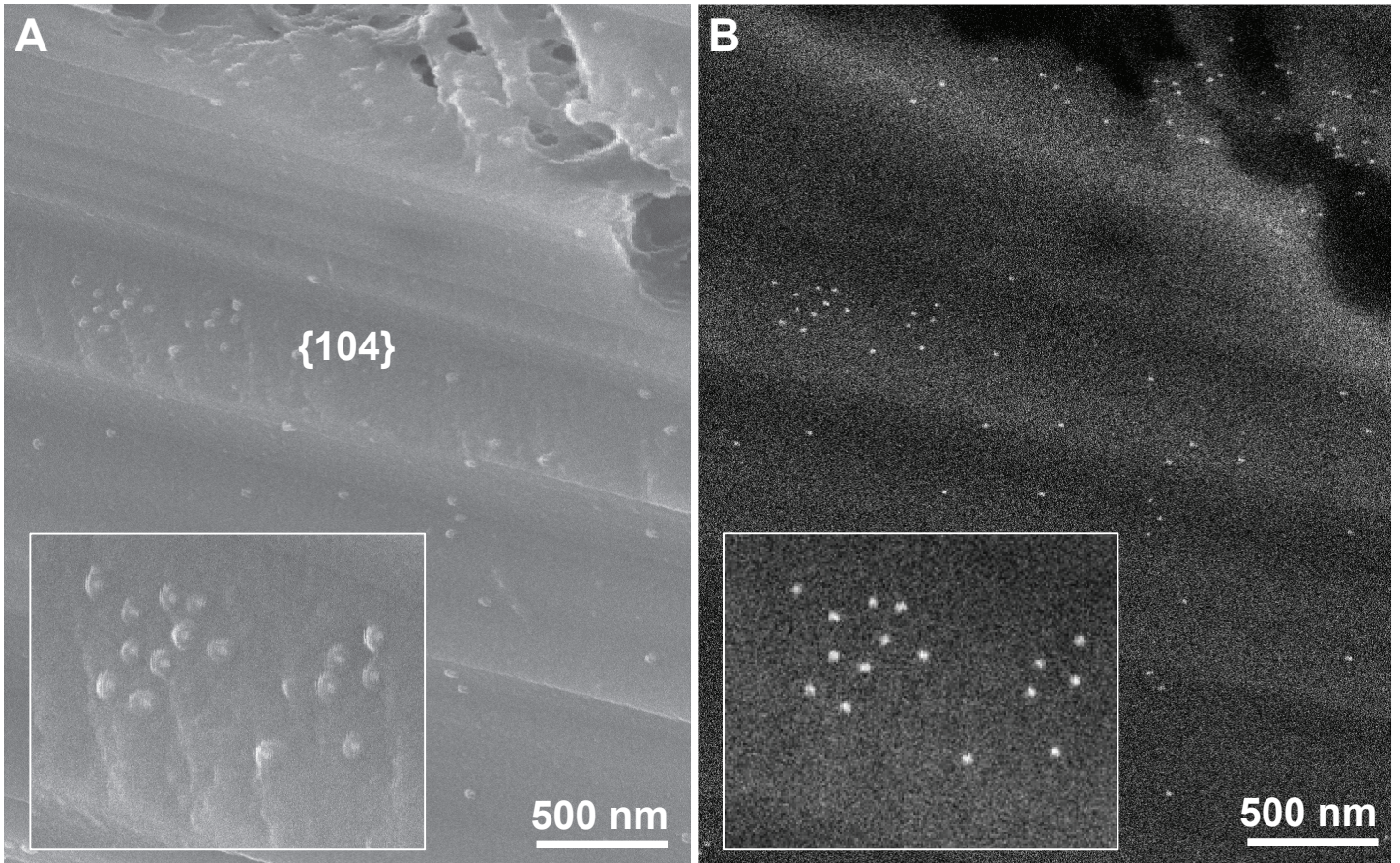


Figure 6. Osteopontin as a constituent of the eggshell matrix in the palisades region in an undecalcified and fractured eggshell sample. Scanning electron microscopy performed in the (A) secondary or (B) backscattered electron imaging mode show gold-particle labeling for osteopontin at the surface of the cleaved calcite along the {104} crystallographic faces.

Chapter 3

Manuscript 2

3.1 Preface

This study reports on a reconciliation of matrix protein (OPN) localization with actual mineral structure and crystallographic faces using a variety of direct and indirect ultrastructural approaches, including scanning and transmission electron microscopy, and immunogold localization of OPN, after eggshell fracture and partial etching of mineral or organic matrix structure. More specifically, ultrastructural localization of OPN in eggshell is demonstrated showing an association of this protein with particular crystallographic faces. The effects of this protein on calcite crystal growth *in vitro* are also shown. To date, prior to this study, no reports exist with this amount of novel ultrastructural detail on matrix organization and matrix-mineral relationships in the eggshell, and with high-resolution localization of OPN in different eggshell compartments. These data provide new insight into the regulation of eggshell and calcite biomineralization by proteins, and more broadly contribute to the current understanding of the effects of protein binding to, and occlusion within, the minerals found in different biomineralizing systems.

Reproduced with permission from *J. Struct. Biol.* (2008), 163(1):84-99

Ultrastructural matrix-mineral relationships in avian eggshell, and effects of osteopontin on calcite growth *in vitro*

Yung-Ching Chien¹, Maxwell T. Hincke², Hojatollah Vali^{1,3} and

Marc D. McKee^{1,3}

¹ Faculty of Dentistry, McGill University, Montreal, QC, Canada, ² Department of Cellular and Molecular Medicine, Faculty of Medicine, University of Ottawa, ON, Canada, ³ Department of Anatomy and Cell Biology, Faculty of Medicine, McGill University, Montreal, QC, Canada

3.2 Abstract

We investigated matrix-mineral relationships in the avian eggshell at the ultrastructural level using scanning and transmission electron microscopy combined with surface-etching techniques to selectively increase topography at the matrix-mineral interface. Moreover, we investigated the distribution of osteopontin (OPN) in the eggshell by colloidal-gold immunolabeling for OPN, and assessed the effects of this protein on calcite crystal growth *in vitro*. An extensive organic matrix network was observed within the calcitic structure of the eggshell that showed variable, region-specific organization including lamellar sheets of matrix, interconnected fine filamentous threads, thin film-like surface coatings of proteins, granules, vesicles and isolated proteins residing preferentially on internal {104} crystallographic faces of fractured eggshell calcite. With the exception of the vesicles and granules, these matrix structures all were immunolabeled for OPN, as were occluded proteins on the {104} calcite faces. OPN inhibited calcite growth *in*

vitro at the {104} crystallographic faces producing altered crystal morphology and circular growth step topography at the crystal surface resembling spherical voids in mineral continuity prominent in the palisades region of the eggshell. In conclusion, calcite-occluded and interfacial proteins such as OPN likely regulate eggshell growth by inhibiting calcite growth at specific crystallographic faces and compartmental boundaries to create a biomineralized architecture whose structure provides for the properties and functions of the eggshell.

Keywords: Eggshell, calcite, calcium carbonate, biomineralization, calcification, osteopontin, extracellular matrix, chicken, ultrastructure

3.3 Introduction

The hard, calcareous avian eggshell serves multiple purposes, primarily acting in fertilized eggs to protect the growing embryo from physical trauma and invasion of microorganisms, to control gas and water exchange, to dampen temperature fluctuations between its contents and the external environment, and finally to provide a source of calcium for the embryonic skeleton (Burley and Vadehra, 1989; Arias, 1993). Like most mineralized structures in biology, there is an abundant organic component to eggshells in addition to the mineral phase, and constituent proteins and proteoglycans are widely thought to regulate mineral deposition and growth, and to determine the final form and properties of the eggshell in the laid egg. Understanding matrix-mineral relationships in such a model system may provide not only a better understanding of the biology behind eggshell formation in birds, but may also provide insight into general principles of biomineralization with relevance to other biological systems. Moreover, eggs and chickens are a nourishing food source ingested worldwide, and economically and nutritionally it is of significant importance to identify the molecular determinants leading to protective shell strength and its other

properties described above. Indeed, eggshell quality is a major concern to the poultry industry since the percentage of broken or cracked (with possible microorganism invasion) eggshells can range from 13 to 20 percent (Roland, 1988; Hincke et al., 2000a).

Avian eggshell consists of mostly inorganic calcite (*ca.* 96%) – the most stable polymorph amongst the calcium carbonate minerals – and an organic matrix (*ca.* 4%) with water (Romanoff and Romanoff, 1949; Erben, 1970; Simons, 1971). The formation of an avian eggshell includes a series of spatio-temporally distinct events that occur within specific regions along the oviduct in the female reproductive system (Arias et al., 1993; Fernandez et al., 1997, 2001, 2003). The assembly and calcitic mineralization of different eggshell compartments are thought to be guided by organic molecules, including noncollagenous proteins and proteoglycans (e.g., Burley and Vadehra, 1989; Lavelin et al., 2000). A large number of egg white proteins, eggshell-specific proteins and other proteins and proteoglycans have been identified and studied in attempts to understand their contribution to eggshell mineralization (e.g., Hincke et al., 1992; Arias et al., 1993; Hincke et al., 1995; Gautron et al., 1996; Fernandez et al., 1997; Gautron et al., 1998; Hincke et al., 1999; Nys et al., 1999; Panheleux et al., 1999; Hincke et al., 2000a, b; Nys et al., 2001, 2004). Indeed, Mann and colleagues (2006, 2007) have recently used a proteomics approach to identify more than 500 proteins associated with the avian eggshell.

Amongst the diverse mixture of proteins found in the avian eggshell matrix, osteopontin (OPN) secreted by oviductal cells has been identified as a prominent protein constituent (Pines et al., 1995; Panheleux et al., 1999). OPN is a highly phosphorylated, acidic, mineral-binding glycoprotein rich in many vertebrate mineralized tissues (including chicken bone), and also abundant in many soft tissue pathologies where ectopic calcification has occurred. OPN is highly

post-translationally modified, particularly by phosphorylation, and has many different peptide domains with different, well-established functions – including mineral-binding domains (Kazanecki et al., 2007). More specifically relevant to the present study, OPN is a potent inhibitor of crystal growth, with significant inhibitory effects on hydroxyapatite, calcium oxalate and calcium carbonate (e.g., hydroxyapatite: Goldberg and Hunter, 1995; McKee and Nanci, 1996; calcium oxalate: McKee et al., 1995; Qiu et al., 2004; calcium carbonate: Hincke and St. Maurice, 2000). Accordingly, in normal vertebrate mineralized tissues having apatite as their main mineral component, OPN is thought to regulate crystal growth physiologically such that crystals attain a form, size and orientation appropriate to their respective tissue (Sodek et al., 2000). Acting together with other mineral-binding proteins, such a protein-guided, hardening strategy for bones and teeth serves multiple important functions in the skeleton and dentition, including meeting many of the biomechanical demands unique to these tissues. Eggshell mineralization, while calcitic, likewise provides some similar functions, and thus we have examined how OPN might be involved in this mineralization process.

With respect to the avian eggshell, OPN is thought to play an important role in regulating its mineralization – initially proposed because OPN gene expression correlates with the daily egg production cycle and reaches its maximal expression during the period of eggshell calcification (Pines et al., 1995). OPN is synthesized and secreted by nonciliated granular cells of the surface epithelium lining the lumen of uterus (shell gland) (Pines et al., 1995; Hincke et al., 2008), and its production is stimulated by entry of the egg into the uterus and the associated mechanical strain due to distension of the uterine wall (Lavelin et al., 1998, 2000). This egg-induced expression of OPN leads to release of OPN into the uterine fluid whereupon it subsequently accumulates as part of the eggshell matrix (Pines et al., 1995; Hincke et

al., 2008). While several reports show OPN expression by cells and localization in eggshell matrix (Pines et al., 1995; Fernandez et al., 2003), data is limited with respect to the ultrastructural distribution of OPN, and its relationship with eggshell structure – both in terms of its organization into the shell matrix, and its association with the crystallographic faces of the calcitic mineral. Localization of shell matrix constituents after decalcification (as is commonly done) of a tissue that is only ~4% organic material is fraught with possible artifacts. Thus, in the present study we report on a reconciliation of matrix protein (OPN) localization with actual mineral structure using a variety of direct and indirect ultrastructural approaches including scanning and transmission electron microscopy, and immunogold localization of OPN, after eggshell fracture and partial etching of mineral or organic matrix structure. More specifically, we describe the ultrastructural localization of OPN in eggshell, demonstrating its association with particular crystallographic faces. We also show the effects of this protein on calcite crystal growth *in vitro*. These data provide new insight into the regulation of eggshell and calcite biomineralization by proteins, and more broadly contribute to our understanding of the effects of protein binding to, and occlusion within, the minerals found in different biomineralizing systems.

3.4 Materials and methods

Eggshells. Laid, unfertilized eggs were obtained from domesticated White Leghorn chickens (*Gallus gallus*). Eggshells were fractured open at the obtuse end, and all egg white and yolk contents discarded. The empty eggshells were rinsed briefly with physiologic saline (150 mM sodium chloride solution) and then with de-ionized water (resistivity >18 Ω). Eggshell samples destined for morphological observations received limited exposure to aqueous solutions to prevent mineral dissolution, and they were immediately dried in air at ambient temperature after

rinsing. To preserve matrix structure for microscopy, some eggshell samples were fixed immediately after rinsing by overnight immersion in a 0.1-5% glutaraldehyde solutions (in 0.1 M sodium cacodylate buffer, pH 7.3), with subsequent storage in the same buffer alone prior to use or further treatment as described below. All shell fragments used in this study were taken from the equatorial region of the eggshell.

Eggshell decalcification, acid etching and bleaching. For eggshell matrix observations, fractured eggshell fragments fixed in glutaraldehyde solution as above were decalcified in 8% EDTA containing 0.1-1% glutaraldehyde (added at this stage to further retain eggshell matrix constituents during mineral dissolution) for 5-7 days under continuous, gentle solution agitation at 4°C. They were then sequentially dehydrated in graded solutions of ethyl alcohol and hexamethyldisilazane (HMDS; Electron Microscopy Sciences), or dehydration was achieved using a critical-point dryer (LADD Research Industries, Burlington, Vermont).

To visualize in three dimensions the association of matrix with mineral, and to create additional surface topography for critical morphological and compositional analysis, aldehyde-fixed and unfixed eggshell samples were either briefly etched (usually for 1 minute, with some samples being etched for longer periods up to 1 hour) with 1 mM hydrochloric acid (HCl, pH 3; Fisher Scientific) to remove surface mineral, or were bleached with 14% sodium hypochlorite (NaOCl, pH >14; Fisher Scientific) for 3, 6, or 12 hours to remove surface organics. Samples were dehydrated by either the critical-point or HMDS drying method (as above) prior to observation.

Light microscopy, immunocytochemistry for OPN, and transmission electron microscopy (TEM). Decalcified eggshell fragments processed as above were embedded after ethyl alcohol dehydration in LR White acrylic resin (London Resin Company, Berkshire, UK) as previously described (McKee and Nanci, 1995).

Survey sections (0.5 μm) of embedded tissue cut with a diamond knife on an ultramicrotome (model Reichert Ultracut E, Leica, Wetzlar, Germany) were stained with toluidine blue and coverslipped. Light micrographs were obtained using a Sony DXC-950 3-CCD camera (Sony, Tokyo, Japan) mounted on an optical microscope (model Leitz DMRBE, Leica, Wetzlar, Germany). For transmission electron microscopy (TEM), selected regions were trimmed, and ultrathin sections (80 nm) were placed on FormvarTM and carbon-coated nickel grids. Grid-mounted tissue sections were processed for colloidal-gold immunocytochemistry by incubation of the sections with primary rabbit anti-chicken OPN polyclonal antibody at a 1:10 dilution (antibody courtesy of Dr. Louis C. Gerstenfeld, Department of Orthopaedic Surgery, Boston University, MA, USA; Gerstenfeld et al., 1990), after which immunolabeling patterns were visualized by incubation with protein A-colloidal gold complex (14 nm gold particles; Dr. G. Posthuma, University of Utrecht, The Netherlands) followed by conventional staining with uranyl acetate and lead citrate, as described previously (McKee and Nanci, 1995). Control incubations consisted of exactly the same incubation steps with the same reagents, except that the OPN antibody was omitted. Incubated grids were examined in a JEOL JEM 2000FXII transmission electron microscope (JEOL Ltd, Tokyo, Japan) operated at an accelerating voltage of 80 kV. Images were recorded using a CCD camera (model 792 Bioscan 1k x 1k wide-angle multi-scan CCD camera, Gatan Inc., Pleasanton, CA).

Immunocytochemistry and scanning electron microscopy (SEM). For morphological imaging of both decalcified and undecalcified eggshell (either fixed with aldehyde solution or left unfixed) and calcite crystals grown *in vitro* (see below), samples were mounted with conductive carbon cement onto metallic SEM stubs. Eggshell samples were oriented to provide a transverse, cross-sectional view of the

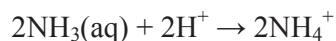
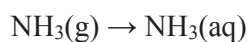
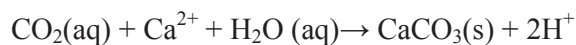
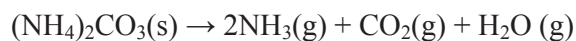
eggshell/membrane; in other cases decalcified eggshell was gently split open in a plane parallel with the eggshell surface to view internal structure in an *en face* manner. Samples were then sputter-coated with a 20-25 nm thick Au-Pd thin film using a Hummer VI Sputter System (Anatech Ltd., Hayward, CA) and imaged using a Hitachi field-emission gun scanning electron microscope (FE-SEM) operating at an accelerating voltage of 3-5 kV (model S-4700, Hitachi High Technologies America, Pleasanton, CA) and using working distances of <12 mm. To localize OPN in eggshell matrix and to investigate eggshell ultrastructure and matrix-mineral relationships, we used SEM coupled with immunogold labeling for OPN. Briefly, undecalcified and aldehyde-fixed, or EDTA-decalcified and fixed, eggshell fragments were incubated by sequentially placing small fragments of eggshell directly into 50 μ l drops of incubation solutions with intervening multiple rinses using this drop method and gentle jet washing. After an initial blocking step using 1% bovine serum albumin in phosphate-buffered saline, eggshell fragments were incubated with primary antibody against OPN followed by protein A-colloidal gold complex as above. When etched or fully decalcified samples were incubated, a final 1% glutaraldehyde fixation step was performed to stabilize the antigen-antibody-colloidal gold complexes. For SEM, the samples were coated with a 40-60 nm-thick carbon layer and examined by FE-SEM using both secondary and backscattered electron imaging modes (Robinson YAG backscattered electron detector, ETP Semra Pty., Canterbury, Australia).

Effect of OPN on calcite crystal growth in vitro. To examine potential effects of OPN on calcite crystal growth, calcite crystals with directed crystallographic orientation were grown on carboxylated, alkane-thiolate self-assembled monolayer (SAM) substrates. The rationale for using SAMs for crystal growth studies is to provide a specific crystallographic plane for oriented crystal growth (Aizenberg et al.,

1999) such that all crystals under experimental conditions have the same crystallographic orientation, thus generally mimicking the patterned crystal growth orientation commonly found in biomineralization processes including the eggshell. The charged crystallographic surface also attracts and accumulates ions in a manner that facilitates the formation of stable mineral nuclei that reach a critical radius (r_c) enabling further crystal growth. The crystals grown on the SAMs can be easily analyzed by various high-resolution microscopies, such as atomic force microscopy (AFM) and SEM. SAM substrates were prepared according to Finklea and Hanshaw (1992). Briefly, commercially available gold substrates (Evaporated Metal Films, Inc., Ithaca, NY) were immersed in dilute thiol-ethanol solutions (11-mercaptoundecanoic acid, 95%, Sigma; ~1.0 mM) for 24-36 hours. The gold substrates modified by the SAM were rinsed with copious amounts of absolute ethanol followed by rinsing with distilled, deionized water (resistance >18 M Ω). The SAM substrates were dried using a stream of pure, dry N₂ gas and used immediately for the calcite crystal growth experiments as outlined below.

Calcite crystals were nucleated and grown from aqueous calcium chloride and OPN solutions exposed to gaseous carbon dioxide. The OPN used for these experiments was full-length, phosphorylated bovine milk OPN (0.15 - 0.78 μ M) as characterized (Sørensen and Peterson, 1993) and supplied by Esben Sørensen (Dept. of Molecular and Structural Biology, University of Aarhus, Denmark) and Arla Foods (Denmark). The growth experiments were performed in a free-drift system at room temperature for various periods of time. The initial calcium concentration in the reactant solutions was fixed at 10 mM. Freshly prepared SAMs substrates were immersed vertically or upside-down in CaCl₂ solution and placed in a closed desiccator containing vials of ammonium carbonate. Growth of calcite is generated

by the diffusion of carbon dioxide vapor into the CaCl_2 solution, according to the following reactions:



The concentration of solution calcium continuously decreases once the nucleation of calcite starts; thus, monitoring the temporal changes of solution calcium level under different conditions can provide a measure of the inhibitory activity of protein on crystal growth. The reactant solution was likewise collected and filtered through a 0.22 μm hydrophilic Durapore (PVDF) low-protein binding membrane filter (Millex-GV₄, Millipore). Solution calcium concentrations were measured by atomic absorption spectrophotometry (model AAnalyst 100 flame atomic adsorption spectrometer, Perkin Elmer, Waltham, MA). For SEM analysis of the crystals formed under the different experimental conditions, SAM substrates with calcite crystals were briefly and gently rinsed using a few drops of deionized water to remove residual solution salts, and then crystal samples were dehydrated in ethyl alcohol and the crystals were examined by SEM. Surface topography of some of the crystals was imaged using thin-film Pt-C surface replicas (viewed by TEM after underlying crystal dissolution with acid) prepared using a freeze-fracture/metal shadowing unit (model Balzers 301, BAL-TEC AG, Balzers, Liechtenstein).

3.5 Results

Eggshells form by oriented calcite growth on the eggshell membranes, producing a structure that has well-established regions which are compartmentalized as follows from the inside (egg white side) to the outside (external surface): *i*) the mammillae (or mammillary bodies / layer), *ii*) the palisades region comprising the thickest layer of the shell, *iii*) the transitional vertical crystal layer, and *iv*) a thin, surface cuticle (Figs. 1a,b) (Dennis et al., 1996). Whereas cross-fractured eggshell viewed by SEM demonstrates mostly its calcitic mineral phase and structure (Fig. 1a), after complete decalcification of the eggshell, an extensive organic matrix network that varied in morphological texture from region to region was observed throughout the full thickness of the shell as viewed by light microscopy after microtome sectioning (Fig. 1b). The distribution of this abundant organic matrix throughout all eggshell regions suggests not only a mineral-compartmentalizing role, but also that a substantial amount of this matrix could well be occluded within the mineral phase (see further observations below).

Mammillae region

Figure 2a illustrates, by SEM, surface and internal detail of a mammillary body. Each mammillae is comprised of a sequentially assembled base plate, a calcium reserve body (CRB) with a centrally located CRB sac, and a CRB cover and crown (Dieckert et al., 1989; Dennis et al., 1996). Several previous studies have given excellent descriptions of the development and structure of these mammillae (Terepka 1963a, 1963b; Wyburn et al., 1973; Dieckert et al., 1989; Dennis et al., 1996). The base plate is the calcified foundation of eggshell, rich in organic matrix. The base plate directly attaches to the outer portion of the shell membranes by incorporating mineralized fibres of the outer shell membrane, and it is generally believed that mineralization of eggshell initiates at the base plate (Schmidt, 1960; Terepka 1963a,

1963b; Tyler, 1969; Wyburn et al., 1973; Dieckert et al., 1989). The overlying CRB is considered to be crucial to embryo development in that this structure is thought to be the main source of calcium required for skeletal growth in the chick embryo (Schmidt, 1960; Dieckert et al., 1989; Dennis et al., 1996). The CRB extends directly above the base plate and includes a centrally located CRB sac rich in spherical-shaped granules (Dennis et al., 1996) (and see below). The CRB is capped by a CRB cover having a different matrix and mineral texture, which in turn sits below a CRB crown that serves as the base for development of the columnar palisades above (Dieckert et al., 1989; Dennis et al., 1996). The conical shape and lateral growth of the mammillae – with fluid-filled and/or air spaces between mammillae – is likely determined by a delimiting layer of protein that resides at the surface of each mammillae (see below) to prevent the merging of neighboring mammillae during mineralization.

At higher magnification, individual sub-compartments of the mammillae showed distinct morphological features. Of note, the periphery of the CRB sac showed a membrane-like protein film directly and intimately covering calcitic mineral (Fig. 2b). As is evident from this plane of fracture, the CRB sac is a distinct, centrally located chamber within mammillae whose boundary is defined by this protein layer which is in turn connected to outwardly projecting matrix fibres and sheets (Figs. 2c,d). At the boundary between the CRB sac and the CRB, numerous proteinaceous vesicular profiles were present, representing most likely the protein that circumferentially surrounds spherical voids (filled with fluid or gas) that are widely dispersed throughout the mammillary and palisades region (Fig. 2d) (see also Fig. 5 and Fig. 7a, as described below). When these vesicular structures and the surrounding fibrous and membranous matrix sheets were digested by NaOCl treatment, the mineral phase is exclusively visualized and here it appeared highly

porous with the spherical voids being readily apparent in the bulk of the CRB at the margins of the CRB sac (Figs. 2e,f).

Based on SEM observations suggesting that the contents of the CRB sac were loosely packed and had been displaced during the fracturing procedure used during sample preparation, we used a combination of mild acid etching and gentle *en face* fracturing of the eggshell in that particular region; abundant granules were indeed preserved inside the CRB sac following this procedure (Figs. 3a-c) as viewed from the shell side. Granules were 200-300 μm in diameter, with thin, fibrous threads of matrix linking the granules (Fig. 3c, and inset).

Colloidal-gold immunolabeling for OPN, detected by SEM in secondary and backscattered imaging modes, and by TEM, was carried out to investigate whether this protein was associated with any of these mammillary structures. All immunoreactions reported in this manuscript are considered as being specific given that control incubations, where primary antibody (Gerstenfeld et al., 1990) was omitted but all other incubation steps remained identical, showed only background labeling (data not shown). Within the CRB sac, the fibre threads between granules were strongly labeled for OPN, whereas the granules themselves were not labeled (Figs. 4a-c). The membranous, protein film delimiting the CRB sac was also not labeled for OPN (data not shown). Beyond the CRB sac and into the body of the calcified CRB proper, moderate immunolabeling for OPN was observed within the interior of the CRB, whereas strong immunolabeling was seen as part of a coating of protein at the surface of the mammillae (Figs. 4d-f).

Palisades region

The palisades of the avian eggshell – constituting roughly 80% of the shell (Fig. 1a) – determine most of the mechanical properties required to protect the growing embryo. Aligned columns (prisms) of calcitic mineral, with regular pores at

specific interfacial sites between these columns, provide the bulk of the eggshell. In addition to the calcite mineral in the palisades (Fig. 5a), an extensive network of organic matrix permeates this mineralized structure (Fig. 5b, and also refer to Fig. 1b). After full decalcification of aldehyde-fixed (included during the decalcification process) eggshell to reveal this organic matrix (Fig. 5b), or after brief etching of the mineral phase with acid of otherwise intact fractured eggshell fragments to likewise reveal surface organics (Figs. 5c,d), prominent structures include aligned sheets of matrix and abundant vesicles, and an interconnecting fibrous network. The sheets (lamellae) of matrix run parallel to each other and often to the surface of the eggshell (Fig. 5b), or they may be at an oblique angle that seems to vary from region to region, and they are connected to each other by thin fibres extending to neighboring lamellae (Figs. 5c,d). After NaOCl treatment used conversely to remove surface organics – rather than remove mineral with acid as above – from the fractured eggshell surface to highlight surface mineral, a subtle streaked appearance was observed as generated by the surface relief caused by linear voids digested into the “raised” mineral surface (Figs. 5 e,f).

After colloidal-gold immunolabeling for OPN in the palisades region, followed by TEM, the lamellar sheets of matrix were strongly labeled for OPN (Fig. 6a). The prominent vesicular structures in the palisades, typically ranging in size from 200-500 μm and being seemingly randomly distributed throughout the palisades region (Fig. 5a) in fractured undecalcified eggshell samples, but aligned along the lamellar matrix sheets in artifactually collapsed fully decalcified samples (Fig. 5b), were not labeled for OPN (Fig. 6a). This localization pattern for OPN was confirmed by SEM and backscattered electron imaging for the vesicles (Figs. 6b,c) and for the matrix lamellae (Figs. 6d,e).

Whereas geologic calcite preferentially cleaves along the $\{104\}$ faces, fractured

eggshell typically shows cleavage not only at the {104} faces but also at {110} crystallographic faces (Fig. 7a), exposing internal structural planes as smooth or stepped (single orientation) surfaces, respectively. Light etching with acid of these internal crystal planes leads to partial removal of the inorganic mineral phase by dissolution, and here produced a characteristic surface microtopography typical for each crystallographic face (Fig. 7b). The {104} faces contained irregularly arranged (“zigzag”), cascading etch steps with a significant number of straight edges parallel to the $\langle \bar{4}41 \rangle$ direction. Frequently observed between etched steps were narrow {104} terraces with small residual bumps / particles (Fig. 7b). In contrast, the {110} faces showed arrays of steps or multiple, short etch pits (Fig. 7b) that ran parallel to the $\langle \bar{4}41 \rangle$ direction. Upon etching for slightly longer times, the {104} faces showed increased topography with abundant and pronounced residual peaks reflecting focal areas protected (by organic material) from the acid (Fig. 7c), whereas the {110} faces remained essentially unaltered and retained their stepped appearance. Conversely, after partial removal of organic matrix by digestion using NaOCl, the {104} faces became significantly pitted while the {110} faces again remained largely unaltered (Fig. 7d). Following colloidal-gold immunocytochemical localization of OPN on similarly fractured, unetched samples, most gold particles were associated with the {104} faces, with more minor labeling being observed on the {110} faces (Figs. 7e,f).

Vertical crystal layer and cuticle

Just external to the palisades region of the eggshell lies the vertical crystal layer (Tyler, 1969) – also called the vertical matrix layer (Dennis et al., 1996). Fractured eggshell in this region when viewed in cross section, whether left undecalcified (Fig. 8a) or decalcified (Fig. 8b), shows that both the mineral and the matrix have a texture and orientation that changes from being either parallel or at an acute angle to the

shell surface in the palisades region to being nearly perpendicular at the outer surface of the eggshell. Brief acid etching revealed a fibrous and vertically oriented matrix laterally interconnected by short matrix struts (Figs. 8b,c). Partial removal of matrix by bleaching increased surface topography to reveal mineral components likewise oriented vertically (Fig. 8d). Spherical voids similar in size and protein-coating structure to those in the palisades region were also observed in the vertical crystal layer, but were much fewer in number (data not shown). While no obvious structural boundary was observed between the palisades and vertical crystal layer compartments, on occasion some parallel sheets of matrix appeared to form an indistinct interface in this region (data not shown). Moderate levels of OPN immunolabeling were observed by SEM (Fig. 8e) and TEM (Fig. 8f) for the matrix found in the vertical crystal layer.

The cuticle is the outermost layer of the eggshell and its thickness varies considerably over the eggshell surface. Dennis et al. (1996) have characterized the cuticle as having a mineral-rich inner cuticle, containing spherulitically arranged hydroxyapatite crystals, and a mostly organic outer cuticle. Post-embedding colloidal-gold immunolabeling for OPN on sections of the cuticle, viewed by TEM, showed a moderate and homogeneous distribution of gold particles across the organic matrix of the cuticle (Fig. 8f).

Eggshell pores

The pore system of the avian eggshell is located at specific locations between the eggshell cones (columns, prisms) to provide for gas and humidity exchange. In chicken eggs, a typical pore (Fig. 9a) has a funnel-shaped orifice opening at the outer shell surface at the level of the cuticle, and a single channel passing through the vertical crystal layer and the palisades region to open at the inner surface of the eggshell between neighboring mammillae. Brief acid etching demonstrates that the

surfaces of each pore are lined by a thin layer of protein (Fig. 9b) connected by struts to the underlying matrix (Fig. 9c). This pore-coating layer of protein showed an abundance of gold particles after immunolabeling for OPN (Fig. 9c).

Effect of OPN on calcite growth in vitro

Calcite crystal growth experiments were conducted in the absence and presence of OPN protein; changes in calcium concentration in reactant solutions were measured by atomic adsorption spectrophotometry, and crystal morphology was assessed by SEM. Without protein, solution calcium decreased after 30 minutes (Fig. 10a), and sizable calcite crystals were observed by SEM after 1 hour of reaction time (Fig. 10b). With OPN added to the CaCl_2 solution, crystal nucleation and growth were delayed by approximately 30 minutes, with solution calcium decreasing significantly only after 1 hour, and with roughly similarly sized (as without protein) crystals forming at about 1.5 hours of reaction time. At relatively low concentrations of OPN ($0.15 \mu\text{M}$), calcite crystal morphology appear as $\{104\}$ rhombohedra (Fig. 10c). A 2-fold increase in OPN concentration ($0.31 \mu\text{M}$) produced significant morphological change in the crystals via modulation of growth mechanisms at the crystal faces (Figs. 10d,g). At this OPN concentration, the calcite crystals formed aggregates of $\{104\}$ rhombohedra and their “patchy” irregular surfaces were comprised of layers of spreading and merging growth islands. The edges and corners of the larger growth islands retained angles corresponding to the crystallographic symmetry of calcite $\{104\}$ (Fig. 10g). When the concentration of OPN was increased about 5-fold to $0.78 \mu\text{M}$ and crystal growth was allowed to proceed for 1.5 hours (Figs. 10e,h), the majority of the crystals developed as aggregates and the calcite $\{104\}$ rhombohedra grew small, new facets at the equatorial edges and corners of the crystals (as shown previously for magnesium addition by Chien et al., 2006). On the larger $\{104\}$ crystal faces, circular voids in

mineral continuity were observed (Fig. 10h) with an appearance similar to those seen in fractured eggshell in the palisades layer (Fig. 10f, and also Figs. 5a and 7a). Attempts to immunolocalize OPN on these synthetically grown crystals were not successful given the significant dissolution of the crystals during the aqueous immunolabeling procedures.

3.6 Discussion

Matrix-mineral ultrastructural relationships in the avian eggshell

Although there are excellent reports on the structure of avian eggshell and, to some extent, its organic matrix (for example, Schmidt, 1960; Terepka 1963a, 1963b; Tyler, 1969; Wyburn et al., 1973; Dieckert et al., 1989; Dennis et al., 1996), little is known about the ultrastructural relationship between matrix constituents and the calcitic mineral phase. The details and implications of these relationships are important to know for understanding eggshell formation; indeed, significant progress has been made in recent years in identifying and explaining how proteins and their peptide motifs interact with minerals (e.g., Hoang et al., 2003; Qiu et al., 2004; De Yoreo et al., 2006). Importantly, these interactions can result in modifications to mineral type, form and function (Berman et al., 1990; Berman et al., 1993). The influence of proteins on biomineralization results not only from interactions of proteins with crystal surfaces, but also from their subsequent occlusion within mineral structure. In the present study, using several high-resolution ultrastructural approaches, we report on heretofore undescribed organic matrix structures within the eggshell, relate them to crystallographic features of the mineral phase by surface-etching techniques, and identify the location of OPN within previously known, and new, matrix structures. We also provide data from *in vitro* crystal growth studies performed in the presence of OPN that demonstrate the ability of this

protein to act as an inhibitor of calcite growth and modify crystal morphology. Taken together, these data provide new insight into how proteins, and particularly OPN, might function in the formation of eggshells, and perhaps even in other biomineralizing systems. Considered below, following our interpretation of the *in vitro* calcite growth studies, is a region-by-region discussion of the eggshell in the context of matrix (OPN)-mineral relationships.

Effects of OPN on calcite crystal growth *in vitro*: Implications for eggshell formation

Our free-drift, calcite growth experiments, with or without OPN, demonstrate the inhibitory effect of purified, phosphorylated OPN on calcite growth at both the micro- (crystal morphology) and nano- (growth step) scales. A similar inhibitory activity for phosphorylated OPN on calcite growth has been shown using a pH stat assay. However, OPN dephosphorylated by alkaline phosphatase was relatively inactive, thus emphasizing the role of the phosphate groups in this inhibitory activity (Hincke and St Maurice, 2000).

In all cases in our present study, the morphology of the crystals were {104} rhombohedra within the times and range of the OPN concentrations used in the growth studies. Modifications in overall crystal morphology, and examination of growth steps at higher magnification, revealed that OPN interacts preferentially with the {104} crystallographic faces of calcite, which in turn inhibits and stabilizes these faces. This *in vitro* result is consistent with the *in vivo* immunolabeling data showing OPN preferentially residing on internal, cleaved {104} faces – existing presumably *in situ* as a mineral-occluded protein. Indeed, studies of synthetic or natural calcite commonly show that in the presence of either inorganic (Ba^{2+} in Astillero et al., 2000; Mg^{2+} in Davis et al., 2000) or organic (aspartic acids in Teng et al., 1998; chiral aspartic acids in Orme et al., 2001) impurities, or even when grown

at near-equilibrium growth conditions (Chien et al., 2006), new faces will develop on the crystals at the equatorial corners and edges (e.g., Mann et al., 1990; Albeck, et al., 1993; Aizenberg et al., 1994; Temmam et al., 2000; Orme et al., 2001; Chien et al., 2006). This occurs because the propagation of growth layers is generally slower toward the equatorial edges and corners than toward the polar edges and corner layers of the {104} faces; edges of growth layers pile up, coalesce, and eventually form new faces at the equatorial corners (Chien et al., 2006). In the present study, the development of new faces on the calcite crystals occurred when OPN was added at a concentration of 0.78 μM in solution and after 1.5 hours of crystal growth.

With increasing OPN concentration, the calcite crystals grown *in vitro* tended to aggregate, with the *c*-axis of each {104} rhombohedron slightly mismatched to that of its neighbors (Figs. 10d,e). Furthermore, the higher concentrations of OPN produced rougher (increased topography) {104} calcite surfaces having abundant growth islands and step edges (macrosteps), thus revealing alterations in the growth mechanism on the {104} faces caused by the added OPN (Figs. 10g,h). However, the growth process at this {104} face was still controlled by the surface structure of the underlying calcite {104}, as indicated by the symmetry-related straight edges of growth islands. At the highest concentration of added OPN (0.78 μM), calcite growth was modulated by OPN at the {104} face to produce a circular growth step pattern (Fig. 10h) that strikingly resembles the vesicular voids – interruptions in mineral continuity – seen in the palisades region of fractured eggshell. While this observation implicates OPN in the process by which these voids are created *in vivo*, the lack of an immunogold labeling reaction on the vesicular proteins that encapsulate these voids indicates that the influence of OPN may be indirect.

The finding of an interaction between OPN and the {104} eggshell calcite faces is remarkable and noteworthy, and is confirmed by our *in vitro* studies of synthetic

calcite inhibition by the added OPN at the {104} faces (Figs. 10c-h). The inhibition of other calcite crystallographic faces by the components of uterine fluid indeed has been previously reported (for example, Fernandez et al., 2004). However, those studies involving uterine fluid obviously contain an extensive mixture of organics and other ions able to affect calcite growth, whereas our study uses a single purified protein – OPN. While in some cases it would be considered desirable to use whole uterine fluid for calcite growth studies, the purpose of our study was to focus on the role of OPN. Our results not only show this nanoscale OPN- $\{104\}$ face interaction, but also demonstrate more macroscale changes as observed *in vitro* by the creation of the documented spherical voids by OPN and overall morphologic changes to crystal shape (Fig. 10).

Ultrastructure and OPN localization in the mammillae of the eggshell

Eggshell is sequentially formed on the shell membranes by a spatio-temporal deposition of organic matrix and inorganic minerals (Fernandez et al., 1997, 2001, 2003). When the egg enters the tubular shell gland portion of the oviduct (red isthmus), and before calcification begins, mammillary matrix is synthesized and deposited at quasi-periodic, discrete locations on the shell membranes (Wyburn et al., 1973; Fernandez et al., 1997). The egg then enters the shell gland pouch (uterus), where mineralization first begins within these initial mammillary base plates (also called knobs, or mammillary tips) located on the outer shell membrane (Wyburn et al., 1973; Fernandez et al., 1997). Granular epithelial cells of the uterus secrete OPN into the uterine fluid which then accumulates in the forming eggshell (Pines et al., 1995; Lavelin et al., 1998, 2000; Hincke et al., 2008). At this time of early calcification, the CRB and the CRB sac are not yet fully developed (Wyburn et al., 1973).

Our observations from fully mature laid eggshell, and from forming eggshells

removed at different stages of development from the uterus (data not shown), indicate that little or no OPN resides within, or on, the shell membrane fibres. These observations differ from those of Fernandez et al. (2003), who describe OPN within the fibres – perhaps attributable to differences in fixation protocols and/or the use of different antibodies. Our negative reaction for OPN associated with the shell membrane fibres does not necessarily preclude its presence there, since in some cases epitopes may be masked and thus not exposed for antibody labeling. As the mammillae develop and calcify, OPN accumulates within base plate and the CRB and at the external surface of the mammillae, where in the latter case OPN organized as a protein coating may serve to inhibit mineralization and define the outermost boundary of each mammillary body. The CRB sac is a unique compartmental unit with unknown function (Dieckert et al., 1989; Dennis et al., 1996). It develops as a chamber-like structure that is bounded by a membranous protein coating (free of OPN) and which contains abundant small granules also lacking OPN. Interconnecting, fine filamentous fibres containing OPN form an interlacing network between the granules. Although additional work is necessary to understand the assembly, organization and function of this complex eggshell compartment, it has been described that spherulitically arranged calcite microcrystals exist in association with these protein granules (Nys et al., 2004), providing a structure whose crystalline architecture and dissolution during embryonic skeletal growth facilitates breaking the weakened shell by the beak of the chick during hatching.

Ultrastructure and OPN localization in the palisades of the eggshell

The aligned matrix lamellae with associated vesicles found in the palisades region of the eggshell demonstrate not only an abundant matrix that intermingles with the calcitic mineral phase, but also a periodic structure most obviously apparent after full decalcification of the eggshell. While some of this arrangement is likely

artificial, arising from partial collapse of the matrix when the mineral phase is removed by decalcification, our inclusion of aldehyde (crosslinking) fixative in the decalcification solution to stabilize as best as possible this organization, together with observations of the matrix on briefly acid-etched samples, indicates that much of this organization is real. Indeed, it appears that most of this OPN-containing matrix, and the vesicular protein structures, is likely occluded within the calcitic mineral. Since the columnar palisade layer is established sequentially in a vertical manner towards the surface of the eggshell, it would seem reasonable to consider that alternating cycles of OPN-containing matrix deposition (and consequently mineral growth inhibition) and calcite growth regulate eggshell formation rates and oriented structure in this region. The alternative possibility – that OPN / matrix deposition and mineral inhibition is a continuous process – cannot be excluded. In any event, regulation of calcite growth by OPN and likely other matrix constituents in some manner produces elongated, matrix-rich calcitic columns in the palisades region that have well-defined forms which provide the bulk of the eggshell important to its functions.

It is interesting to compare how calcite growth in the geologic setting, which is not regulated by such a matrix, produces calcite crystal habits seen as scalenohedrons, also known as “dog tooth spar.” Competitive growth of calcite crystals clearly plays a role in the formation of the eggshell (Garcia-Ruiz et al., 1995), as does the constituents and organization of the organic matrix in modifying what would otherwise be unrestricted, geologic-type growth of calcite. The most obvious difference between geologic calcite scalenohedrons and eggshell calcite is that the eggshell has a repetitive and organized structure. Although competitive growth surely explains significant features of the eggshell pattern, the refined, repetitive and organized structure of eggshell can only come about from additional influences, such

as those provided by an organic matrix. In contrast to the geologic growth pattern having acute, angular ends and more disorganized structure, eggshell structure is characterized by its repetitive, architectural pattern.

The absence of an association of OPN with the palisade vesicles, which correlate with the peripheries of the voids in mineral continuity observed in fractured undecalcified eggshell, is noteworthy. The mineral inhibition activity presumably creating these voids therefore likely resides with other matrix components; indeed, the eggshell-specific proteins ovocleidin-116 (Hincke et al., 1999) and ovocalyxin-32 (Gautron et al., 2001) have been identified previously by us in these structures.

Of particular interest is our localization of OPN to the {104} crystallographic face of calcite in fractured eggshell. Fracturing of the eggshell during sample preparation characteristically followed the {104} and {110} cleavage planes of calcite. After brief acid-etching of these faces, a characteristic surface microtopography was obtained along the Periodic Bond Chain (PBC) orientation – a theory developed by Hartman and Perdok (1955) and Hartman (1987). Briefly, when considering an elementary growth slice (i.e. a slice of crystal whose thickness is equal to the interplanar distance of the corresponding crystallographic faces), a PBC is defined as an uninterrupted stoichiometric linkage of the strongest bonds in the first coordination sphere of the molecular units of the crystal; thus, the detachment energy of the molecular units is higher and probability for molecular units to attach is lower along the PBC directions than along any other crystallographic directions. Upon exposure to acid and dissolution, crystal face etching (dissolution) therefore proceeds rapidly along the PBC directions to give characteristic, etched topographic features. For calcite, Heijnen (1985) demonstrated three non-equivalent PBCs ($\bar{4}41$), $\langle 010 \rangle$ and $\langle 2\bar{2}1 \rangle$) where the {104} face contains two or more PBCs in their elementary crystal slices enabling

crystal dissolution / growth by a layer-spreading mechanism, whereas the {110} face has only one PBC, and etching on these faces occurs rapidly only along the PBC direction in one-dimension. Experimental observations on inorganic calcite have shown that the crystal morphology and the surface microtopography on different crystallographic faces are generally consistent with the PBC analysis of Heijnen (Heijnen, 1985; Staudt et al., 1994; Astilleros et al., 2000). Relating this to our observations in the present study where eggshell calcite was lightly etched with acid to dissolve mineral (Figs. 7b,c), or was “etched” with sodium hypochlorite to remove organic material (Fig. 7d), we noted that {104} cleavage faces contained abundant matrix proteins, and typical irregular (“zigzag”) etching steps with straight edges normally parallel to the $\langle \bar{4}41 \rangle$ PBC direction on the surfaces, while the {110} faces display elongated etched pits aligned in only one direction and the amount of organic matrix on this surfaces was limited. OPN bound to the {104} face provides an explanation for the acid-resistant, residual peaks of mineral observed after brief acid etching (Fig. 7c) where each peak is likely capped by one or more organic matrix molecules that could include OPN. The occlusion of proteins such as OPN (and likely other organics) into the calcitic structure of the eggshell likely modifies the propagation of cleavage planes when an eggshell is fractured (relative to pure calcite which preferentially fractures along the {104} cleavage planes); this has been shown previously for sea urchin calcite (Berman et al., 1990; Seto et al., 2004). The alternating cleavage pattern observed here in fractured eggshell occurring between the {104} and {110} cleavage planes can now be explained by the preferential localization of protein (including OPN) to the {104} face. This interpretation is consistent with discussions of the quality and mechanical strength of eggshells being largely determined by the micro-structural organization of calcite crystals in the palisades region (Rodriguez-Navarro et al., 2002).

Ultrastructure and OPN localization in the vertical crystal layer and cuticle of the eggshell

In the vertical crystal / matrix layer there is a change in the alignment and texture of the eggshell matrix and mineral from that of the palisades region; the matrix has a general vertical orientation, with interconnecting horizontal struts. While OPN does not appear to be preferentially associated with either of these matrix structures, there is moderate immunolabeling for this protein in this region. In the cuticle, OPN was likewise moderately distributed throughout its full thickness. These observations are consistent with those reported by Lavelin et al. (1998), where a reduction in OPN gene expression prior to laying of the egg was described for the shell gland. Although the terminal phases of eggshell construction occur in a uterine fluid which is supersaturated in calcium and bicarbonate with respect to calcite (Gautron et al., 1997), the role of inhibitory phosphoprotein(s) such as OPN on cessation of calcite deposition has not yet been elucidated.

Ultrastructure and OPN localization in pore walls of the eggshell

The remarkably strong association of OPN with proteinaceous limiting membrane coating the calcite column surface and defining the pore space suggests a crucial role for OPN in developing and maintaining eggshell pores. The avian eggshell contains a large numbers of pores, up to several tens of thousands as reported by Rahn et al. (1987), Peebles and Brake (1985) and Tullet et al. (1975). These pores form a shell-traversing channel network that allows water and gas exchange necessary for the growing embryo, while at the same time not significantly diminishing the mechanical properties of eggshell required to protect the embryo. The pore systems must also need to be capable of resisting micro-organism invasion, and it has been reported that embryo mortality is inversely related to the density of pores existing in eggshell (Peebles and Brake, 1985; Board et al., 1977; Tullet et al.,

1975). In the present study, our description of OPN as a prominent component of a distinct, delimiting protein layer at the margins of the calcitic columns and defining the pore space may be a means by which calcification is not only inhibited and/or terminated at the calcite column boundary, but is done so in a definitive way that preserves the patency of the pore channel. Such an inhibitory, compartmental boundary function for OPN would define pore structure and dimensions, and prevent calcification of the pore system during eggshell formation.

3.7 Conclusions

In summary, we have documented many features of matrix ultrastructure in the avian eggshell, and have related them to eggshell compartments and mineral structure and organization. We have described an extensive matrix network co-existing with a calcitic mineral phase, have localized the mineral-binding, inhibitory protein OPN (as determined *in vitro* by a crystal growth inhibition assay and SEM of crystal morphology) within this network, and have shown a preferential binding of OPN to the {104} crystallographic faces of eggshell calcite – whose appearance at fractured surfaces suggest that it resides as an occluded protein. In the eggshell, OPN likely functions to guide calcite orientation by influencing crystal growth and morphology. OPN is also a prominent interfacial protein, accumulating at the boundaries of various eggshell structures where we propose it terminates calcification at those margins to maintain different eggshell compartments and the patency of the eggshell pores.

3.8 Acknowledgements

This work was funded by the Natural Sciences and Engineering Research Council of Canada, and by a studentship to Y.-C. Chien from the Strategic Training Initiative

in Health Research program of the Canadian Institutes of Health Research. The authors also thank Line Mongeon and Lydia Malynowsky for their skillful technical assistance with the microscopy work. MDM is a member of the Jamson T.N. Wong Laboratories for calcified tissue research, and a scholar of the Fonds de la Recherche en Santé du Québec.

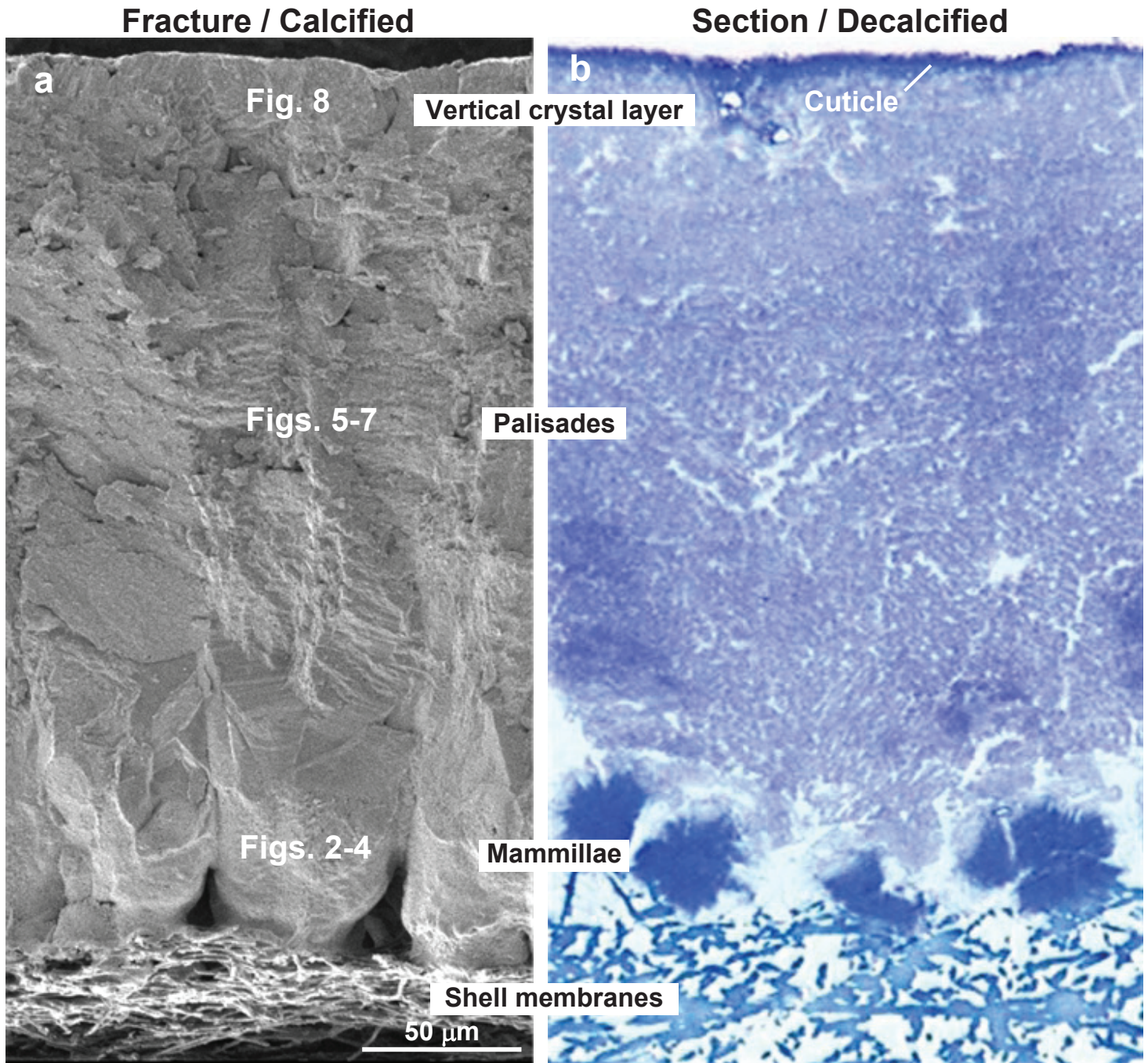


Figure 1. Cross-sectional profile of avian eggshell. (a) Scanning electron micrograph of a cross-fractured eggshell without decalcification showing the major eggshell compartments (as indicated) and the shell membranes. The major mineral phase of the eggshell is calcite. Detailed observations for each compartment are described in subsequent figures (as indicated). (b) Light micrograph of cross-sectioned eggshell stained with toluidine blue after complete decalcification, plastic embedding and microtome sectioning. An abundant matrix is present throughout all compartments of the eggshell.

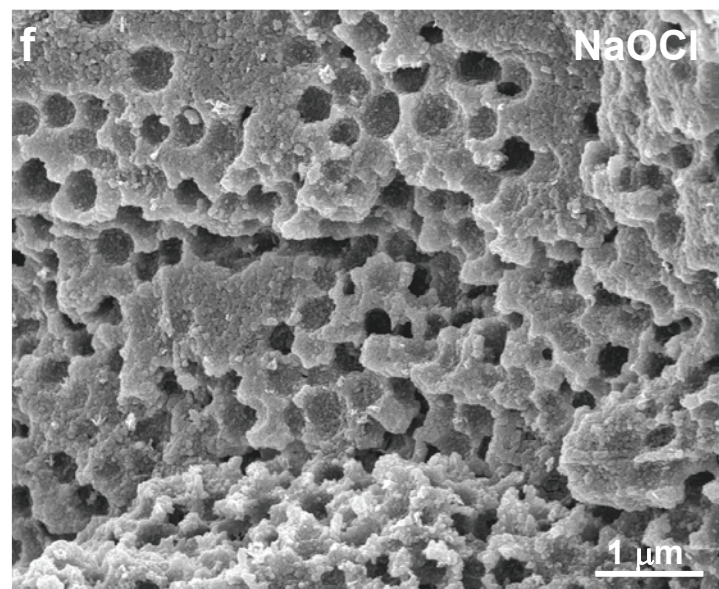
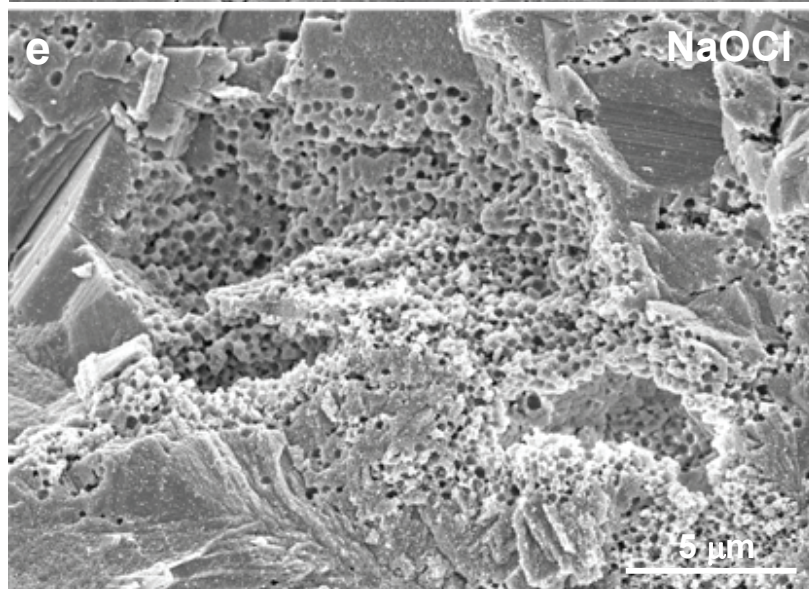
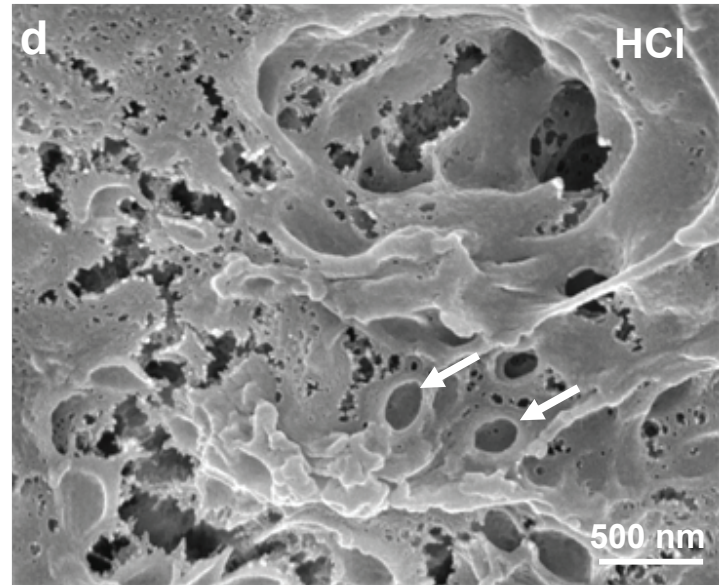
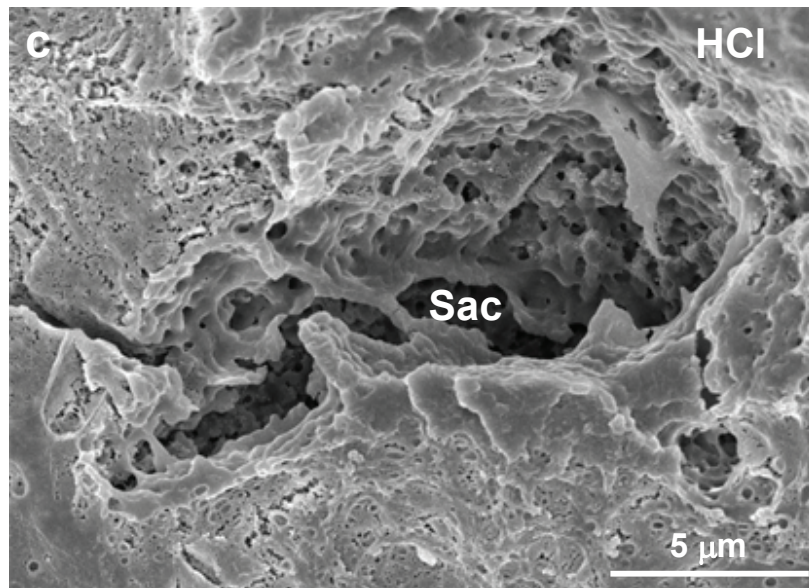
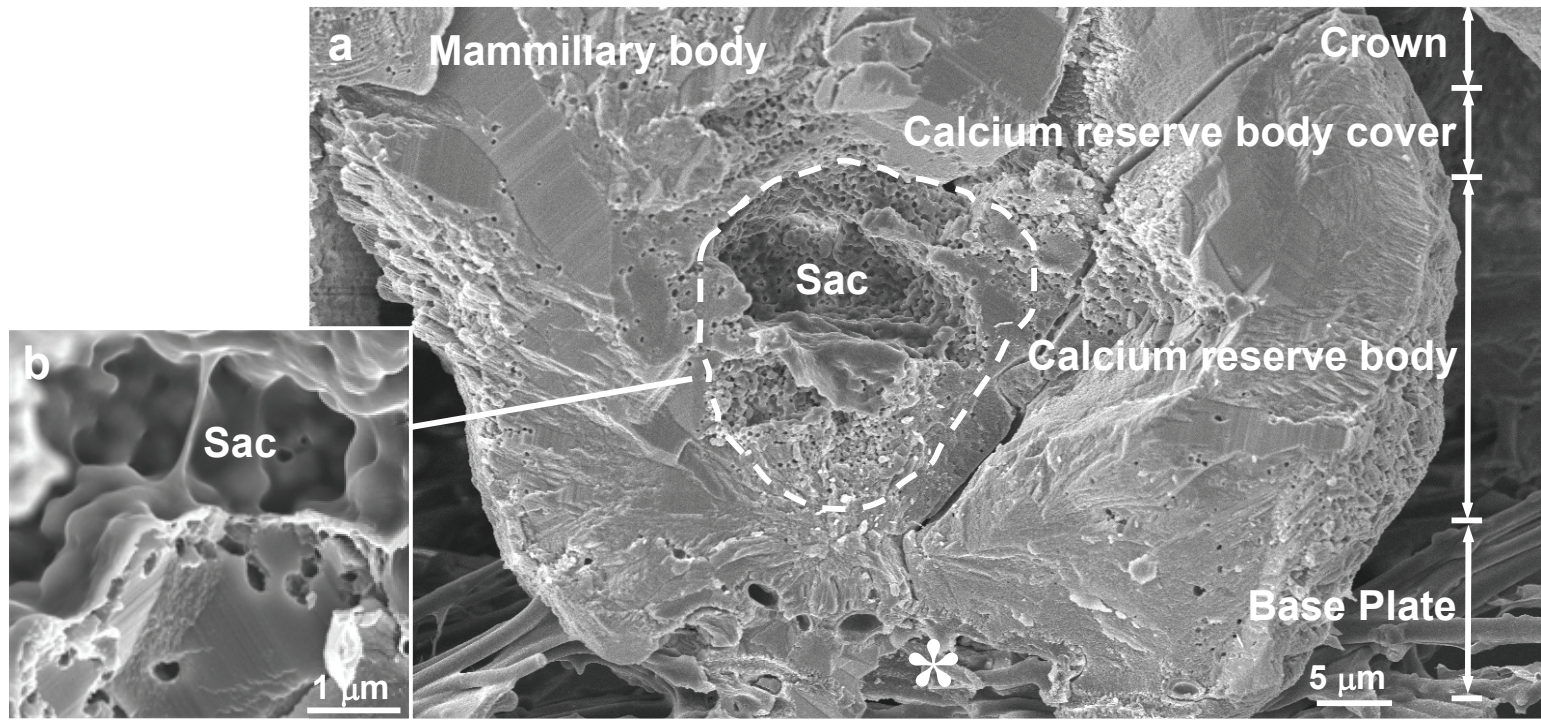


Figure 2. Ultrastructure of mammillary bodies in eggshell observed by SEM. (a) Constituting the mammillary body starting from the membrane side (asterisk) are the base plate and calcium reserve body (CRB) sac (dashed line), cover and crown. (b) A membranous film lines the margins of the CRB sac defining a space within the calcified mammillae. (c) Slight acid etching with hydrochloric acid (1 mM HCl for 1 minute) in aldehyde fixative reveals that the membrane of the CRB sac is continuous with the surrounding matrix of the mammillae. (d) Located within the CRB sac membrane are abundant hemi-vesicular structures (arrows). Sample was slightly acid-etched (1 mM HCl for 1 minute in fixative). (e,f) After digestion of the CRB sac membrane and subjacent matrix with sodium hypochlorite (14% NaOCl for 6 hours), the surrounding mineral phase is revealed showing cleaved calcite and abundant spherical voids.

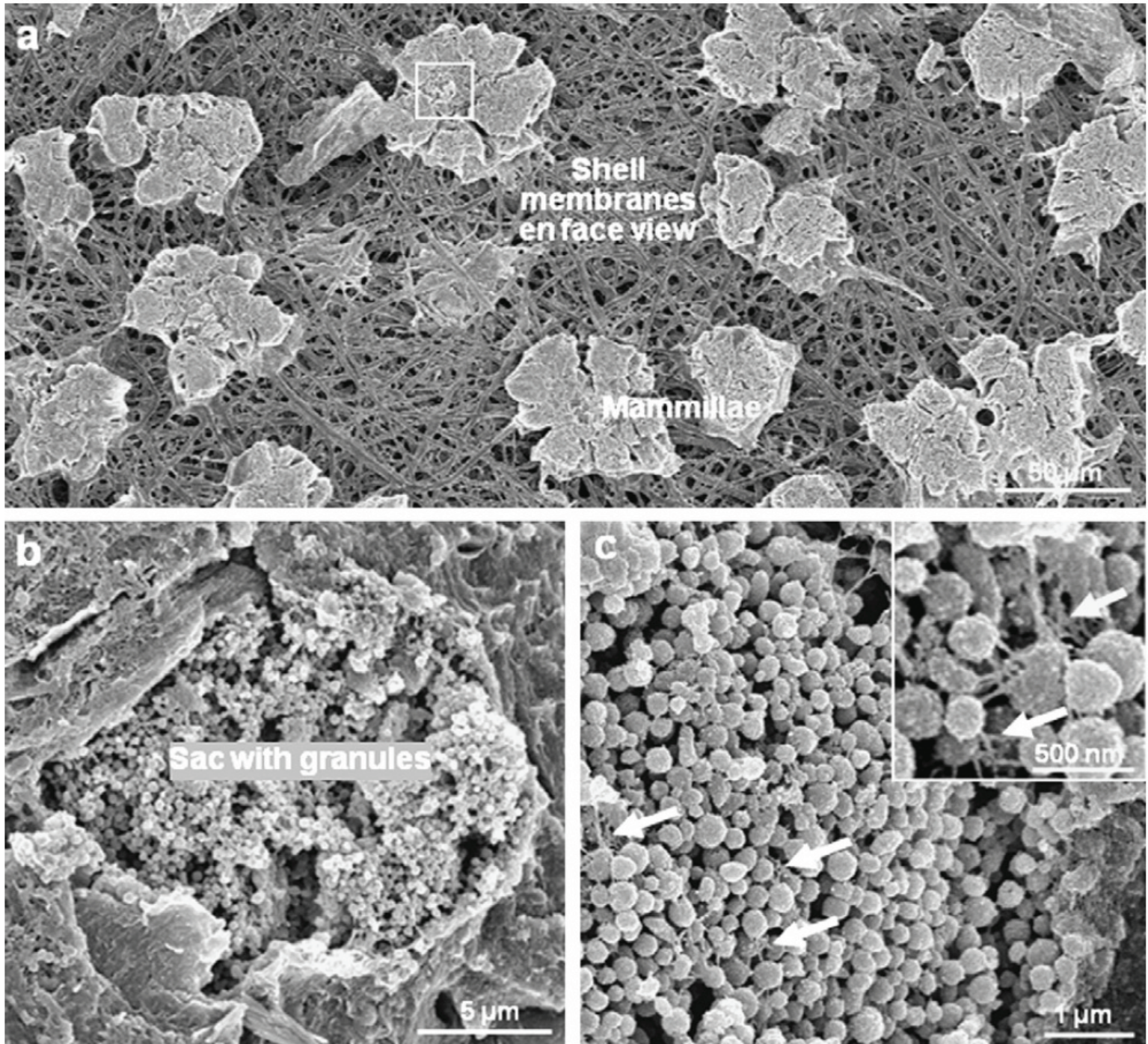


Figure 3. Scanning electron micrographs of an eggshell mildly acid-etched (1 mM HCl for 1 minute in fixative) and split in a plane parallel with the eggshell surface at the level of the mamillae to provide an *en face* view of the internal structure of the mamillary bodies. (a) Mammillae are patterned on the shell membranes in a pseudo-periodic manner. (b,c) Abundant granules (not seen in Fig. 2) inside the CRB sac are preserved by this sample preparation method. The granules are typically 200-300 nm in diameter and are linked by thin, fibrous threads (arrows).

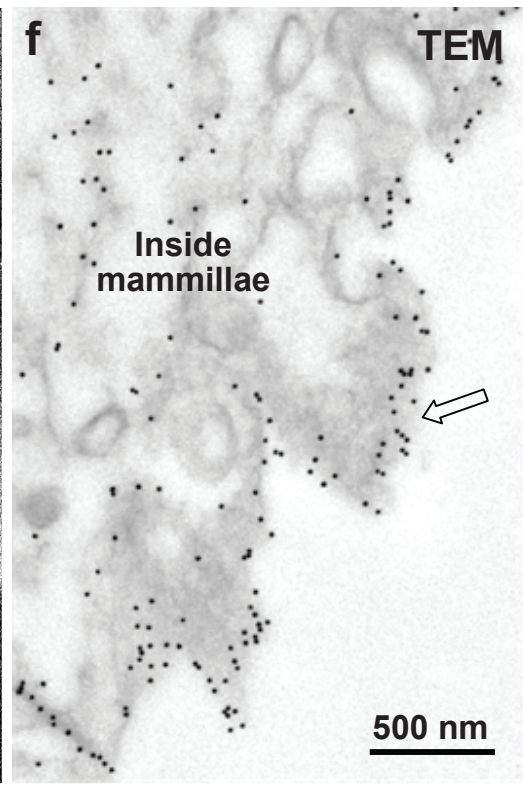
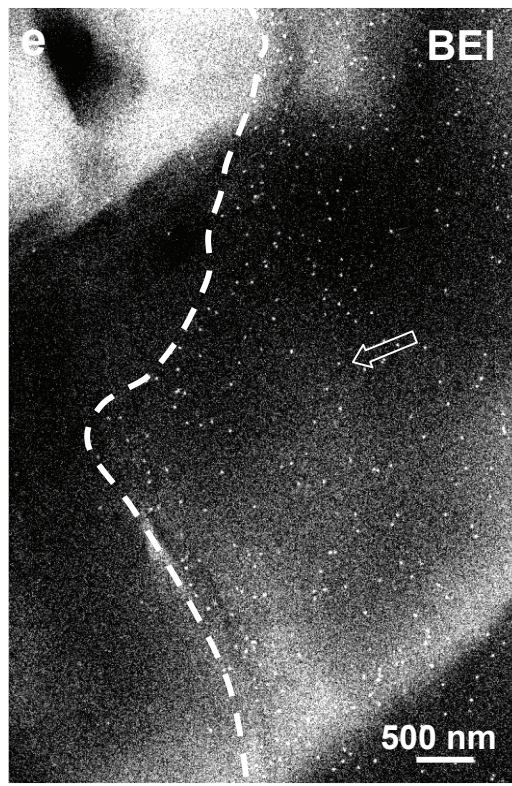
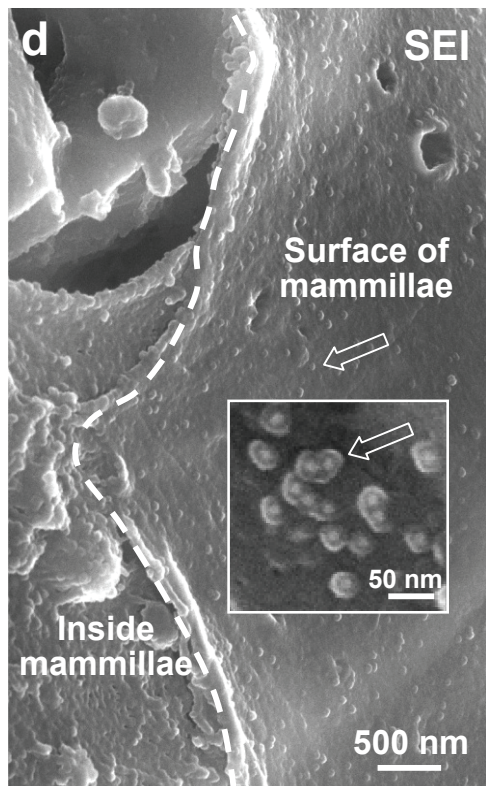
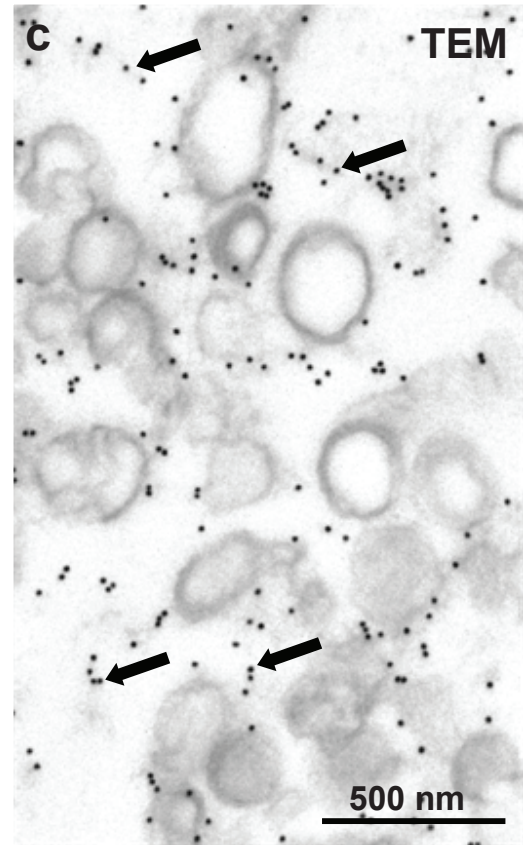
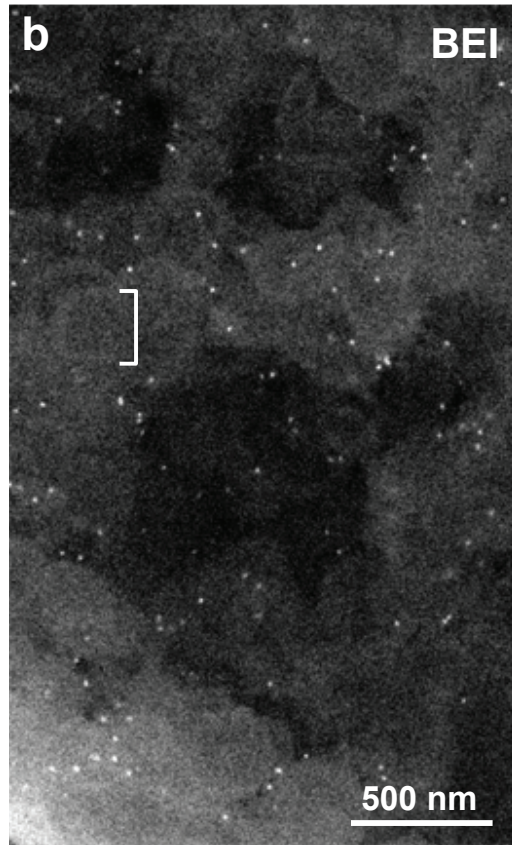
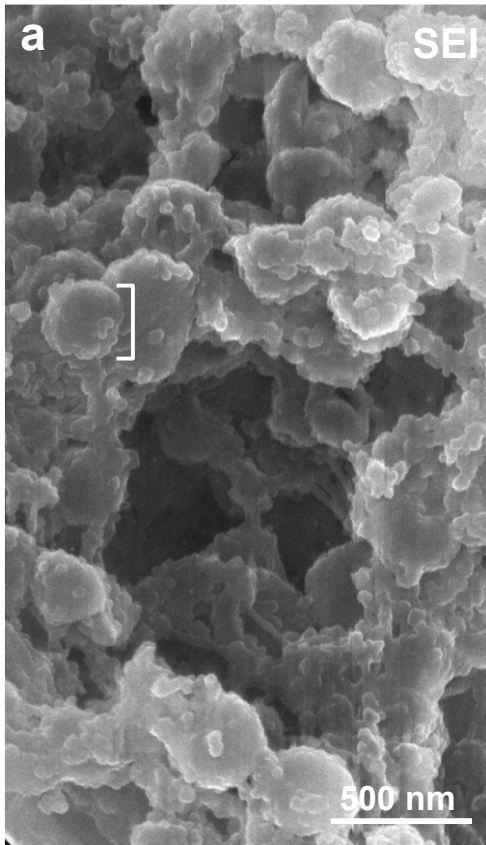


Figure 4. Colloidal-gold immunolabeling for OPN of eggshell mamillary structure viewed by SEM and TEM. (a) SEM secondary electron imaging (SEI), (b) SEM backscattered electron imaging (BEI) of slightly acid-etched eggshell (1 mM HCl for 1 minute in fixative), and (c) TEM viewing of decalcified ultrathin sections, all labeled for OPN by application of primary antibody followed by protein A-colloidal gold conjugate, show OPN associated with the network of thin, fibrous matrix (solid black arrows), but not with granules (brackets), within the CRB sac. (d) SEM secondary electron imaging (SEI), (e) SEM backscattered electron imaging (BEI) (1 mM HCl for 1 minute in fixative), and (f) TEM viewing of fully decalcified ultrathin sections, all labeled for OPN, show abundant gold particles associated with an organic layer coating the surface of the mamillae (open arrows), and with matrix inside the mamillary body (f). The halo structure surrounding each gold particle viewed by SEM SEI (inset, d) represents the protein A shell of the colloidal-gold conjugate bound to the surface of the gold particle. Gold particles appear white by SEM, and black (electron-dense) by TEM.

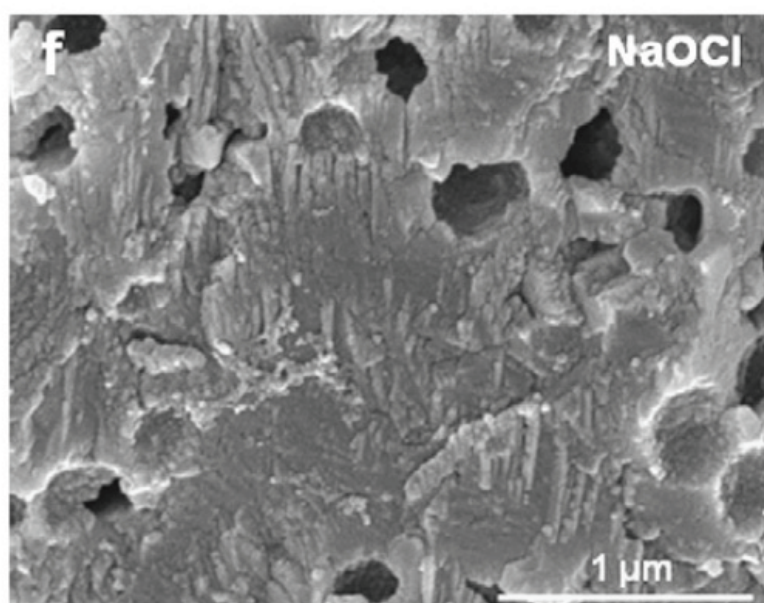
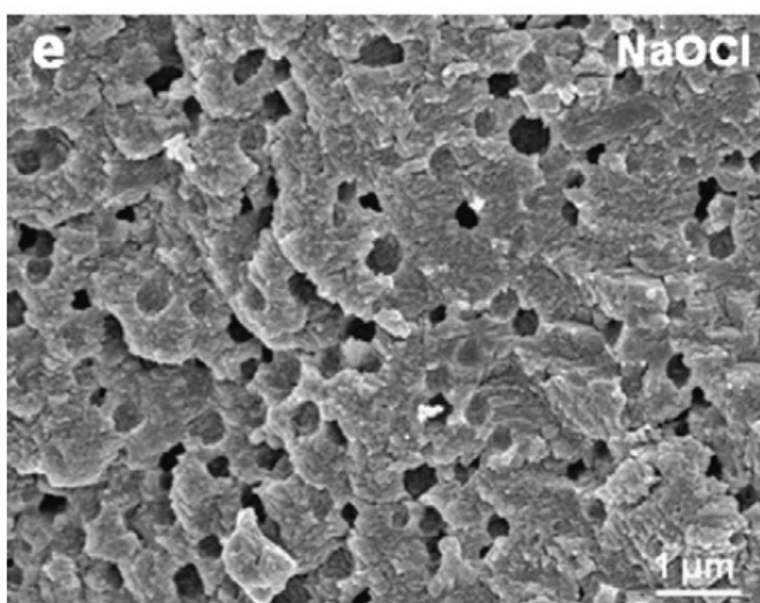
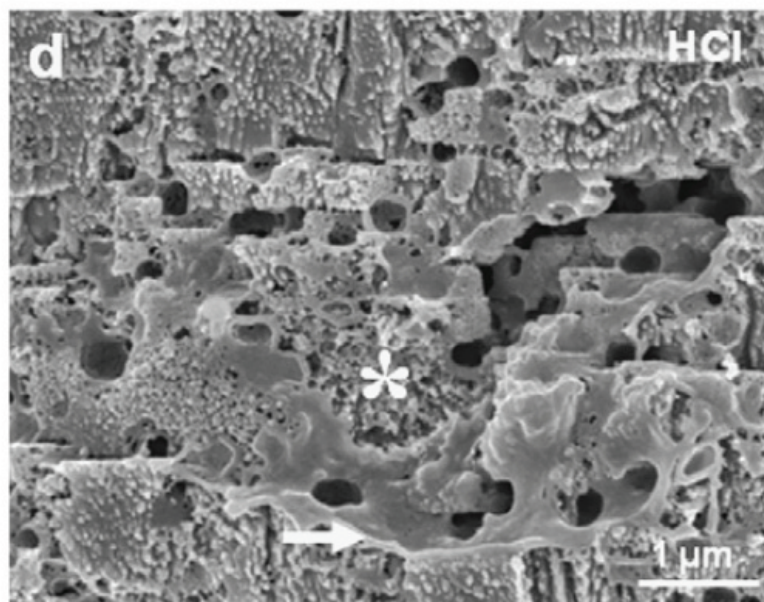
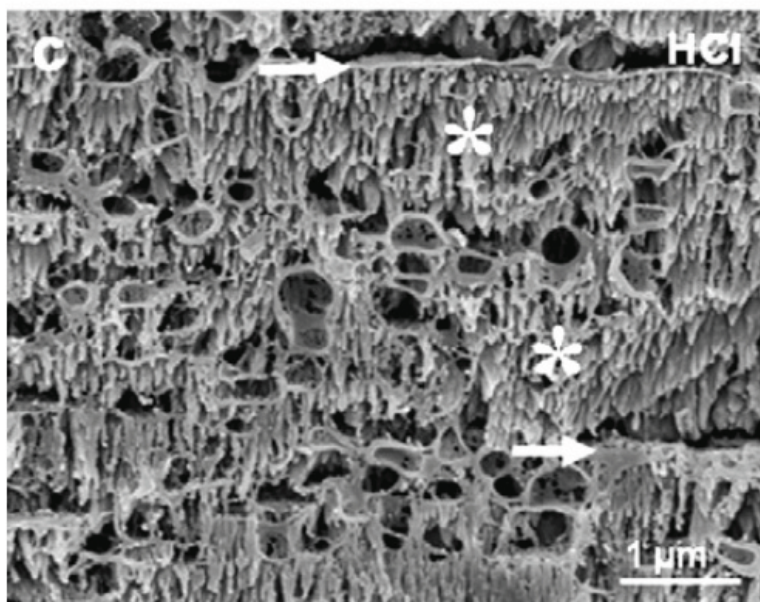
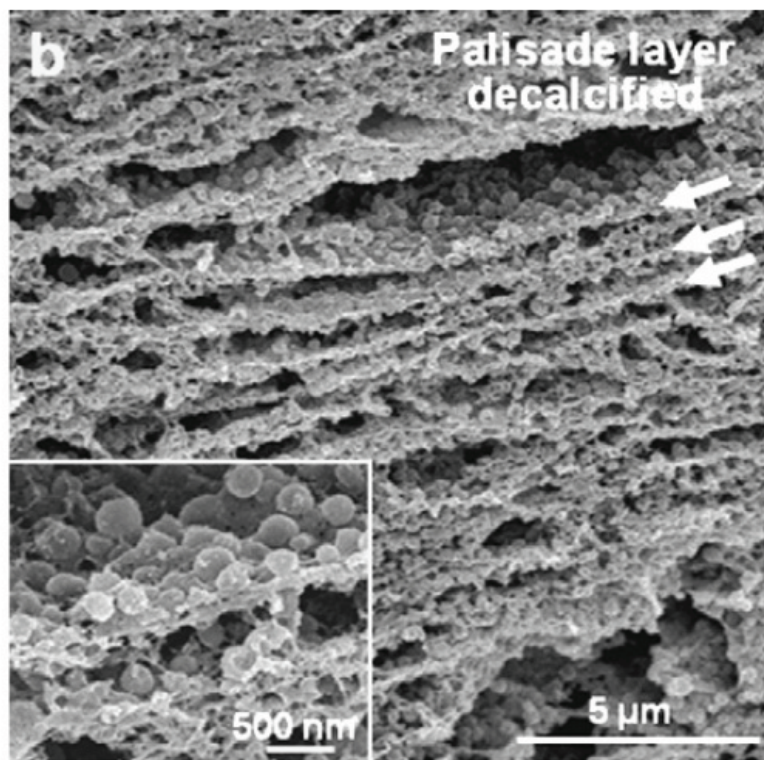
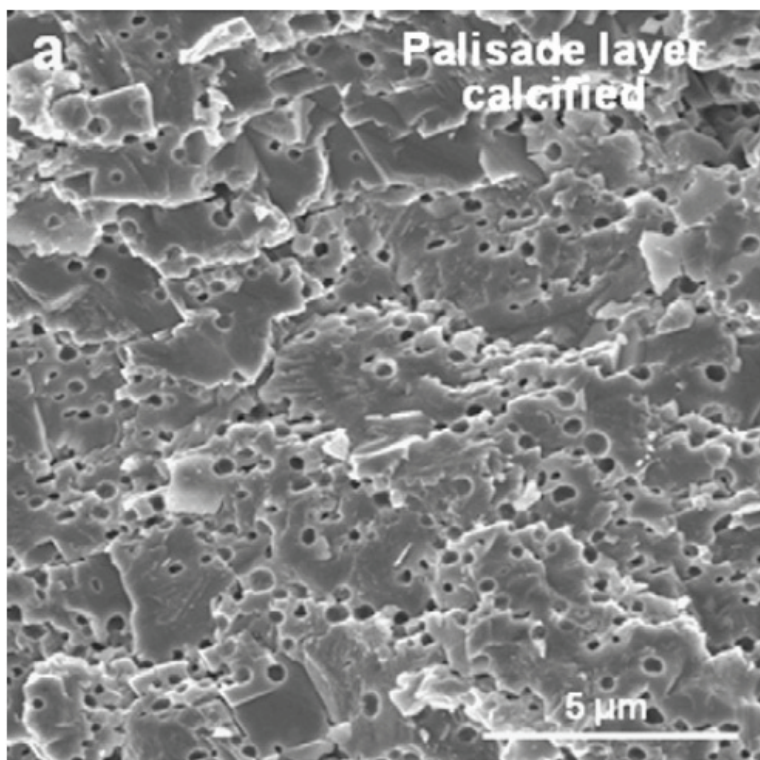


Figure 5. Ultrastructure of the palisade layer in eggshell by SEM. (a) Cross-fractured eggshell displays irregular cleaved calcite profiles in which are found numerous spherical voids. (b) After initial fixation with aldehyde, followed by simultaneous fixation and complete decalcification with EDTA, an extensive network of organic matrix is revealed permeating the previously highly-mineralized eggshell structure. This matrix consists of lamellar sheets (arrows) coated with abundant vesicles (inset). (c,d) After brief hydrochloric acid (1 mM HCl for 1 minute) etching of fixed, native eggshell fragments to partially remove surface mineral, additional prominent structures in this region include vertically aligned, fine fibrous matrix (asterisks) interconnecting the parallel lamellar sheets of matrix (arrows). (e,f) After sodium hypochlorite treatment (14% NaOCl for 6 hours) to remove surface organics from fractured eggshell fragments, a fine, depressed surface texture is noted on the cleaved calcite faces.

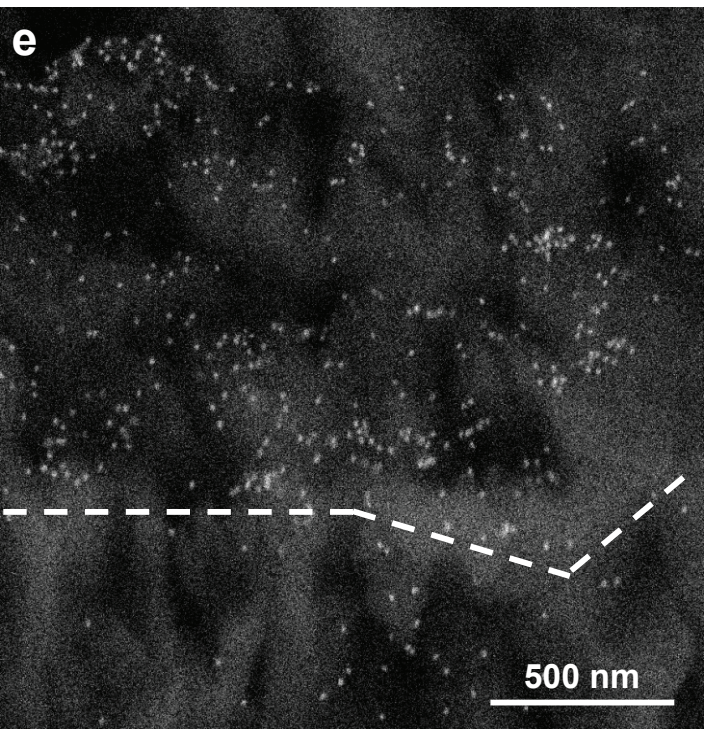
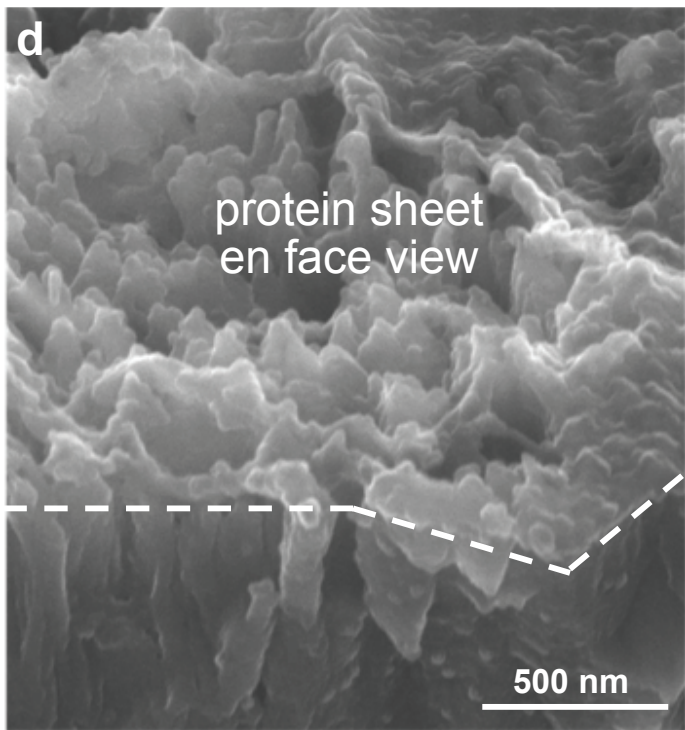
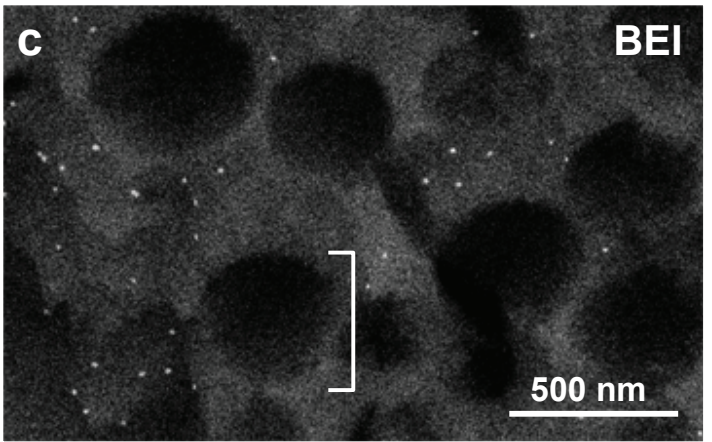
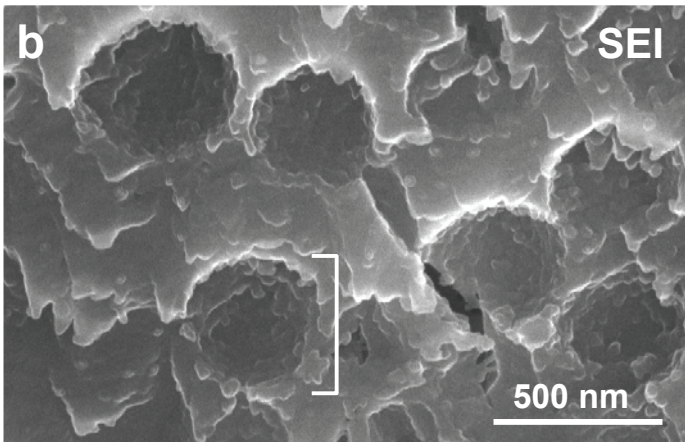
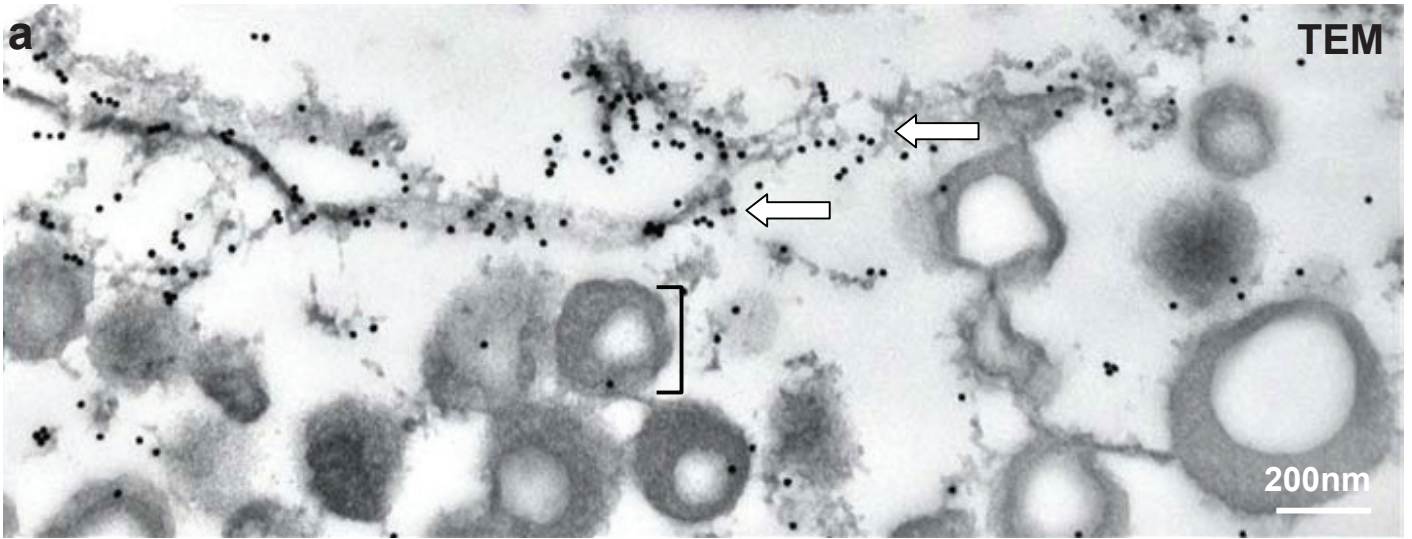


Figure 6. Colloidal-gold immunolabeling for OPN in eggshell palisade structure viewed by SEM and TEM. (a) Ultrathin section of fixed and decalcified eggshell in the palisades region observed by TEM after immunolabeling for OPN. Strong immunolabeling for OPN is associated with the lamellar sheets of matrix (arrows), with some moderate labeling of the interconnecting fibrous matrix between the vesicles, whereas the vesicles themselves are not labeled for OPN (brackets). The absence of OPN labeling of the vesicular structures (brackets) was confirmed by (b) secondary electron imaging (SEI) SEM and (c) backscattered electron imaging (BEI) (immunolabeling for OPN on a freshly cleaved eggshell without decalcification). (d) SEI and (e) BEI SEM imaging, in an *en face* view, after immunogold labeling for OPN on a fresh-fractured eggshell showing strong labeling of a matrix lamellae (e).

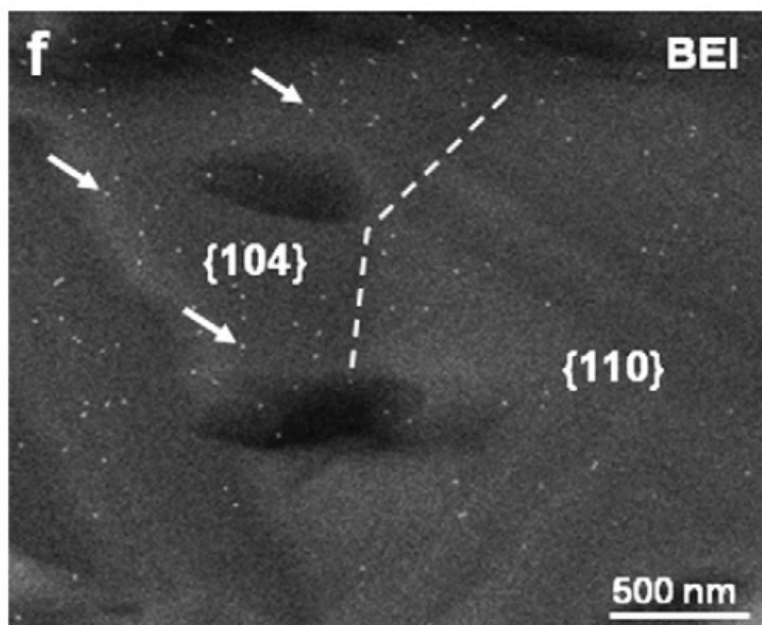
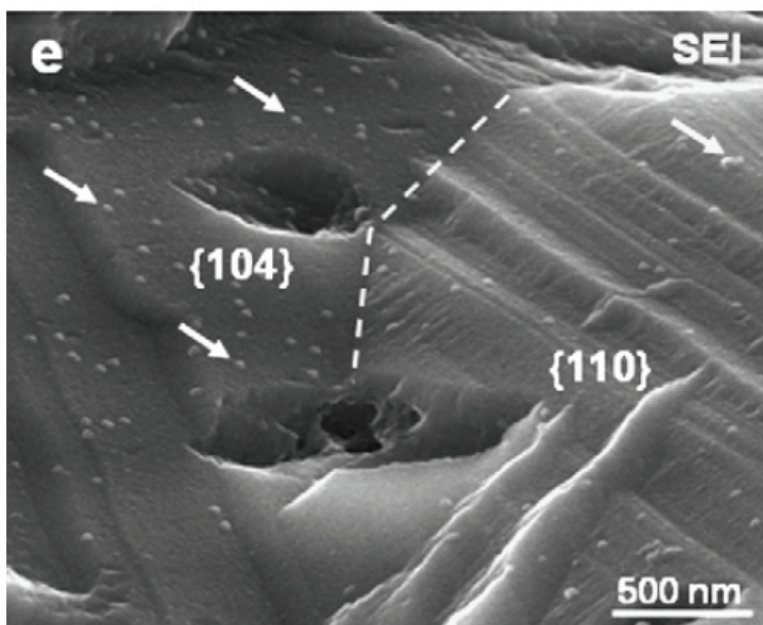
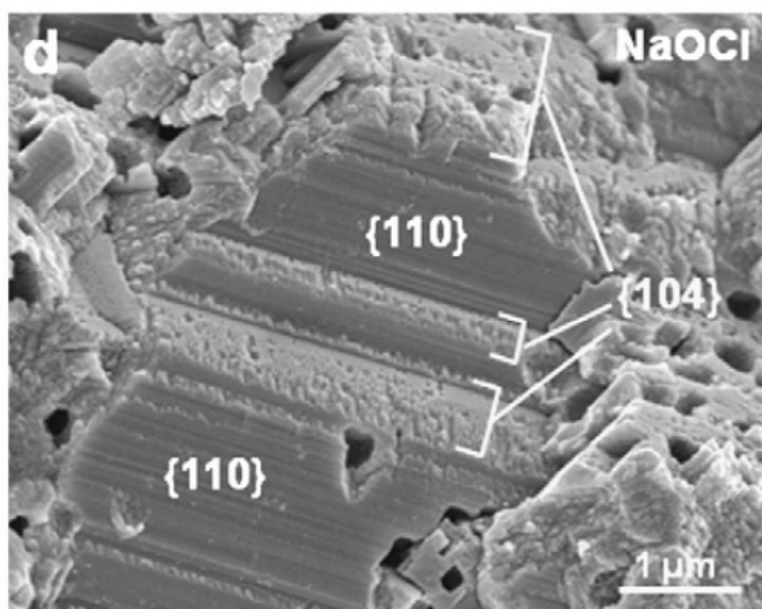
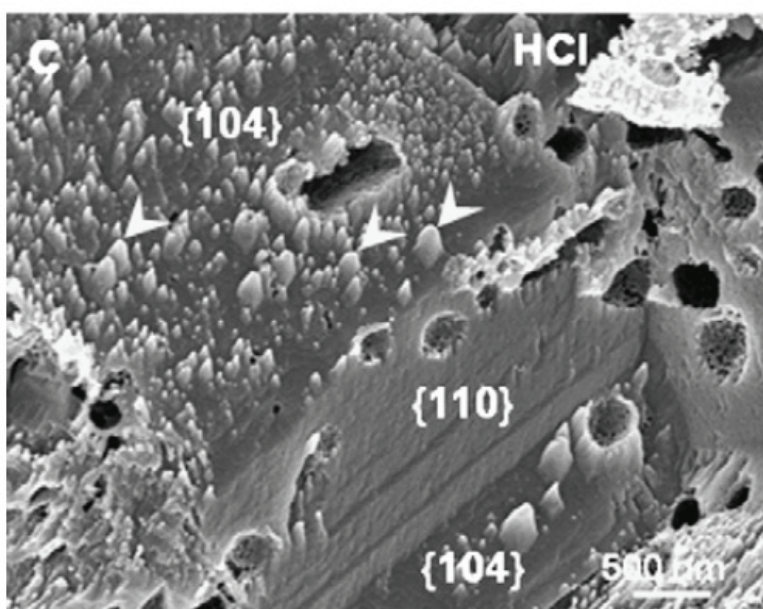
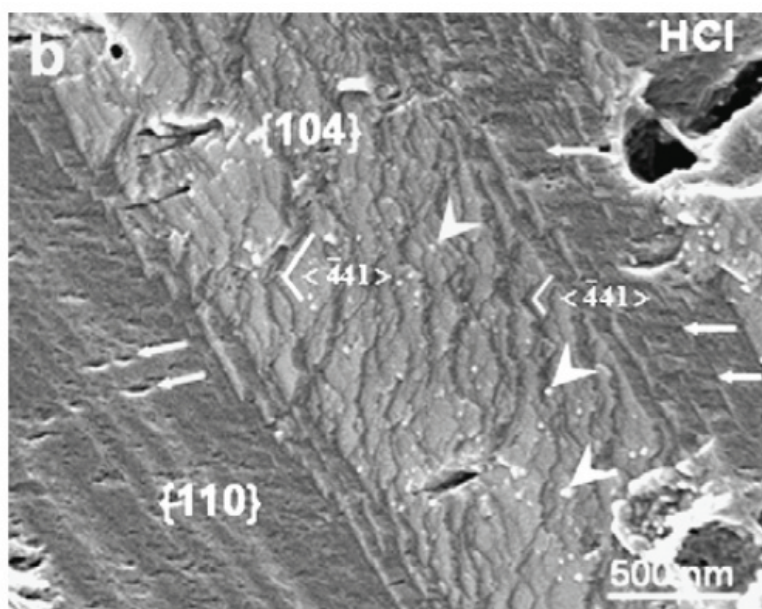
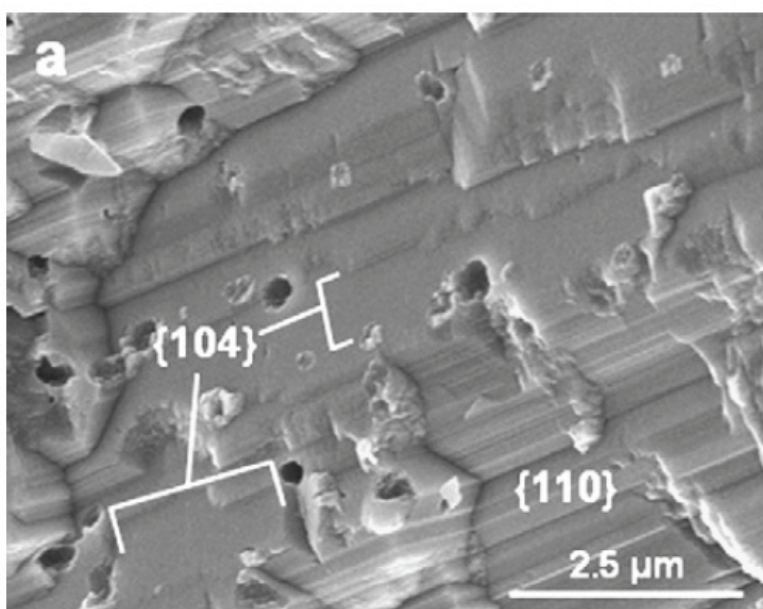


Figure 7. SEM imaging of typical calcite crystallographic cleavage faces from cross-fractured eggshell in the palisades region, and immunolocalization of OPN. (a) The $\{104\}$ and $\{110\}$ crystallographic faces (as indicated) exhibit smooth or stepped (single orientation) surfaces, respectively. (b) A characteristic surface microtopography typical for each crystallographic face is produced by light acid etching with hydrochloric acid (1 mM HCl for 1 minute in fixative) to remove surface mineral. The $\{104\}$ faces contained “zigzagging,” cascading etch steps frequently with straight edges parallel to the $\langle 41 \rangle$ direction (two of the step orientations are labeled with thin white lines just to the left of the denotation). Small, residual bumps / particles (arrowheads), possibly representing protein molecules, remain after acid etching on the narrow $\{104\}$ terraces between etch steps. The $\{110\}$ faces display arrays of parallel steps or multiple, short etch pits (arrows). (c) Acid etching for slightly longer times (1 hour) produces abundant and pronounced residual peaks (arrowheads) on the $\{104\}$ faces, whereas the $\{110\}$ faces still show generally the same topography as in (b). (d) After partial removal of organic matrix using sodium hypochlorite (14% NaOCl for 3 hours), the $\{104\}$ faces became highly pitted as would be expected from removal of protein (and/or proteoglycans or other matrix constituents), while the $\{110\}$ faces remained largely stepped as in native specimens without NaOCl treatment. (e) Secondary electron imaging (SEI) SEM and (f) backscattered electron imaging (BEI) SEM of fractured surfaces (freshly fractured and not etched) after colloidal-gold immunolabeling for OPN show abundant gold particles residing on the $\{104\}$ faces, with smaller amounts of labeling seen on the $\{110\}$ faces.

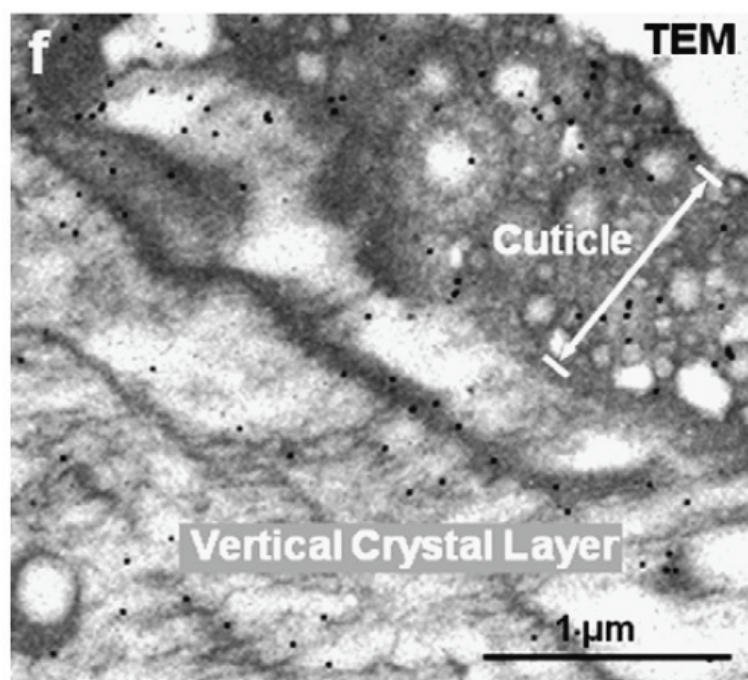
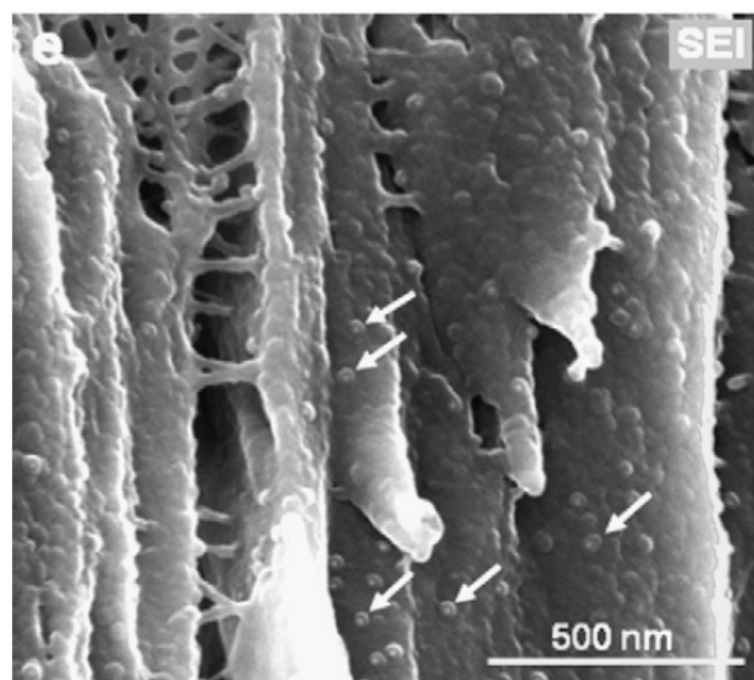
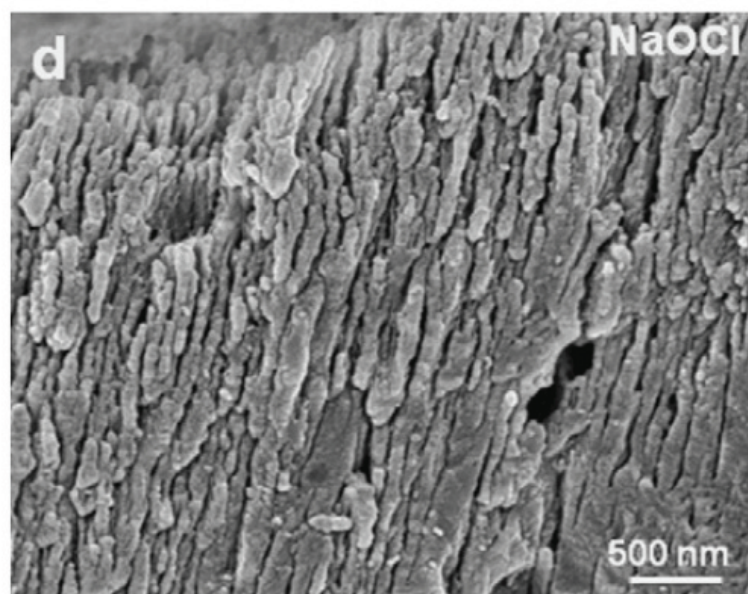
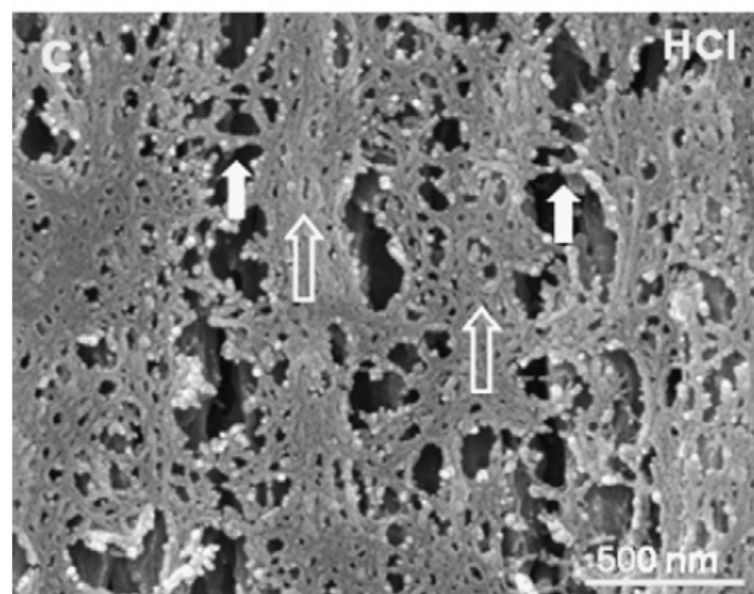
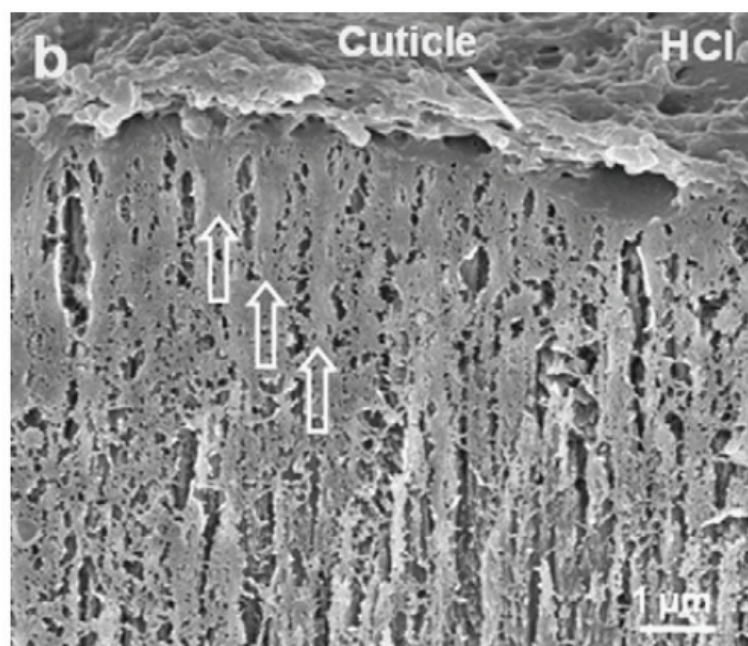
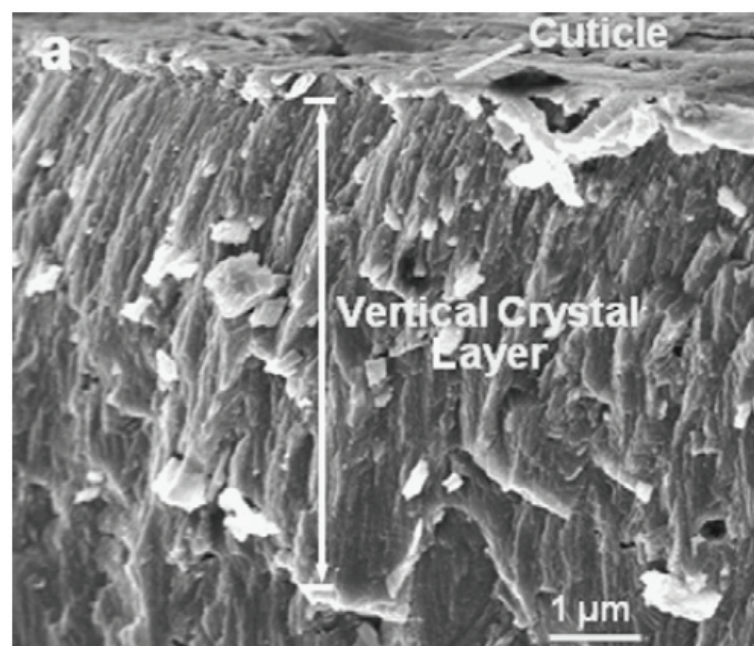


Figure 8. Ultrastructure of the vertical crystal layer and cuticle in eggshell, and immunolocalization of OPN. (a) Freshly fractured undecalcified, and (b,c) hydrochloric acid-etched (1 mM HCl for 1 minute) eggshell at the surface of the shell showing that the mineral and matrix organization change (from the palisades layer) to having a vertically oriented (perpendicular to the eggshell surface) texture (open arrows) in the so-called vertical crystal layer. Vertically oriented matrix and mineral are interconnected laterally by short matrix struts (solid arrows), as revealed by brief acid etching (c). (d) As shown by partial removal of organic matrix by sodium hypochlorite treatment (14% NaOCl for 3 hours), mineral components are likewise generally oriented vertically. (e) Secondary electron imaging (SEI) SEM (samples slightly etched with 1 mM HCl for 1 minutes before immunolabeling) shows OPN immunolocalization (gold particles indicated by arrows) associated with the matrix in this region. (f) TEM of thin sections after full decalcification and post-embedding colloidal-gold labeling for OPN shows moderate immunolabeling over the matrix of both the vertical crystal layer and the cuticle.

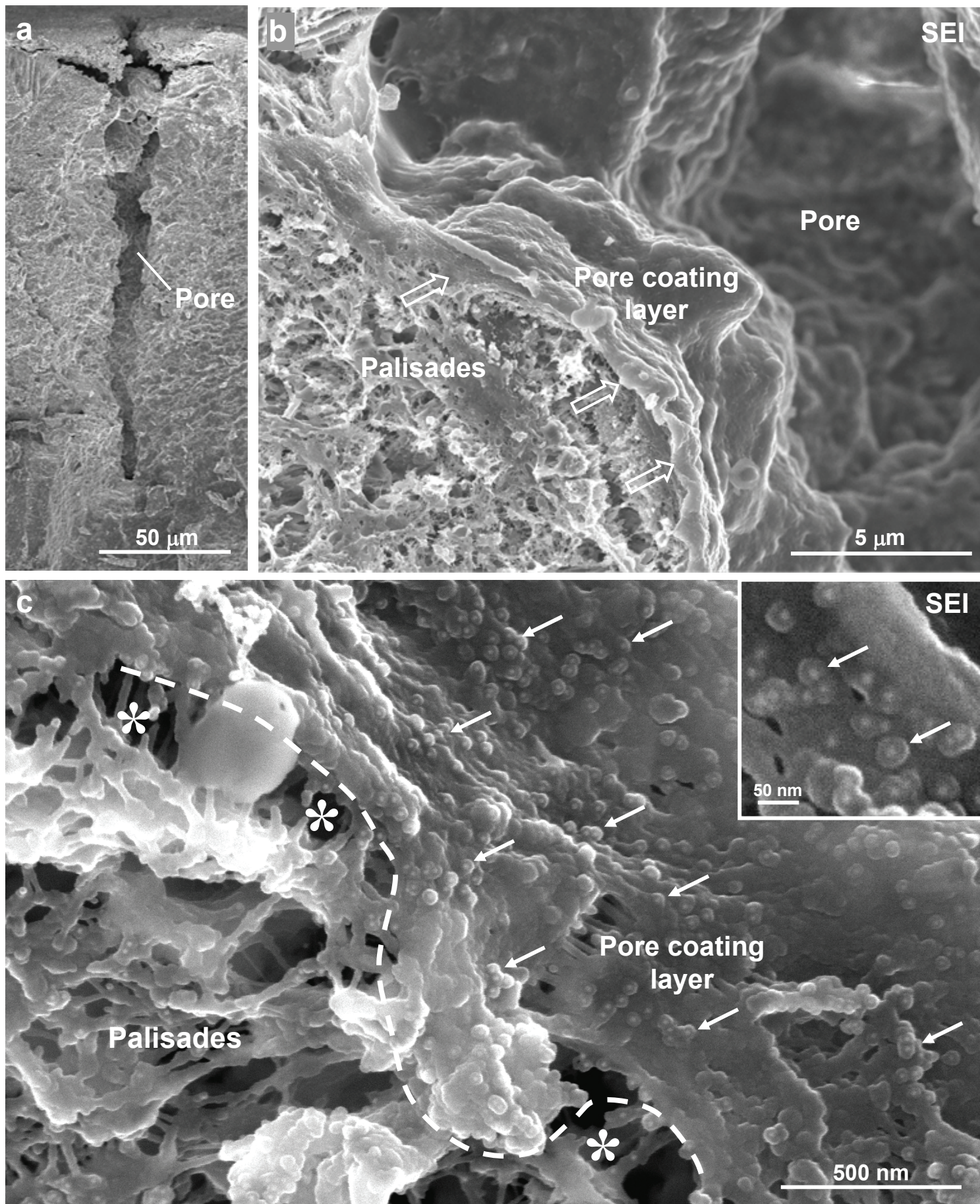


Figure 9. Ultrastructure by SEM secondary electron imaging (SEI) and OPN immunolocalization in the pore system of the eggshell. (a) Pores consists of a funnel-shaped orifice opening at the cuticle, and a single channel passing through the vertical crystal layer and the palisades to open between neighboring mammillae. (b) Pores are lined on their walls by a thin layer of protein (open arrows). (c) Higher magnification of the protein coating delimiting the pore space and defining the outermost boundary of a palisades column (dashed line) shows that it is connected by matrix struts (asterisks) to the underlying palisades matrix. After immunogold labeling for OPN, abundant gold particles (arrows) are associated with this pore-coating layer of protein. Panels b and c are from samples lightly etched with hydrochloric acid (1 mM HCl for 1 minute in fixative).

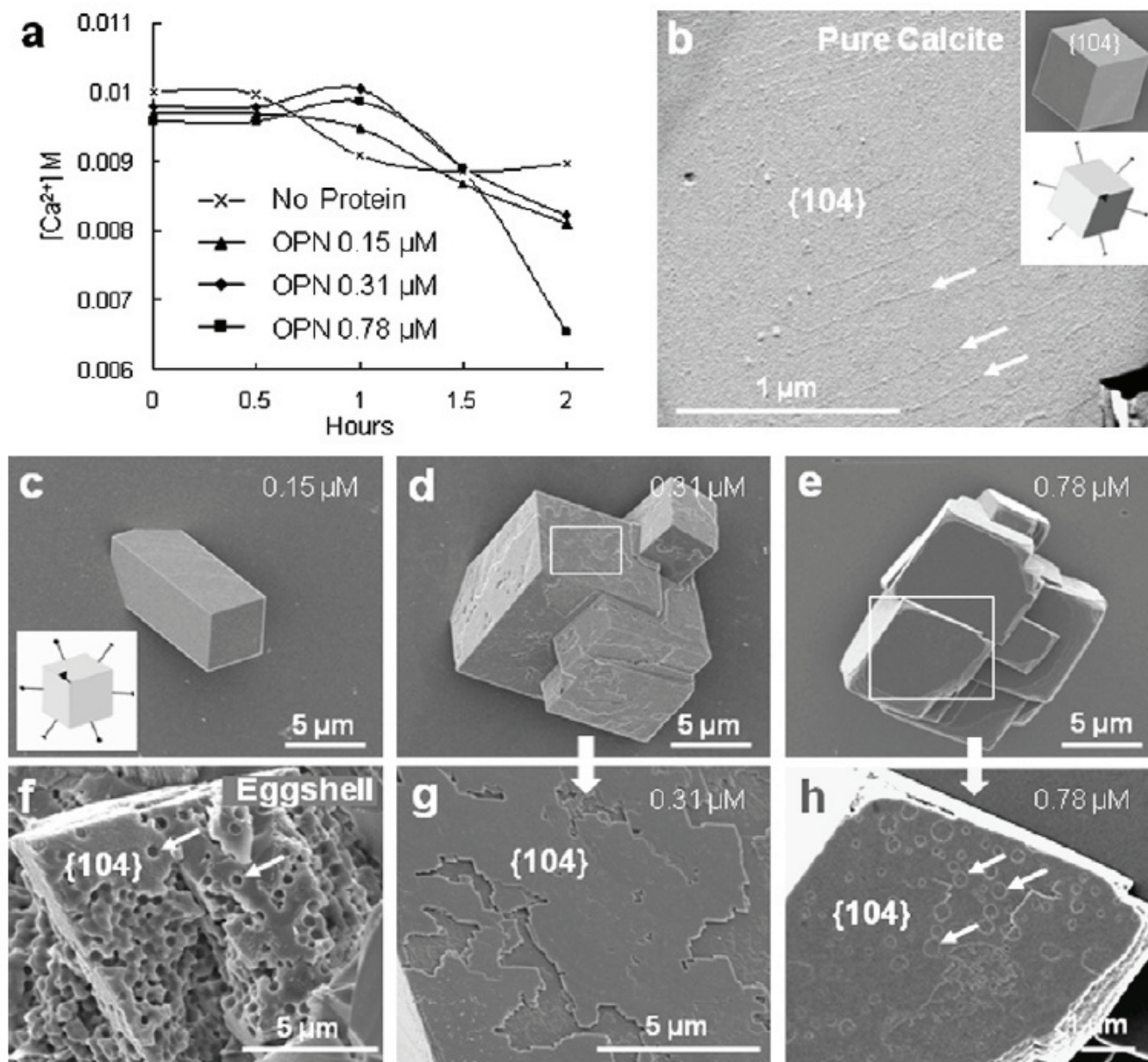


Figure 10. Effect of OPN on calcite growth *in vitro*. (a) With a fixed initial concentration, solution calcium $[Ca^{2+}]$ decreased when the nucleation and then growth of calcite occurred on a carboxylated self-assembling monolayer substrate. When compared to no added protein, the addition of OPN to the growth solution significantly delays crystal nucleation and growth by approximately 30 minutes. $[Ca^{2+}]$ decreases significantly only after 1 hour, and sizeable crystals form at about 1.5 hours of reaction time. (b) TEM of Pt-C replica, and SEM (inset), of pure calcite (grown without protein) consisting of $\{104\}$ rhombohedron (as inset), grows mainly by the propagation of step arrays (arrows). Schematic drawing of a calcite $\{104\}$ rhombohedron (inset) prepared by SHAPE computer software (SHAPE Windows V 6.0 Professional, Copyright 2002 by Eric Dowty). (c) 0.15 mM, (d) 0.31 mM, and (e) 0.78 mM addition of OPN. (c-e) With increasing addition of OPN in the growth solutions, calcite crystals grown for 1.5 hours retain the $\{104\}$ rhombohedron shape, but often form as aggregates (d,e). (f) Fractured eggshell in the palisades region for comparison with panel h. (g,h) Higher magnification SEM views of the boxed areas in panels d and e showing that the surface topography of the $\{104\}$ face loses its calcite symmetry with increasing OPN levels. At the higher concentration of OPN (0.78 mM), a circular growth step pattern (arrows, in panel h) is produced that is remarkably similar to the vesicular voids seen in the palisades region of fractured eggshell (arrows, in panel f).

Chapter 4

Manuscript 3

4.1 Preface

This report presents a brief review of avian eggshell ultrastructure in terms of mineral, organic matrix (and more specifically OPN) and matrix-mineral relationships.

Reproduced with permission from *Cells, Tissues, Organs* (2009), 189(1-4):38-43

Avian eggshell structure and osteopontin

Yung-Ching Chien¹, Maxwell T. Hincke², and Marc D. McKee^{1,3}

¹Faculty of Dentistry, McGill University, Montreal, QC, Canada, ²Department of Cellular and Molecular Medicine, University of Ottawa, ON, Canada, ³Department of Anatomy and Cell Biology, McGill University, Montreal, QC, Canada

4.2 Abstract

The avian eggshell primarily consists of calcium carbonate mineral (calcite) and matrix proteins. Here we review matrix-mineral relationships in the eggshell at the ultrastructural level using scanning and transmission electron microscopy, and describe the distribution of osteopontin (OPN) as determined by colloidal-gold immunolabeling for OPN. A rich protein network integrated within the calcitic structure of the eggshell shows variable, region-specific organization that included layered fibrous planar sheets of matrix, thin filamentous threads, thin film-like surface coatings, vesicular structures and isolated proteins residing on cleaved {104} crystallographic faces of the eggshell calcite. Except for the vesicular structures, these matrix structures all immunolabeled strongly for OPN. Given the potent mineralization-inhibiting function of OPN, we discuss how this protein might regulate eggshell growth rate, and inhibit calcification at specific compartmental boundaries to provide eggshell form.

Key Words: Osteopontin, avian eggshell, calcite, biomineralization.

Abbreviations: EDTA — ethylenediamine tetra-acetic acid; OPN — osteopontin

4.3 Introduction

The avian eggshell is composed mainly of inorganic calcite and an organic matrix (Romanoff and Romanoff, 1949). Its structure and composition serve in physical protection, prevention of desiccation and allowing for gaseous exchange for the growing embryo. Eggshell calcification is one of the fastest known mineralizing biosystems, with gram amounts of calcitic mineral being deposited within a matter of hours. The

structural organization of the eggshell is thought to be directed by organic molecules assembled as a matrix and interacting with calcite during the mineralization process (Burley and Vadehra, 1989; Lavelin et al., 2000). Amongst many organic matrix components of the eggshell, osteopontin (OPN) is a highly phosphorylated, acidic glycoprotein suggested to play an important role in regulating mineralization of the eggshell (Panheleux et al., 1999; Pines et al., 1995). Localization of OPN by microscopy in decalcified eggshell has been reported (Fernandez et al., 2003; Pines et al., 1995), and some details of the structure and mineral phase in the different eggshell compartments have been described by Dennis et al. (Dennis et al., 1996), but sites of OPN incorporation into the extracellular matrix at the ultrastructural level have not yet been determined. Knowledge of the distribution of OPN in these compartments is important given the potent effects of this protein on inhibiting and regulating crystal growth in a wide variety of mineralizing biological systems. Our objective here was to provide information on the distribution of OPN as it relates to extracellular matrix ultrastructure in the eggshell, and to determine whether OPN associates with any specific crystallographic faces of its calcitic mineral phase. Moreover, an improved understanding of how OPN and other matrix molecules interact with calcite will provide insight into how regulatory proteins interact with crystallographic faces to define crystal growth, and will allow insight into the fate and final function of these proteins once incorporated into fully formed eggshell.

4.4 Materials and methods

Eggshells from white leghorn chickens (*Gallus gallus*) were fractured at their equatorial region and air-dried, or were chemically fixed with aldehyde to preserve the structural organization of the organic matrix followed by partial or full decalcification with hydrochloric acid or EDTA. We used a combination of transmission electron microscopy (TEM), field-emission scanning electron microscopy (SEM), and colloidal-gold immunolabeling methods to investigate matrix-mineral relationships in the eggshell and to observe OPN localization at the ultrastructural level. Eggshell fragments where calcitic columns were intentionally fractured along different planes were observed by SEM and after incubation with rabbit anti-chicken OPN antibody (from Dr. L.C.

Gerstenfeld, Boston University, MA) followed by protein A-colloidal gold conjugate. Some samples were briefly etched with hydrochloric acid or sodium hypochlorite to observe structure after partial removal of mineral or matrix, respectively. For microtome sectioning of eggshells, aldehyde-fixed, decalcified eggshell samples were embedded in LR White resin.

4.5 Results and Discussion

Morphology and ultrastructural matrix-mineral relationships in avian eggshell

Eggshell structure first develops as a periodically spaced array of rounded, cone-shaped mammillae (or mammillary bodies) on the outer surface of the fibrous shell membrane, which then grow in length and width and extend outwards to form the palisade layer, ending with a thin transitional vertical crystal layer which is then finally covered with a cuticle (Fig. 1a). Sub-compartments exist within each of these regions, with the most noticeable being the calcium reserve body (with accompanying calcium reserve body base plate, calcium reserve body cover, and calcium reserve body crown) (Dennis et al., 1996; Dieckert et al., 1989; Terepka, 1963a; Terepka, 1963b; Wyburn et al., 1973) in the mammillae. Calcite is present as the major mineral phase in all regions except the cuticle, the latter also containing calcium-phosphate mineral (apatite) (Dennis et al., 1996). Following initial formation of the tips of the mammillary bodies on the shell membrane, eggshell is sequentially constructed via a precise spatio-temporal deposition of organic matrix and inorganic mineral (Fernandez et al., 1997; Fernandez et al., 2003).

Mammillae

After ovulation, the forming egg receives each of its layers as it traverses a specialized region of the oviduct. The shell membranes are deposited in the proximal (white) isthmus, followed by entry of the egg into the distal (red) isthmus where the initial early mammillary matrix molecules are synthesized by isthmal cells and deposited onto the membrane in a discrete, periodic array with a spacing of about 50-200 μm between mammillae (Figs. 1b,c) (Fernandez et al., 1997; Wyburn et al., 1973). The immature egg then enters the shell gland (uterus) where calcification commences within the tips of the mammillae (also called mammillary knobs) (Fernandez et al., 1997;

Wyburn et al., 1973). Calcified mammillae serve as the foundation for the elongated calcitic prisms (also called cones or columns) of the final eggshell (Fig. 1a), each of which shows a generally coherent X-ray diffraction pattern (Nys et al., 2004). The base plates of the mammillae are rich in organic matrix and are penetrated by membrane fibres of the outer shell membrane. It is generally thought that mineralization of the eggshell is initiated within the base plate (Dieckert et al., 1989; Schmidt, 1960; Terepka, 1963a; Terepka, 1963b; Wyburn et al., 1973). The calcium reserve body refers to an important region of the mammillae where microcrystals of calcite are spherulitically arranged and whose dissolution serve as a source of calcium to nourish the embryo (Nys et al., 2004) and to provide calcium for initial embryonic skeletal development (Fig. 1d) (Dennis et al., 1996; Dieckert et al., 1989; Schmidt, 1960). The calcium reserve body connects directly to the base plate and includes a calcium reserve body sac located at its centre. The calcium reserve body sac is a chamber-like structure (Dennis et al., 1996) that is demarcated at its periphery by a thin protein matrix sheet and encloses numerous granules interconnected by thin threads of protein (Chien et al., 2008). The calcium reserve body is capped by a cover that has a different matrix structure, and a highly mineralized crown that serves as the base for the columns of calcite in the palisades above. Each mammillae as a whole is enclosed by a thin organic film at its surface that presumably functions to limit mineralization from extending beyond these margins and prevents the merging of neighboring mammillae.

Palisades

The palisades region constitutes the thickest part of a mature eggshell, and is represented by the region where the calcitic columns become fully formed and abut extensively against one another, leaving only narrow pores that traverse the eggshell. A prominent feature observed within fractured calcite prisms in the palisades are numerous spherical voids, presumably filled with either gas or fluid, that measure between 200-500 μm (Fig. 2a). When examined in decalcified specimens, the voids are circumscribed by an organic halo (Fig. 2b). Also in this region, extended, layered and interconnected sheets of matrix run roughly parallel to the eggshell surface (Fig. 2b). These matrix sheets have a finer substructure consisting of thinner, more flocculent filaments radiating in different directions from this layered matrix organization. The generally parallel

arrays of matrix sheets and spherical structures was confirmed by brief acid-etching of the samples, which partly removes surface minerals and exposes the underlying structural arrangement of matrix underneath (Chien et al., 2008). It is not clear whether this matrix architecture represents occlusion of organic material within large calcite crystals, or rather reflects intervening layers of matrix alternating with a coherently oriented arrangement of multiple calcite crystals. When eggshells are fractured, calcite cleavage commonly occurs at the {104} crystallographic faces (Fig. 2a) (Berman et al., 1988). Characteristic surface microtopography can be accentuated on crystallographic faces by slight acid etching, which is useful for face identification, and on these cleaved faces we observed proteins, such as OPN, in isolated forms distinct from that seen as the layered matrix structures described above (Chien et al., 2008).

Association of OPN with eggshell ultrastructure

Mammillae and OPN.

OPN is synthesized by granular cells in the surface epithelium of the shell gland (uterus) (Fernandez et al., 2003; Pines et al., 1995). It is secreted into the uterine fluid along with other matrix proteins where it then accumulates within the mineralizing eggshell. Colloidal-gold immunolabeling of OPN in epithelial cells shows intense labeling for OPN in secretory granules (Fig. 2c). In the bulk of the mammillae, OPN accumulates to a moderate degree, whereas the prominent granules contained within the calcium reserve body sac do not contain OPN. At the surface of the mammillae, intense OPN immunolabeling is associated with a thin coating of protein which, given the inhibitory properties of OPN on calcite growth (Hincke and St Maurice, 2000), may serve to restrict further calcite growth at this boundary in order to delineate the final form of the mammillae. This accumulation of OPN at the boundary of the eggshell mammillae may be analogous to its mineralization-inhibiting function within the OPN-rich protein layer (laminae limitantes) seen at the surface of mineralized bone covered with quiescent bone-lining cells and surrounding osteocyte lacunae and associated canaliculi (McKee and Nanci, 1996).

Palisades and OPN.

In the palisades region of the eggshell, OPN is strongly associated with sheets of matrix generally parallel to the shell surface (Fig. 2d). The association of OPN with

parallel sheets of matrix, and more diffusely with the {104} crystallographic faces of eggshell calcite (Figs. 2e and f), may function in regulating palisade growth by orienting calcite crystals and by regulating the speed of mineralization. Inappropriately rapid mineralization in this biological context might otherwise result in crystal morphologies commonly seen in geological settings where crystal habits not regulated by organics appear as large, radiating and angular scalenohedrons also known as “dogtooth spar.”

The vesicular structures found in the palisades layer that are rich in protein and are dispersed along the matrix sheets lack OPN (Fig. 2d). While the biological function of these protein-circumscribed, non-mineralized voids in the calcite prisms is not well understood, we have observed that the eggshell-specific matrix proteins, ovocleidin-116 and ovocalyxin-32, are prominent components of the vesicle walls (Gautron et al., 2001; Hincke et al., 1999). Further investigation is required to determine their function / significance in the forming and mature eggshell.

4.6 Acknowledgements

The authors thank NSERC (Canada) for funding this work, Dr. Hojatollah Vali for his insightful discussions, and Line Mongeon for help with electron microscopy.

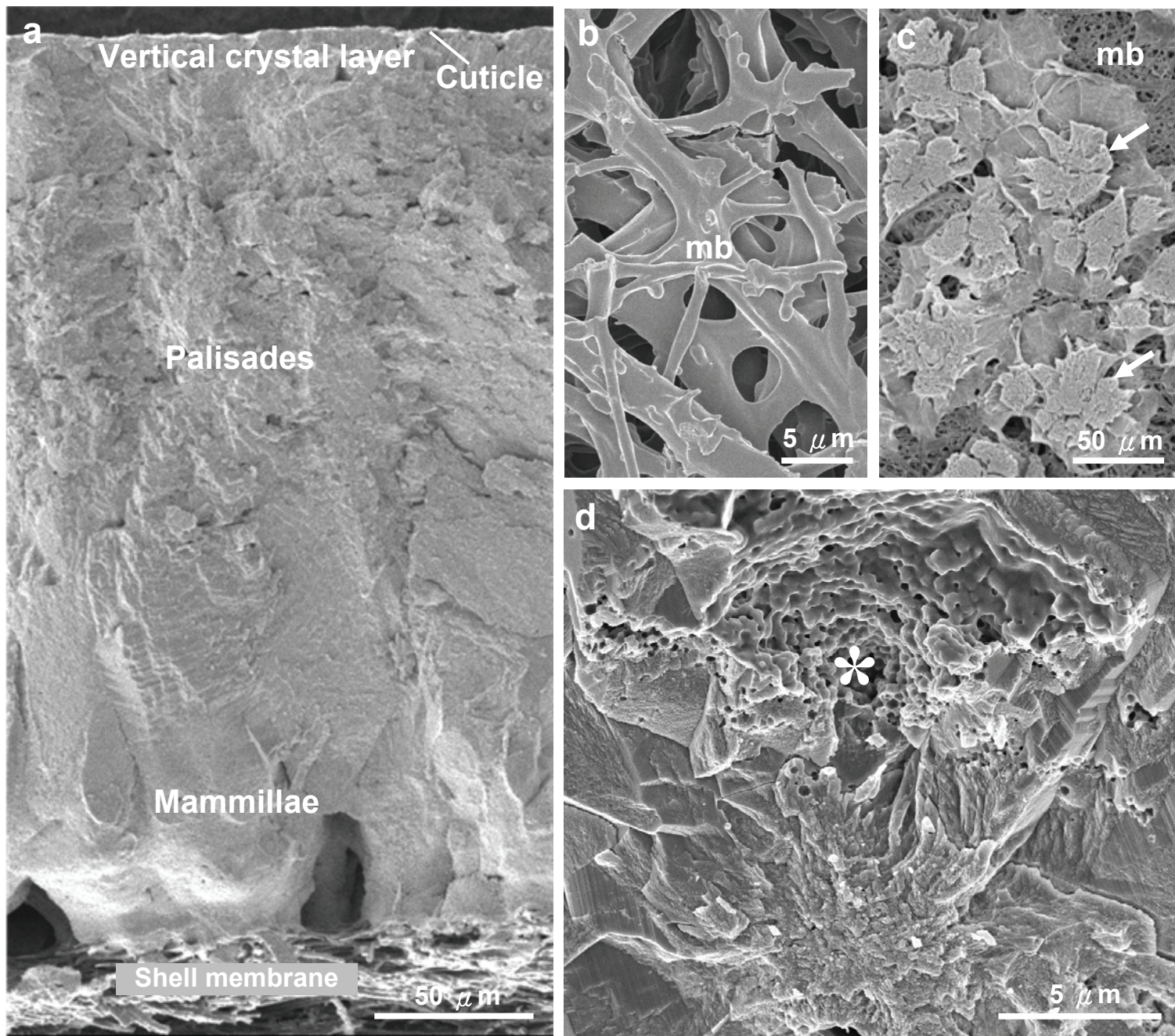


Fig. 1. Scanning electron micrographs of fractured avian eggshell and eggshell membranes. (a) Full-thickness view of cross-fractured eggshell attached to its shell membrane and with major structural compartments indicated. (b) En face view (eggshell/outer side) of the fibrous shell membrane (mb) after removal of the eggshell. (c) En face view of shell membrane (mb) with portions of mammillae (arrows) remaining attached after fracturing the eggshell parallel to the membrane surface and after a slight acid etching. (d) Cross-fractured eggshell at the level of the calcium reserve body (CRB) of a mammillae, in whose center normally resides the CRB sac and its constituent granules, whose space is indicated here by the asterisk. These structures have been lost in this sample during the fracture preparation, but this region was intentionally selected to show the outline of this compartment.

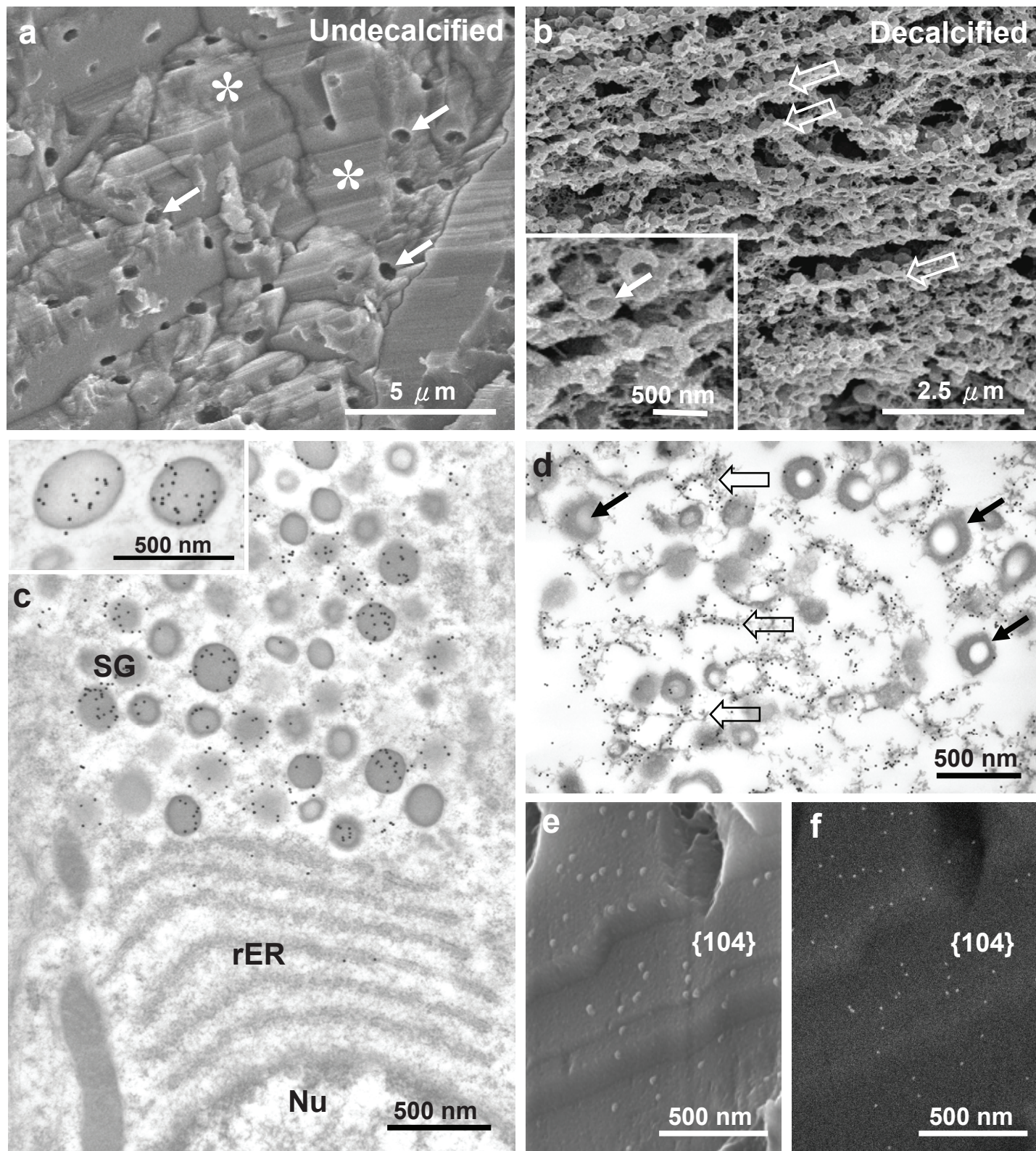


Fig. 2. Scanning and transmission electron micrographs of undecalcified and decalcified eggshell and epithelial cells of the shell gland. (a) Cross-fractured eggshell in the palisades region showing cleaved calcite faces (asterisks) and spherical voids (arrows). (b) Fully decalcified eggshell palisade layer showing arrayed sheets of matrix (open arrows) with many spherical vesicles (closed arrow, inset) aligned along and between these matrix sheets. (c) Non-ciliated granular epithelial cells of the shell gland after immunogold labeling for OPN followed by TEM showing abundant gold particles associated with secretory granules (SG). rER, rough endoplasmic reticulum; Nu, nucleus. (d) Immunogold labeling for OPN followed by TEM on decalcified palisades region showing gold-particle labeling associated with flocculent sheets of matrix (open arrows) whereas the palisades vesicles (closed arrows) are not labeled for OPN. (e, f) SEM image in secondary (e) and backscattered (f) electron imaging mode of fractured eggshell without decalcification showing gold particle complexes (small white spots) labeling OPN at the {104} crystallographic faces.

Chapter 5

Manuscript 4

5.1 Preface

As shown in the previous chapters, the avian eggshell is a highly structured and compartmentalized calcitic architecture constructed by sequential and orderly deposition of both matrix and mineral phases. Once built for the protection of the developing embryo from the exterior environment, dissolution of mineral from its inner surface (shell resorption) accounts for more than 80% of the calcium required by the avian embryo for skeletal mineralization. As a follow-up to the previous report where ultrastructural details of unincubated (unresorbed) eggshell were described (Chapter 3), this study presents a detailed systematic (over time) ultrastructural study of how the inner surface (mammillary layer) of the shell dissolves to release calcium. Major changes occur in the structure and mineralization status of the so-called calcium reserve body located centrally within individual mammillae comprising the mammillary layer. Significantly, the protein-rich organic matrix described previously in Chapter 3 – involved in the construction of the shell – slowly becomes exposed as part of the calcite/shell dissolution process and might then serve as a conduit that facilitates further resorption to provide calcium for the embryo and then to weaken the shell for chick hatching (pipping). These data are consistent with the notion that a possible dissolution mechanism for biominerals in general may involve an extensive and occluded organic matrix within the mineral phase that facilitates and guides dissolution patterns where loss of mineral occurs as part of a biologic process.

Reproduced with permission from *J. Struct. Biol.* (2009) as doi:

10.1016/j.jsb.2009.07.005

Ultrastructure of avian eggshell during resorption following egg fertilization

Yung-Ching Chien¹, Maxwell T. Hincke² and Marc D. McKee^{1,3}

¹ Faculty of Dentistry, McGill University, Montreal, QC, Canada, ² Department of Cellular and Molecular Medicine, Faculty of Medicine, University of Ottawa, ON, Canada, ³ Department of Anatomy and Cell Biology, Faculty of Medicine, McGill University, Montreal, QC, Canada

5.2 Abstract

For skeletal mineralization, the avian embryo mobilizes calcium from its calcitic eggshell. This occurs through dissolution of specific interior regions of the shell in a process that also weakens the shell to allow hatching. Here, we have examined eggshell ultrastructure during dissolution occurring between laying of a fertilized egg (with incubation) and hatching of the chick (*Gallus gallus*). We have focused on changes in shell mammillae where the majority of dissolution takes place. Using scanning electron microscopy, we describe differences in matrix-mineral structure and relationships not observed in unfertilized eggs (unresorbed eggshell). We document changes in the calcium reserve body – an essential sub-compartment of mammillae – consistent with it being an early, primary source of calcium essential for embryonic skeletal growth. Dissolution events occurring in the calcium reserve sac and in the base plate of the calcium reserve body, and similar changes in surrounding bulk mammillae structure, all correlate with advancing skeletal embryonic calcification. The changes in mammillae sub-structures can generally be

characterized as mineral dissolutions revealing fine surface topographies on remaining mineral surfaces and the exposure of an extensive, intracrystalline (occluded) organic matrix network. We propose that this mineral-occluded network regulates how shell mineral is dissolved by providing dissolution channels facilitating calcium release for the embryonic skeleton.

Keywords: Eggshell, eggshell resorption, calcite, calcification, chicken, ultrastructure

5.3 Introduction

The avian eggshell is a unique mineralized structure produced by birds to isolate and protect the developing embryo from the exterior environment. This hard, calcareous shell protects the growing embryo from physical trauma, invasion by microorganisms and dehydration, and it allows gaseous exchange while buffering against temperature fluctuations to maintain an appropriate growing temperature for the embryo. In addition to these functions, the eggshell provides, via its physiologic dissolution, a primary source of calcium for the developing embryonic skeleton of the chick (Burley and Vadehra, 1989; Arias, 1993) and a possible means to prevent respiratory acidosis in the embryo (Dawes and Simkiss, 1971), although the latter hypothesis remains unproven (Crooks and Simkiss, 1974; Gabrielli, 2004; Everaert et al., 2008).

During the second half of avian embryonic development (for the domestic chicken, starting at day 11 of egg incubation until hatching of the chick from the shell at day 21; (Hamburger and Hamilton, 1951), the avian embryo receives a large amount of calcium from extra-embryonic sources to fulfill the metabolic/anabolic needs of skeletal growth, neuromuscular activity and other physiologic functions. In fertilized eggs of the domestic chicken, the extra-embryonic sources of calcium come from the

yolk and the eggshell (Simkiss, 1961). More specifically, the eggshell is the major source of calcium and provides more than 80% of this key ion for the chick embryo (Johnston and Comar, 1955; Romanoff, 1960; Simkiss, 1967; Crooks and Simkiss, 1974). During embryonic development, calcium is successively mobilized first from the yolk at the earliest stages (from laying until the 11th day of incubation), and then from the eggshell for the remainder of the incubation period, as clearly demonstrated in a ^{45}Ca tracer study performed by Johnston and Comar (1955). Resorption of the eggshell to release calcium for the growing embryo is initiated at approximately day 11-12 of incubation, and continues until hatching at 21 days. While the majority of the shell calcium is used by the embryo to mineralize its skeleton, a significant amount is also transferred into phosphatidylcholine-rich platelets residing in the yolk sac (Moran, 2007). The storage of this latter calcium in the form of high-density, calcium-phosphate lipoprotein platelets is particularly important for newborn hatchlings to continue their skeletal development and mineralization uninterrupted after loss of chorioallantoic membrane attachment to the shell causing aborted access to shell calcium near the time of hatching (Cheville and Coignoul, 1984). As a final point, the net loss of mineral from the eggshell during the resorption process also weakens the shell for the pipping process allowing emergence of the chick from the shell.

During eggshell resorption, the calcitic mineral phase is dissolved by the acidic conditions generated by H^+ release occurring during the conversion of carbon dioxide (CO_2) to bicarbonate ion (HCO_3^-) via the actions of carbonic anhydrase (Narbaitz, 1974; Tuan and Zrike, 1978; Anderson et al., 1981; Tuan, 1984; Tuan and Ono, 1986; Tuan, 1987). Calcium is transported into the embryonic bloodstream by uni-directionally traversing the ectodermal cells of the chorioallantoic membrane (Terepka et al., 1976; Clark and Simkiss, 1980; Tuan, 1987). The chorioallantoic membrane is an extra-embryonic, placenta-like tissue important for developmental

functions, where it is particularly important for the transport of Ca^{2+} ions (Garrison and Terepka, 1972b; Garrison and Terepka, 1972a; Terepka et al., 1976). The region of the chorioallantoic membrane in contact with the eggshell contains two distinct cell types: villus-cavity cells specifically engaged in eggshell dissolution and calcium transport (Narbaitz et al., 1981; Narbaitz, 1987), and supporting capillary-covering cells which constitute most of the chorioallantoic membrane surface. As calcium transport activity increases, the villus-cavity cells specifically undergo morphologic changes and secrete enzymes involved in calcite dissolution and calcium transport (Narbaitz, 1977; Anderson et al., 1981; Narbaitz et al., 1981; Gabrielli, 2004). A number of proteins are expressed by villus-cavity cells of the chorioallantoic membrane concomitant with the onset of resorption activity – an apical vacuolar H^+ -ATPase which secretes protons towards the shell, carbonic anhydrase which partakes in the acidification process resulting in dissolution of the shell mineral, and a calcium-binding protein involved in the uptake and transportation of calcium (Tuan et al., 1978; Tuan and Zrike, 1978; Narbaitz et al., 1995).

Although a reasonable amount of information is available concerning the cellular and biochemical mechanisms underlying avian eggshell resorption, few systematic studies describing morphologic changes (especially ultrastructural changes) have been reported, and little is known of the evolution of matrix-mineral relationships during this process. In a recent study we detailed unincubated eggshell ultrastructure using a variety of sample preparation etching techniques and electron microscopy. In the present study, we use similar approaches to describe changes in eggshell structure during resorption following fertilization, incubation and embryonic growth. Particularly, we examine in detail a sub-compartment of eggshell mammillae, the calcium reserve body (CRB) sac, in terms of its role as a source of calcium for the growing chick. We also demonstrate delicate dissolution features on the bulk of the

mineral in mammillary bodies – likewise a rich calcium source – and describe an occluded and interlacing organic matrix network contained therein. These data support the suggestion that a possible dissolution mechanism for biominerals may involve an extensive and occluded organic matrix within the mineral phase that facilitates and guides dissolution patterns.

5.4 Materials and methods

Eggshells. Eggshells from fertilized, laid and incubator-warmed and turned eggs from domesticated White Leghorn chickens (*Gallus gallus*) were examined at different days after laying until hatching of the chicks at 21 days. Eggshells were fractured open from their obtuse ends, and carefully detached from the chorioallantoic membrane and the developing embryo. Eggshell fragments from each sample were rinsed briefly with physiologic saline and de-ionized water, and then they were immediately dried in air at room temperature. To assess the preserving effects of fixative on matrix structure for microscopy, some eggshell samples were fixed immediately after rinsing by overnight immersion in a 5% glutaraldehyde solution (in 0.1 M sodium cacodylate buffer, pH 7.3) with subsequent short-term storage in the same buffer alone prior to use. All shell fragments used in this study were taken from the equatorial region of the eggshell.

Eggshell acid etching. To compare fertilized and incubated eggshell dissolution after physiologic resorption with an experimental resorption of an unincubated shell by acid etching, both aldehyde-fixed and unfixed eggshell samples were exposed for 12-24 hours on their inner surface to 1 mM hydrochloric acid (HCl, pH 3; Fisher Scientific, Ottawa, Ontario); shell membranes were left in place during the dissolution. Eggshell samples were then briefly washed in distilled water and sequentially dehydrated in graded solutions of ethyl alcohol and hexamethyldisilazane

(Electron Microscopy Sciences, Hatfield, Pennsylvania), or dehydration was achieved using a critical-point dryer (model 29000, LADD Research Industries, Burlington, Vermont) prior to observation as described below.

Light microscopy. Undecalcified, air-dried eggshells at different stages of resorption were embedded after ethyl alcohol dehydration in LR White acrylic resin (London Resin Company, Berkshire, UK) as described previously (Chien et al., 2008; Hincke et al., 2008a), and then sections approximately 100 μm thick were cut perpendicular to the surface of the eggshell using a diamond saw rotating disc (model VC-50 Precision Diamond Saw, LECO, St. Joseph, Michigan). The sections were mechanically polished by hand using 2500A abrasive paper (ImperialTM WetordryTM 401Q, 3M, London, Ontario) to a thickness of approximately 10-20 μm suitable for light microscopy. Light micrographs were obtained using a Sony DXC-950 3-CCD camera (Sony, Tokyo, Japan) mounted onto an optical microscope (model Leitz DMRBE, Leica, Wetzlar, Germany).

Scanning electron microscopy (SEM) and energy-dispersive X-ray spectroscopy (EDS). For morphological imaging of fertilized, incubated and resorbed eggshell (either fixed with aldehyde solution or left unfixed), samples were mounted with conductive carbon cement onto metallic stubs prior to viewing by scanning electron microscopy (SEM). Eggshell samples were oriented to provide a transverse, cross-sectional view of the eggshell and its membranes. In cases where the eggshell and shell membrane were fortuitously detached during the rinsing and fracturing, these samples were used to provide both shell and membrane viewing in an *en face* orientation. Samples were then sputter-coated with a 20-25 nm thick Au-Pd thin film using a Hummer Sputter System (model VI, Anatech Ltd., Hayward, CA) and imaged using a field-emission gun scanning electron microscope operating at an accelerating voltage of 3-5 kV (model S-4700, Hitachi High Technologies America, Pleasanton,

CA) and using working distances of <12 mm. For energy-dispersive X-ray spectroscopy (EDS) analysis, samples were coated with a 10-15 nm-thick carbon layer and examined by SEM using the secondary electron imaging mode. The EDS analyses were performed using an Oxford INCA microanalysis system (model D-7200) with its installed software INCA Microanalysis Suite (Version 4.04).

5.5 Results

Prior to calcium release from a resorbing eggshell of a fertilized and incubated egg, the intact eggshell has a well-established structure with compartmentalized regions (Dennis et al., 1996; Chien et al., 2008; Chien et al., 2009), as illustrated here by light microscopy of ground sections and by SEM of cross-sections of freshly fractured shell as seen in unfertilized eggs (Fig. 1a and b). The calcified shell attaches to the shell membranes via conical-shaped mammillae (also called mammillary bodies) – with each consisting of an outer crown and inner base plate between which is found the calcium reserve body (CRB) with a CRB sac at its centre (Terepka, 1963b; Terepka, 1963a; Wyburn et al., 1973; Dieckert et al., 1989; Dennis et al., 1996; Chien et al., 2008; Chien et al., 2009). As the resorption of calcium from the eggshell has been reported to be most extensive at its equatorial region, with less resorption towards the acute end and almost no resorption at the obtuse end (Dokocil et al., 1985), incubated eggs were fractured open from the obtuse end to preserve the equatorial region where the resorption of calcium is known to be most pronounced; these resorbing regions of the shell also match areas of chorioallantoic membrane apposition to the innermost surface of the eggshell membranes. Eggshells became perceptibly fragile starting at day 15 of incubation, especially at the equatorial regions, where the tips of the base plates of the mammillary bodies had noticeably disintegrated/resorbed such that the shell membranes began to detach

from the remaining eggshell (Fig. 1c and d). This innermost shell resorption was clearly responsible for releasing shell membrane fibres embedded in the tips of the mammillae. At day 20-21, when the fetal chick was fully grown and ready to hatch, the shell membrane had completely detached from the shell (Fig. 1e and f), being drawn inwards with displacement of the chorioallantoic membrane caused by shrinkage of the membrane and/or by movements of the chick.

Calcium reserve body (CRB) sac granules and associated fibrous matrix

Since the CRB is considered to be a crucial structural unit serving as an early source of calcium required for skeletal growth in the chick embryo (Schmidt, 1960; Dieckert et al., 1989; Dennis et al., 1996), we carefully investigated CRB structure in eggshell samples at different days of incubation of fertilized eggs. The CRB structural contents, predominantly consisting of spherical granules interconnected by thin matrix fibres (Chien et al., 2008), have been proposed to contain calcite microcrystals (Nys et al., 2004), but this has yet to be shown, and the possibility that they include amorphous calcium carbonate cannot be excluded. From our study, SEM viewing of cross-sections of fractured shell from 12-day incubated eggs showed well-developed CRB sacs containing abundant and loosely packed granules, and an interconnecting fibrous network of matrix, all distinctively different from the surrounding mammillary body structure (Fig. 2a-d). As observed at higher magnification, spherulitic granules within the CRB sac commonly had a nano-granular texture at their surface (Fig. 2b and c). The size of these granules in undecalcified specimens, roughly 250-300 μm in diameter, is similar to that reported in the literature (Dennis et al., 1996; Chien et al., 2008), and is also the size observed in fully decalcified (with HCl) samples (inset of Fig. 2b), thus indicating that the organic matrix of these granules is abundant and pervasive throughout the granules. When partially resorbed physiologically (Fig. 2, excluding inset), the grainy-surfaced

granules appeared to be coated or filled with nanometre-sized minerals (Fig. 2b and c). The granules and thickened fibrous matrix varied in abundance and density from region to region within a single CRB sac, possibly because at this early time of resorption there was only partial or uneven dissolution of mineral. Some regions showed thickened interconnecting fibrous matrices between granules (Fig. 2c), and occasionally some rhombic crystallites were observed resembling typical calcite rhombohedra (Fig. 2d).

To examine more closely the calcification status of the CRB sac structures, we performed energy dispersive x-ray microanalysis (EDS) on both the granules and the fibrous matrix in fertilized resorbing eggshells, and compared this to analyses from experimentally acid-etched unfertilized eggshells. EDS on day 13-incubated eggshell CRB revealed abundant calcium and a small amount of sulfur within both the granules (Fig. 3a) and the fibres (data not shown) (the oxygen peaks are from the carbonate content of the mineral, and the carbon peaks arise from the carbon coating applied during specimen preparation). While mineral phase identification is not possible by EDS, our acid-etching approach to decalcify the samples was used to verify the calcium content; calcium was not detected after HCl acid treatment, although the sulfur peak was still discernible (Fig. 3b). Sulfur was not detected in the regions of the mammillary body immediately surrounding the CRB sac (Fig. 3c). While our acid-etching treatment removed entirely the calcium from the CRB sac structures, EDS of these same structures from physiologically resorbing shell of fertilized eggs up to about 16 days of incubation showed a calcium peak (data not shown), after which they were lost as part of the resorption process.

Changes in the structure of eggshell mammillary bodies induced by calcium resorption

In an intact eggshell, either without fertilization of the egg or immediately after

laying of a fertilized egg, the CRB sac is distinctly bounded by a continuous, membrane-like protein film directly apposed to the surrounding calcitic mineral of the encasing mammillary body. Fractures through this site viewed by SEM show cleaved calcite mineral with smooth and clean fracture faces (Fig. 4a; Chien et al., 2008). At the initial stages of eggshell resorption associated with embryonic growth (*i.e.* on day 12 of incubation), these same interfacial areas just adjacent to the CRB sac (particularly the base plate region) showed noticeable signs of dissolution. This caused shrinking, detachment and perforation of the delimiting membranous protein film circumscribing the CRB sac as it lost its subjacent mineral support (Fig. 4b); from this, tiny struts of matrix fibres connecting the residual CRB sac membrane to the mammillary matrix were exposed (Fig. 4c and d). Mineral in the base plate directly adjacent to the disintegrating CRB sac membrane was partially dissolved and appeared as nano-granular crystallites interwoven with an exposed matrix network (Fig. 4d). Mineral at other sites surrounding the CRB sac showed substantially less dissolution than the base plate at this stage of egg incubation.

Throughout mammillary bodies and the palisades layer of intact eggshells, vesicular/void structures typically ranging in diameter from 200-300 nm are widely dispersed within the solid calcite crystals, and they are lined by protein (Fig. 4e; (Chien et al., 2008). During day 11-12 of fertilized egg incubation (*i.e.* early chick skeletal mineralization; (Bellairs and Osmond, 2005), the calcitic mineral dissolved peripherally around these vesicular structures exposing the circumscribing protein, which then collapsed centrally (without supporting mineral) but maintained fine matrix struts connecting it with underlying connecting matrix fibres surrounding the voids (Fig. 4f).

Early in the eggshell resorption process there was a subtle and orderly dissolution of mineral throughout the densely mineralized regions constituting the

bulk of the mammillary bodies. Unresorbed mammillary bodies after fracture typically show stepped (single orientation fracture steps) (inset in Fig. 5a), smooth cleavage or conchoidal surfaces. However, on day 12 of incubation with resorption, these previously highly mineralized regions were furrowed and pitted, and the fractured surfaces appeared to be tiled by crystallites or dissolution islands with many straight edges roughly parallel to the $\langle\bar{4}41\rangle$ step orientations of calcite – something typical for pure calcite – but modified here (presumably as a result of occluded protein) with irregular pits and grooves (Fig. 5a and b). At higher magnification on the terraces of dissolution islands, fibrous matrices previously embedded/occluded within the mineral were either exposed and slightly raised above the surrounding flat mineral surfaces (Fig. 5b), or were removed by the fracturing and remained as small channels (Fig. 5b). With progression of dissolution/resorption at this and slightly later times of incubation, layer by layer of mineral was removed to expose an extensive interconnected matrix network previously occluded within the mineral phase (Fig. 5c). Disintegration of once-solid calcite mineral into clusters of nano-granular crystallite-containing faces revealed an underlying permeating network of organic matrix (Fig. 5d), which in turn could accelerate dissolution by providing porous channels and increasing the surface area of mineral exposed for dissolution. This implies that protein-rich regions may resorb preferentially, leaving behind "residual" crystallites lingering "interstitially" within the organic matrix (Fig. 5e). The intricate network of organic matrix remains well-exposed and appears insoluble (Fig. 5f).

From days 12-15 of incubation, the eggshell becomes the principal supply of calcium for the chick embryo and the intake of calcium from the shell escalates to provide for the extensive mineralization needs of widespread intramembranous and endochondral ossification (Bellairs and Osmond, 2005). After day 15 of incubation,

when the base plate of the eggshell becomes frail and readily detaches from the shell membranes, the CRB structures were frequently disintegrated as well. Figure 6 shows *en face* (Fig. 6a) and cross-sectional views (Figs. 6b and c) of mammillary bodies of eggshells after incubation for 16 days. At this stage, where significant dissolution has occurred, most of the CRB contents were lost; either these delicate structures were dislodged during fracturing/detachment of the shell membrane during sample preparation, or they were removed by resorption, leaving behind essentially empty CRB sacs appearing as central hollow cavities. On occasion, a complete CRB sac appeared undisturbed with its modified contents preserved (Fig. 6c-e); the contents being a relatively loosely packed, flocculent fibrous matrix (Fig. 6d and e) and a few remaining granules (Fig. 6e).

From day 17 of egg incubation until the chick hatches on day 21, the high demand for calcium release persists while the skeleton continues to develop (Bellairs and Osmond, 2005). During this time, from day 17 onwards, entire mammillary bodies showed morphologic features consistent with extensive dissolution and removal of the inner part of the shell (Fig. 7a-c) with the shell membrane being barely attached or completely separated from the eggshell at the time of sample harvesting. The CRB structures were not present in all these late-stage samples, occasionally leaving behind empty dissolved centres within each partial mammillae (Fig. 7d). The remaining portions of the upper mammillary bodies showed heavy uni-directional etching/resorption leaving behind a jagged mineral profile (Fig. 7e). At all times of egg incubation, no apparent changes were observed in the palisades or other regions of the shell.

5.6 Discussion

The chick embryo relies solely on yolk calcium for development from around day 7-10 of egg incubation (Johnston and Comar, 1955). To provide for future calcium requirements, the chorioallantoic membrane first makes contact with the shell membranes on about day 9-10 of incubation (Simkiss, 1967), but the cells in this membrane responsible for enzyme expression are not fully differentiated until day 12-14 (Coleman and Terepka, 1972; Narbaitz, 1977; Narbaitz et al., 1981; Gabrielli, 2004). The total calcium of the embryo and the yolk starts to rise thanks to the influx of calcium from eggshell into the incubated egg on the 12th day of incubation (Crooks and Simkiss, 1974; Packard and Packard, 1984; Moran, 2007). Our observations describing ultrastructural changes in the eggshell, which are coordinated by the chorioallantoic membrane, match well with these metabolic changes of calcium in the egg and chick embryo (Johnston and Comar, 1955; Crooks and Simkiss, 1974; Packard and Packard, 1984; Moran, 2007) generally correlating with the skeletal growth of the chick (Bellairs and Osmond, 2005).

Despite many excellent studies describing avian eggshell resorption (Sajner, 1955; Tyler, 1958; Tyler and Simkiss, 1959; Terepka, 1963b; Terepka, 1963a; Schmidt, 1965; Bellairs and Boyde, 1969; Erben, 1970; Simons, 1971; Bond et al., 1988; Dennis et al., 1996), little has been done in terms of a systematic analysis of changes in shell ultrastructure over time (*i.e.* after different days of incubation spanning the resorption period). In the present study, we build on our previous report describing ultrastructural details of unincubated eggshell ultrastructure and composition (Chien et al., 2008; Chien et al., 2009) by here using SEM and other methods to visualize loss of mineral, and to characterize matrix-mineral ultrastructural relationships, as they progress over time during the resorption (thinning and weakening) of the eggshell that occurs in the mammillae of fertilized,

incubated eggs. In particular, we have analyzed changes in the components of a structural sub-compartment of the mammillae – the CRB sac (described in detail in Dennis et al., 1996; Chien et al., 2008) – long thought to be an important calcium source for the growing embryo. Significantly, we have verified for the first time that the granules and fibrous matrix in the CRB sac are indeed calcified – not with well-crystallized euhedral calcite crystals – but with aggregations of nano-crystallites. The CRB contents are subsequently physiologically depleted of calcium and ultimately lost during the period of days 11-16 of egg incubation, and thus this location is not likely (as is conventionally considered) to be the major source of calcium for embryonic skeletal growth. For this, our observations of mammillary body dissolution from day 11 onwards points to the mammillae as being the major source of calcium for skeletal growth, especially starting at day 16 when the CRB calcium has been depleted. Finally, we make the key observation that a rich proteinaceous network is exposed in the mammillary bodies during resorption/dissolution of shell calcite; this organic network important initially for shell construction (Chien et al., 2008) might then serve as a conduit increasing internal surface area and acid diffusion – in turn affecting surfaces energies and dissolution kinetics – to facilitate resorption to provide calcium for the embryo and to thin the shell for chick hatching (pipping). This unique matrix-facilitated dissolution of biomineral composites may be widespread across different phyla and conserved in evolutionary history, and for the first time here is being proposed for avian eggshell.

Calcification of CRB granules and associated fibrous matrix

The CRB sac is a unique compartmental sub-unit within each mammillae that has drawn considerable attention for its potential role as a source of calcium for the growing chick embryo (Dieckert et al., 1989; Dennis et al., 1996; Chien et al., 2008;

Chien et al., 2009). Its chamber-like structure is bounded by a delimiting, membrane-like thin film, and centrally it contains abundant small granules interconnected by filamentous fibres (Dennis et al., 1996; Chien et al., 2008). The distinctive contents of the CRB are believed to be composed of proteins and mineral, although this is only recently beginning to be elucidated, and thus their detailed characterization was part of the present study. Osteopontin – a noncollagenous, acidic phosphoprotein intimately associated with biominerals in many tissues (Sodek et al., 2000) – is present throughout eggshell matrix (Pines et al., 1995) with an additional specific localization to the thin filamentous fibres in the CRB sac (Chien et al., 2008). It has been described that the CRB matrices are associated with spherulitically arranged calcite microcrystals (Nys et al., 2004), which may have greater solubility as compared to pure inorganic rhombohedral calcite, but no data for this was provided. Wyburn et al. (1973) reported that a fully developed CRB could only be observed at the middle stage of eggshell formation when mammillary body formation was essentially completed and the palisades layer was beginning its construction.

In the present study, we definitively show that the granules and associated thin fibrous threads in the CRB sac are mineralized (presumably as amorphous calcium carbonate or calcite nano-crystals), as clearly indicated by comparative morphological observations and by microanalytical (EDS) analyses of loss of calcium from fertilized eggs incubated for different times – experimental decalcification with hydrochloric acid confirmed the calcium loss. The fact that these granules and interconnecting fibres showed variable degrees of calcification, with the mineral phase ranging from nano-granular mineral to rhombic crystallites, may reflect the transformation of an amorphous calcium carbonate (ACC) precursor (Addadi et al., 2003) into variably crystalline calcite – all in close association with an

organic “matrix” phase. ACC phases are widespread among plant and animal tissues (Simkiss, 1994; Weiner et al., 2003), and they have recently garnered significant attention as an important precursor phase apparently central to many biomineralization mechanisms (e.g., Addadi et al., 2003; Gago-Duport et al., 2008; Nebel et al., 2008; Neira-Carrillo et al., 2008; Pipich et al., 2008; Politi et al., 2008; Pouget et al., 2009). Biogenic ACC may be permanently stabilized by organic substances for structural strengthening purposes, or may transform into crystalline forms with time (Aizenberg et al., 1996; Aizenberg et al., 2002; Addadi et al., 2003; Aizenberg et al., 2003; Sethmann et al., 2005). In this context, it is possible that the calcification of the granules and associated fibres in the CRB sac initially began as ACC stabilized by mineral-regulating proteins such as the osteopontin found there (Chien et al., 2008), and that subsequently all (or a portion of) the ACC gradually transformed into fine crystals of calcite. As such, this form of a calcified composite in the CRB sacs, relatively unstable and soluble if exposed to enzyme and/or acid, would be a rapidly mobilizable source of calcium for the chick embryo, particularly for early stages of extensive skeletal growth. However, although difficult to detect experimentally, current experimental data do not support the existence of ACC in avian eggshells. Mineral textural analyses of avian eggshell using X-ray analysis and polarized light show no evidence that ACC is present in completed, laid calcitic eggshell (Rodriguez-Navarro et al., 2007). More recently, this same group found no ACC phase in crystal growth studies in vitro (Hernandez-Hernandez et al., 2008), although others growing calcium carbonate in vitro observed its transient presence when quail eggshell proteins were present (Lakshminarayanan et al., 2006). Despite this for avian eggshell, in the case of calcium carbonate sea urchin spine and larval skeleton, for example, higher resolution studies show that the “single crystal” biominerals are actually a mosaic of domains delimited by distinct or occluded organic proteinaceous

layers (Berman et al., 1988; Berman et al., 1990) and contain transient ACC (Wilt, 1999; Wilt, 2002). Further investigation with high resolution methods is required to establish whether ACC is present in avian eggshell, and if so, whether it occurs only at a specific stage of eggshell formation (or resorption).

Ultrastructure of resorbed eggshell mammillae

While likely important as a source of calcium for the embryo during early stages of shell resorption, we show here that the physiologic decalcification and ultimate loss of the CRB sac contents occurring by day 16 of egg incubation. This leaves behind empty CRB sacs as centrally located hollows within the mammillae, and precludes their functioning similarly at later stages of embryonic growth. The timing of the appearance of these empty CRB sacs in our study corresponds well with observations in previous studies describing that naturally detached shell membrane was associated with a distinctive "hole" region in the centre of each eroded mammillae that was surrounded by some remaining calcite minerals (Tyler and Simkiss, 1959; Terepka, 1963b; Terepka, 1963a). Without knowledge of the existence of the CRB, this non-uniform dissolution of the mammillary bodies was taken to represent a preferential central dissolution during resorption of an otherwise generally homogeneous mammillary body (e.g., (Bond et al., 1988).

Dieckert et al. (1989) first suggested that the calcium resorbed from the eggshell for embryonic skeletal development derives mostly from the mineral of the CRB and the underlying base plate of the mammillary body. Our data are consistent with this, where we show ultrastructural details of extensive resorption in these specific structures/regions. Additionally, and not reported previously, we document subtle dissolution features appearing in the mineral phase throughout the mammillary bodies, particularly surrounding the CRB and in the base plates at the early resorption stage. Our previous work has characterized in detail the extensive

protein matrix of eggshells (Chien et al., 2008), and our data here show that widespread calcite dissolution during physiologic shell resorption was influenced extensively by this mineral-occluded matrix – whether this was present peripherally at structural interfaces, or was “guided” internally by the matrix.

In fully decalcified eggshell (experimentally decalcified, using acid or calcium chelation), mammillary bodies appear as the shell region with the highest density of matrix (Dieckert et al., 1989; Dennis et al., 1996; Chien et al., 2008). This protein-rich calcified region, located on the inner side of the shell where the vast majority of the mineral dissolution (resorption) takes place, is consistent with the view that protein-loaded mineral of the mammillae may be more susceptible to dissolution than the palisades region which contains less protein. Such regions, varying in structure and in protein-to-mineral ratios, might reflect a “graded structure” where gradual changes in the matrix and mineral interphases, or sudden changes at interfaces, would variably alter the physicochemical and functional properties of the composite material at those sites (Weiner et al., 2006).

Mineral-occluded macromolecules/matrices have been known to produce and accelerate unusual internal etching/dissolution of biominerals (references and examples below), as opposed to organic-crystal surface interactions inhibiting dissolution exclusively at mineral surfaces (Weiner and Dove, 2003). For teeth, it is recognized that the enamel of deciduous teeth is more susceptible to acid attack, and more frequently show caries, than that of permanent teeth (Hunter et al., 2000; Angker et al., 2004) – attributable to their higher organic content (Mortimer, 1970; Müller and Schmitz-Feuerhake, 1996), and this has recently been confirmed *in vitro* (Wang et al., 2006). In a calcite system, (Estroff et al., 2004) reported on the growth and dissolution of calcite crystals grown in an organic hydrogel rich in carboxylate groups; gel aggregates nonspecifically intercalated into the crystals

during growth, and dissolution was accelerated with irregular etched crevasses (compared to pure, nonorganic-containing calcite crystals) when exposed to various etchants. In addition, intracrystalline proteins have been shown to be situated within the structure of biominerals such that distortion of the crystal lattice occurs (Pokroy et al., 2006) which also modulates their thermodynamic properties (De Yoreo and Vekilov, 2003) – rendering them more unstable and soluble. In particular examples most closely related to our work here, Ryall and colleagues (Fleming et al., 2003) have shown that the inclusion of urinary proteins into calcium oxalate crystals (as commonly seen in kidney stones) increase lattice strains and reduce crystallite size because of intracrystalline defects and discontinuities, all of which increase solubility of the crystals. Moreover, proteolytic degradation of the occluded proteins created channels within the crystals facilitating the dissolution of the mineral phase (Ryall et al., 2001; Ryall et al., 2005; Ryall et al., 2007; Grover et al., 2008).

Indeed, we hypothesize that such an occluded protein network within the avian eggshell – as we have demonstrated previously (Chien et al., 2008) and here – may exactly serve such a purpose; namely, to facilitate calcium release required to satisfy the dynamic skeletal growth needs of the embryo. Moreover, shell dissolution may solubilize anti-microbial eggshell matrix proteins to upregulate antimicrobial protection as the eggshell becomes progressively weaker to facilitate hatching as we have previously proposed (Hincke et al., 2008b). Our view is that eggshell resorption is modulated and guided by an intracrystalline matrix network in the eggshell of the domestic chicken, and this may likewise function universally in other avian species, in some reptilian eggs (Erben, 1970; Packard and Packard, 1980; Packard et al., 1984), and possibly even previously in dinosaur eggs (*e.g.*, from theropod dinosaurs) whose eggshells contain internal knob-like elements (Zelenitsky

et al., 1996; Zelenitsky et al., 2002) similar to the mammillary structure of the chicken eggshell.

5.7 Acknowledgements

This work was funded by a grant from the Natural Sciences and Engineering Research Council of Canada (to MTH and MDM), and by a studentship to YCC from a Strategic Training Initiative in Health Research program funded by the Canadian Institutes of Health Research. The authors also thank Line Mongeon and Lydia Malynowsky for their skillful technical assistance with some of the microscopy work. MDM is a member of the Jamson T.N. Wong Laboratories for Calcified Tissue Research and the Centre for Bone and Periodontal Research.

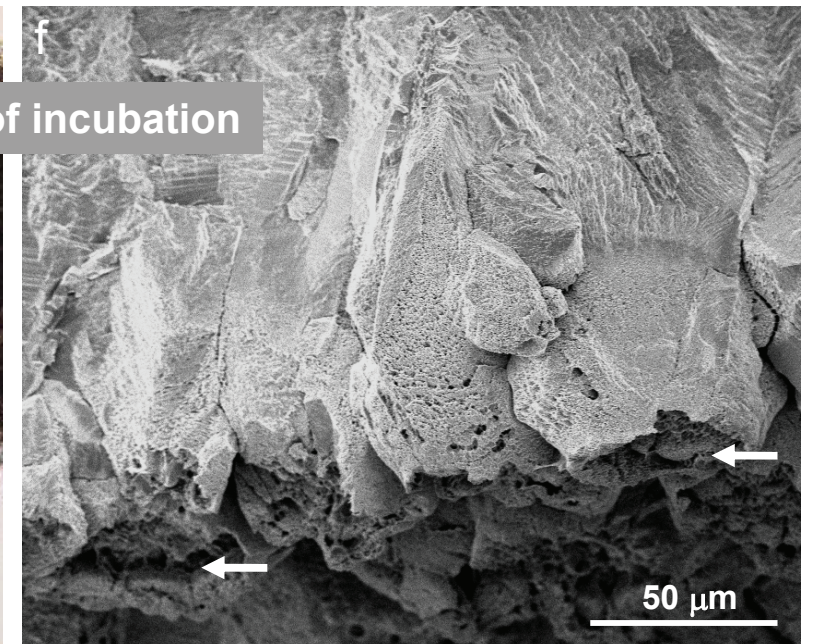
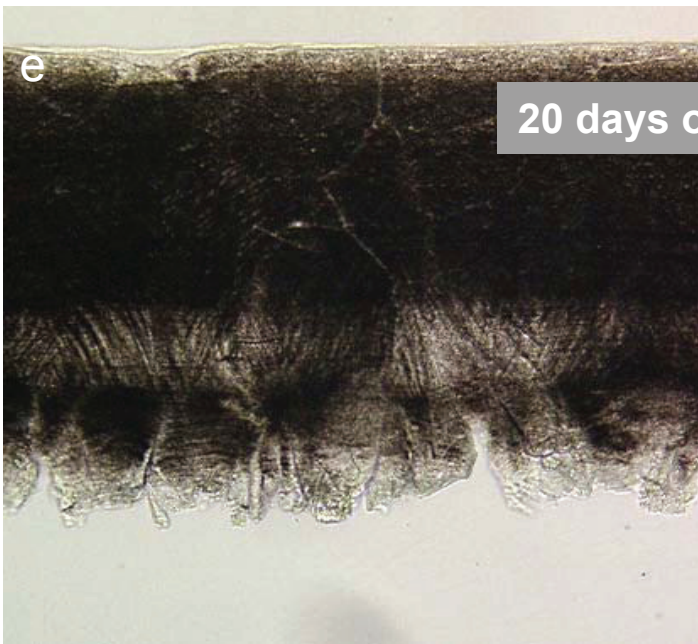
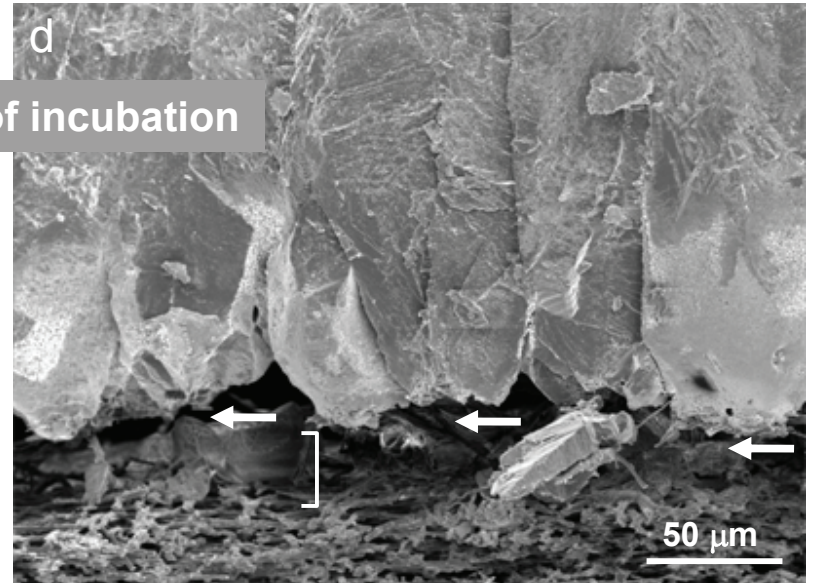
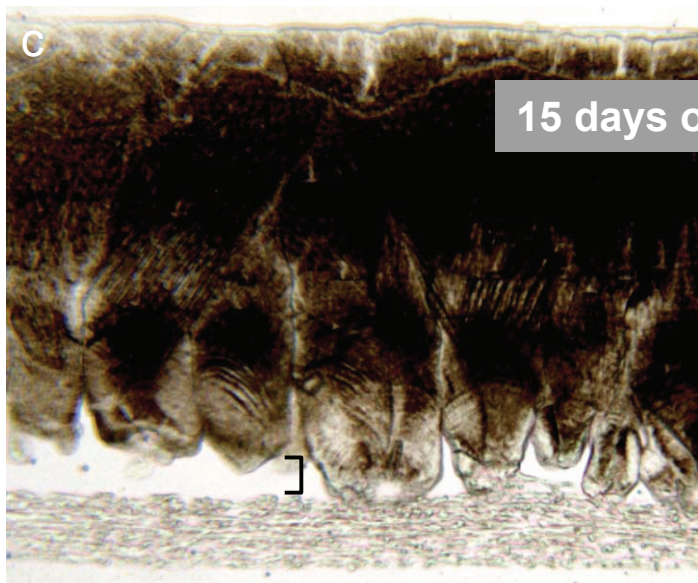
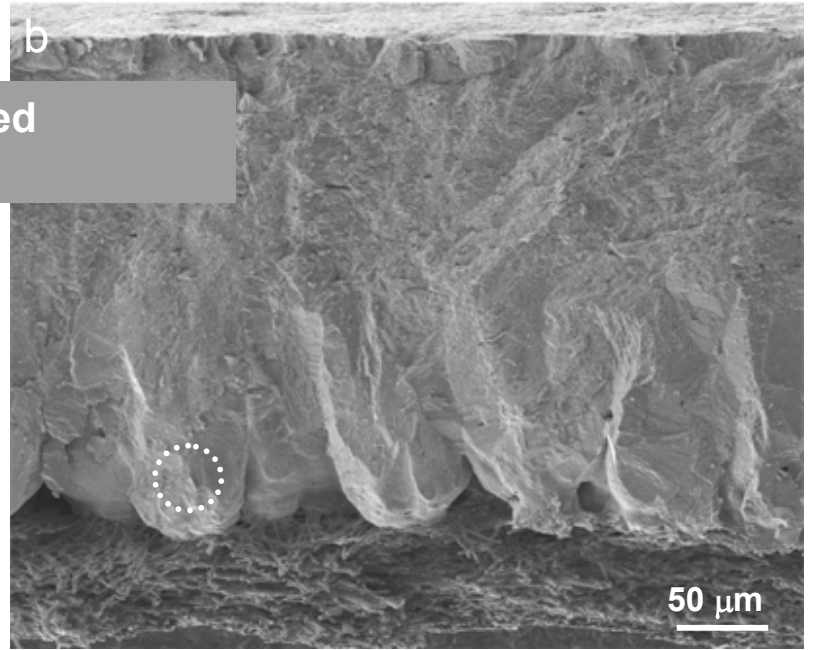
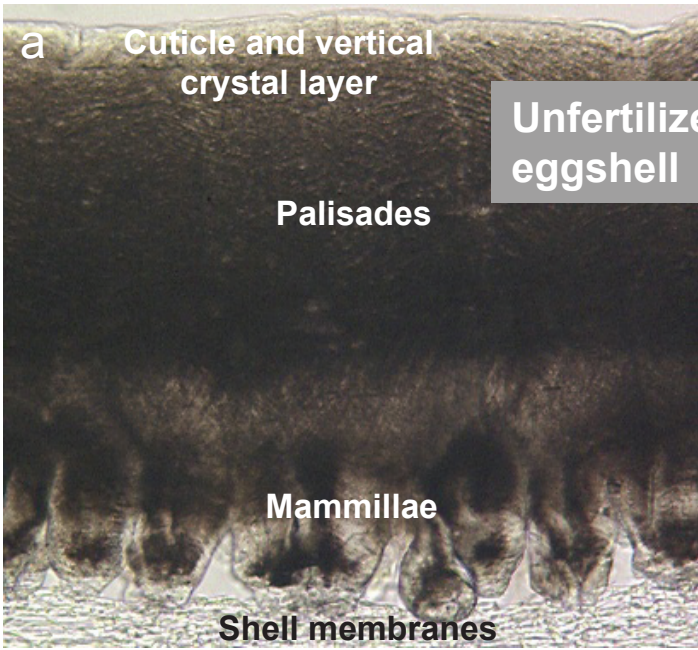


Figure 1. Cross-sectional profiles by light microscopy of ground sections of eggshell (left panels) and by SEM of fractured eggshell (right panels) from an unfertilized egg and from eggshells of fertilized eggs incubated for various periods of time. (a,b) Eggshell from an unfertilized egg showing the intact major shell compartments and the shell membranes (as labeled). The white dotted circle in panel (b) indicates the approximate location of the interior calcium reserve body described in subsequent figures. (c,d) Fertilized eggshells incubated for 15 days showing disintegration of a portion of the base plate at the tips of the mammillae (arrows) with detachment or partial detachment of the shell membranes (brackets). (e,f) After 20 days of incubation (just prior to hatching), the shell membrane detaches completely from the eggshell, whose irregular, porous and dissolved appearance reflect a loss of material and cohesion in this inner part of the eggshell.

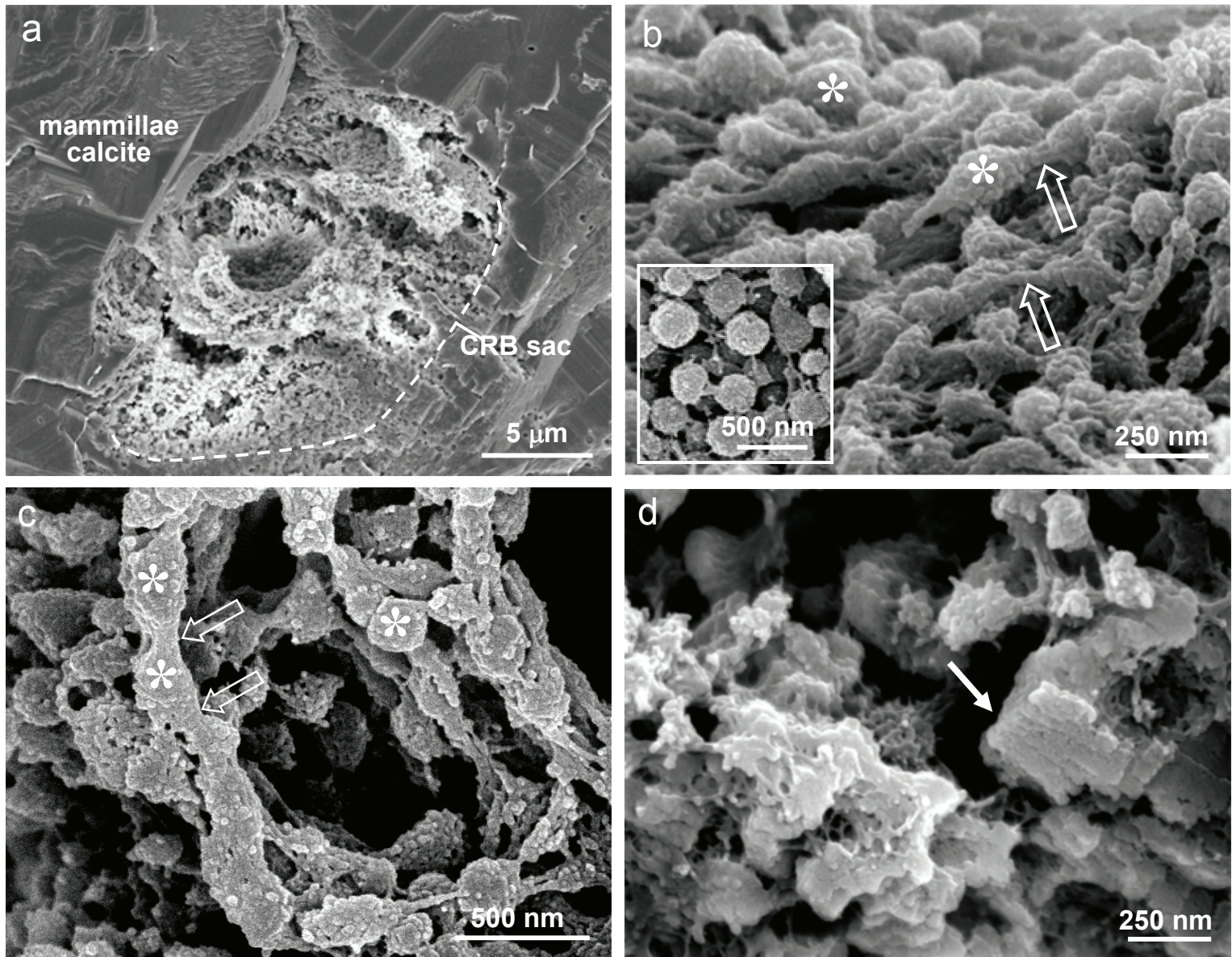


Figure 2. SEM of a calcium reserve body (CRB) sac and its contents in a fertilized eggshell at day 12 of incubation corresponding to the onset of eggshell resorption. (a) Ultrastructure of a CRB sac (partially outlined with dashed line) surrounded by the bulk calcitic mineral phase of the mammillae. (b) Within the CRB sac, abundant granules (asterisks) with a grainy-textured surface are interconnected by a network of extended matrix fibres (open arrows). The size of these granules, typically 250-300 nm in diameter, are comparable to the spherical granules as reported in the literature and as observed after complete experimental decalcification (inset). (c) Interconnecting matrix fibres (open arrows) vary in thickness as they connect the granules (asterisks) in the CRB sac. (d) Isolated rhombic crystallites (arrow), with distinct edges and angular corners resembling classic calcite rhombohedrons grown in the absence of protein, can sometimes be found within the CRB sac and show a layered appearance.

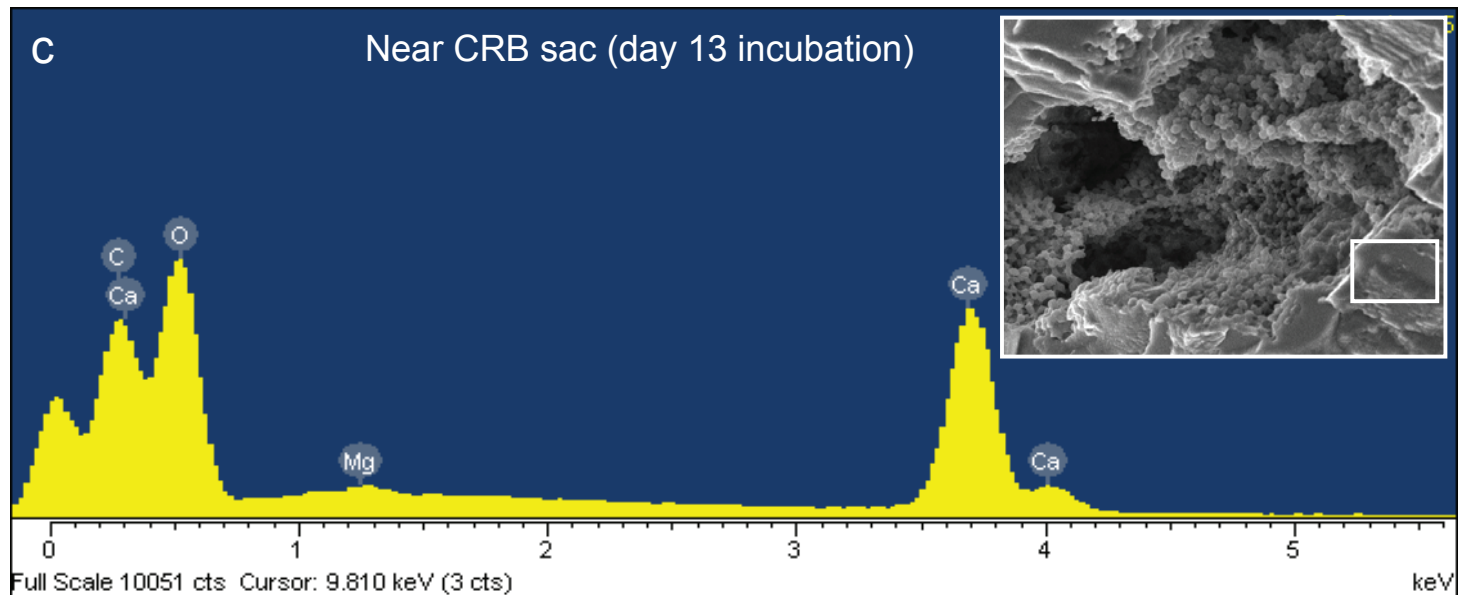
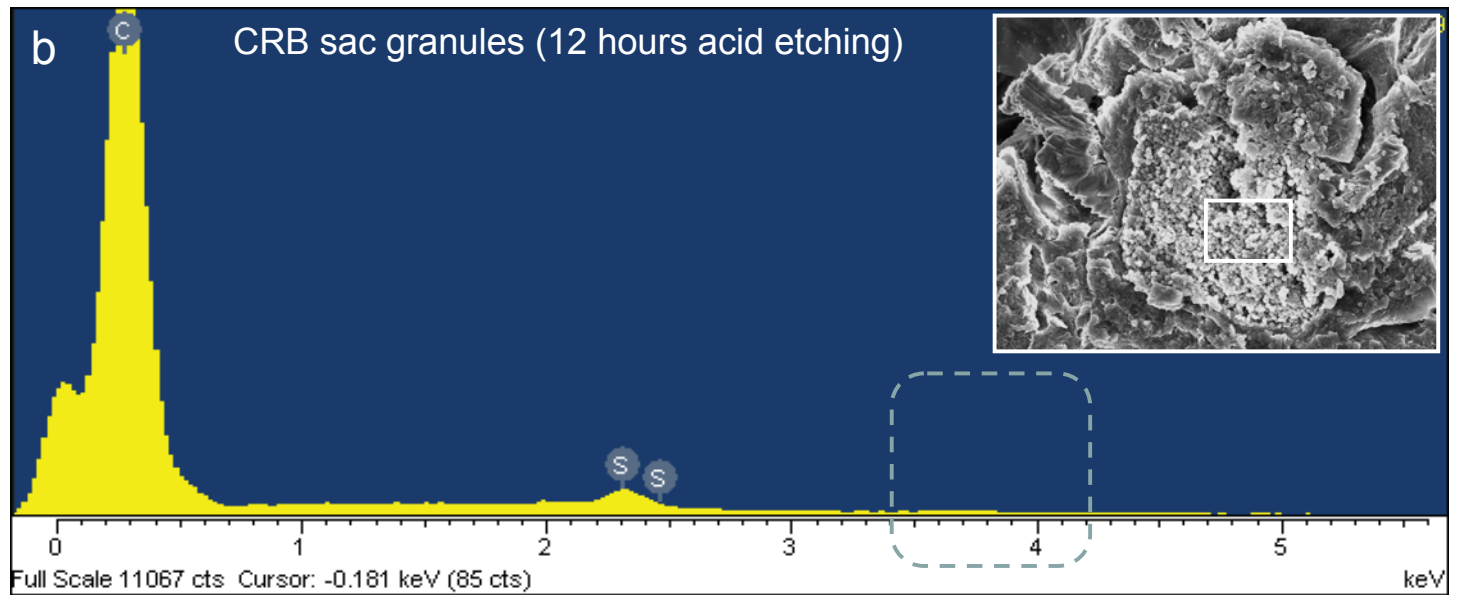
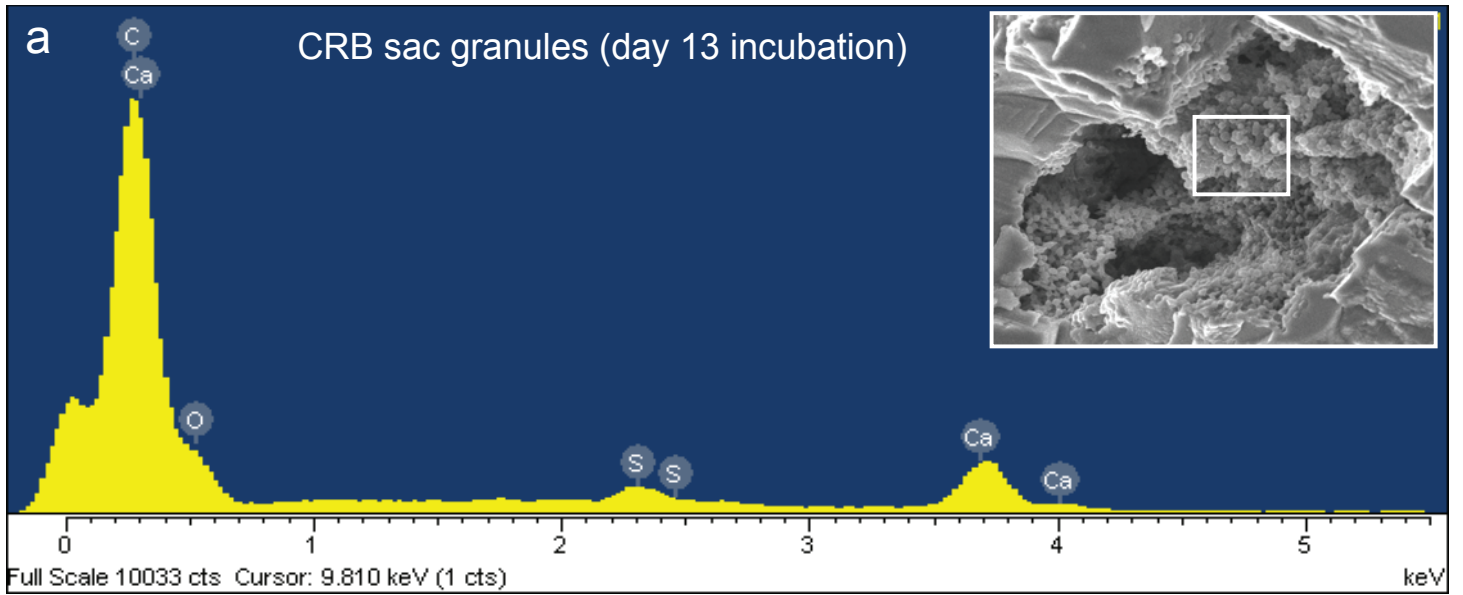


Figure 3. Energy dispersive x-ray spectroscopy (EDS) obtained by SEM on the contents and periphery of the CRB sac. (a) Prominent calcium (Ca) and sulfur (S) $K\alpha$ peaks are detected from both the granules and matrix fibres in the CRB sac from a fertilized egg incubated for 13 days. (b) As a control, EDS on fragments of intact eggshells (unincubated), immersed in 1 mM HCl for 12 hours in fixative to intentionally remove mineral, show granules and matrix fibres but no calcium signal (dashed outline); the persistent sulfur (S) peak presumably derives from the organic matrix. (c) EDS of the mammillary body near the periphery of a CRB sac (same sample as panel a) shows a strong calcium (Ca) signal but no sulfur peak, indicating less sulfur-containing organic matrix in this region. A trace amount of magnesium (Mg) is also detected. Smaller inset boxes demarcate areas of EDS analysis.

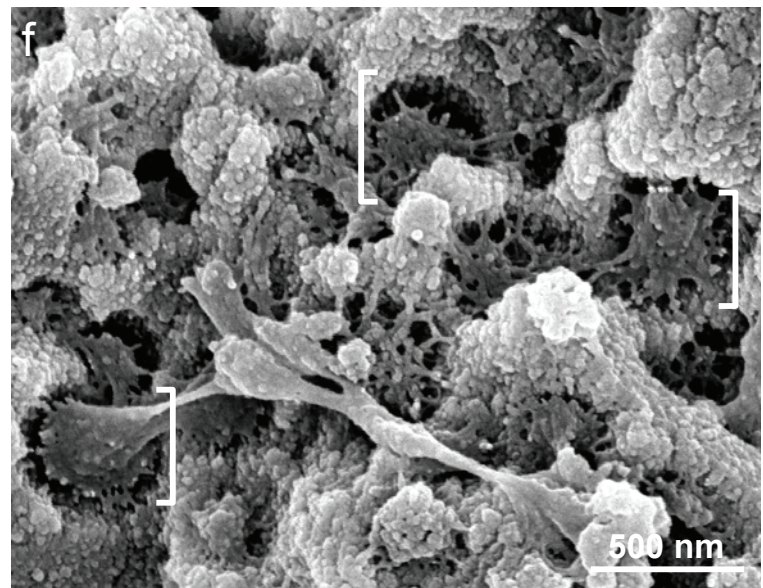
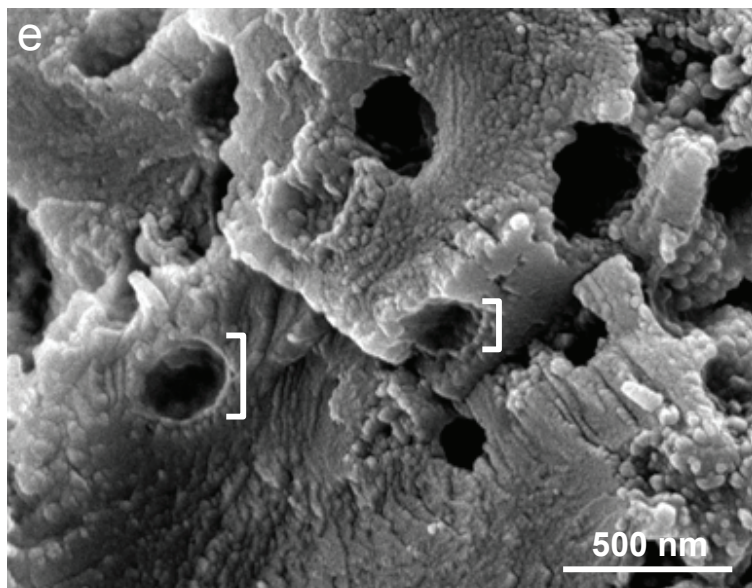
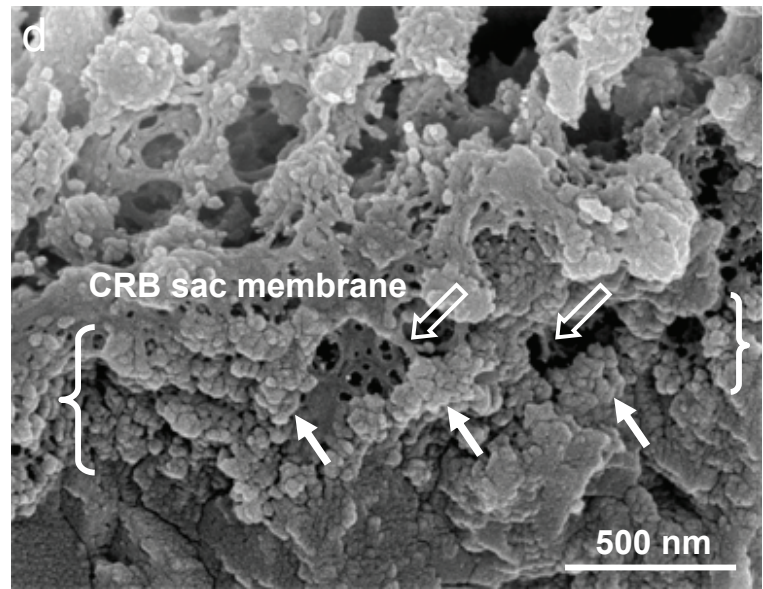
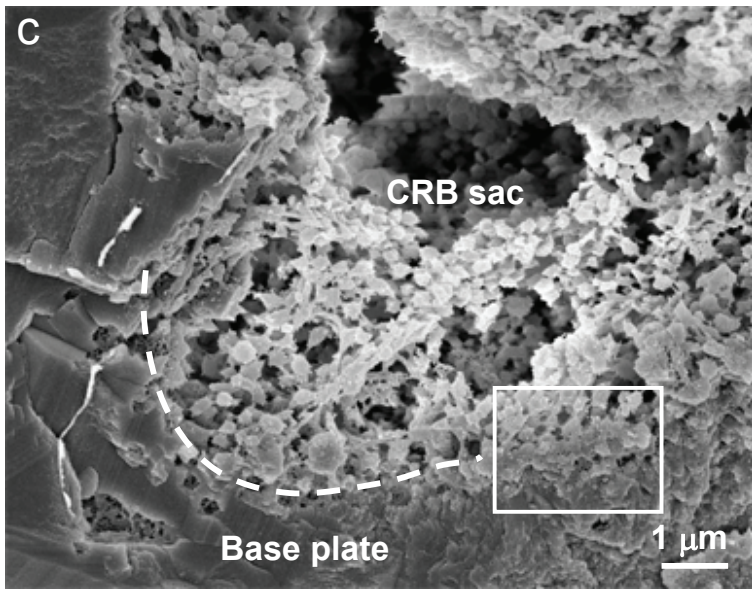
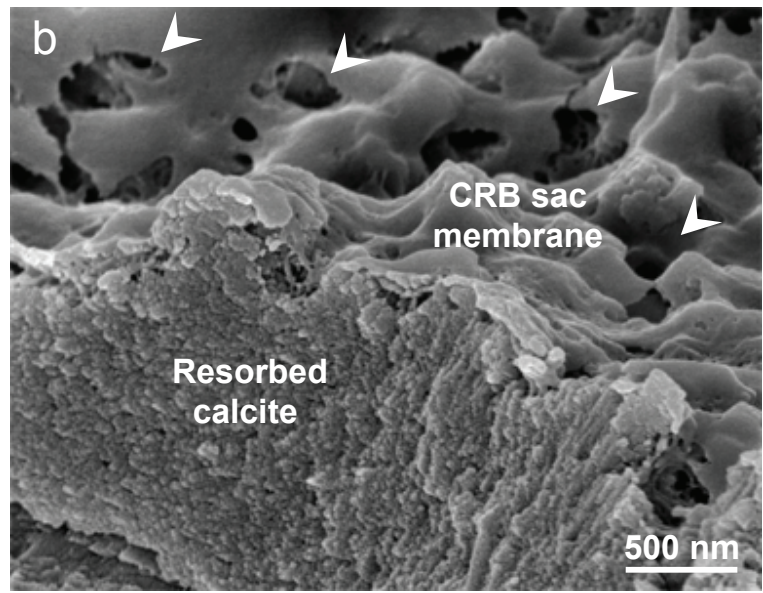
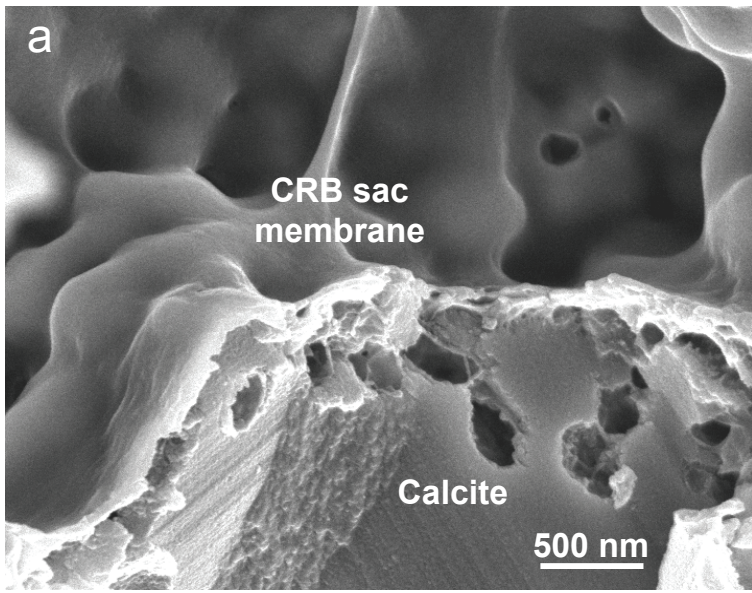


Figure 4. Morphological changes in the peripheral regions of the CRB sac attributable to mineral dissolution in 12-day incubated fertilized eggs (excluding panels a and e, which are from an intact and unincubated egg) viewed by SEM. (a) In an intact eggshell, the CRB sac is delimited by a continuous, membranous protein film, which closely approximates the calcitic mineral of the surrounding mammillary body. (b) With the onset of shell resorption starting at about 12 days of incubation, this membrane becomes perforated (arrowheads) coincident with loss of structural support caused by mineral dissolution. (c,d) More pronounced dissolution is observed on the peripheral mineral beneath the CRB sac (bracket in d, from boxed area in panel c) than in the rest of the base plate of the mamillae. The dissolution of peripheral calcite discloses minute struts of matrix (open arrows) attaching the CRB sac to the peripheral mammillary matrix. Calcite mineral directly in contact with the CRB sac membrane appear disintegrated as nano-granular crystallites (solid arrows). (e) In an intact eggshell, vesicles/voids (brackets) are common throughout the mammillae, where they range in size from about 200-300 nm, where their margins appear to be coated by a thin film of protein. (f) In 12-day incubated and resorbed eggshell, dissolution occurs in the peripheral calcitic mineral surrounding these vesicular structures such that the circumscribing protein film contracts toward the centre of the voids leaving extended tiny matrix struts delicately attached to the margin of spherical voids (brackets) .

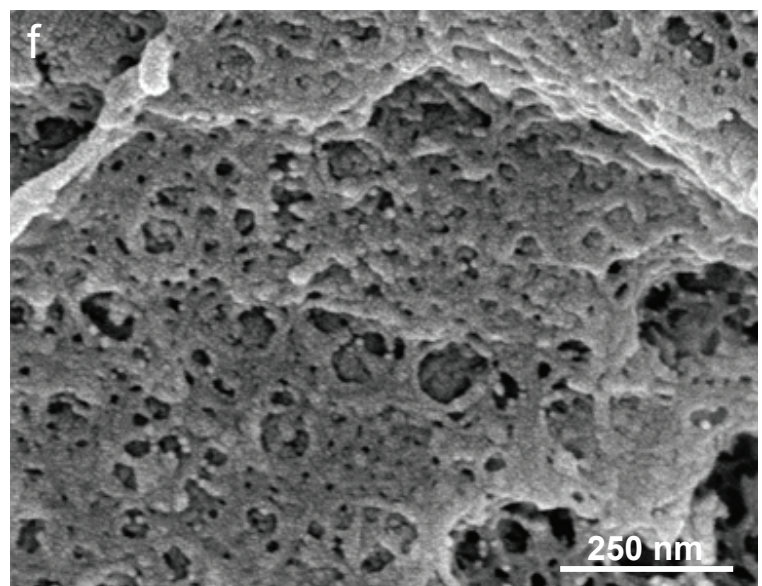
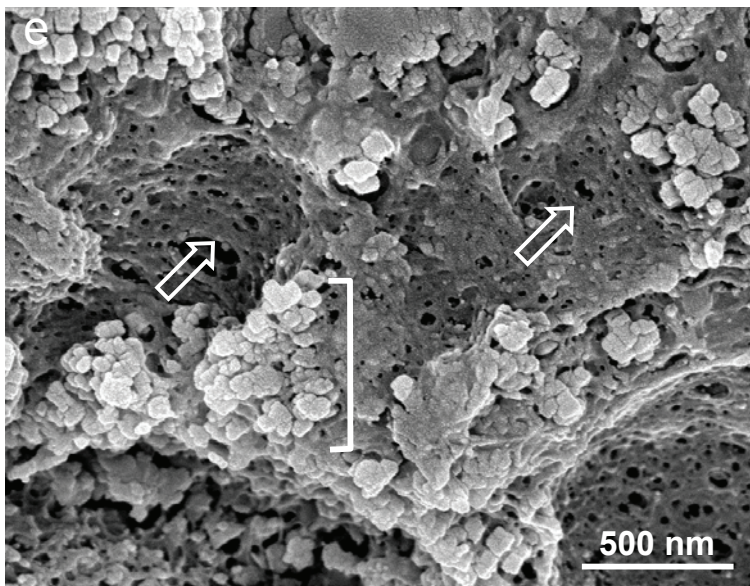
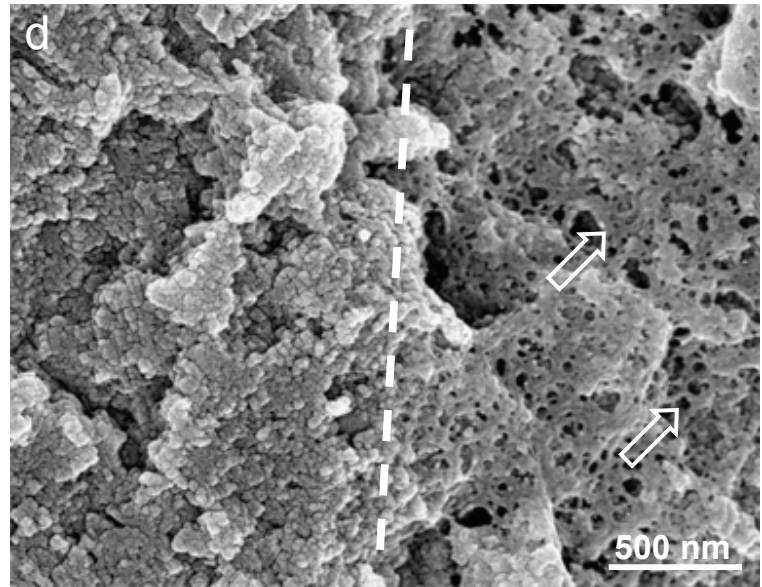
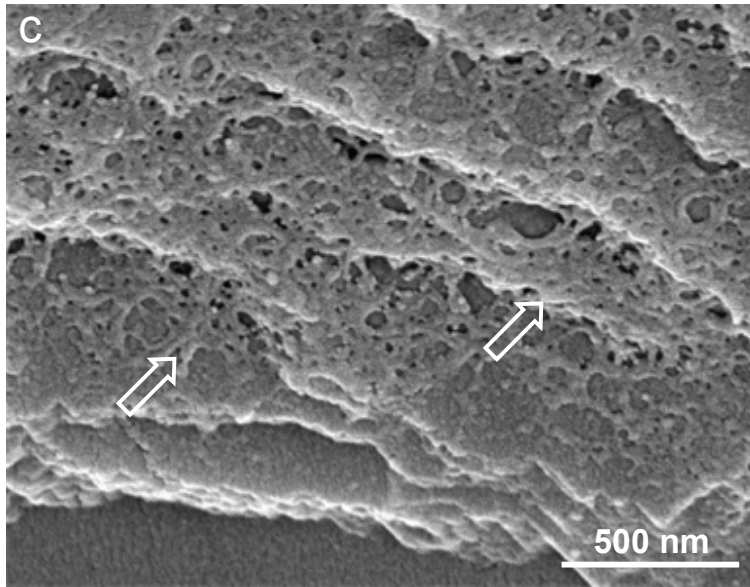
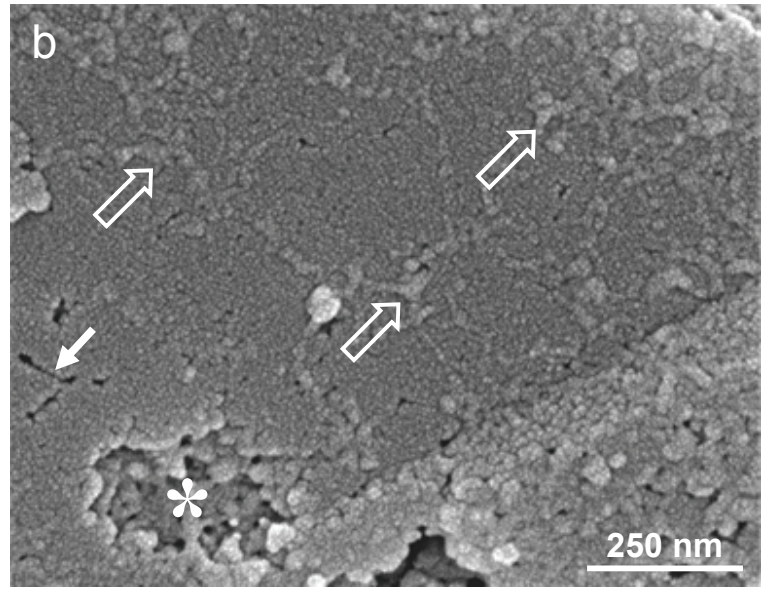
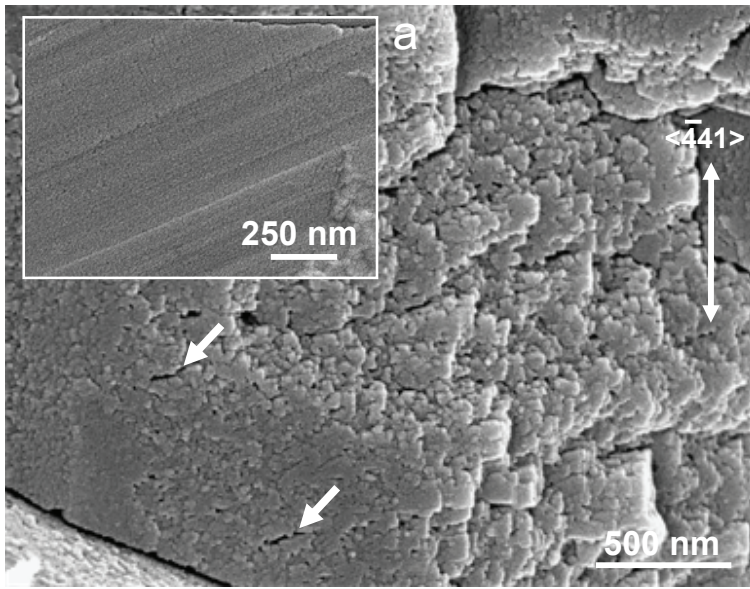


Figure 5. Dissolution of mineral in the shell mammillary bodies of fertilized eggs incubated for 12 days, and exposure of organic matrix by this process, as viewed by SEM. (a) Cross-fractured eggshell displays surfaces covered by irregular dissolution islands and crystallites, with many straight $\langle 41 \rangle$ edges of calcite (aligned in the direction of double-headed arrow) and some evident irregular pits and grooves (white solid arrows), in contrast to the stepped and continuous cleavage surface from intact eggshell (inset). (b) On the terrace of a dissolution island, loss of mineral reveals a fibrous network (open arrows) that was previously embedded within the mineral and which is now slightly raised above the surface. Where similar organic structures were removed during the fracturing, small surface channels remain (white solid arrows). An irregular dissolution pit (asterisk) reveals matrix deep within the mineral bulk. (c) In other regions, extended sheets of similar matrix (open arrows) formerly occluded within the mineral phases are exposed as more mineral is removed. (d) At earlier stages of this dissolution process, as seen in other regions, bulk mineral starts to dissolve to form a nano-granulated textured mineral (left side of dashed line), while immediately adjacent regions show greater dissolution revealing the permeating organic matrix network (open arrows, and right side of dashed line). (e) In some areas, nano-crystals (bracket) reside in the interstices of the organic matrix (open arrows). (f) High magnification of the protein network exposed by shell dissolution during resorption.

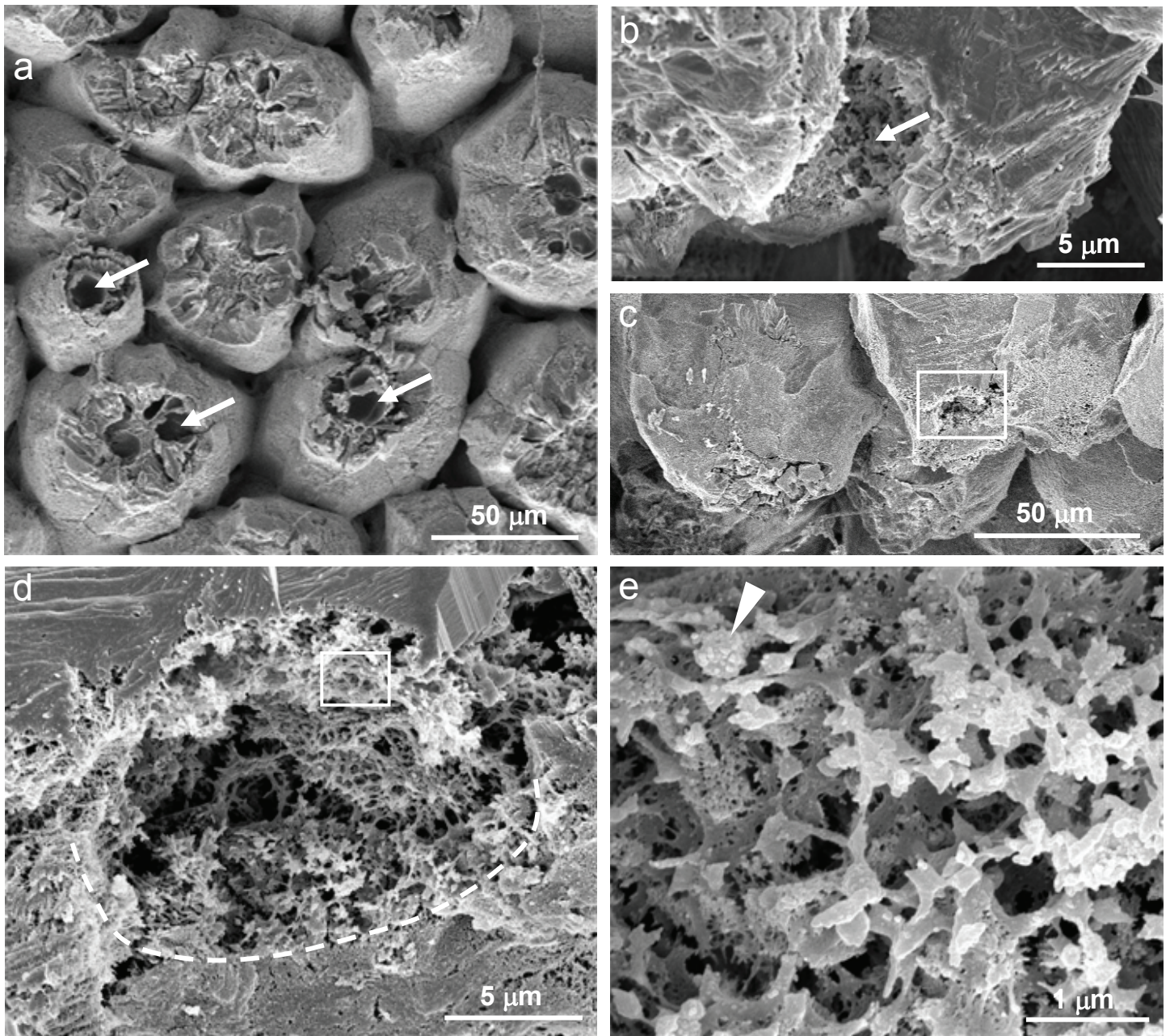


Figure 6. SEM of resorbed eggshell mammillae and the CRB from fertilized eggs incubated for 16 days. (a) As detected in *en face* views of mammillary bodies at this stage of resorption, CRB contents are mostly removed during fracturing/detachment of the shell membrane, and appear as central hollows (arrows). (b) Cross-fractured view of an empty CRB sac (arrow). (c-e) In an instance where a CRB sac retains some of its contents, examination at successively higher magnifications (subsequent panels indicated by white boxes) reveal details of these modified contents. A porous, loosely packed flocculent matrix comprises the majority of remaining structural elements, with an occasional granule being observed (arrowhead). Compare with Figure 2 (12 days of incubation).

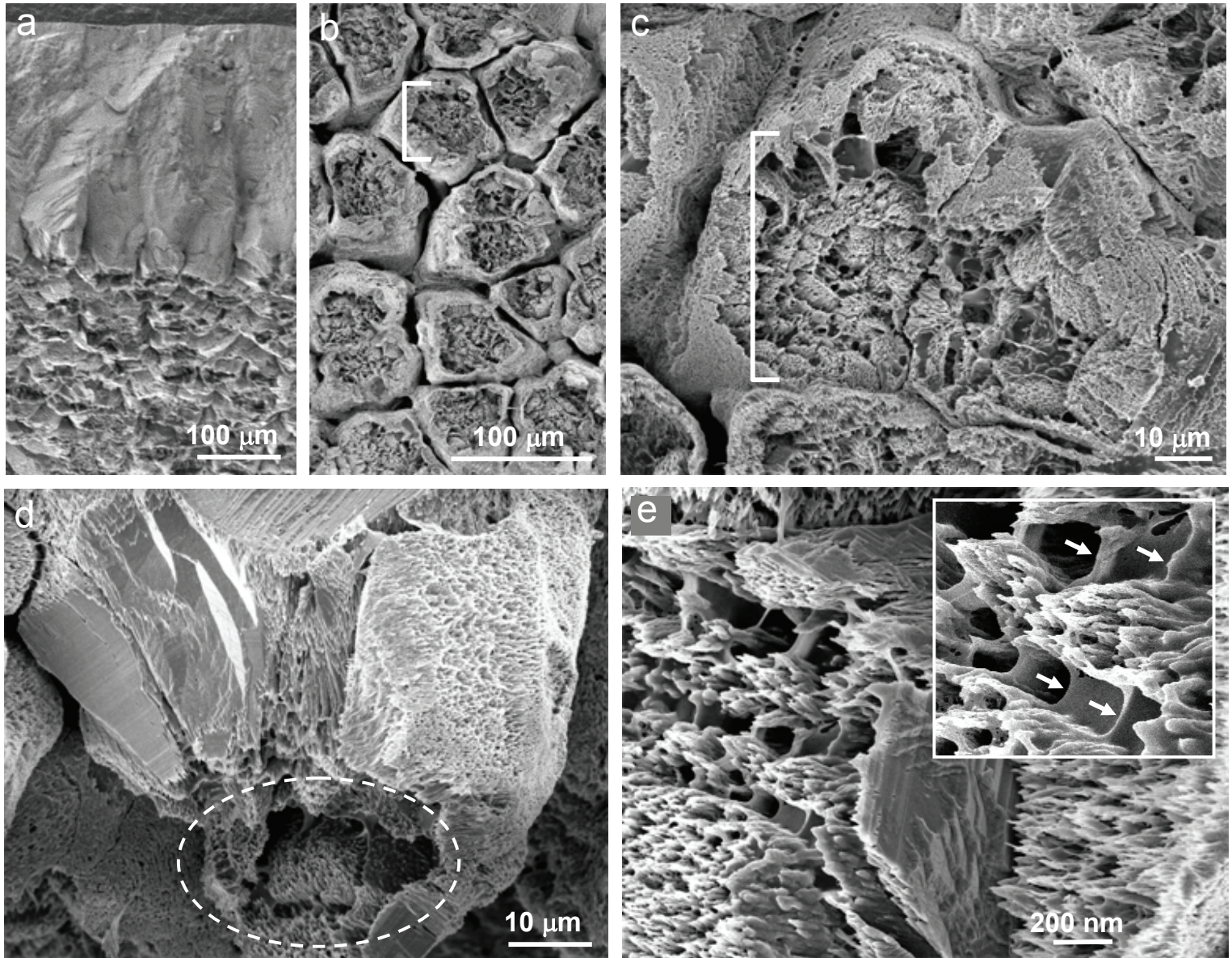


Figure 7. SEM of resorbed eggshell mammillae and the CRB from fertilized eggs incubated for 19 days. (a-c) The shell membrane is separated from the shell, and pronounced morphological changes are evident in comparison to earlier times of incubation/resorption. Mammillae are truncated and shortened (a), and resorption and loss of shell structure has advanced within each mamillae to a level generally above the CRB. In *en face* views of the resorbed mammillae (b,c), CRBs are generally missing, and the porous mammillae show eroded mineral and matrix (brackets). (d) On occasion, hollows can be found where CRBs previously resided (dashed oval). (e) High magnification view of remaining mineral profiles show uni-directional spikes of calcite, linked laterally by thin films or fibres of organic matrix (arrows).

Chapter 6

Manuscript 5

6.1 Preface

This study continues to elucidate how OPN regulates crystal growth, this time in a pathologic biosystem related to urolithiasis (kidney stone formation) and focuses on a mineral phase commonly found in human kidney stones – calcium oxalate dihydrate (COD). The data presented here demonstrate specific, non-equilibrated actions of phosphorylated full-length OPN and a short acidic peptide sequence of OPN in modulating COD growth and crystal morphologies. Furthermore, the OPN peptide preferentially binds and uniquely occludes into a specific crystallographic face of COD. Using Monte Carlo-based computational simulations, a possible adsorption mechanism is proposed to clarify the binding and intracrystalline occlusion of protein into COD – something that might also be relevant to many biomineralizing systems involving other mineral phases.

Reproduced with permission from *J. Biol. Chem.* (2009) as

doi:10.1074/jbc.M109.021899

Modulation of calcium oxalate dihydrate growth by selective crystal-face binding of phosphorylated osteopontin and poly-aspartate peptide showing occlusion by sectoral (compositional) zoning

**Yung-Ching Chien¹, David L. Masica,² Jeffrey J. Gray,^{2,3} Sarah Nguyen¹,
Hojatollah Vali^{1,4} and Marc D. McKee^{1,4}**

From the ¹Faculty of Dentistry, McGill University, Montreal, QC, Canada, ²Program in Molecular Biophysics, The Johns Hopkins University, Baltimore, Maryland, USA, ³Department of Chemical and Biomolecular Engineering, The Johns Hopkins University, Baltimore, Maryland, USA, ⁴Department of Anatomy and Cell Biology, Faculty of Medicine, McGill University, Montreal, QC, Canada

6.2 Abstract

Calcium oxalate dihydrate (COD) mineral and the urinary protein osteopontin/uroponin (OPN) are commonly found in kidney stones. To investigate the effects of OPN on COD growth, COD crystals were grown with phosphorylated OPN or a poly-aspartic acid-rich peptide of OPN (DDLDDDDD, poly-Asp₈₆₋₉₃). Crystals grown with OPN showed increased dimensions of the {110} prismatic faces attributable to selective inhibition at this crystallographic face. At high concentrations of OPN, elongated crystals with dominant {110} faces were produced, often with intergrown, interpenetrating twin crystals. Poly-Asp₈₆₋₉₃ dose-dependently elongated crystal morphology along the {110} faces in a manner similar to OPN. In crystal growth studies using fluorescently tagged poly-Asp₈₆₋₉₃ followed by imaging of crystal interiors using confocal microscopy, sectoral (compositional) zoning in COD was observed resulting from selective binding and incorporation (occlusion) of peptide exclusively into {110}

crystal sectors. Computational modeling of poly-Asp₈₆₋₉₃ adsorption to COD {110} and {101} surfaces also suggests increased stabilization of the COD {110} surface and negligible change to the natively stable {101} surface. Ultrastructural, colloidal-gold immunolocalization of OPN by transmission electron microscopy in human stones confirmed an intracrystalline distribution of OPN. In summary, OPN and its poly-Asp₈₆₋₉₃ sequence similarly affect COD mineral growth – the {110} crystallographic faces become enhanced and dominant attributable to {110} face inhibition by the protein/peptide, and peptides can incorporate into the mineral phase. We thus conclude that the poly-Asp₈₆₋₉₃ domain is central to OPN's ability to interact with the {110} faces of COD, where it binds to inhibit crystal growth with subsequent intracrystalline incorporation (occlusion).

6.3 Introduction

Calcium oxalate is the major mineral phase of human renal calculi, constituting roughly 70% by weight of the stones (Wesson et al., 1998). Two polymorphs of calcium oxalate – calcium oxalate monohydrate (COM) and calcium oxalate dihydrate (COD) – are the most abundant mineral types, but others may exist in smaller amounts, including calcium-phosphate minerals. It has been reported that the occurrence of COM, the more thermodynamically stable polymorph of calcium oxalate, is often at the core of most kidney stones, and is approximately twice as frequent as COD (Mandel and Mandel, 1989), although both crystal types typically exist to some degree in most stones (Durrbaum et al., 2001; Mandel et al., 1987). COM is commonly found in the urine of 'stone formers,' but seldom is seen in healthy urine; on the other hand, COD crystals are typically found in the urine of both healthy people and stone formers and are routinely excreted during urination (Cerini et al., 1999; Dyer and Nordin, 1967; Elliot and Rabinowitz, 1980). Importantly, in patients with severe uremia and hypercalciuria, elongated, large rod-shaped COD crystals are not only often observed, but are the sole mineral phase present in the kidneys in these pathologies (Daudon, 2008; Lewis et al., 1974).

In comparing physiologic differences between calcium oxalate polymorphs, one study has shown that for a given amount of added crystals, approximately 50% more

COM than COD crystals bound to inner medullary collecting duct cells *in vitro* (Wesson and Worcester, 1996). Other studies have reported that COD crystals are less prone than COM crystals to adhere to cell surfaces, suggesting that COD might thus contribute to a lesser degree than COM to the retention of mineral in the renal collecting ducts leading to kidney stone formation (Cerini et al., 1999; Mandel, 1994). This is supported by the fact that COM crystals are large cationic particulates, presenting more calcium ions than COD crystals at their surface that would have a stronger affinity for anionic molecules on renal epithelial cell membranes (Verkoelen et al., 2000; Wesson and Worcester, 1996). Further to this, COM and COD crystals bind to cultured renal cells with different face-selective affinities (Lieske et al., 1996; Lieske et al., 1997; Sheng et al., 2005; Wesson and Ward, 2006), and COM crystals are known to be more injurious to cell membranes than COD crystals (Wiessner et al., 1986). In this regard, Wesson et al. (Wesson et al., 1998) proposed that the preferential formation of COD crystals *in vivo* protects against urolithiasis because they are less likely to adhere to renal tubular cells and are thus more readily excreted. This notion is supported by direct experimental measurements of the macromolecular adhesion force on specific crystal faces of COM or COD at the near-molecular level (Sheng et al., 2005; Wesson and Ward, 2006). Given this, conversely, inhibition of the formation of COD crystals could lead to preferential COM deposition and the formation of kidney stones.

Although calcium and oxalate ionic concentrations are frequently supersaturated with respect to both COM and COD mineral polymorphs, normal human urine likely contains factors that can modulate calcium oxalate crystallization into COD (Wesson and Worcester, 1996). In this context, the presence of urinary macromolecular inhibitors of crystal growth can cause preferential crystallization of COD, rather than COM, from a supersaturated solution of calcium chloride and sodium oxalate (Wesson and Worcester, 1996). Substantial elegant work has been performed on COM growth and the effect of citrate and peptides/proteins as crystal growth modifiers. Some macromolecules, including urinary osteopontin (OPN), contain poly-anionic regions and net negative charges that have been shown to inhibit calcium oxalate crystallization (Grohe et al., 2007; Langdon et al., 2009; Qiu et al., 2004; Sheng et al., 2005; Taller et al., 2007) and influence calcium oxalate growth in favor of COD (Durrbaum et al., 2001; Pedraza et al.,

2008; Ryall et al., 2005; Wesson and Worcester, 1996). Although there appears to be preferential inhibition of COM, several studies present evidence for higher affinity of OPN binding to COD, and here we investigate this further to show effects of OPN (and a peptide of OPN) on COD crystal growth and provide information on peptide/protein occlusion that might facilitate crystal dissolution as originally proposed by Ryall and colleagues (see below) (Grover et al., 2008; Ryall et al., 2005).

OPN is a highly acidic, glycosylated phosphoprotein produced by many types of epithelial cells and can be found in normal plasma and in various body fluids such as bile, urine and milk (Brown et al., 1992; Rittling and Denhardt, 1999). In normal kidneys, OPN is secreted by the thin and thick ascending limbs of the loop of Henle and distal nephrons (Asplin et al., 1998; Khan, 1997; Lopez et al., 1993; Shiraga et al., 1992; Tawada et al., 1999; Xie et al., 2001). OPN contains a 15-20% aspartic acid residue content, and the mineral-binding and inhibitory properties of OPN have often been partly attributed to an aspartic acid-rich sequence within this protein (Fisher et al., 2001; Hoyer et al., 2001; Rittling and Denhardt, 1999; Wesson and Worcester, 1996). Likewise, post-translational phosphorylation of OPN has been shown to markedly enhance the mineral-binding and inhibitory ability of this protein (Hoyer et al., 2001; Kazanecki et al., 2007). Furthermore, OPN also contains sialic acid (Rittling and Denhardt, 1999; Shiraga et al., 1992), which may play an indirect role in crystal binding by forming a bridge between transiently expressed crystal-binding molecules and the cell surface (Verkoelen et al., 2000). Several studies have shown that OPN has a higher affinity for COD than COM in normal urinal precipitates, with some evidence given for the incorporation of protein into calcium oxalate crystals (Ryall et al., 2005; Ryall et al., 2001; Wesson et al., 1998).

OPN consistently localizes to kidney stones (Kohri et al., 1993), and at physiologically relevant concentrations applied *in vitro*, acts as a potent inhibitor of the nucleation, growth and aggregation of calcium oxalate crystals (Asplin et al., 1998; Hoyer et al., 2001; Shiraga et al., 1992). In a rat model of urolithiasis, although increased OPN mRNA expression was associated with increased renal calculi formation, the urinary excretion level of OPN was less than in controls, discussed as being attributable to incorporation of OPN into stones (Kohri et al., 1993; Yasui et al., 2001). In general, the inclusion of OPN, plus other urinary macromolecules, into renal calculi has been

suggested to be part of a cellular defense mechanism designed to inhibit crystal growth and limit the growth of kidney stones, to interrupt inorganic crystal structure of the calcium oxalate minerals, and to provide an organic volume whose degradation by permeating proteases creates channels facilitating dissolution of the mineral phase (Grover et al., 2008; Ryall et al., 2005). Given these possibilities, our aim was to determine whether full-length phosphorylated OPN, and a poly-Asp peptide of OPN, affect COD crystal growth and morphology, and if so, we further aimed to identify the contribution of face-specific binding and intracrystalline incorporation (occlusion) of OPN peptide into COD. Combining experimental and computational approaches, we have identified preferential binding and unique occlusion of a peptide of OPN at a specific crystallographic face of COD. Furthermore, we present a possible adsorption mechanism in a model where multiple peptide carboxylate groups bind calcium atoms at the COD {110} surface. Taken together, our findings provide new information on the pathogenesis of renal calculi by describing specific actions of phosphorylated full-length OPN and a short peptide sequence of OPN (not having post-translational modifications) on specific COD crystal faces that modulate calcium oxalate growth and crystal morphologies.

6.4 Materials and methods

Kidney stones and immunolocalization of OPN by light and electron microscopy. Kidney stones from two female patients (age 66 and 69) obtained from the Kidney Stone Clinic of the Royal Victoria Hospital, McGill University Hospital Centre, were characterized as being calcium oxalate-containing stones by routine x-ray diffraction performed by a commercial service on a fragment of each stone. The bulk of the stones were washed briefly multiple times with tap water, and fixed in 1% glutaraldehyde and 1% paraformaldehyde in 0.1 M sodium cacodylate buffer (pH 7.2) for 2 days. Stones were decalcified in a 4.13% EDTA solution containing 1% glutaraldehyde.

For light microscopy immunohistochemistry, the decalcified kidney stone samples were embedded in paraffin and 5- μ m sections were immunostained for OPN using rabbit anti-human OPN (LF-123) polyclonal antibodies (antibodies courtesy of Dr. Larry W. Fisher, National Institutes of Health, Bethesda, MD, USA). Briefly, deparaffinized

sections were treated with 1% bovine testicular hyaluronidase (Sigma, St. Louis, MO) at 37°C for 30 minutes, followed by incubation with anti-OPN LF-123 antibody diluted 1:200 in 5% normal goat serum/0.2% BSA in Tris-buffered saline (TBS) with 0.01% Tween-20 (TBST) (50 mM Tris-HCl, 150 mM NaCl, 0.01% Tween-20, pH 7.6). Sections were washed with TBST, and secondary biotinylated goat anti-rabbit IgG (Caltag Laboratories, InVitrogen, Carlsbad, CA, USA) antibody incubation was followed by TBST washing and application of the Vectastain ABC-AP kit (Vector Laboratories, Burlingame, CA, USA) for an additional 45 minutes at room temperature. Colour development was achieved by treatment with Fast Red TR/Naphthol AS-MX phosphate (Sigma) containing 1 mM levamisole to inhibit endogenous alkaline phosphatase activity. Sections were counterstained with methyl green (Vector Laboratories, Burlingame, CA, USA) and mounted with coverslips using Kaiser's glycerol jelly. Light micrographs were obtained using a DXC-950 3-CCD camera (Sony, Tokyo, Japan) mounted on an optical microscope (model Leitz DMRBE, Leica Wetzlar, Germany).

For ultrastructural immunolocalization of OPN in the kidney stones, aldehyde-fixed samples were fully decalcified with EDTA (also containing aldehyde), dehydrated, and then embedded in LR White acrylic resin (London Resin Company, Berkshire, UK) as previously described (McKee and Nanci, 1995). Survey sections (0.5 μm) of embedded tissue were cut with a diamond knife on an ultramicrotome (model Reichert Ultracut E, Leica), stained for light microscopy with toluidine blue, and coverslipped. For transmission electron microscopy (TEM), selected regions were trimmed, and ultrathin sections (80 nm) were placed on polyvinyl formvar- and carbon-coated nickel grids. Grid-mounted tissue sections were processed for colloidal-gold immunocytochemistry by incubation of the sections with primary anti-OPN LF-123 antibody (1:10 dilution), after which immunolabeling patterns were visualized by incubation with protein A-colloidal gold complex (14 nm). Contrasting of the sections was performed using conventional uranyl acetate and lead citrate staining, and this was followed by their examination using a JEM 2000FXII transmission electron microscope (JEOL, Tokyo, Japan) operated at 80 kV.

Precipitation of calcium oxalate crystals from human urine. The metastable limit of human urine with respect to oxalate – slightly below 4 mM sodium oxalate final concentration – was determined as described by Ryall et al. (Ryall et al., 1985), and the protocol to precipitate calcium oxalate crystals from human urine was adapted from Doyle et al (Doyle et al., 1991). Briefly, fresh morning urine (200-500 ml volume) was collected without added anti-bacterial agents from 6 males between the ages of 23 and 45, with each having no history of kidney stones. The pH of each sample was taken and urine analysis was performed, to identify and discard abnormal samples, using ChemStrip 5L (Roche, Basel, Switzerland), which identifies the presence of leukocytes, glucose, ketones, or red blood cells in the samples. Urinary protein concentrations were quantified by the Micro BCA Protein Assay Reagent Kit (Pierce Biotechnology, Thermo Fisher Scientific, Rockford, IL, USA) as well as by the mini-Lowry method. A 200 mM solution of sodium oxalate was added to the urine samples to get a final concentration of 4 mM sodium oxalate, and the samples were left at room temperature for intervals of one to 3 hours. Crystals precipitated in the samples were collected by centrifugation at 8,200 rpm for 30 minutes, followed by filtration harvesting through a hydrophilic polypropylene membrane (0.2-0.8 mm pore size, Gelman Sciences, Pall Corporation, East Hills, NY, USA) and washing with distilled and de-ionized water. To obtain/release crystal-bound proteins, 30 mg of crystals were demineralized with 7 ml of 0.25 M EDTA at pH 8.0 and 4°C, for a period of 3 days with gentle agitation (Doyle et al., 1991). Dialysis was done against distilled, de-ionized water, to remove EDTA, using cellulose membranes with a 12 kDa molecular-weight cutoff (Sigma) for over 24 hours at 4°C. The extracts were collected in 15 ml conical tubes and concentrated 5-fold with the appropriate volume of distilled, de-ionized water.

Western blotting for OPN from urine-precipitated crystal extracts. Twenty µl of total protein extract from the precipitated crystals were separated by SDS-PAGE. The proteins were electrophoretically transferred to an Immobilon-P transfer membrane (Millipore). The membranes were blocked with 3% bovine serum albumin (BSA) (Sigma) in PBS and then probed with the following primary antibodies: 1) monoclonal mouse anti-human OPN Mb53 antibody (1:5,000 dilution, kindly provided by Dr. A. Chambers, University of Western Ontario, Canada), 2) polyclonal rabbit anti-human

OPN LF-124 (anti-N-terminal) or polyclonal rabbit anti-human LF-123 (anti-C-terminal) antibodies (LF-124 used at 1:2,000 dilution; LF-123 used at 1:10,000 dilution; kindly provided by Dr. Larry W. Fisher, National Institutes of Health, Bethesda, MD, USA). This was followed by the appropriate horseradish peroxidase (HRP)-conjugated secondary anti-bodies that included: 1) goat anti-mouse-HRP/1:2,000 (Dupont Biotechnology, Johnston, IA, USA) for the monoclonal antibody, 2) goat anti-rabbit/1:2,000 (Pierce Biotechnology, Thermo Fisher Scientific, Rockford, IL, USA) for the polyclonal antibodies. The blots were visualized by chemiluminescence using ECL Plus (Amersham Biosciences, GE Healthcare, Buckinghamshire, UK).

OPN, poly-Asp peptide of OPN, and calcium oxalate dihydrate (Weddelite) crystal growth in vitro. To investigate the effects of full-length OPN and an acidic OPN peptide on COD growth, COD crystals were grown from aqueous $\text{CaCl}_2\text{-Na}_2\text{C}_2\text{O}_4$ solutions in the presence of OPN or the synthetic poly-Asp peptide. The OPN used for these experiments was full-length, phosphorylated bovine milk OPN as characterized (Sorensen and Petersen, 1993) and supplied by Esben Sørensen (Department of Molecular and Structural Biology, University of Aarhus, Denmark) and Arla Foods (Denmark). Synthetic, linear poly-aspartic acid-rich (poly-Asp) peptide, with or without a fluorescein (FAM) tag, was constructed according to the sequence of the aspartate-rich domain of bovine OPN (poly-Asp₈₆₋₉₃, residues 86-93, DDLDDDDDD) at the Sheldon Biotechnology Centre of McGill University, and peptide was purified by HPLC. Commercial poly-aspartic acid (MW range 5,000-15,000 daltons, range of 37-113 residues, Sigma), was also used to compare effects with the linear synthesized poly-Asp₈₆₋₉₃. OPN, poly-Asp₈₆₋₉₃ or commercial poly-aspartic acid were added to the sodium oxalate solution prior to the crystal growth experiments, with various final concentrations ranging from 0.15 - 5 μM which span the physiologic range (Thurgood et al., 2008), and extend beyond.

The detailed procedure for the growth of COD crystals was essentially that described by Lepage and Tawashi (Lepage and Tawashi, 1982). The growth experiments were performed in a free-drift system at 4°C. In brief, 3 ml of 0.005 M sodium oxalate ($\text{Na}_2\text{C}_2\text{O}_4$, Fisher Scientific, room temperature), with or without added protein or peptide, was added to 5 ml of 1 M calcium chloride solution at 4°C (CaCl_2 , Fisher Scientific) in

15 ml conical polypropylene tubes (Sarstedt). The $\text{Na}_2\text{C}_2\text{O}_4$ solution was added to the centre of the air-liquid interface of the CaCl_2 solution using a micropipette. The mixture was left without agitation for 24 hours at 4°C . The COD crystals that formed were collected by centrifugation at 10,000 g for 10 minutes at 4°C . COD crystals are stable in air at 4°C for 2 weeks; however, when these crystals are kept in normal saline at 37°C , they are stable only for 24 hours. This is attributable to the gradual transformation of the dihydrate form of calcium oxalate to the monohydrate form, which is more stable in normal saline at 37°C (Lepage and Tawashi, 1982). As COD is insoluble in alcohol (Bartholomew and Rebello, 1979), the crystals were washed briefly with distilled, de-ionized water (resistance $>18\text{ M}\Omega$) and dehydrated sequentially in gradient 50%, 70% and 100% ethyl alcohol solutions; the 100% ethyl alcohol was changed three times to ensure that the dehydration was complete. The crystals were kept at 4°C and rehydrated sequentially as needed.

Morphological imaging of COD crystals by scanning electron microscopy (SEM). COD crystals grown *in vitro* were mounted with conductive carbon cement onto metallic SEM stubs. Samples were then sputter-coated with a 20-25 nm thick Au-Pd thin film using a Hummer VI Sputter System (Anatech Ltd., Hayward, CA) and imaged using a Hitachi field-emission gun scanning electron microscope (FE-SEM) operating at an accelerating voltage of 3-5 kV (model S-4700, Hitachi High Technologies America, Pleasanton, CA) and using working distances of $<12\text{ mm}$.

Fluorescence microscopy and laser confocal microscopy of crystals grown with poly-Asp₈₆₋₉₃. COD crystals grown in the presence of fluorescein-tagged poly-Asp₈₆₋₉₃ (as above) were suspended in absolute alcohol and deposited on microscope glass slides. Samples were viewed as whole mounts by immunofluorescence microscopy and pictures were taken with Leica model DC300F camera mounted on a phase contrast/fluorescence microscope (Leica DM IL). For imaging of fluorescent peptide in the interior of the grown crystals using laser confocal microscopy, glass slides with COD containing fluorescein-tagged poly-Asp₈₆₋₉₃ were coverslipped using Geltol mounting medium (Thermo Electron Corporation, Pittsburgh, PA, USA). Imaging at different focal planes was acquired using a Zeiss 510-META confocal microscope (Carl Zeiss GmbH, Jena, Germany) and fluorescein was visualized using 488-nm excitation (argon laser) and a

505–530-nm band-pass emission filter. All images were acquired at Nyquist resolution (70 nm/pixel) as recommended by the manufacturer, using a X63 numerical aperture (NA) 1.4 oil-immersion Plan-Apochromat objective lens (Zeiss). Line averaging (16X) was used to minimize noise. Optical sectioning was carried out using an interval of 0.5 μm , and stacks of image slices were analyzed using LSM Image Browser Release v4.2.

SHAPE computer modeling and software identification of crystallographic faces. The morphologies of COD crystals were identified and indexed by comparing an observed morphology and the angles of its polar-type corners of faces (i.e., crystal corners intersecting the *c*-axis of the COD crystal) to graphic renditions prepared by the computer software SHAPE (Dowty, 2002), with reference to unit cell parameters, *d*-spacing, and X-ray powder diffraction file data for COD. SHAPE software renditions based on entered crystallographic parameters for COD matched exactly the observed SEM morphologies, validating differences in relative inhibition of specific faces. Two-dimensional schematic drawings of compositional sectoral zoning were prepared and calculated by re-orienting the 3-D morphological SHAPE drawings to match the orientations of selected crystals in light micrographs.

RosettaSurface energy calculations and structure predictions for poly-Asp₈₆₋₉₃. All simulations were performed using the RosettaSurface Monte Carlo plus-minimization structure-prediction program (Masica and Gray, 2009). Each execution of the program folds a peptide from a fully extended conformation and results in one energy-minimized candidate solution- and adsorbed-state structure. Large structural ensembles of 10^5 candidate solution- and adsorbed-state structures were generated from which the 100 lowest-energy structures, from each state, were chosen for further analysis. RosettaSurface accounts for solvent and solvent entropy via the Effective Energy Function-1 (EEF-1) implicit solvent model (Lazaridis and Karplus, 1999).

COD crystal coordinates were constructed for simulation using CrystalMakerTM (Palmer, 2005) starting from the COD unit cell (Tazzoli and Domeneghetti, 1980). Lattice plane terminations were chosen based on exposure of positively charged atoms (calcium) expected to interact with our negatively charged poly-Asp₈₆₋₉₃ peptide, and based on reasonable estimates of relative stability for individual crystallographic faces. While multiple lattice plane terminations were run in the simulations, we present here the data

for simulations of the {110} face during growth of an atomic plane terminating in high-calcium density potentially available for extensive electrostatic peptide/protein binding which could in turn stabilize this termination. For the {101} face modeled here, we chose the normally stable termination leading to charge neutrality with the uppermost calcium-containing layer being partly buried under oxalate or lattice-incorporated H₂O groups.

6.5 Results

Immunohistochemical staining of human calcium oxalate kidney stones for osteopontin (Figure 1a, a rhombic-shaped crystal at its centre) often show layers/lamellae of concentrically deposited organic matrix surrounding apparent niduses of calcification; the layered appearance of the stones reflects the alternating cycles of crystal and matrix protein deposition at the growing stone surface (McKee et al., 1995). OPN is most abundantly localized within the lamellae as reported on previously using colloidal-gold immunolabeling (McKee et al., 1995). In addition to the strong immunolabeling of the lamellae, moderate OPN labeling was detected within the mineral compartment of the kidney stones (here intentionally decalcified during sample preparation to allow ultrathin sectioning and colloidal-gold immunolocalization of OPN by TEM; Figures 1b,c). In addition to immunogold labeling for OPN of the thin protein layer circumscribing individual crystals in decalcified samples of the stones (Figure 1b), generally vacant, more central areas often had some residual matrix retained by the aldehyde (added to the decalcifying solution specifically for this purpose of retaining protein) that had clearly angular profiles reflecting the previously existing crystalline mineral phase (Figure 1c).

In the urine calcium oxalate precipitation experiments, crystals formed by increasing the calcium concentration and examined by SEM showed the typical di-pyramidal shapes characteristic of COD (Figure 1d). Western blotting of urine was positive for OPN, and the total protein extract obtained from precipitated, washed and subsequently decalcified crystals revealed particularly abundant OPN released from the COD crystals (Figure 1e). Taken together, these results confirm previous reports describing that OPN is a major protein component of urine in healthy persons, that OPN is abundant in

human kidney stones, and that OPN binds to COD crystals. More specifically, the intracrystalline immunogold localization data provide supporting evidence that a portion of the OPN likely resides within the mineral phase.

To elucidate how OPN might modify crystal chemistry and habit, and whether OPN and OPN peptides might incorporate into COD crystals, COD precipitation experiments were carried out in aqueous $\text{CaCl}_2\text{-Na}_2\text{C}_2\text{O}_4$ solutions in the presence of full-length purified OPN or a synthesized 8-amino acid poly-Asp peptide of OPN. In these crystal growth experiments, more than 90% of the crystals precipitated as COD having characteristic tetragonal symmetry. Figure 2 shows that upon addition of OPN to the growth solution, the COD was more cuboidal in its crystal habit with the formation of extensive $\{110\}$ prismatic faces (Figure 2a), in contrast to having a $\{101\}$ more dipyrnidal structure in the pure (control) system without protein/peptide (lower inset in Figure 2a). The $\{110\}$ prismatic faces of COD gained in morphologic importance (in their dimension) with increasing OPN, a result indicating that OPN interacts and modifies particularly these faces (Figures 2b-d). At an OPN concentration of 0.93 mM, elongated crystals started to appear attributable to $\{110\}$ face-inhibition by OPN (Figure 2c). At higher OPN concentrations, practically all COD crystals exhibited the elongated shape, often intergrown as penetration twins (Figure 2d).

Given the high content of negatively charged aspartic acid residues in OPN and the presence of a contiguous stretch of these amino acids (residues 86-93) proposed to bind to calcium at the positively charged surface of COD, we performed COD precipitation experiments in which synthetic linear poly-Asp₈₆₋₉₃ was used in the same crystal growth conditions to compare the effects of this peptide with full-length OPN. Increases in poly-Asp₈₆₋₉₃ concentration, although less effective than full-length OPN (crystals showed delayed and less elongation), likewise enhanced the $\{110\}$ prismatic face dimensions (Figure 3a). Similar experiments using commercially purchased poly-Asp (Sigma), a large polymer of aspartic acid, exerted the most significant modification of COD morphology (Figure 3b), not altogether surprising given the relatively high-molecular weight (5-15 kDa) linear repeats of high unit charge.

To examine possible incorporation of the poly-Asp₈₆₋₉₃ linear peptide into the COD crystal interior, conventional and confocal fluorescence microscopy were used to

examine the localization of fluorescently tagged poly-Asp₈₆₋₉₃ (FAM-poly-Asp₈₆₋₉₃). By conventional fluorescence light microscopy, COD crystals grown in the presence of FAM-poly-Asp₈₆₋₉₃ displayed various polygonal fluorescence patterns (Figure 4a) indicating incorporation (occlusion) of the peptide into COD crystals. The pattern of incorporation was that of sectoral compositional zoning crystallographically related to the elongated {110} face, and thus could be indexed as {110} zoning (insets in Figure 4a) using SHAPE crystal analysis software. The incorporation of FAM-poly-Asp₈₆₋₉₃ at the {110} prismatic faces of COD crystals led not only to its inclusion but to the dose-dependent effect on the area and shape of these prismatic faces (Figure 4b). The formation of these compositional zoning patterns in COD crystals was confirmed by laser scanning confocal microscopy (Figure 4c), which enables “optical sectioning” to exclude out-of-focus flare and thus allows direct imaging of crystal interiors. (Grohe et al., 2007) These two-dimensional zoning patterns vary in appearance with the “depth” of the optical focus and allowing confirmation of the sectoral zoning through different focal planes (Figure 4c). Figure 5 summarizes how increasing OPN and poly-Asp₈₆₋₉₃ concentrations inhibit the {110} faces of COD leading to their increased relative prominence and resulting in elongated COD crystal morphology and specific {110} sectoral zoning within these crystals.

To investigate the mechanism underlying this face-specific interaction of poly-Asp₈₆₋₉₃ with COD, we modeled poly-Asp₈₆₋₉₃ adsorption to {110} and {101} crystal faces of COD (Figures 6a,b) using a Monte Carlo plus-minimization structure-prediction algorithm. In previous studies we have shown that this approach successfully predicted the binding of the salivary protein statherin to hydroxyapatite, in agreement with experimental solid-state NMR data (Makrodimitris et al., 2007; Masica and Gray, 2009). Our calculations predict considerably stronger poly-Asp₈₆₋₉₃ binding at the COD {110} surface relative to that of the COD {101} surface (Table 1). This prediction suggests stronger inhibition (higher relative stabilization) of the COD {110} surface compared to the {101} surface – a prediction consistent with our experimental observations demonstrating a gain in relative prominence of the {110} faces on COD crystals grown in the presence of protein/peptide (Figure 3).

In the majority of the top-scoring configurations for poly-Asp₈₆₋₉₃ adsorbed to the high-calcium density {110} surface, the carboxylate residues of the peptide bind to calcium very strongly (Figures 6c and e). This strong, electrostatic binding of poly-Asp₈₆₋₉₃ to the {110} face typically occurs through four or five aspartate carboxylate groups linked with crystal-surface calcium atoms such that a high degree of lattice matching can be observed between the peptide and {110} face (Figures 6c,e). The binding between carboxylate residues and calcium on the {110} face of COD yielded an average distance of 0.47 nanometres for the top-100 scoring decoys. In contrast, in the case of poly-Asp₈₆₋₉₃ binding to the {101} face, the aspartate and leucine residues contribute only moderate hydrogen bonding with the {101} crystal surface upon peptide adsorption (Figures 6d,f; hydrogen bonds shown as yellow dashed lines represent degenerated, resonant donor-acceptor pairs) (Kortemme et al., 2003; Morozov et al., 2004). This significant binding of the peptide by hydrogen bonds to the COD {101} face is frequently balanced by desolvation penalties, thus rendering a binding energy near zero.

Modeling also indicates that the poly-Asp₈₆₋₉₃ peptide is mostly linear and unstructured in solution, but becomes slightly more structured (less dispersed) upon adsorption to the {101} face, and less structured (more dispersed) upon adsorption to the high-calcium {110} face (data not shown).

6.6 Discussion

Normal human urine is supersaturated with respect to calcium oxalate minerals, and it has been estimated that 1×10^7 calcium oxalate crystals can be produced and excreted daily in a healthy (non-stone forming) individual (Koul et al., 1999). In the face of these high ionic concentrations, inhibitory mechanisms must be in place to prevent pathologic calcification in the kidney and urine. In addition to small-molecule inhibitors like citrate, currently available *in vitro* and *in vivo* evidence suggest that urinary proteins such as OPN and trefoil factor 1 (TFF1) present in urine likewise serve as inhibitors of calcification (Chutipongtanate et al., 2005; Kleinman et al., 2004; McKee et al., 1995; Wesson et al., 2003; Worcester, 1996), and moreover, may potentially decrease crystal retention and aggregation (Koul et al., 1999; Wesson et al., 2003). In addition, emerging

data show that OPN may potentially direct the formation of COD, and in the process incorporate (occlude) into the crystal structure (Ryall et al., 2005; Ryall et al., 2001; Wesson et al., 1998). Interesting proposals for this occlusion include facilitating dissolution of the crystals from the inside-out by providing intracrystalline channels for fluid movement, and facilitating phagocytosis of crystals by renal tubular cells for clearance of crystals from the urine (Chauvet and Ryall, 2005; Fleming et al., 2003; Grover et al., 2008; Ryall et al., 2001).

In the present study, our objective was to examine how full-length OPN and one of its acidic peptides affected COD crystal growth and morphology, and where small biologically relevant peptides might incorporate into COD. Such information would provide insight into when, where and how biological molecules affect crystal growth and subsequent “maturation” or dissolution/clearance within the kidney and urine. Our data, deriving from several different experimental approaches, *i*) confirm the presence and binding of OPN in kidney stones and in COD crystals precipitated from healthy human urine, *ii*) show immunogold localization at the ultrastructural level consistent with the notion that OPN epitopes can be found at the surface of, and within, crystal interiors, *iii*) demonstrate OPN peptide occlusion into COD in a sectoral compositional zoning pattern, and *iv*) show that both full-length OPN and its poly-Asp₈₆₋₉₃ peptide have significant and similar effects on COD crystal morphology – effects that ultimately might modify the fate of these crystalline particles in the context of this modification either reducing or promoting stone formation.

The concentric, lamellar immunohistochemical staining pattern for OPN commonly seen in kidney stones confirms that the protein is deposited in cyclical episodes that represent “growth rings” over time as the calcified mass grows within the urine/kidney. Both the concentric lamellae of matrix and perpendicularly arranged interlamellar organic structures (radial striations) all immunolabel intensely for OPN (Khan, 1997; McKee et al., 1995). We extend these findings by showing that in addition to a surface coating of protein, a fine, flocculent organic material is frequently present in decalcified samples within the boundaries of profiles that clearly reflect crystalline structures present prior to the decalcification procedure (Figure 1c). More specifically, we show that the crystal-coating layer and the internal flocculent material label strongly for OPN.

Collectively, these localization studies at the light and electron microscopic levels suggest extensive incorporation of organics (and OPN) into all compartments of kidney stones.

A better temporal appreciation of organic inclusion into kidney stones can be obtained by intentionally and controllably inducing COD precipitation in urine which contains proteins that would likely be present and sequestered (more slowly) into kidney stones because of their mineral-binding potential. The morphology of such precipitated COD shows {101} tetragonal di-pyramidal shapes typically seen in human urinary calculi (Berg et al., 1979; Berg et al., 1976; Gibson, 1974; Werness et al., 1981) (our Figure 1d). The {101} tetragonal di-pyramid COD is the “equilibrium morphology” of COD generally equilibrated with growth medium, and this form often can be found in either pure growth solutions (as discussed below) or in impurity-loaded complex fluids where reactions have a propensity to reach an equilibrium state. Different growth conditions frequently used for the study of calcium oxalate commonly show at least some crystals of both the monohydrate and dihydrate forms. In an example of an equilibrated state, calcium oxalate crystals found in the major sources of commercially available fetal bovine serum (FBS) routinely supplied as a growth- and differentiation-inducing supplement for cells in culture have been reported to sequester numerous proteins from the serum, and most of the COD crystals adopted the {101} tetragonal di-pyramidal shape (Pedraza et al., 2008). In this same study, Western blotting for OPN from protein extracts derived from the crystals separated from the FBS confirmed likewise in this case the presence of abundant OPN bound by the crystals.

To assess the inhibitory potentials of OPN and its poly-Asp₈₆₋₉₃ peptide on COD crystals, we performed COD growth experiments in the absence or presence of these organic molecules at physiologically relevant (or higher) concentrations (Thurgood et al., 2008). With increasing protein/peptide, the COD crystals become elongated along the *c*-axis to form rod-shaped morphologies as the {110} tetragonal prismatic faces became dominant; these were capped with small {101} pyramids and other diminishing faces ({121} and {001}). This rod-shaped COD morphology – identified and referred to as the dodecahedral form of COD by Daudon and colleagues (Daudon, 2008) based on *in vivo* observations at optical-microscopic resolution – rapidly became the predominant

shape, with penetration twins of these crystals becoming frequent at relatively high concentrations of OPN, linear poly-Asp₈₆₋₉₃ or commercial poly-Asp. The rod-shaped COD morphology is commonly seen in plant tissues where calcium oxalates are a common mineral phase. Interestingly, this form of COD has also been reported in patients having severe uremia (Lewis et al., 1974) or severe hypercalciuria (Daudon et al., 2004; Daudon, 2008). Calcium oxalate crystalluria particles experimentally induced in the urine of rats often showed elongated, dumbbell-shaped morphologies that were similarly reflected by the organic component of these particles following their decalcification (McKee et al., 1995). It is very likely that the elongated, rod-shaped COD represents a severe pathologic form of calcium oxalate commonly seen in both human stone disease and in a variety of animal models. To the best of our knowledge, this comprises the first *in vitro* report describing how a urinary protein or its peptide fragments facilitate the formation of rod-shaped COD crystals to resemble those observed in some severe renal stone diseases. Thus, our work here provides mechanistic insight into the lithogenic conditions and etiology that lead to the formation of various forms of COD in patients, and thus may be useful in clinical diagnosis (Daudon, 2008).

The development and preponderance of the {110} prismatic faces of COD observed in the present study reflect a kinetic response to increasing OPN/peptide concentration in solution, suggesting that these organic molecules inhibit growth through direct inhibitory binding of OPN/peptide to these crystallographic faces. Such face-specific binding inhibits crystal growth perpendicular to that face, as discussed for biologic calcification systems (Addadi and Weiner, 1985). The more OPN/peptide molecules present in a solution, the farther the COD morphology deviates from the equilibrium state, and more elongated crystals are formed (Figures 5a, b). Conserved among many mammalian and avian species, our selected poly-Asp₈₆₋₉₃ peptide is a linear, contiguous stretch of amino acids rich in aspartic acid as found in the primary sequence of OPN (Oldberg et al., 1986) – and proposed to be one of the potent mineral-binding motifs of this protein (Hoyer et al., 2001; Sodek et al., 2000). It has been shown that small, linear acidic polypeptides, some artificially constructed and others reflecting real protein sequence, can potentially regulate the kinetics of biomineral growth (inhibition (Elhadj et al., 2006b;

Hoyer et al., 2001; Wang et al., 2006) or acceleration (Elhadj et al., 2006a; Kim et al., 2006)) and impurity-mineral interactions (Stephenson et al., 2008).

To provide information on a possible mechanism for binding, inhibition and occlusion of poly-Asp₈₆₋₉₃ related to COD crystal growth, we have used a modeling/simulation method (to our knowledge, the only one available) capable of accurately predicting the folding of a protein/peptide onto a solid-state (here mineral) surface (Makrodimitris et al., 2007; Masica and Gray, 2009). This method allows for structural visualization and calculation of comparative adsorption energies of peptides to different mineral faces. The computational modeling predicts that the small, highly charged poly-Asp₈₆₋₉₃ peptide is unstructured in solution, without specific orientation of functional side chains. Upon adsorption to COD crystals, the peptide may bind the crystal surface in one or more of many configurations. The binding energy of poly-Asp₈₆₋₉₃ at the {101} face is approximately zero because the peptide-COD hydrogen bonding is frequently balanced by desolvation. Also, this face is stable and facilitates minimal electrostatic interaction. Therefore, polyAsp₈₆₋₉₃ adsorption at the COD {101} face is weak and minimally disruptive to the peptide intramolecular interactions (i.e., transient binding). Conversely, the strong binding predicted at the high-calcium terminated {110} COD surface is disruptive to peptide intra-molecular contacts. Binding of poly-Asp₈₆₋₉₃ to the {110} surface is mostly electrostatic, with minimal hydrogen bond contributions to the binding energy.

That poly-Asp₈₆₋₉₃ peptide was less inhibitory than full-length OPN is not surprising given the large number of acidic amino acid stretches found in OPN, and given that the protein is extensively post-translationally modified by phosphorylation. All these features of OPN, in its full-length form, would provide additional negative charges potentially clustered as groups and available for inhibitory crystal binding (Gericke et al., 2005; Kazanecki et al., 2007; Pampena et al., 2004). In all scenarios, charge density may be a critical factor in determining the binding of OPN peptides. In addition to charge density, other characteristics of OPN and poly-Asp₈₆₋₉₃ peptide in solution, such as hydrophilicity, may also account for abilities to influence growth of calcium oxalate minerals (Elhadj et al., 2006a; Stephenson et al., 2008).

Fluorescent molecules and fluorescently-tagged proteins have been previously and effectively used to study protein-mineral interactions (in COM studies (Grohe et al., 2007; Hunter et al., 2009; O'Young et al., 2009; Taller et al., 2007; Touryan et al., 2001)). Extending this approach to COD and using a poly-Asp₈₆₋₉₃ peptide not previously examined by others, we have visualized by light and confocal microscopy the incorporation behavior of this peptide into the crystal structure of COD and revealed distinctive and informative 3-dimensional sectoral (compositional) zoning patterns (Hunter et al., 2009; O'Young et al., 2009; Reeder and Grams, 1987; Touryan et al., 2001) that provide significant new insight into protein occlusion into biominerals. A promising scenario is that the selective, specific incorporation and segregation of fluorescent FAM-poly-Asp₈₆₋₉₃ into pyramidal regions of a COD crystal, reflecting continuous binding to the {110} prismatic faces during COD growth, thus provides an example of creating an experimental visual record of the temporal and spatial occlusion of organics within a biomineral. The fluorescently labeled pyramidal growth sectors begin their formation at the centre of the COD crystal and extend to the bases of the pyramids reflecting continuous and gradual enlargement of the {110} faces attributable to peptide inhibition at these sites. Different pyramidal growth sectors within the same crystal meet centrally at their apices, and changes in fluorescence across adjacent growth sectors are abrupt – no fluorescence is seen in adjacent growth sectors that are not {110} sectors. This abrupt change in fluorescent peptide incorporation corresponds to sector boundaries reflecting interfacial compositional changes in COD crystal structure. Taken together, these results demonstrate that poly-Asp₈₆₋₉₃ (and very likely other acidic peptides of OPN generated by proteolytic cleavage) binds to COD, inhibits growth normal to the {110} face, and exclusively occludes into its {110} growth sectors. These results are consistent with a variety of other *in vitro* studies suggesting intracrystalline OPN in urinary COD crystals (Grover et al., 2008; Ryall et al., 2005; Ryall et al., 2001; Wesson et al., 1998).

Of interest here, as deduced from simulation, is a possible scenario where the majority of polyAsp₈₆₋₉₃-carboxylate groups bind the {110} COD surface, but leave remaining carboxylate groups available (or partially available) for binding of initially non-lattice calcium in solution. Strong peptide binding at the {110} crystal surface,

followed by the chelation of free calcium ions by solvent-exposed peptide carboxylate groups, might participate in the observed occlusion of peptide during further slow mineralization at that face.

The concept of protein inclusion (occlusion) into the crystal structure of biominerals has been commonly accepted as a strategy adapted by organisms to attain control over mineralization (Albeck et al., 1996). In regulating biomineralization, intracrystalline proteins likely simultaneously (or uniquely) impart additional functional properties to the final structure of the biomineral, such as, amongst others, mechanical strength, optical characteristics, or varying textures (Aizenberg et al., 1995; Berman et al., 1988). In calcitic avian eggshell, for example, an extremely abundant organic matrix network occludes into the mineral phase, and OPN is a prominent protein of this matrix (Chien et al., 2008). Intracrystalline organics can also be components of biominerals that dislocate the mineral structure, distorting crystal lattice (Pokroy et al., 2006) and modifying their thermodynamic properties (De Yoreo, 2003), thus rendering them more unstable and dissolvable. In this regard, recent studies have shown that urinary proteins situated within the bulk mineral phase of calcium oxalate raise lattice strains and reduce crystallite size because of intracrystalline defects and discontinuities, which in turn allow proteolytic invasion and crystal dissolution (Fleming et al., 2003; Ryall et al., 2001; Ryall et al., 2007).

In our *in vitro* crystal growth experiments, the selective and nonequilibrated incorporation of peptide within COD crystals results in the formation of compositional zoning. The consequent sectoral intracrystalline heterogeneity suggests that the sectors containing occluded peptides may have different functional properties from neighboring sectors within the same crystal. In the context of the discussion above relating largely to the work done by Ryall and colleagues, and in linking this to physiologic defenses designed to decrease detrimental pathologic calcification as seen in uro/nephrolithiasis, one consequence of this may be that COD sectors with occluded peptide are susceptible to proteolytic, degradative “attack” by proteases, whose removal of occluded organics would increase the dissolution rate of the mineral phase or increase the urinary clearance of these particles. Moreover, in this scenario, these {110} sectors become dominant with increases in peptide concentration, and more intracrystalline peptides are

sequestered within the COD, which in turn might ultimately promote their dissolution and/or clearance fate. Additional information about the surface and internal structure of the {110} faces and sectors is required to clarify whether this preferential interaction of peptides of OPN may favor the binding of COD crystals to renal epithelial cells, and whether it is involved in the internalization of COD crystals via the phagocytic/endosomal pathway (Grover et al., 2008; Lieske and Deganello, 1999).

6.7 Conclusions

The data reported here are consistent with an increasing number of reports describing protein/peptide occlusion in the “inorganic” phase of biomineralizing systems, and they provide an explanation for the presence and intracrystalline localization of abundant OPN and other proteins in kidney stones and in COD crystals artificially precipitated from urine. Intracrystalline proteins in biominerals can modify internal structure and physical properties of the mineral in which they reside. Proteins found in urine that incorporate into calcium oxalate crystals may perform a role in forming or inhibiting calcium oxalate urolithiasis. Our results show that with increasing OPN or poly-Asp₈₆₋₉₃ concentrations in growth solutions, the {110} faces are greatly increased and eventually dominate the crystal morphology. The poly-Asp₈₆₋₉₃ peptide of OPN may be central to OPN’s effects on the {110} faces of COD, since its actions were similar on these faces. Finally, mineral-binding peptides of OPN may incorporate into {110} faces to develop {110} sectoral compositional zones in the crystals which may serve additional purposes related to crystal dissolution at later times.

6.8 Acknowledgements

This work was funded by Canadian Institutes of Health Research grant MT11360 to MDM, and by the Arnold and Mabel Beckman Foundation. The authors also wish to thank Dr. Denise Arsenault for her input during the course of this study, and Dr. Esben Sørensen and Arla Foods for the generous supply of osteopontin protein.

6.9 Supporting Data

Coordinate files in Protein Data Bank format for the ten lowest-scoring models of the OPN peptide bound to the {101} and {110} faces of COD.

Table 1. Poly-Asp₈₆₋₉₃ peptide-COD adsorption energies in kcal/mol (estimated by RosettaSurface)^a

COD Crystal Surface	{101}	{110} high calcium
Adsorption Energy (kcal/mol)	-2.5±5.7	-23.4±6.2

^a Binding energy (kcal/mol) is the difference between the mean energies of 100 lowest-energy adsorbed- and solution-state candidate structures (error given is standard deviation).

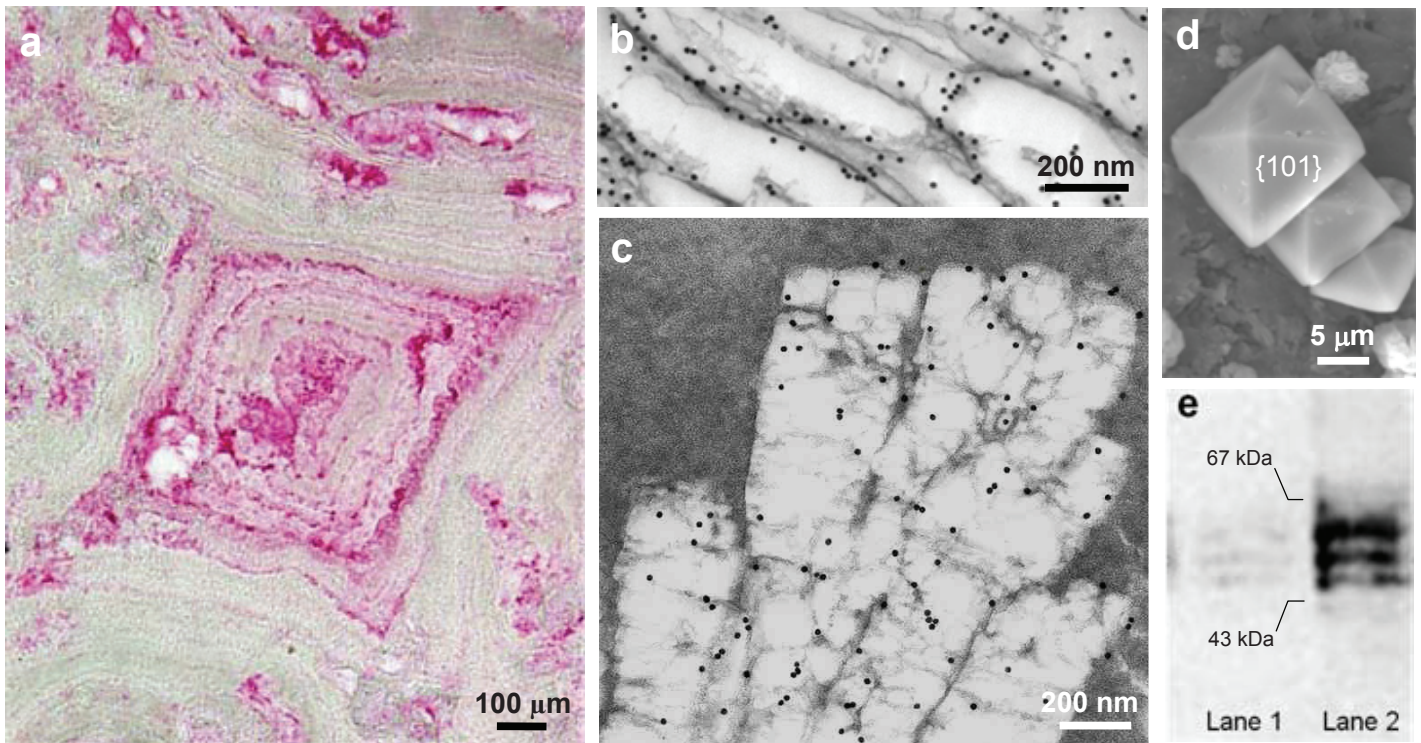


Figure 1. (a) Immunohistochemical localization of OPN in human kidney stone by light microscopy. Concentric layers/lamellae of organic matrix, rich in OPN, radiate from apparent niduses of calcification. (b,c) At the ultrastructural level, colloidal-gold immunolabeling for OPN viewed by transmission electron microscopy shows OPN variably concentrated either at crystallite surfaces (b), here seen as voids after sample decalcification, or within the crystallites (within the void) and associated with a flocculent organic material evident after decalcification (c). (d) Scanning electron micrograph of calcium oxalate dihydrate (COD) crystals precipitated from normal male human urine by oxalate addition. Typical di-pyramidal COD crystals show prominent {101} crystallographic faces. (e) Western blots for OPN of normal human urine (Lane 1) and the protein extract of COD crystals precipitated from normal human urine (Lane 2).

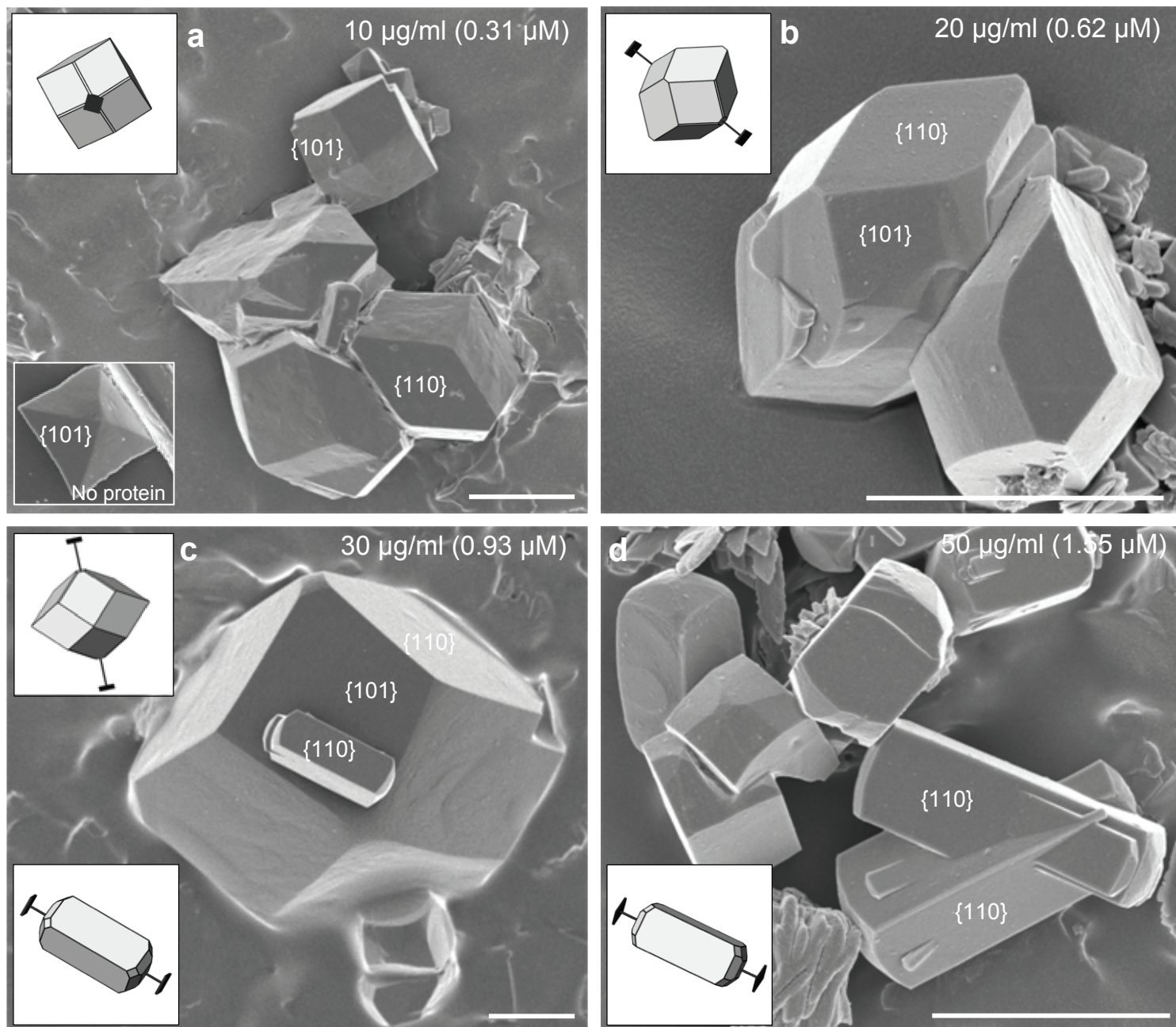


Figure 2. (a-d) Scanning electron micrographs of COD grown in solution in the presence of full-length, phosphorylated OPN at the indicated concentrations. With increasing amounts of OPN, the {110} prismatic crystallographic faces of COD grow in dimension and become predominant at the expense of the {101} faces, the latter being the predominant crystal face formed in the absence of added protein (lower inset in panel a). At the highest concentration of OPN used (d), most COD crystals are elongated and often intergrown as penetration twins. Schematic insets show SHAPE software-derived renditions of the crystals used for face identification and *c*-axis determination (blue extension bars). Scale bars equal 5 µm.

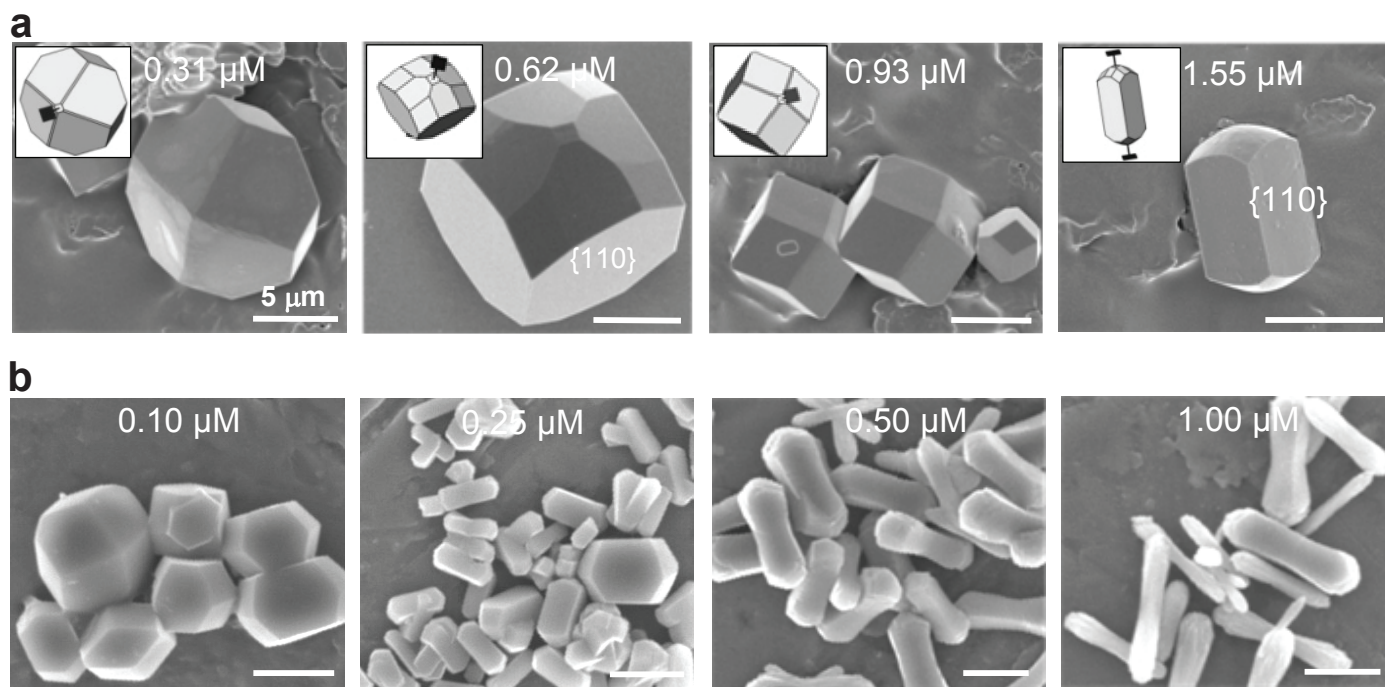


Figure 3. Scanning electron micrographs of COD grown in solution in the presence of synthetic, low- (a) and high- (b) molecular weight aspartic-acid rich peptides at the indicated concentrations. (a) Increases in linear poly-Asp₈₆₋₉₃ concentration (sequence from OPN bovine sequence), while not as effective as full-length OPN, induced a similar elongating effect on COD crystal morphology – increasing the {110} faces at the expense of the {101} faces. (b) High-molecular weight and poly-Asp (Sigma) was more potent in similarly generating rod-shaped crystal morphologies, with some additional “rounding” effect at the poles of the elongated crystals. Schematic insets show SHAPE software-derived renditions of the crystals used for face identification and *c*-axis determination (blue extension bars). Scale bars equal 5 μm .

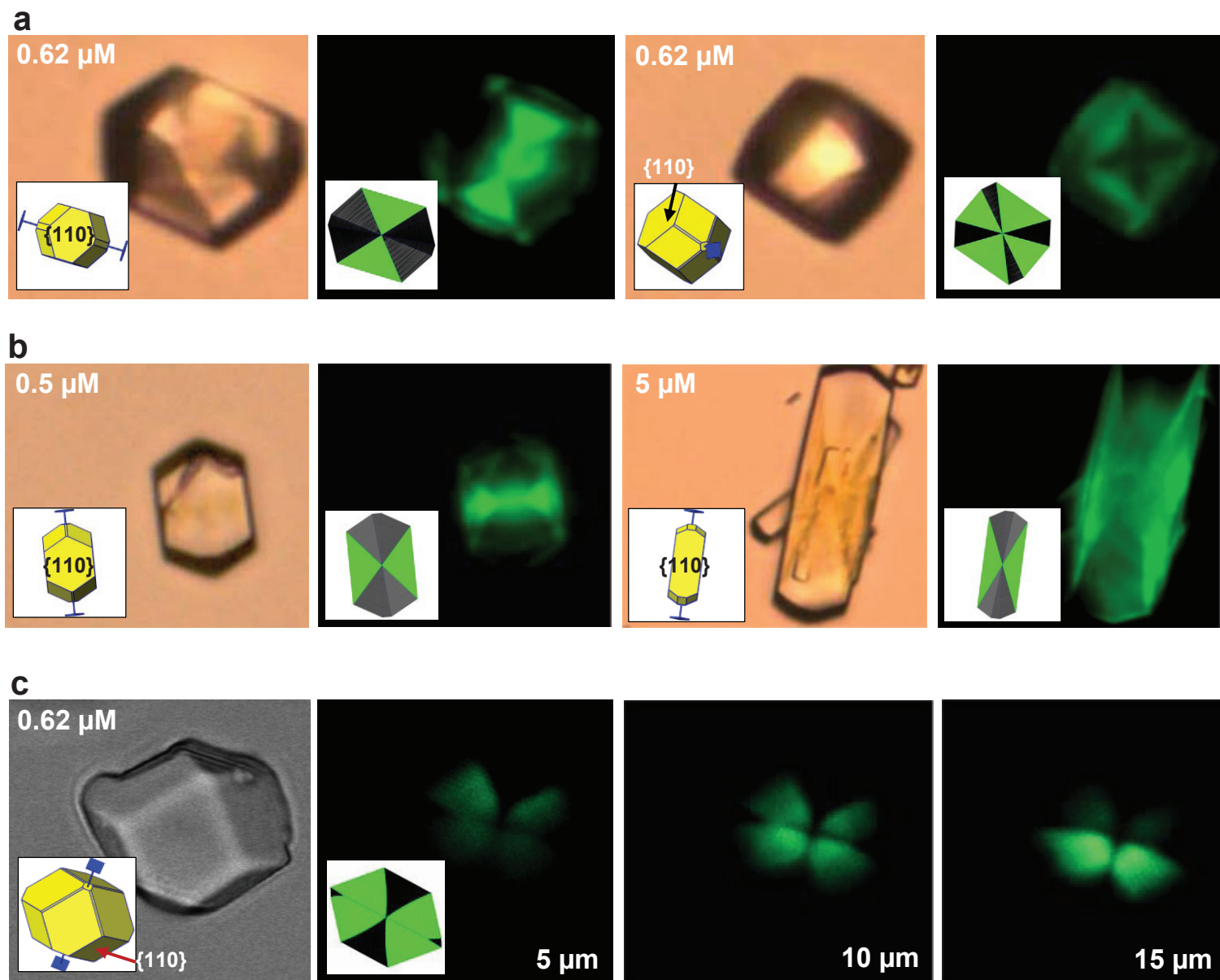


Figure 4. Conventional fluorescence micrographs, and laser confocal micrographs, of COD crystals grown in the presence of fluorescently-tagged poly-Asp₈₆₋₉₃ at the indicated concentrations. (a,b) Pyramidal, compositional (sectoral) zoning is observed in COD crystals reflecting selective incorporation during growth of fluorescently-tagged poly-Asp₈₆₋₉₃ specifically into {110} crystal sectors. Because of differences in orientation, the zoning pattern changes in appearance despite the crystals having similar morphology. Concentration of peptide affects the relative dimensions of the sectors, as well as the area and shape of {110} prismatic faces (as in Figure 3a). In this non-confocal image, fluorescence may originate from the interior of the crystal as well as from exterior faces. (c) Laser scanning confocal microscopy with focal plane imaging performed within crystal interiors (here shown for a crystal at a scanning depth of 5, 10 and 15 μm from the top of the crystal) confirms sectoral compositional zoning within COD crystals, revealing the boundaries of {110} crystal sectors. The overall morphology of the imaged crystal is shown by transmitted light in the left-most panel. Schematic insets show SHAPE software-derived renditions of the crystals used for face identification and *c*-axis determination (blue extension bars).

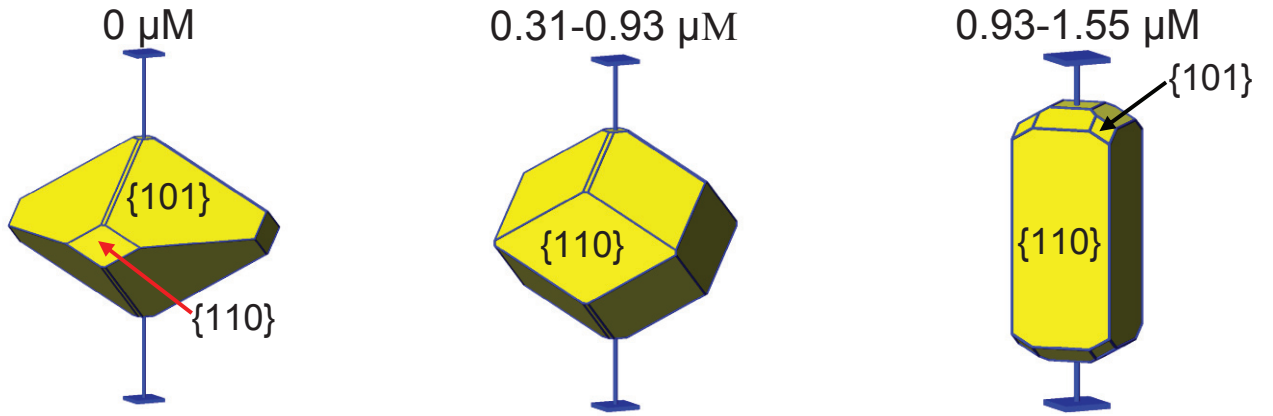
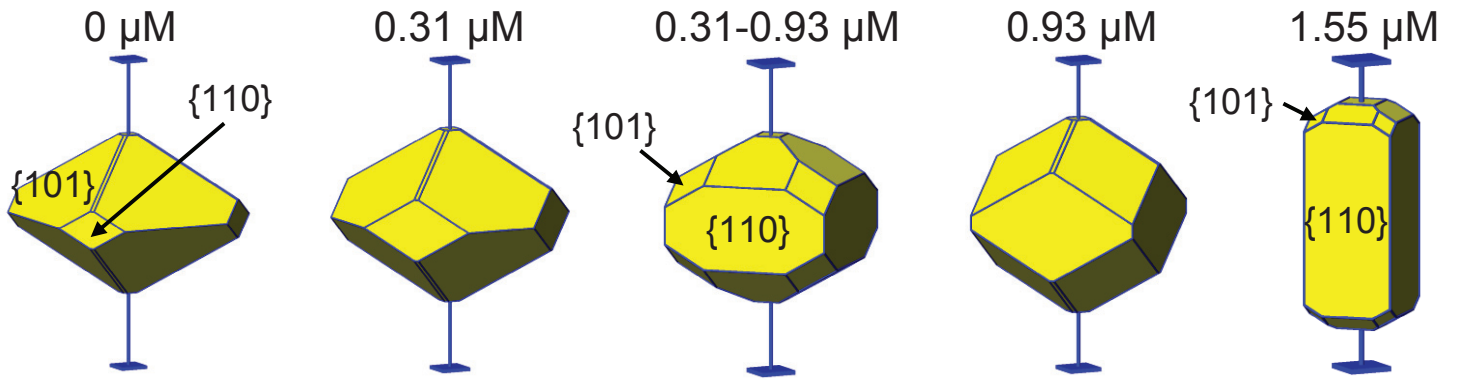
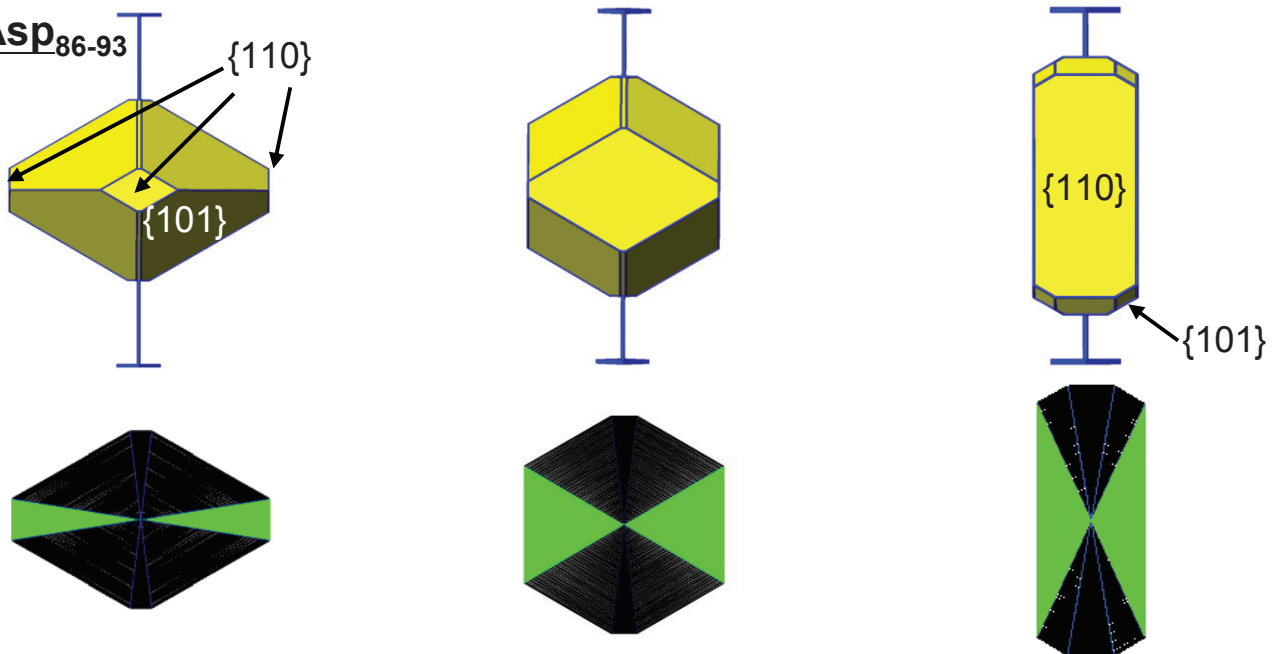
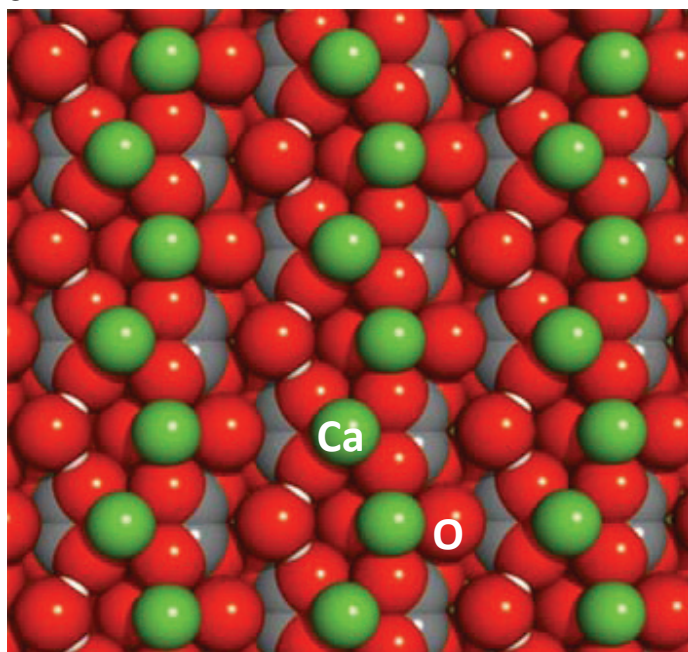
(a) OPN**(b) Poly-Asp₈₆₋₉₃****(c) Poly-Asp₈₆₋₉₃**

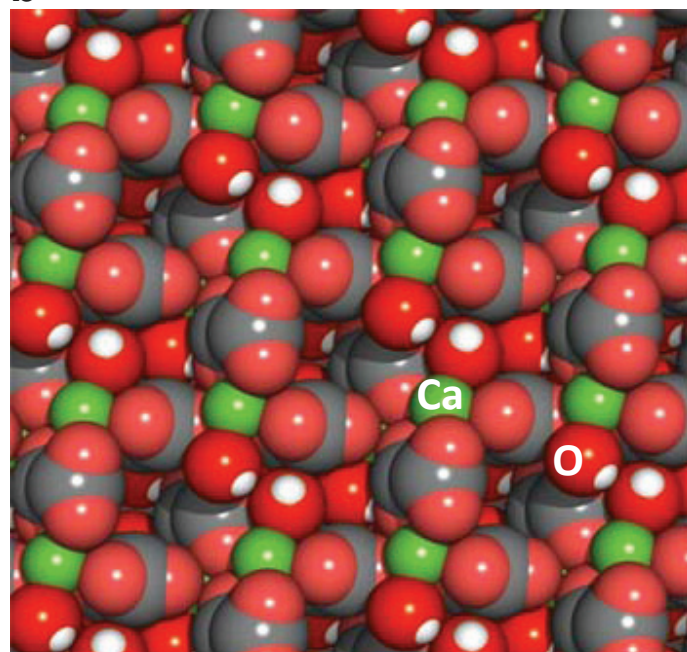
Figure 5. Summary of data using SHAPE software renditions of effects of full-length OPN and poly-Asp₈₆₋₉₃ peptide on COD crystal growth morphology (a,b), and of occlusion of poly-Asp₈₆₋₉₃ into COD in a sectoral compositional zoning pattern arising from {110} face binding of this peptide (c). Increases in OPN or poly-Asp₈₆₋₉₃ concentrations in growth solution kinetically result in similar effects on COD crystal morphology – the same faces {110} are significantly inhibited and become predominant, and COD crystals elongate along their *c*-axis. {110} sectoral zones become dominant with increases in poly-Asp₈₆₋₉₃ concentration, and the 3 schematics in the bottom row represent 2-dimensional planes taken from the center of COD crystals where poly-Asp₈₆₋₉₃ incorporation (in increasing solution concentration from left-to-right) is shown by green triangles in two (of four) adjoining pyramidal sectors. The {110} sectors (green) gain in proportion relative to other crystal-face sectors (black) as poly-Asp₈₆₋₉₃ concentration increases.

$\{110\}$

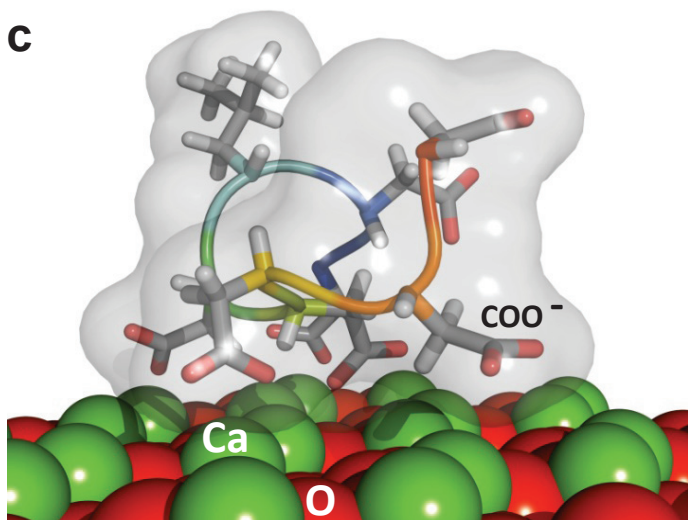
a

 $\{101\}$

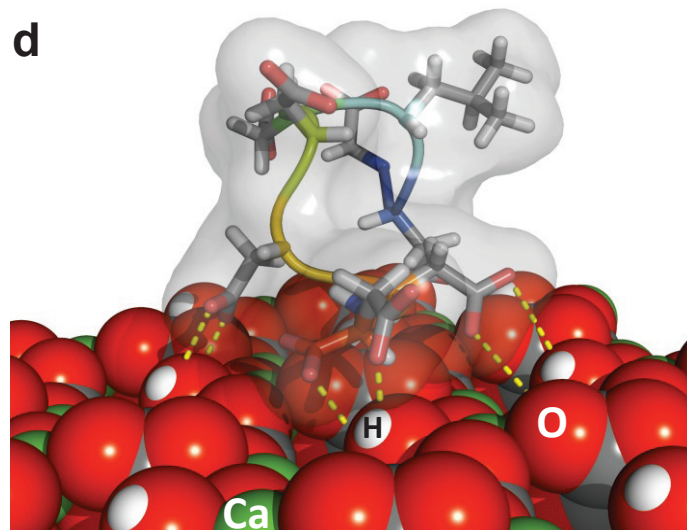
b



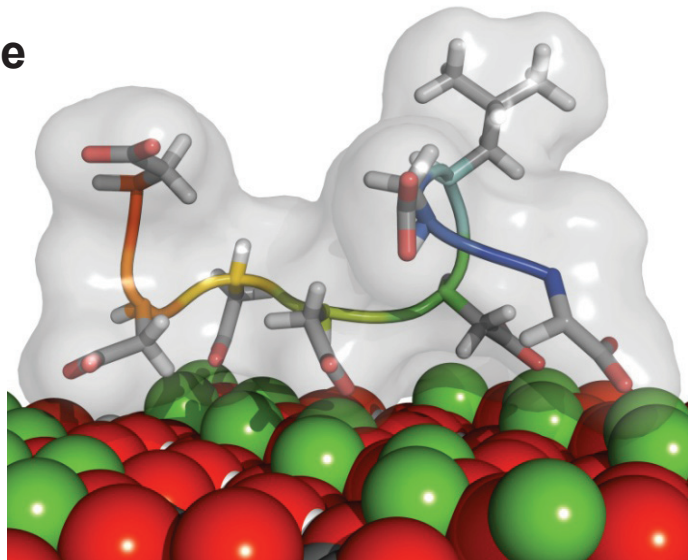
c



d



e



f

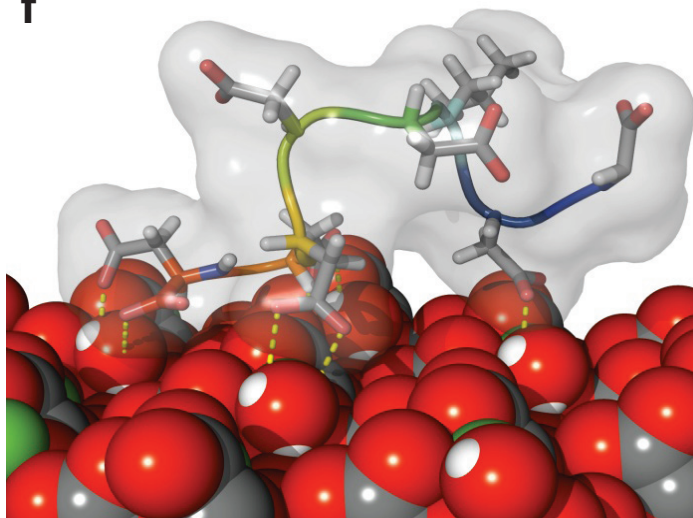


Figure 6. Molecular modeling of poly-Asp₈₆₋₉₃ peptide binding to {110} and {101} crystallographic faces of COD. Atomic configurations used for modeling at the surfaces of the {110} face (a) and {101} face (b) of COD. (c-f) Representative, top-scoring (low-energy) models of poly-Asp₈₆₋₉₃ adsorbed onto COD. (c,e) Two lateral views (approximately 90° to each other) of poly-Asp₈₆₋₉₃ bound to a high-calcium density plane in the {110} face of COD (with the N-terminal of the peptide extending beyond the image plane in panel (c), and with the N-terminal of the peptide to the right in panel (e)). Some degree of lattice matching for five carboxylate (COO⁻) side chains aligned with calcium (Ca) atoms occurs on the {110} face in this profile. (d,f) Two lateral views (approximately 90° to each other) of poly-Asp₈₆₋₉₃ bound to the {101} face of COD (with the N-terminal of the peptide extending beyond the image plane in panel (d), and with the N-terminal of the peptide to the right in panel (f)). Hydrogen bonding is schematically illustrated by dashed yellow lines connecting donor-acceptor pairs. (Ca, green; C, grey; O, red; H, white).

Chapter 7

Conclusions

Construction of the avian eggshell is one of the fastest known mineralizing systems in biology, with gram amounts of calcium carbonate mineral (calcite) and matrix proteins being deposited within hours. Yet, despite this rapid construction, the architecture of the avian eggshell is remarkably ordered and compartmentalized for achieving its biologically functionalized purposes. The studies presented in this thesis provide substantial new information describing the detailed ultrastructure of a hardened composite material consisting of a protein network and calcite mineral – the avian eggshell. An extensive matrix network with variable, region-specific ultrastructure and highly systematic organization co-exists with a calcitic mineral phase within the eggshell, and this is described across the thickness of this biological structure.

Within the matrix network in the eggshell, the inhibitory protein OPN is intimately associated with most of the matrix found throughout the thickness of the shell except for the vesicular structures in the palisades layer and the membrane structures of the calcium reserve body sac. This protein is secreted from the epithelial cells of the eggshell gland during shell formation. Both *in vivo* and *in vitro*, OPN preferentially interacts with the {104} face of calcite where it likely functions to guide calcite orientation by inhibiting/stabilizing this specific face and modifying calcite morphology in the eggshell. In addition, OPN appears at eggshell {104} fractured surfaces, suggesting that it resides as an occluded protein. OPN is also a prominent interfacial protein, accumulating at the boundaries of various eggshell compartments where it may inhibit or terminate calcification at those margins to delimit different eggshell structural units and retain the patency of the eggshell pores (used for gaseous exchange). In this way, OPN might also regulate eggshell growth to establish the characteristic cone / columnar architecture to assure normal biologic functions of the eggshell. Definitive studies on OPN function in eggshell will require *in vitro* crystal growth systems that more faithfully

reflect the total composition of eggshell. Alternatively, transgenesis in chickens while not on the immediate horizon, would allow for *in vivo* assessment of the role of OPN if mutations and/or deletions in the OPN gene could be established in this animal.

As a primary source of calcium essential for chick embryonic skeletal growth, avian eggshell releases calcium ions through physiologic dissolution of specific interior regions in a process that serves multiple functional purposes, including shell-weakening for hatching and serum acid-base balance in chick embryo. Following the detailed ultrastructural investigations of unincubated eggshell, my systematic (over time) study of eggshell ultrastructure during dissolution of a fertilized, incubated egg clearly demonstrates that the inner surface (mammillary layer) of the shell is where the majority of dissolution takes place to release calcium and bears major morphological changes. Essentially, dissolution events occurring in the mammillary layer of the shell – the calcium reserve body sac, the base plate of the calcium reserve body, and the surrounding bulk mammillae structure in particular – all can be correlated with developing embryonic skeletal calcification. The calcium reserve body – an essential sub-compartment of mammillae – functions as an early source of calcium; eventually it is lost, perhaps resorbed, during embryonic development and the bulk mammillae take over the calcium-supplying task. My ultrastructural results provide clear, direct visualization of eggshell resorption – which previously was only shown partially or inconclusively mostly from chemically treated samples – and thus lays a foundation for further mechanistic investigations. Importantly, the proteinaceous organic matrix – previously occluded in calcitic mineral phase of avian eggshell and involved in the construction of the shell – is slowly exposed during the shell dissolution process and could function as a channel that assists in the release of calcium for the embryo.

The internal structure and physical properties of biominerals can be modified by intracrystalline proteins incorporated within the mineral bulk. An increasing number of studies have led to the acceptance of the occlusion of peptides, proteins or even larger matrix structures in the mineral phase of biominerals. Urinary proteins that incorporate within calcium oxalate crystals can play a key role in forming or inhibiting calcium oxalate urolithiasis. The study presented in Chapter 6 provides a detailed, protein/peptide

concentration-dependent reporting of the alterations in crystal morphology occurring during COD growth with OPN and one of its peptides, with resulting morphologies being commonly observed in the etiology of severe human kidney stone diseases. The selected aspartic acid-rich peptide of OPN plays a key part on the morphological modification of COD, as it exerts similar effects as full-length OPN on these particular faces of COD. OPN or the selected peptide binds to specific {110} faces of COD and inhibits crystal growth with subsequent site/face specific intracrystalline incorporation. This preferential incorporation of OPN and its peptide develops {110} sectoral compositional zones, which are dose-dependent, and may convert COD crystals into a more dissolvable structure. The binding and occlusion of urinary proteins/peptides to calcium oxalate mineral is thought to serve as a defense mechanism protecting against further mineralization and the enlargement of renal calculi. These findings provide important insights on kidney stone formation and biomineralization processes adopted as a natural protective mechanism against pathologic calcification.

In summary, I have examined the interaction of OPN and one of its peptides with two different mineral phases – calcite and calcium oxalate dihydrate – using in vitro cell-free growth assays and by examining in detail the formation and dissolution/resorption structures of the avian eggshell. In doing so, I have provided new information on how proteins interact with mineral phases relevant to biomineralizing systems.

Chapter 8

Reference List

- Abraham, F.F., 1974. Homogeneous nucleation theory. Academic Press, New York.
- Adachi, E., T. Hayashi, 1986. *In vitro* Formation of Hybrid Fibrils of Type-V Collagen and Type-I Collagen - Limited Growth of Type-I Collagen into Thick Fibrils by Type-V Collagen. *Connective Tissue Research* 14, 257-66.
- Addadi, L., J. Moradian, E. Shay, N.G. Maroudas, S. Weiner, 1987. A chemical model for the cooperation of sulfates and carboxylates in calcite crystal nucleation: Relevance to biomineralization. *Proc Natl Acad Sci U S A* 84, 2732-6.
- Addadi, L., S. Raz, S. Weiner, 2003. Taking advantage of disorder: Amorphous calcium carbonate and its roles in biomineralization. *Advanced Materials* 15, 959-70.
- Addadi, L., S. Weiner, 1985. Interactions between acidic proteins and crystals: stereochemical requirements in biomineralization. *Proc. Natl. Acad. Sci. U. S. A.* 82, 4110-4.
- Addadi, L., S. Weiner, 2001. Crystals, asymmetry and life. *Nature* 411, 753-5.
- Addadi, L., S. Weiner, M. Geva, 2001. On how proteins interact with crystals and their effect on crystal formation. *Z Kardiol* 90 Suppl 3, 92-8.
- Addison, W.N., Y. Nakano, T. Loisel, P. Crine, M.D. McKee, 2008. MEPE-ASARM peptides control extracellular matrix mineralization by binding to hydroxyapatite: an inhibition regulated by PHEX cleavage of ASARM. *J Bone Miner Res* 23, 1638-49.
- Aizenberg, J., A.J. Black, G.H. Whitesides, 1999a. Oriented growth of calcite controlled by self-assembled monolayers of functionalized alkanethiols supported on gold and silver.

Journal of the American Chemical Society 121, 4500-4509.

Aizenberg, J., A.J. Black, G.M. Whitesides, 1999b. Control of crystal nucleation by patterned self-assembled monolayers. *Nature* 398, 495-98.

Aizenberg, J., Albeck, S., Weiner, S., Addadi, L., 1994. Crystal protein interactions studied by overgrowth of calcite on biogenic skeletal elements. *J. Cryst. Growth* 142: 156-64.

Aizenberg, J., Black, A.J., Whitesides, G.H., 1999. Oriented growth of calcite controlled by self-assembled monolayers of functionalized alkanethiols supported on gold and silver. *J. Am. Chem. Soc.* 121: 4500-9.

Aizenberg, J., D.A. Muller, J.L. Grazul, D.R. Hamann, 2003. Direct fabrication of large micropatterned single crystals. *Science* 299, 1205-8.

Aizenberg, J., G. Lambert, S. Weiner, L. Addadi, 2002. Factors involved in the formation of amorphous and crystalline calcium carbonate: a study of an ascidian skeleton. *J. Am. Chem. Soc.* 124, 32-9.

Aizenberg, J., J. Hanson, M. Ilan, L. Leiserowitz, T.F. Koetzle, L. Addadi, S. Weiner, 1995. Morphogenesis of calcitic sponge spicules: a role for specialized proteins interacting with growing crystals. *FASEB J.* 9, 262-8.

Aizenberg, J., M. Ilan, S. Weiner, L. Addadi, 1996. Intracrystalline macromolecules are involved in the morphogenesis of calcitic sponge spicules. *Connect. Tissue Res.* 34, 255-61.

Aizenberg, J., S. Weiner, L. Addadi, 2003. Coexistence of amorphous and crystalline calcium carbonate in skeletal tissues. *Connect. Tissue Res.* 44, 20-25.

Albeck, S., Aizenberg, J., Addadi, L., Weiner, S., 1993. Interactions of various skeletal intracrystalline components with calcite crystals. *J. Am. Chem. Soc.* 115: 11691-11697.

- Albeck, S., L. Addadi, S. Weiner, 1996. Regulation of calcite crystal morphology by intracrystalline acidic proteins and glycoproteins. *Connect. Tissue Res.* 35, 365-70.
- Ali, S.Y., 1983. Calcification of cartilage, in: Hall, B K, (Ed.), *Cartilage, Structure, Function and Biochemistry*, Academic Press, New York, pp. 343-378.
- Anderson, H.C., 1967. Electron microscopic studies of induced cartilage development and calcification. *J Cell Biol* 35, 81-101.
- Anderson, R.E., C.V. Gay, H. Schraer, 1981. Ultrastructural localization of carbonic anhydrase in the chorioallantoic membrane by immunocytochemistry. *J Histochem Cytochem* 29, 1121-7.
- Angker, L., C. Nockolds, M.V. Swain, N. Kilpatrick, 2004. Quantitative analysis of the mineral content of sound and carious primary dentine using BSE imaging. *Arch. Oral Biol.* 49, 99-107.
- Archibald, D.D., S.B. Qadri, B.P. Gaber, 1996. Modified calcite deposition due to ultrathin organic films on silicon substrates. *Langmuir* 12, 538-546.
- Arias, J.L, Carrino DA, Fernandez MS, Rodriguez JP, Dennis JE, Caplan AI (1992) Partial biochemical and immunochemical characterization of avian eggshell extracellular matrices. *Arch Biochem Biophys* 298:203-302
- Arias, J.L, Fernandez MS, Dennis JE, Caplan AI (1991) Collagens of the chicken eggshell membranes. *Connect Tissue Res* 26:37-45
- Arias, J.L., Fink, D. J., Xiao, S.-Q, Heuer, A. H., and Caplan, A. I., 1993. Biomineralization and eggshells: cell-mediated acellular compartments of mineralized extracellular matrix. *International Review of Cytology* 145, 217-250.
- Arias, J.L., Fink, D. J., Xiao, S.-Q, Heuer, A. H., and Caplan, A. I., 1993. Biomineralization and

- eggshells: cell-mediated acellular compartments of mineralized extracellular matrix. *Int. Rev. Cytol.* 145, 217-250.
- Arias, J.L., Fink, D.J., Xiao, S.-Q, Heuer, A.H., Caplan, A.I., 1993. Biomineralization and eggshells: Cell-mediated acellular compartments of mineralized extracellular matrix. *Int. Rev. Cytol.* 145: 217-250.
- Arias, J.L., M.S. Fernandez, J.E. Dennis, A.I. Caplan, 1991a. Collagens of the chicken eggshell membranes. *Connect Tissue Res* 26, 37-45.
- Arias, J.L., M.S. Fernandez, J.E. Dennis, A.I. Caplan, 1991b. The fabrication and collagenous substructure of the eggshell membrane in the isthmus of the hen oviduct. *Matrix* 11, 313-20.
- Arnold, S., U. Plate, H.P. Wiesmann, U. Stratmann, H. Kohl, H.J. Hohling, 2001. Quantitative analyses of the biomineralization of different hard tissues. *J Microsc* 202, 488-94.
- Asplin, J.R., D. Arsenault, J.H. Parks, F.L. Coe, J.R. Hoyer, 1998. Contribution of human uropontin to inhibition of calcium oxalate crystallization. *Kidney Int.* 53, 194-9.
- Astilleros, J.M., Pina, C.M., Fernandez-Diaz, L., Putnis, A., 2000. The effect of barium on calcite {104} surfaces during growth. *Geochim. Cosmochim. Acta* 64: 2965-2972.
- Atmani, F., F.J. Opalko, S.R. Khan, 1996. Association of urinary macromolecules with calcium oxalate crystals induced in vitro in normal human and rat urine. *Urol Res* 24, 45-50.
- Atmani, F., P.A. Glenton, S.R. Khan, 1998. Identification of proteins extracted from calcium oxalate and calcium phosphate crystals induced in the urine of healthy and stone forming subjects. *Urol Res* 26, 201-7.
- Ausprunk, D.H., 1986. Distribution of hyaluronic acid and sulfated glycosaminoglycans during

- blood-vessel development in the chick chorioallantoic membrane. *Am J Anat* 177, 313-31.
- Barabási, A.-L., E.H. Stanley, 1995. *Fractal concepts in surface growth* Cambridge University Press, Cambridge.
- Bartholomew, R.S., P.F. Rebello, 1979. Calcium oxalate crystals in the aqueous. *Am. J. Ophthalmol.* 88, 1026-8.
- Bautista, D.S., Z. Saad, A.F. Chambers, K.S. Tonkin, F.P. O'Malley, H. Singhal, S. Tokmakejian, V. Bramwell, J.F. Harris, 1996. Quantification of osteopontin in human plasma with an ELISA: basal levels in pre- and postmenopausal women. *Clin Biochem* 29, 231-9.
- Bazylnski, D.A., 1996. Controlled biomineralization of magnetic minerals by magnetotactic bacteria. *Chemical Geology* 132, 191-198.
- Belcher AM, Wu XH, Christensen RJ, Hansma PK, Stucky GD, Morse DE (1996) Control of crystal phase switching and orientation by soluble mollusc-shell proteins. *Nature* 381:56-58
- Bellairs, R., A. Boyde, 1969. Scanning electron microscopy of the shell membranes of the hen's egg. *Z. Zellforsch. Mikrosk. Anat.* 96, 237-49.
- Bellairs, R., M. Osmond, 2005. *The atlas of chick development*, 2nd ed. Elsevier, Amsterdam.
- Beniash, E., J. Aizenberg, L. Addadi, S. Weiner, 1997. Amorphous calcium carbonate transforms into calcite during sea-urchin larval spicule growth. *Proc R Soc London B Ser* 264, 461-65.
- Beniash, E., L. Addadi, S. Weiner, 1999. Cellular control over spicule formation in sea urchin embryos: A structural approach. *J Struct Biol* 125, 50-62.
- Berg, W., J.D. Schnapp, H.J. Schneider, A. Hesse, E. Hienzsch, 1976. Crystalloptical and spectroscopical findings with calcium oxalate crystals in the urine sediment: a contribution to the genesis of oxalate stones. *Eur. Urol.* 2, 92-7.

- Berg, W., P. Lange, C. Bothor, D. Rossler, 1979. Submicroscopic investigations on calcium oxalate stone genesis. *Eur. Urol.* 5, 136-43.
- Berman A, Addadi L, Weiner S. 1988, Interactions of sea-urchin skeleton macromolecules with growing calcite crystals – a study of intracrystalline proteins. *Nature* 331:546-8
- Berman, A., Addadi, L., Kvick, A., Leiserowitz, L., Nelson, M., Weiner, S. 1990. Intercalation of sea urchin proteins in calcite: Study of a crystalline composite material. *Science* 250: 664-7.
- Berman, A., D.J. Ahn, A. Lio, M. Salmeron, A. Reichert, D. Charych, 1995. Total Alignment of Calcite at Acidic Polydiacetylene Films - Cooperativity at the Organic-Inorganic Interface. *Science* 269, 515-8.
- Berman, A., Hanson, J., Leiserowitz, L., Koetzle, T.F., Weiner, S., Addadi, L., 1993. Biological control of crystal texture: A widespread strategy for adapting crystal properties to function. *Science* 259: 776-9.
- Berridge, M.J., M.D. Bootman, P. Lipp, 1998. Calcium--a life and death signal. *Nature* 395, 645-8.
- Bettencourt, V., A. Guerra, 2000. Growth increments and biomineralization process in cephalopod statoliths. *Journal of Experimental Marine Biology and Ecology* 248, 191-205.
- Bezeaud, A., M.C. Guillin, 1984. Quantitation of prothrombin activation products in human urine. *Br J Haematol* 58, 597-606.
- Board, R.G., Tullett, S.G., Perrott, H.R., 1977. Arbitrary classification of pore systems in avian eggshells. *J. Zool.* 182: 251-65.
- Bond, G.M., R.G. Board, V.D. Scott, 1988. A Comparative-Study of Changes in the Fine-Structure of Avian Eggshells during Incubation. *Zool. J. Linn. Soc.* 92, 105-13.
- Borowitzka, L.J., A.D. Brown, 1974. The salt relations of marine and halophilic species of the

- unicellular green alga, *Dunaliella*. The role of glycerol as a compatible solute. Arch Mikrobiol 96, 37-52.
- Borowitzka, M.A., 1982. Morphological and Cytological Aspects of Algal Calcification. International Review of Cytology-a Survey of Cell Biology 74, 127-62.
- Brown, L.F., B. Berse, L. Van de Water, A. Papadopoulos-Sergiou, C.A. Perruzzi, E.J. Manseau, H.F. Dvorak, D.R. Senger, 1992. Expression and distribution of osteopontin in human tissues: widespread association with luminal epithelial surfaces. Mol. Biol. Cell 3, 1169-80.
- Brownlee, C., N. Nimer, L.F. Dong, M.J. Merrett, 1994. Cellular regulation during calcification in *Emiliana huxleyi*, in: Green, J C, Leadbeater, B S C, (Eds.), The Haptophyte Algae, Clarendon Press, New York, pp. 133-48.
- Burley RW, Vadehra DV (1989) The Avian Egg, Chemistry and Biology, Toronto, J. Wiley & Sons
- Burley, R.W., Vadehra, D.V., 1989. In: The Avian Egg: Chemistry and Biology, Wiley, New York, NY, USA.
- Burton, W.K., N. Cabrera, F.C. Frank, 1951. The Growth of Crystals and the Equilibrium Structure of Their Surfaces. Philosophical Transactions of the Royal Society of London Series a-Mathematical and Physical Sciences 243, 299-358.
- Butler, W.T., 1989. The nature and significance of osteopontin. Connect Tissue Res 23, 123-36.
- Butler, W.T., A.L. Ridall, M.D. McKee, 1996. Osteopontin, in: Bilezikian, J P, et al., (Eds.), Principles of bone biology, Academic Press, San Diego, pp. 167-81.
- Cabrera, N., D.A. Vermileya, 1958. Growth and perfection of crystals. John Wiley & Sons, New York; Chapman and Hall, London.
- Cancel, A.M., D.A. Chapman, G.J. Killian, 1999. Osteopontin localization in the Holstein bull

- reproductive tract. *Biol Reprod* 60, 454-60.
- Carrino, D.A., J.P. Rodriguez, A.I. Caplan, 1997. Dermatan sulfate proteoglycans from the mineralized matrix of the avian eggshell. *Connect Tissue Res* 36, 175-93.
- Cerini, C., S. Geider, B. Dussol, C. Hennequin, M. Daudon, S. Veessler, S. Nitsche, R. Boistelle, P. Berthezene, P. Dupuy, A. Vazi, Y. Berland, J.C. Dagorn, J.M. Verdier, 1999. Nucleation of calcium oxalate crystals by albumin: involvement in the prevention of stone formation. *Kidney Int.* 55, 1776-86.
- Chauvet, M.C., R.L. Ryall, 2005. Intracrystalline proteins and calcium oxalate crystal degradation in MDCK II cells. *J. Struct. Biol.* 151, 12-7.
- Chernov, A.A., 1961. Layer-Spiral Growth of Crystals. *Uspekhi Fizicheskikh Nauk* 73, 277-331.
- Chernov, A.A., 1984. *Modern Crystallography III: Crystal Growth*. Springer-Verlag, Berlin.
- Chernov, A.A., 1989. Formation of Crystals in Solutions. *Contemporary Physics* 30, 251-76.
- Chevillat, N., F. Coignoul, 1984. Calcium in the turkey yolk sac during late development and postembryonic involution. *Am. J. Vet. Res.* 45, 2458-66.
- Chien, Y.C., M.T. Hincke, H. Vali, M.D. McKee, 2008. Ultrastructural matrix-mineral relationships in avian eggshell, and effects of osteopontin on calcite growth in vitro. *J. Struct. Biol.* 163, 84-99.
- Chien, Y.C., M.T. Hincke, M.D. McKee, 2009. Avian eggshell structure and osteopontin. *Cells Tissues Organs* 189, 38-43.
- Chien, Y.C., Mucci, A., Paquette, J., Sears, S.K., Vali, H., 2006. Comparative study of nanoscale surface structures of calcite microcrystals using FE-SEM, AFM, and TEM. *Microsc. Microanal.* 12: 302-10.

- Chutipongtanate, S., Y. Nakagawa, S. Sritippayawan, J. Pittayamateekul, P. Parichatikanond, B.R. Westley, F.E. May, P. Malasit, V. Thongboonkerd, 2005. Identification of human urinary trefoil factor 1 as a novel calcium oxalate crystal growth inhibitor. *J. Clin. Invest.* 115, 3613-22.
- Clark, N.B., K. Simkiss, 1980. Time, targets, and triggers: A study of calcium regulation in the bird, in: Epple, A, Stetson, M H, (Eds.), *Avian Endocrinology.*, Academic Press, New York, pp. 191-208.
- Coleman, J.R., A.R. Terepka, 1972. Electron probe analysis of the calcium distribution in cells of the embryonic chick chorioallantoic membrane. I. A critical evaluation of techniques. *J. Histochem. Cytochem.* 20, 401-13.
- Consortium, I.C.G.S., 2004. Sequence and comparative analysis of the chicken genome provide unique perspectives on vertebrate evolution, *Nature*, Vol. 432, pp. 695-716.
- Constantz, B.R., A. Meike, 1989. Calcite centers of calcification in *Mussa angulosa* (Scleractinia), in: Crick, R E, (Ed.), *Origin, Evolution, and Modern Aspects of Biomineralization in Plants and Animals*, Plenum, New York, pp. 201-7.
- Craig, A.M., J.H. Smith, D.T. Denhardt, 1989. Osteopontin, a transformation-associated cell adhesion phosphoprotein, is induced by 12-O-tetradecanoylphorbol 13-acetate in mouse epidermis. *J Biol Chem* 264, 9682-9.
- Crenshaw, M.A., 1980. Mechanisms of shell formation and dissolution, in: Rhoads, D C, Lutz, R A, (Eds.), *Skeletal growth of aquatic organisms*, Plenum Publishing Corporation, New York, pp. 115-32.
- Crooks, R.J., K. Simkiss, 1974. Respiratory acidosis and eggshell resorption by the chick embryo. *J.*

- Exp. Biol. 61, 197-202.
- Daudon, M., F. Barbey, P. Jungers, 2004. [Value of the study of crystalluria in clinical practice]. Rev. Med. Suisse Romande 124, 455-9.
- Daudon, M., Jungers, P, Bazin, D., 2008. Stone morphology: implication for pathogenesis, in: Evan, A P, et al., (Eds.), Second International Urolithiasis Research Symposium American Institute of Physics, Indianapolis, Indiana Vol. 1049, pp. 199-215.
- Davis, K.J., Dove, P.M., De Yoreo, J.J., 2000. The role of Mg^{2+} as an impurity in calcite growth. Science 290: 1134-37.
- Dawes, C.M., K. Simkiss, 1971. The effects of respiratory acidosis in the chick embryo. J. Exp. Biol. 55, 77-84.
- De Vrind-De Jong, E.W., J.P.M. De Vrind, 1997. Algal deposition of carbonates and silicates, Vol. 35, pp. 267-307.
- De Vrind-De Jong, E.W., P.R. Van Emburg, J.P.M. De Vrind, 1994. Mechanisms of calcification: *Emiliana huxleyi* as a model system, in: Green, J C, Leadbeater, B S C, (Eds.), The Haptophyte Algae, Clarendon Press, New York, pp. 149-166.
- De Yoreo, J.J., A.K. Burnham, P.K. Whitman, 2002. Developing KH_2PO_4 and KD_2PO_4 crystals for the world's most powerful laser. International Materials Reviews 47, 113-52.
- De Yoreo, J.J., P.G. Vekilov, 2003. Principles of crystal nucleation and growth, in: Dove, P M, J.J. De Yoreo, and S. Weiner, (Eds.), Biomineralization, The Mineralogical Society of America, Washinton, D.C., Vol. 54, pp. 57-93.
- De Yoreo, J.J., Qiu, S.R., Hoyer, J.R., 2006. Molecular modulation of calcium oxalate crystallization. Am. J. Physiol. Renal Physiol. 291: F1123-31.

- Denhardt, D.T., M. Noda, 1998. Osteopontin expression and function: role in bone remodeling. *J Cell Biochem Suppl* 30-31, 92-102.
- Denhardt, D.T., X. Guo, 1993. Osteopontin: a protein with diverse functions. *FASEB J* 7, 1475-82.
- Dennis, J.E., S.Q. Xiao, M. Agarwal, D.J. Fink, A.H. Heuer, A.I. Caplan, 1996. Microstructure of matrix and mineral components of eggshells from white leghorn chickens (*Gallus gallus*). *J. Morphol.* 228, 287-306.
- Dieckert, J.W., Dieckert, M.C., Creger, C.R., 1989. Calcium reserve assembly: A basic structural unit of the calcium reserve system of the hen egg shell. *Poult. Sci.* 68: 1569-84.
- Dimuzio, M.T., A. Veis, 1978a. Phosphophoryns-major noncollagenous proteins of rat incisor dentin. *Calcif Tissue Res* 25, 169-78.
- Dimuzio, M.T., A. Veis, 1978b. The biosynthesis of phosphophoryns and dentin collagen in the continuously erupting rat incisor. *J Biol Chem* 253, 6845-52.
- Dodds, R.A., J.R. Connor, I.E. James, E.L. Rykaczewski, E. Appelbaum, E. Dul, M. Gowen, 1995. Human osteoclasts, not osteoblasts, deposit osteopontin onto resorption surfaces: an in vitro and ex vivo study of remodeling bone. *J Bone Miner Res* 10, 1666-80.
- Dominguez-Vera, J.M., J. Gautron, J.M. Garcia-Ruiz, Y. Nys, 2000. The effect of avian uterine fluid on the growth behavior of calcite crystals. *Poult Sci* 79, 901-7.
- Donoghue, P.C., I.J. Sansom, 2002. Origin and early evolution of vertebrate skeletonization. *Microsc Res Tech* 59, 352-72.
- Doskocil, M., J. Blazek, P. Nemcova, B. Starkova, 1985. Über die Struktur der Schale des Huhnereies und ihre Veränderungen während der Bebrütung. Eine rasterelektronenmikroskopische Studie. *Anat. Anz.* 159, 117-26.

- Dowty, E., 2002. SHAPE. Windows Professional Kingsport, TN.
- Doyle, I.R., R.L. Ryall, V.R. Marshall, 1991. Inclusion of proteins into calcium oxalate crystals precipitated from human urine: a highly selective phenomenon. *Clin. Chem.* 37, 1589-94.
- Durrbaum, D., A.L. Rodgers, E.D. Sturrock, 2001. A study of crystal matrix extract and urinary prothrombin fragment 1 from a stone-prone and stone-free population. *Urol. Res.* 29, 83-8.
- Dyer, R., B.E. Nordin, 1967. Urinary crystals and their relation to stone formation. *Nature* 215, 751-2.
- Edyvane, K.A., C.M. Hibberd, R.M. Harnett, V.R. Marshall, R.L. Ryall, 1987. Macromolecules inhibit calcium oxalate crystal growth and aggregation in whole human urine. *Clin Chim Acta* 167, 329-38.
- Elhadj, S., E.A. Salter, A. Wierzbicki, J.J. De Yoreo, N. Han, P.M. Dove, 2006b. Peptide controls on calcite mineralization: Polyaspartate chain length affects growth kinetics and acts as a stereochemical switch on morphology. *Cryst. Growth Des.* 6, 197-201.
- Elhadj, S., J.J. De Yoreo, J.R. Hoyer, P.M. Dove, 2006a. Role of molecular charge and hydrophilicity in regulating the kinetics of crystal growth. *Proc. Natl. Acad. Sci. U. S. A.* 103, 19237-42.
- Elliot, J.S., I.N. Rabinowitz, 1980. Calcium oxalate crystalluria: crystal size in urine. *J. Urol.* 123, 324-7.
- Emler RB (1982) Echinoderm calcite: a mechanical analysis from larval spicules. *Biol Bull* 163:264-275
- Epstein, S., R. Buchsbaum, H. Lowenstam, H.C. Urey, 1951. Carbonate-Water Isotopic Temperature Scale. *Geological Society of America Bulletin* 62, 417-26.
- Erben, H.K., 1970. Ultrastrukturen und mineralisation rezenter und fossiler eischalen bei vogeln und reptilien. *Biomineralization* 1: 1-66.

- Estroff, L.A., L. Addadi, S. Weiner, A.D. Hamilton, 2004. An organic hydrogel as a matrix for the growth of calcite crystals. *Org. Biomol. Chem.* 2, 137-41.
- Everaert, N., L. De Smit, M. Debonne, A. Witters, B. Kamers, E. Decuyper, V. Bruggeman, 2008. Changes in acid-base balance and related physiological responses as a result of external hypercapnia during the second half of incubation in the chicken embryo. *Poult. Sci.* 87, 362-7.
- Falini, G., S. Albeck, S. Weiner, L. Addadi, 1996. Control of aragonite or calcite polymorphism by mollusk shell macromolecules. *Science* 271, 67-69.
- Fernandez, M.S., Araya, M., Arias, J.L., 1997. Eggshells are shaped by a precise spatio-temporal arrangement of sequentially deposited macromolecules. *Matrix Biol.* 16: 13-20.
- Fernandez, M.S., C. Escobar, I. Lavelin, M. Pines, J.L. Arias, 2003. Localization of osteopontin in oviduct tissue and eggshell during different stages of the avian egg laying cycle. *J Struct Biol* 143, 171-80.
- Fernandez, M.S., Moya, A., Lopez, L., Arias, J.L., 2001. Secretion pattern, ultrastructural localization and function of extracellular matrix molecules involved in eggshell formation. *Matrix Biol.* 19: 793-803.
- Fernandez, M.S., Passalacqua, K. Arias, J.I., Arias, J.L., 2004. Partial biomimetic reconstitution of avian eggshell formation. *J. Struct. Biol.* 148: 1-10.
- Finklea, H.O., Hanshew, D.D., 1992. Electron-transfer kinetics in organized thiol monolayers with attached pentaammine (pyridine) ruthenium redox centers. *J. Am. Chem. Soc.* 114: 3173-3181.
- Fisher, L.W., D.A. Torchia, B. Fohr, M.F. Young, N.S. Fedarko, 2001. Flexible structures of SIBLING

- proteins, bone sialoprotein, and osteopontin. *Biochem. Biophys. Res. Commun.* 280, 460-5.
- Fisher, L.W., N.S. Fedarko, 2003. Six genes expressed in bones and teeth encode the current members of the SIBLING family of proteins. *Connect Tissue Res* 44 Suppl 1, 33-40.
- Fleming, D.E., A. Van Riessen, M.C. Chauvet, P.K. Grover, B. Hunter, W. van Bronswijk, R.L. Ryall, 2003. Intracrystalline proteins and urolithiasis: a synchrotron X-ray diffraction study of calcium oxalate monohydrate. *J. Bone Miner. Res.* 18, 1282-91.
- Fortin, D., F.G. Ferris, T.J. Beveridge, 1997. Surface-mediated mineral development by bacteria. *Geomicrobiology: Interactions between Microbes and Minerals* 35, 161-180.
- Frankel, R.B., D.A. Bazylinski, 2003. Biologically induced mineralization by bacteria, in: Dove, P M, et al., (Eds.), *Biom mineralization*, The Mineralogical Society of America, Washinton, D.C., Vol. 54, pp. 95-114.
- Gabrielli, M.G., 2004. Carbonic anhydrases in chick extra-embryonic structures: a role for CA in bicarbonate reabsorption through the chorioallantoic membrane. *J. Enzyme Inhib. Med. Chem.* 19, 283-6.
- Gago-Duport, L., M.J. Briones, J.B. Rodriguez, B. Coveló, 2008. Amorphous calcium carbonate biomineralization in the earthworm's calciferous gland: pathways to the formation of crystalline phases. *J. Struct. Biol.* 162, 422-35.
- Garcia-Ruiz, J.M., Rodriguez Navarro, A., Kalin, O., 1995. Textural analysis of eggshells. *Mat. Sci. Eng. C3*: 95-100.
- Garrison, J.C., A.R. Terepka, 1972a. Interrelationships between sodium ion, calcium transport and oxygen utilization in isolated chick chorioallantoic membrane. *J. Membr. Biol.* 7, 146-163.

- Garrison, J.C., A.R. Terepka, 1972b. Calcium-stimulated respiration and active calcium transport in isolated chick chorioallantoic membrane. *J. Membr. Biol.* 7, 128-145.
- Gautron, J., Hincke, M.T., Mann, K., Panheleux, M., Bain, M., McKee, M.D., Solomon, S.E., Nys, Y., 2001a. Ovocalyxin-32, a novel chicken eggshell matrix protein. Isolation, amino acid sequencing, cloning, and immunocytochemical localization. *J. Biol. Chem.* 276: 39243-52.
- Gautron J, Hincke MT, Panhéleux M, Garcia-Ruiz JM, Boldicke T, Nys Y. 2001b Ovotransferrin is a matrix protein of the hen eggshell membranes and basal calcified layer. *Connective Tiss Res* 42:255-67
- Gautron, J., Bain, M., Solomon, S.E., Nys, Y., 1996. Soluble matrix of hen's eggshell extracts changes in vitro the rate of calcium carbonate precipitation and crystal morphology. *Br. Poult. Sci.* 37: 853-66.
- Gautron, J., E. Murayama, A. Vignal, M. Morisson, M.D. McKee, S. Rehault, V. Labas, M. Belghazi, M.L. Vidal, Y. Nys, M.T. Hincke, 2007. Cloning of ovocalyxin-36, a novel chicken eggshell protein related to lipopolysaccharide-binding proteins, bactericidal permeability-increasing proteins, and plunc family proteins. *J Biol Chem* 282, 5273-86.
- Gautron, J., Hincke, M. T., Nys, Y., 1997. Precursor matrix proteins in the uterine fluid change with stages of eggshell formation in hens. *Connect. Tissue Res.* 36: 195–210.
- Gautron, J., Hincke, M.T., Panheleux, M., Garcia-Ruiz, J.M., Nys, Y. 1998. Identification and characterization of matrix proteins from hen's eggshell, pp. 19-23, in: Goldberg, M., Boskey, A., and Robinson, C., (Ed.) *Chemistry and Biology of Mineralized Tissues. Proceeding of the Sixth International Conference.* American Academy of Orthopaedic Surgeons, Vittel, France.

- Gericke, A., C. Qin, L. Spevak, Y. Fujimoto, W.T. Butler, E.S. Sorensen, A.L. Boskey, 2005. Importance of phosphorylation for osteopontin regulation of biomineralization. *Calcif. Tissue Int.* 77, 45-54.
- Gerstenfeld L.C., Gotoh Y, McKee M.D., Nanci A, Landis W.J., Glimcher M.J. 1990 Expression and ultrastructural immunolocalization of a major 66 kDa phosphoprotein synthesized by chicken osteoblasts during mineralization in vitro. *Anat Rec* 228:93-103
- Giachelli, C.M., L. Liaw, C.E. Murry, S.M. Schwartz, M. Almeida, 1995. Osteopontin expression in cardiovascular diseases. *Ann N Y Acad Sci* 760, 109-26.
- Giachelli, C.M., N. Bae, M. Almeida, D.T. Denhardt, C.E. Alpers, S.M. Schwartz, 1993. Osteopontin is elevated during neointima formation in rat arteries and is a novel component of human atherosclerotic plaques. *J Clin Invest* 92, 1686-96.
- Gibson, R.I., 1974. Descriptive Human Pathological Mineralogy. *Am. Mineral.* 59, 1177-82.
- Goldberg, H.A., Hunter, G.K., 1995. The inhibitory activity of osteopontin on hydroxyapatite formation in vitro. *Ann. N. Y. Acad. Sci.* 760: 305-8.
- Gorski, J.P., E.A. Kremer, Y. Chen, S. Ryan, C. Fullenkamp, J. Delviscio, K. Jensen, M.D. McKee, 1997. Bone acidic glycoprotein-75 self-associates to form macromolecular complexes in vitro and in vivo with the potential to sequester phosphate ions. *J Cell Biochem* 64, 547-64.
- Gotliv, B.A., L. Addadi, S. Weiner, 2003. Mollusk shell acidic proteins: In search of individual functions. *Chembiochem* 4, 522-9.
- Gotoh Y., Salih E., Glimcher M.J., Gerstenfeld L.C. 1995 Characterization of the major non-collagenous proteins of chicken bone: Identification of a novel 60 kDa non-collagenous phosphoprotein. *Biochem Biophys Res Commun* 208:863-70

- Graf, K., Y.S. Do, N. Ashizawa, W.P. Meehan, C.M. Giachelli, C.C. Marboe, E. Fleck, W.A. Hsueh, 1997. Myocardial osteopontin expression is associated with left ventricular hypertrophy. *Circulation* 96, 3063-71.
- Gratz, A.J., P.E. Hillner, P.K. Hansma, 1993. Step Dynamics and spiral growth on calcite. *Geochim. Cosmochim. Acta* 57, 491-5.
- Grégoire, C., G.H. Duchateau, M. Florkin, 1955. La trame protidique des nacres et des perles. *Ann Inst Oceanogr Monaco* 31, 1-36.
- Grohe, B., J. O'Young, D.A. Ionescu, G. Lajoie, K.A. Rogers, M. Karttunen, H.A. Goldberg, G.K. Hunter, 2007. Control of calcium oxalate crystal growth by face-specific adsorption of an osteopontin phosphopeptide. *J. Am. Chem. Soc.* 129, 14946-51.
- Grover, P.K., L.A. Thurgood, D.E. Fleming, W. van Bronswijk, T. Wang, R.L. Ryall, 2008. Intracrystalline urinary proteins facilitate degradation and dissolution of calcium oxalate crystals in cultured renal cells. *Am. J. Physiol. Renal Physiol.* 294, F355-61.
- Hamburger, V., H.L. Hamilton, 1951. A series of normal stages in the development of the chick embryo. *J. Morphol.* 88, 49-92.
- Hamilton R.M.G. 1986 The microstructure of the hens egg-shell – a short review. *Food Microstruct* 5:99-110
- Hartman, P., 1987. Modern PBC theory, In: Sunagawa, I. (Ed.), *Morphology of Crystals: Part A*, Terra Scientific, Tokyo, p.p. 269-319.
- Hartman, P., Perdok, W.G., 1955. On the relations between structure and morphology of crystals. I. *Acta Crystallogr.* 8: 49-52.
- He, G., T. Dahl, A. Veis, A. George, 2003. Nucleation of apatite crystals in vitro by self-assembled

- dentin matrix protein 1. *Nat Mater* 2, 552-8.
- Hedgepeth, R.C., L. Yang, M.I. Resnick, S.R. Marengo, 2001. Expression of proteins that inhibit calcium oxalate crystallization in vitro in the urine of normal and stone-forming individuals. *Am J Kidney Dis* 37, 104-12.
- Heijnen, W.M.M., 1985. The morphology of gel grown calcite. *Neues Jahrbuch Fur Mineralogie-Monatshefte*. 8: 357-71.
- Hernandez-Hernandez, A., J. Gomez-Morales, A.B. Rodriguez-Navarro, J. Gautron, Y. Nys, J.M. Garcia-Ruiz, 2008. Identification of Some Active Proteins in the Process of Hen Eggshell Formation. *Cryst. Growth Des.* 8, 4330-9.
- Heywood, B.R., S. Mann, 1994. Template-Directed Nucleation and Growth of Inorganic Materials. *Advanced Materials* 6, 9-20.
- Hincke M.T., Gautron J., Tsang C.P.W., McKee M.D., Nys Y. 1999 Molecular cloning and ultrastructural localization of the core protein of an eggshell matrix proteoglycan Ovocleidin-116. *J. Biol. Chem.* 274:32915-23
- Hincke M.T., Nairn A.C. 1992 Phosphorylation of Elongation Factor 2 during Calcium - Mediated Secretion from Rat Parotid Acini. *Biochem J* 282:877-882
- Hincke, M.T., Bernard, A.M., Lee, E.R., Tsang, C.P., Narbaitz, R., 1992. Soluble protein constituents of the domestic fowl's eggshell. *Br. Poult. Sci.* 33: 505-16.
- Hincke, M.T., St. Maurice, M., Nys, Y., Gautron, J., Panheleux, M., Tsang, C.P.W., Bain, M., Solomon, S.E., McKee, M.D., 2000a. Eggshell matrix proteins and shell strength: Molecular biology of eggshell matrix proteins and industrial applications, In: Sim, J. S., Nakai, S., and Guenter, W., ((Eds.), *Egg Nutrition and Biotechnology*, CAB International, Wallingford,

p.p. 447-461.

- Hincke, M.T., Gautron, J., Panheleux, M., Garcia-Ruiz, J.M., McKee, M.D., Nys, Y., 2000b. Identification and localization of lysozyme as a component of eggshell membranes and eggshell matrix. *Matrix Biol.* 19: 443-53.
- Hincke, M.T., M. St. Maurice, 2000. Phosphorylation-dependent modulation of calcium carbonate precipitation by chicken eggshell matrix proteins, in: Goldberg M, A, Boskey , C, Robinson (Eds.), *Chemistry and Biology of Mineralized Tissues.*, Am. Acad. Orthop. Surg., Rosemont, IL, pp. 13-17.
- Hincke, M.T., Chien Y.C., Gerstenfeld L.C., McKee M.D., 2008a. Colloidal-gold immunocytochemical localization of osteopontin in avian eggshell gland and eggshell. *J. Histochem. Cytochem.* 56, 467-76.
- Hincke, M.T., O. Wellman-Labadie, M.D. McKee, J. Gautron, Y. Nys, K. Mann, 2008b. Biosynthesis and structural assembly of eggshell components, in: Mine, Y, (Ed.), *Egg Bioscience and Biotechnology*, Wiley-Interscience, Hoboken, N.J., pp. 97-128.
- Hincke, M.T., Tsang C.P., Courtney M., Hill V., Narbaitz R, 1995. Purification and immunochemistry of a soluble matrix protein of the chicken eggshell (ovocleidin 17). *Calcif Tissue Int* 56, 578-83.
- Hoang, Q.Q., Sicheri, F., Howard, A.J., Yang, D.S., 2003. Bone recognition mechanism of porcine osteocalcin from crystal structure. *Nature* 425: 977-80.
- Hoyer, J.R., 1994. Uropontin in urinary calcium stone formation. *Miner Electrolyte Metab* 20, 385-92.
- Hoyer, J.R., J.R. Asplin, L. Otvos, 2001. Phosphorylated osteopontin peptides suppress crystallization by inhibiting the growth of calcium oxalate crystals. *Kidney Int.* 60, 77-82.

- Hoyer, J.R., L. Otvos, Jr., L. Urge, 1995. Osteopontin in urinary stone formation. *Ann N Y Acad Sci* 760, 257-65.
- Hu, D.D., Lin E.C., Kovach N.L., Hoyer J.R., Smith J.W., 1995. A biochemical characterization of the binding of osteopontin to integrins alpha v beta 1 and alpha v beta 5. *J Biol Chem* 270, 26232-8.
- Hunter, G.K., B. Grohe, S. Jeffrey, J. O'Young, E.S. Sorensen, H.A. Goldberg, 2009. Role of phosphate groups in inhibition of calcium oxalate crystal growth by osteopontin. *Cells Tissues Organs* 189, 44-50.
- Hunter, G.K., P.V. Hauschka, A.R. Poole, L.C. Rosenberg, H.A. Goldberg, 1996. Nucleation and inhibition of hydroxyapatite formation by mineralized tissue proteins. *Biochem J* 317 (Pt 1), 59-64.
- Hunter, M.L., N.X. West, J.A. Hughes, R.G. Newcombe, M. Addy, 2000. Erosion of deciduous and permanent dental hard tissue in the oral environment. *J. Dent.* 28, 257-63.
- Iizuka, J., Y. Katagiri, N. Tada, M. Murakami, T. Ikeda, M. Sato, K. Hirokawa, S. Okada, M. Hatano, T. Tokuhisa, T. Uede, 1998. Introduction of an osteopontin gene confers the increase in B1 cell population and the production of anti-DNA autoantibodies. *Lab Invest* 78, 1523-33.
- Johnston, P.M., C.L. Comar, 1955. Distribution and contribution of calcium from the albumen, yolk and shell to the developing chick embryo. *Am. J. Physiol.* 183, 365-70.
- Kaartinen, M.T., W. Sun, N. Kaipatur, M.D. McKee, 2005. Transglutaminase crosslinking of SIBLING proteins in teeth. *J Dent Res* 84, 607-12.
- Kashchiev, D., 1999. *Nucleation: Basic theory with applications*. Butterworths-Heinemann, Oxford.
- Kawasaki, K., K.M. Weiss, 2003. *Mineralized tissue and vertebrate evolution: the secretory*

- calcium-binding phosphoprotein gene cluster. *Proc Natl Acad Sci U S A* 100, 4060-5.
- Kazanecki, C.C., D.J. Uzwiak, D.T. Denhardt, 2007. Control of osteopontin signaling and function by post-translational phosphorylation and protein folding. *J Cell Biochem* 102, 912-24.
- Kerr, J.M., L.W. Fisher, J.D. Termine, M.F. Young, 1991. The cDNA cloning and RNA distribution of bovine osteopontin. *Gene* 108, 237-43.
- Khan, S.R., 1997. Animal models of kidney stone formation: an analysis. *World J. Urol.* 15, 236-43.
- Khan, S.R., J.M. Johnson, A.B. Peck, J.G. Cornelius, P.A. Glenton, 2002. Expression of osteopontin in rat kidneys: induction during ethylene glycol induced calcium oxalate nephrolithiasis. *J Urol* 168, 1173-81.
- Kiefer, M.C., D.M. Bauer, P.J. Barr, 1989. The cDNA and derived amino acid sequence for human osteopontin. *Nucleic Acids Res* 17, 3306.
- Kim, I.W., M.R. Darragh, C. Orme, J.S. Evans, 2006. Molecular "tuning" of crystal growth by nacre-associated polypeptides. *Cryst. Growth Des.* 6, 5-10.
- Kleinman, J.G., J.A. Wesson, J. Hughes, 2004. Osteopontin and calcium stone formation. *Nephron Physiol.* 98, p43-7.
- Kohri, K., S. Nomura, Y. Kitamura, T. Nagata, K. Yoshioka, M. Iguchi, T. Yamate, T. Umekawa, Y. Suzuki, H. Sinohara, T. Kurita, 1993. Structure and expression of the mRNA encoding urinary stone protein (osteopontin). *J. Biol. Chem.* 268, 15180-4.
- Kohri, K., Y. Suzuki, K. Yoshida, K. Yamamoto, N. Amasaki, T. Yamate, T. Umekawa, M. Iguchi, H. Sinohara, T. Kurita, 1992. Molecular cloning and sequencing of cDNA encoding urinary stone protein, which is identical to osteopontin. *Biochem Biophys Res Commun* 184, 859-64.

- Komeili, A., H. Vali, T.J. Beveridge, D.K. Newman, 2004. Magnetosome vesicles are present before magnetite formation, and MamA is required for their activation. *Proc. Natl. Acad. Sci. U. S. A.* 101, 3839-44.
- Kon, S., M. Maeda, T. Segawa, Y. Hagiwara, Y. Horikoshi, S. Chikuma, K. Tanaka, M.M. Rashid, M. Inobe, A.F. Chambers, T. Uede, 2000. Antibodies to different peptides in osteopontin reveal complexities in the various secreted forms. *J Cell Biochem* 77, 487-98.
- Konya, E., T. Umekawa, M. Iguchi, T. Kurita, 2003. The role of osteopontin on calcium oxalate crystal formation. *Eur Urol* 43, 564-71.
- Kortemme, T., A.V. Morozov, D. Baker, 2003. An orientation-dependent hydrogen bonding potential improves prediction of specificity and structure for proteins and protein-protein complexes. *J. Mol. Biol.* 326, 1239-59.
- Koul, H.K., S. Koul, S. Fu, V. Santosham, A. Seikhon, M. Menon, 1999. Oxalate: from crystal formation to crystal retention. *J. Am. Soc. Nephrol.* 10 Suppl 14, S417-21.
- Lakshminarayanan, R., X.J. Loh, S. Gayathri, S. Sindhu, Y. Banerjee, R.M. Kini, S. Valiyaveetil, 2006. Formation of transient amorphous calcium carbonate precursor in quail eggshell mineralization: an in vitro study. *Biomacromolecules* 7, 3202-9.
- Langdon, A., G.R. Wignall, K. Rogers, E.S. Sorensen, J. Denstedt, B. Grohe, H.A. Goldberg, G.K. Hunter, 2009. Kinetics of calcium oxalate crystal growth in the presence of osteopontin isoforms: an analysis by scanning confocal interference microscopy. *Calcif. Tissue Int.* 84, 240-8.
- Lasa, M., P.L. Chang, C.W. Prince, L.A. Pinna, 1997. Phosphorylation of osteopontin by Golgi apparatus casein kinase. *Biochem Biophys Res Commun* 240, 602-5.

- Lavelin I, Yarden N, Ben-Bassat S, Bar A, Pines M (1998) Regulation of osteopontin gene expression during egg shell formation in the laying hen by mechanical strain. *Matrix Biol* 17:615-23
- Lavelin, I., Meiri, N., Pines, M., 2000. New insight in eggshell formation. *Poult. Sci.* 79: 1014-7.
- Lavelin, I., N. Meiri, M. Einat, O. Genina, M. Pines, 2002. Mechanical strain regulation of the chicken glypican-4 gene expression in the avian eggshell gland. *Am J Physiol Regul Integr Comp Physiol* 283, R853-61.
- Lazaridis, T., M. Karplus, 1999. Effective energy function for proteins in solution. *Proteins: Struct., Funct., Genet.* 35, 133-152.
- Lepage, L., R. Tawashi, 1982. Growth and characterization of calcium oxalate dihydrate crystals (weddellite). *J. Pharm. Sci.* 71, 1059-62.
- Lewis, R.D., H.A. Lowenstam, G.R. Rossman, 1974. Oxalate nephrosis and crystalline myocarditis. Case report with postmortem and crystallographic studies. *Arch. Pathol.* 98, 149-55.
- Liaw, L., V. Lindner, S.M. Schwartz, A.F. Chambers, C.M. Giachelli, 1995. Osteopontin and beta 3 integrin are coordinately expressed in regenerating endothelium in vivo and stimulate Arg-Gly-Asp-dependent endothelial migration in vitro. *Circ Res* 77, 665-72.
- Lieske, J.C., F.G. Toback, S. Deganello, 1996. Face-selective adhesion of calcium oxalate dihydrate crystals to renal epithelial cells. *Calcif. Tissue Int.* 58, 195-200.
- Lieske, J.C., R. Leonard, F.G. Toback, 1995. Adhesion of calcium oxalate monohydrate crystals to renal epithelial cells is inhibited by specific anions. *Am J Physiol* 268, F604-12.
- Lieske, J.C., R. Norris, H. Swift, F.G. Toback, 1997. Adhesion, internalization and metabolism of calcium oxalate monohydrate crystals by renal epithelial cells. *Kidney Int.* 52, 1291-301.
- Lieske, J.C., S. Deganello, 1999. Nucleation, adhesion, and internalization of calcium-containing

urinary crystals by renal cells. *J. Am. Soc. Nephrol.* 10 Suppl 14, S422-9.

- Liu, S., P.S. Rowe, L. Vierthaler, J. Zhou, L.D. Quarles, 2007. Phosphorylated acidic serine-aspartate-rich MEPE-associated motif peptide from matrix extracellular phosphoglycoprotein inhibits phosphate regulating gene with homologies to endopeptidases on the X-chromosome enzyme activity. *J Endocrinol* 192, 261-7.
- Lopez, C.A., J.R. Hoyer, P.D. Wilson, P. Waterhouse, D.T. Denhardt, 1993. Heterogeneity of osteopontin expression among nephrons in mouse kidneys and enhanced expression in sclerotic glomeruli. *Lab. Invest.* 69, 355-63.
- Lowenstam, H., L. Margulis, 1980. Calcium regulation and the appearance of calcareous skeletons in the fossil record, in: Omori, M, Watabe, N, (Eds.), *The Mechanisms of Biomineralization in Animals and Plants*, Tokai University Press, Tokyo, pp. 289-300.
- Lowenstam, H.A., 1981. Minerals formed by organisms. *Science* 211, 1126-31.
- Lowenstam, H.A., S. Weiner, 1989. *On biomineralization*. Oxford University Press, New York.
- Luo, G., P. Ducy, M.D. McKee, G.J. Pinero, E. Loyer, R.R. Behringer, G. Karsenty, 1997. Spontaneous calcification of arteries and cartilage in mice lacking matrix GLA protein. *Nature* 386, 78-81.
- Makrodimitris, K., D.L. Masica, E.T. Kim, J.J. Gray, 2007. Structure prediction of protein-solid surface interactions reveals a molecular recognition motif of statherin for hydroxyapatite. *J. Am. Chem. Soc.* 129, 13713-22.
- Mandel, N.S., 1994. Crystal-membrane interaction in kidney stone disease. *J. Am. Soc. Nephrol.* 5, S37-45.
- Mandel, N.S., G.S. Mandel, 1989. Urinary tract stone disease in the United States veteran population.

- II. Geographical analysis of variations in composition. *J. Urol.* 142, 1516-21.
- Mandel, N.S., G.S. Mandel, A.T. Hasegawa, 1987. The effect of some urinary stone inhibitors on membrane interaction potentials of stone crystals. *J. Urol.* 138, 557-62.
- Mann K. 1999. Isolation of a glycosylated form of the chicken eggshell protein ovocleidin and determination of the glycosylation site. Alternative glycosylation/phosphorylation at an N-glycosylation sequon. *FEBS Lett* 463:12-14
- Mann K., Siedler F. 1999 The amino acid sequence of ovocleidin 17, a major protein of the avian eggshell calcified layer. *Biochem Mol Biol Int* 47:997-1007
- Mann, K., J. Gautron, Y. Nys, M.D. McKee, T. Bajari, W.J. Schneider, M.T. Hincke, 2003. Disulfide-linked heterodimeric clusterin is a component of the chicken eggshell matrix and egg white. *Matrix Biol* 22, 397-407.
- Mann, K., B. Macek, J.V. Olsen, 2006. Proteomic analysis of the acid-soluble organic matrix of the chicken calcified eggshell layer. *Proteomics* 6, 3801-10.
- Mann, K., J.V. Olsen, B. Macek, F. Gnad, M. Mann, 2007. Phosphoproteins of the chicken eggshell calcified layer. *Proteomics* 7, 106-15.
- Mann, S., 1983. Mineralization in Biological-Systems. *Structure and Bonding* 54, 125-74.
- Mann, S., 2001. *Biom mineralization : principles and concepts in bioinorganic materials chemistry.* Oxford University Press, Oxford.
- Mann, S., D.D. Archibald, J.M. Didymus, B.R. Heywood, F.C. Meldrum, V.J. Wade, 1992. Biom mineralization - Biomimetic Potential at the Inorganic-Organic Interface. *MRS Bulletin* 17, 32-36.
- Mann, S., Didymus, J.M., Sanderson, N.P., Heywood, B.R., Samper, E.J.A., 1990. Morphological

- influence of functionalized and non-functionalized-alpha,omega-dicarboxylates on calcite crystallization. *J. Chem. Soc., Faraday Trans.* 86: 1873-80.
- Markel, K., U. Roser, U. Mackenstedt, M. Klostermann, 1986. Ultrastructural Investigation of Matrix-Mediated Biomineralization in Echinoids (*Echinodermata, Echinoidea*). *Zoomorphology* 106, 232-43.
- Marsh, M.E., 1989. Self-association of calcium and magnesium complexes of dentin phosphophoryn. *Biochemistry* 28, 339-45.
- Martin, A., V. David, J.S. Laurence, P.M. Schwarz, E.M. Lafer, A.M. Hedge, P.S. Rowe, 2008. Degradation of MEPE, DMP1, and release of SIBLING ASARM-peptides (minhibins): ASARM-peptide(s) are directly responsible for defective mineralization in HYP. *Endocrinology* 149, 1757-72.
- Masica, D.L., J.J. Gray, 2009. Solution- and adsorbed-state structural ensembles predicted for the statherin-hydroxyapatite system. *Biophys. J*, Accepted.
- Masuda, K., Takahashi, N., Tsukamoto, Y., Honma, H., Kohri, K. 2000. N-glycan structures of an osteopontin from human bone. *Biochem. Biophys. Res. Commun.* 268, 814-17.
- McConnaughey, T., 1989. C-13 and O-18 Isotopic Disequilibrium in Biological Carbonates .1. Patterns. *Geochim. Cosmochim. Acta* 53, 151-162.
- McKee M.D., Nanci A. 1995 Post-embedding colloidal-gold immunocytochemistry of noncollagenous extracellular matrix proteins in mineralized tissues. *Microsc Res Tech* 31:44-62
- McKee, M.D., Nanci A., 1995. Osteopontin and the bone remodeling sequence. Colloidal-gold immunocytochemistry of an interfacial extracellular matrix protein. *Ann N Y Acad Sci* 760,

177-89.

- McKee, M.D., A. Nanci, S.R. Khan, 1995. Ultrastructural immunodetection of osteopontin and osteocalcin as major matrix components of renal calculi. *J. Bone Miner. Res.* 10, 1913-29.
- McKee, M.D., A. Nanci, 1996. Osteopontin at mineralized tissue interfaces in bone, teeth, and osseointegrated implants: ultrastructural distribution and implications for mineralized tissue formation, turnover, and repair. *Microsc Res Tech* 33, 141-64.
- Mine, Y., C. Oberle, Z. Kassify, 2003. Eggshell matrix proteins as defense mechanism of avian eggs. *Journal of Agricultural and Food Chemistry* 51, 249-253.
- Moore, M.A., Y. Gotoh, K. Rafidi, L.C. Gerstenfeld, 1991. Characterization of a cDNA for chicken osteopontin: expression during bone development, osteoblast differentiation, and tissue distribution. *Biochemistry* 30, 2501-8.
- Moran, E.T., Jr., 2007. Nutrition of the developing embryo and hatchling. *Poult. Sci.* 86, 1043-9.
- Morozov, A.V., T. Kortemme, K. Tsemekhman, D. Baker, 2004. Close agreement between the orientation dependence of hydrogen bonds observed in protein structures and quantum mechanical calculations. *Proc. Natl. Acad. Sci. U. S. A.* 101, 6946-51.
- Morse, J.W., 1978. Dissolution kinetics of calcium-carbonate in sea-water. VI. near-equilibrium dissolution kinetics of calcium carbonate-rich deep-sea sediments. *Am J Sci* 278, 344-53.
- Morse, J.W., R.S. Arvidson, 2002. The dissolution kinetics of major sedimentary carbonate minerals. *Earth Sci Rev* 58, 51-84.
- Mortimer, K.V., 1970. The relationship of deciduous enamel structure to dental disease. *Caries Res.* 4, 206-23.
- Mucci, A., 1986. Growth kinetics and composition of magnesian calcite overgrowths precipitated

- from seawater - quantitative influence of ortho-phosphate ions. *Geochim. Cosmochim. Acta* 50, 2255-65.
- Mucci, A., J.W. Morse, 1983. The Incorporation of Mg^{2+} and Sr^{2+} into Calcite Overgrowths - Influences of Growth-Rate and Solution Composition. *Geochimica Et Cosmochimica Acta* 47, 217-33.
- Müller, R., I. Schmitz-Feuerhake, 1996. Comparison Between Deciduous and Permanent Teeth in Relation to their Utility for EPR Dosimetry, in: Schmitz-Feuerhake, I, Schmidt, M, (Eds.), *Proceedings of the International Workshop on the German Society for Radiation Protection Strahlentelex mit ElektrosmogReport*, University of Portsmouth, Portsmouth, England, pp. 380-81.
- Mullin, J.W., 1992. *Crystallization*, 3rd ed. Butterworths, Oxford.
- Mutaftschiev, B., 1993. Nucleation, in: Hurle, D T J, (Ed.), *Handbook on crystal growth*, North-Holland, Amsterdam, pp. 187-248.
- Nagata T, Todescan R, Goldberg HA, Zhang Q, Sodek J (1989) Sulfation of secreted phosphoprotein I (SPPI, osteopontin) is associated with mineralized tissue formation. *Biochem Biophys Res Commun* 165:234-40
- Nakagawa, Y., V. Abram, F.J. Kezdy, E.T. Kaiser, F.L. Coe, 1983. Purification and characterization of the principal inhibitor of calcium oxalate monohydrate crystal growth in human urine. *J Biol Chem* 258, 12594-600.
- Nancollas.Gh, M.M. Reddy, 1971. Crystallization of Calcium Carbonate II. Calcite Growth Mechanism. *Journal of Colloid and Interface Science* 37, 824-30.
- Narbaitz, R., 1974. On the mechanism of shell mineral solubilization by the chick embryo. *Calcif.*

- Tissue Res. 16, 339-42.
- Narbaitz, R., 1977. Structure of the intra-chorionic blood sinus in the chick embryo. *J. Anat.* 124, 347-54.
- Narbaitz, R., 1987. Role of vitamin D in the development of the chick embryo. *J. Exp. Zool. Suppl.* 1, 15-23.
- Narbaitz, R., B. Bastani, N.J. Galvin, V.K. Kapal, D.Z. Levine, 1995. Ultrastructural and immunocytochemical evidence for the presence of polarised plasma membrane H(+)-ATPase in two specialised cell types in the chick embryo chorioallantoic membrane. *J. Anat.* 186 (Pt 2), 245-52.
- Narbaitz, R., S. Kacew, L. Sitwell, 1981. Carbonic anhydrase activity in the chick embryo chorioallantois: regional distribution and vitamin D regulation. *J. Embryol. Exp. Morphol.* 65, 127-37.
- Nebel, H., M. Neumann, C. Mayer, M. Epple, 2008. On the structure of amorphous calcium carbonate--a detailed study by solid-state NMR spectroscopy. *Inorg. Chem.* 47, 7874-9.
- Neilsen, A.E., 1964. Kinetics of precipitation. Pergamon Press, Oxford.
- Neira-Carrillo, A., D.F. Acevedo, M.C. Miras, C.A. Barbero, D. Gebauer, H. Colfen, J.L. Arias, 2008. Influence of conducting polymers based on carboxylated polyaniline on in vitro CaCO₃ crystallization. *Langmuir* 24, 12496-507.
- Nishio, S., T. Iseda, H. Takeda, H. Iwata, M. Yokoyama, 2000. Inhibitory effect of calcium phosphate-associated proteins on calcium oxalate crystallization: alpha2-HS-glycoprotein, prothrombin-F1 and osteopontin. *BJU Int* 86, 543-8.
- Nys, Y., Gautron, J., Garcia-Ruiz, J.M., Hincke, M.T., 2004. Avian eggshell mineralization:

- Biochemical and functional characterization of matrix proteins. *Comptes Rendus Palevol* 3: 549-62.
- Nys, Y., Gautron, J., McKee, M.D., Garcia-Ruiz, J.M., Hincke, M.T., 2001. Biochemical and functional characterization of eggshell matrix proteins in hens. *Worlds Poult. Sci. J.* 57: 401-13.
- Nys, Y., Hincke, M.T., Arias, J.L., Garcia-Ruiz, J.M., Solomon, S.E., 1999. Avian eggshell mineralization. *Poultry and Avian Biology Reviews* 10: 143-66.
- Nys, Y., J. Zawadzki, J. Gautron, A.D. Mills, 1991. Whitening of brown-shelled eggs: mineral composition of uterine fluid and rate of protoporphyrin deposition. *Poult. Sci.* 70, 1236-45.
- Ogawa, H., T. Takahashi, T. Kuwayama, M. Kawashima, 2003. Presence of calcitonin receptors in shell gland of the guineafowl and changes in binding property during an oviposition cycle. *Poult Sci* 82, 1302-6.
- Okada, A., S. Nomura, Y. Saeki, Y. Higashibata, S. Hamamoto, M. Hirose, Y. Itoh, T. Yasui, K. Tozawa, K. Kohri, 2008. Morphological conversion of calcium oxalate crystals into stones is regulated by osteopontin in mouse kidney. *J Bone Miner Res* 23, 1629-37.
- Oldberg, A., A. Franzen, D. Heinegard, 1986. Cloning and sequence analysis of rat bone sialoprotein (osteopontin) cDNA reveals an Arg-Gly-Asp cell-binding sequence. *Proc. Natl. Acad. Sci. U. S. A.* 83, 8819-23.
- Orme, C.A., A. Noy, A. Wierzbicki, M.T. McBride, M. Grantham, H.H. Teng, P.M. Dove, J.J. DeYoreo, 2001. Formation of chiral morphologies through selective binding of amino acids to calcite surface steps. *Nature* 411, 775-9.
- O'Young, J., S. Chirico, N. Al Tarhuni, B. Grohe, M. Karttunen, H.A. Goldberg, G.K. Hunter, 2009.

- Phosphorylation of osteopontin peptides mediates adsorption to and incorporation into calcium oxalate crystals. *Cells Tissues Organs* 189, 51-5.
- Packard, G.C., M.J. Packard, 1980. Evolution of the cleidoic egg among reptilian antecedents of birds. *Am. Zool.* 20, 351-62.
- Packard, M.J., G.C. Packard, 1984. Comparative aspects of calcium metabolism in embryonic reptiles and birds, in: Seymour, R. S., (Ed.), *Respiration and metabolism of embryonic vertebrates.* , Dr. W. Junk Publishers, Dordrecht, Vol. 3, pp. 155-79.
- Packard, M.J., T.M. Short, G.C. Packard, T.A. Gorell, 1984. Sources of calcium for embryonic development in eggs of the snapping turtle *Chelydra-serpentina*. *J. Exp. Zool.* 230, 81-7.
- Palmer, D., 2005. CRYSTAL MAKER. Yarnton, Oxfordshire, UK.
- Pampena, D.A., K.A. Robertson, O. Litvinova, G. Lajoie, H.A. Goldberg, G.K. Hunter, 2004. Inhibition of hydroxyapatite formation by osteopontin phosphopeptides. *Biochem. J.* 378, 1083-7.
- Panda, D., G.C. Kundu, B.I. Lee, A. Peri, D. Fohl, I. Chackalaparampil, B.B. Mukherjee, X.D. Li, D.C. Mukherjee, S. Seides, J. Rosenberg, K. Stark, A.B. Mukherjee, 1997. Potential roles of osteopontin and α V β 3 integrin in the development of coronary artery restenosis after angioplasty. *Proc Natl Acad Sci U S A* 94, 9308-13.
- Panheleux, M., Bain, M., Fernandez, M.S., Morales, I., Gautron, J., Arias, J.L., Solomon, S.E., Hincke, M., Nys, Y., 1999. Organic matrix composition and ultrastructure of eggshell: A comparative study. *Br. Poult. Sci.* 40: 240-52.
- Parsons A.H. 1982 Structure of the eggshell. *Poultry Sci* 61:2013-21
- Patarca, R., G.J. Freeman, R.P. Singh, F.Y. Wei, T. Durfee, F. Blattner, D.C. Regnier, C.A. Kozak, B.A.

- Mock, H.C. Morse, 3rd, et al., 1989. Structural and functional studies of the early T lymphocyte activation 1 (Eta-1) gene. Definition of a novel T cell-dependent response associated with genetic resistance to bacterial infection. *J Exp Med* 170, 145-61.
- Patarca, R., R.A. Saavedra, H. Cantor, 1993. Molecular and cellular basis of genetic resistance to bacterial infection: the role of the early T-lymphocyte activation-1/osteopontin gene. *Crit Rev Immunol* 13, 225-46.
- Pedraza, C.E., Y.C. Chien, M.D. McKee, 2008. Calcium oxalate crystals in fetal bovine serum: implications for cell culture, phagocytosis and biomineralization studies in vitro. *J. Cell. Biochem.* 103, 1379-93.
- Peebles, E.D., Brake, J., 1985. Relationship of eggshell porosity to stage of embryonic development in broiler breeders. *Poult. Sci.* 64: 2388-91.
- Pereira-Mouries, L., M.J. Almeida, C. Ribeiro, J. Peduzzi, M. Barthelemy, C. Milet, E. Lopez, 2002. Soluble silk-like organic matrix in the nacreous layer of the bivalve *Pinctada maxima*. *European Journal of Biochemistry* 269, 4994-5003.
- Perl-Treves, D., L. Addadi, 1990. Molecular Recognition in Pathological Crystallizations - Gout Interactions between Albumin and Sodium Urate Monohydrate Crystals. *Mol Cryst Liq Cryst* 187, 1-16.
- Perry, C.C., 2003. Silicification: the processes by which organisms capture and mineralize silica., in: Dove, P M, J.J. De Yoreo, and S. Weiner, (Ed.), *Biomineralization*, The Mineralogical Society of America, Washinton, D.C., Vol. 54, pp. 291-327.
- Pines, M., V. Knopov, A. Bar, 1995. Involvement of osteopontin in egg shell formation in the laying chicken. *Matrix Biol.* 14, 765-71.

- Pipich, V., M. Balz, S.E. Wolf, W. Tremel, D. Schwahn, 2008. Nucleation and growth of CaCO_3 mediated by the egg-white protein ovalbumin: a time-resolved *in situ* study using small-angle neutron scattering. *J. Am. Chem. Soc.* 130, 6879-92.
- Pokroy, B., A.N. Fitch, F. Marin, M. Kapon, N. Adir, E. Zolotoyabko, 2006. Anisotropic lattice distortions in biogenic calcite induced by intra-crystalline organic molecules. *J. Struct. Biol.* 155, 96-103.
- Politi, Y., R.A. Metzler, M. Abrecht, B. Gilbert, F.H. Wilt, I. Sagi, L. Addadi, S. Weiner, P.U. Gilbert, 2008. Transformation mechanism of amorphous calcium carbonate into calcite in the sea urchin larval spicule. *Proc. Natl. Acad. Sci. U. S. A.* 105, 17362-6.
- Pouget, E.M., P.H. Bomans, J.A. Goos, P.M. Frederik, G. de With, N.A. Sommerdijk, 2009. The initial stages of template-controlled CaCO_3 formation revealed by cryo-TEM. *Science* 323, 1455-8.
- Prince CW, Osawa T, Butler WT, Tomana M, Bhowan AS, Bhowan M, Schrohenloher RE, 1987. Isolation, characterization and biosynthesis of a phosphorylated glycoprotein from rat bone. *J. Biol. Chem.* 262:2900-7.
- Qiu, S.R., A. Wierzbicki, C.A. Orme, A.M. Cody, J.R. Hoyer, G.H. Nancollas, S. Zepeda, J.J. De Yoreo, 2004. Molecular modulation of calcium oxalate crystallization by osteopontin and citrate. *Proc. Natl. Acad. Sci. U. S. A.* 101, 1811-5.
- Rahima, M., A. Veis, 1988. Two classes of dentin phosphophoryns, from a wide range of species, contain immunologically cross-reactive epitope regions. *Calcif Tissue Int* 42, 104-12.
- Rahn, H., Paganelli, C.V., Ar, A.J., 1987. Pores and gas exchange of avian eggs: A review. *J. Exp. Zool. Suppl.* 1: 165-72.

- Reddy, M.M., Nancollas G.H, 1971. Crystallization of calcium carbonate I: isotopic exchange and kinetics. *Journal of Colloid and Interface Science* 36, 166-172.
- Reeder, R.J., 1983. Carbonates: mineralogy and chemistry. Mineralogical Society of America, Washington, D.C.
- Reeder, R.J., J.C. Grams, 1987. Sector Zoning in Calcite Cement Crystals - Implications for Trace-Element Distributions in Carbonates. *Geochim. Cosmochim. Acta* 51, 187-94.
- Rittling, S.R., D.T. Denhardt, 1999. Osteopontin function in pathology: lessons from osteopontin-deficient mice. *Exp. Nephrol.* 7, 103-13.
- Robey P.G. 1996 Vertebrate mineralized matrix proteins: structure and function. *Connect Tiss Res* 35:131-6
- Rodriguez-Navarro, A., Kalin, O., Nys, Y., Garcia-Ruiz, J.M., 2002. Influence of the microstructure on the shell strength of eggs laid by hens of different ages. *Br. Poult. Sci.* 43: 395-403.
- Rodriguez-Navarro, A.B., A. Yebra, Y. Nys, C. Jimenez-Lopez, J.M. Garcia-Ruiz, 2007. Analysis of avian eggshell microstructure using X-ray area detectors. *Eur. J. Mineral.* 19, 391-8.
- Roland, D.A.S., 1988. Egg shell problems: estimates of incidence and economic impact. *Poult. Sci.* 67: 1801-3.
- Romanoff, A.L., 1960. The avian embryo; structural and functional development. Macmillan, New York.
- Romanoff, A.L., Romanoff, A.J., 1949. In: *The Avian Egg*, Wiley, New York, NY, USA.
- Rose, M.L., M.T. Hincke, 2009. Protein constituents of the eggshell: eggshell-specific matrix proteins. *Cell Mol Life Sci* 66, 2707-19.
- Rucker, J.B., R.E. Carver, 1969. A survey of the carbonate mineralogy of cheilostome bryozoa. *J*

Paleont 43, 791-9.

Ryall, R.L., 1997. Urinary inhibitors of calcium oxalate crystallization and their potential role in stone formation. *World Journal of Urology* 15, 155-64.

Ryall, R.L., C.M. Hibberd, V.R. Marshall, 1985. A method for studying inhibitory activity in whole urine. *Urol. Res.* 13, 285-9.

Ryall, R.L., D.E. Fleming, I.R. Doyle, N.A. Evans, C.J. Dean, V.R. Marshall, 2001. Intracrystalline proteins and the hidden ultrastructure of calcium oxalate urinary crystals: Implications for kidney stone formation. *J. Struct. Biol.* 134, 5-14.

Ryall, R.L., D.E. Fleming, P.K. Grover, M. Chauvet, C.J. Dean, V.R. Marshall, 2000. The hole truth: intracrystalline proteins and calcium oxalate kidney stones. *Mol Urol* 4, 391-402.

Ryall, R.L., M.C. Chauvet, P.K. Grover, 2005. Intracrystalline proteins and urolithiasis: a comparison of the protein content and ultrastructure of urinary calcium oxalate monohydrate and dihydrate crystals. *BJU Int.* 96, 654-63.

Ryall, R.L., P.K. Grover, A.M. Stapleton, D.K. Barrell, Y. Tang, R.L. Moritz, R.J. Simpson, 1995. The urinary F1 activation peptide of human prothrombin is a potent inhibitor of calcium oxalate crystallization in undiluted human urine in vitro. *Clin Sci (Lond)* 89, 533-41.

Ryall, R.L., P.K. Grover, L.A. Thurgood, M.C. Chauvet, D.E. Fleming, W. van Bronswijk, 2007. The importance of a clean face: the effect of different washing procedures on the association of Tamm-Horsfall glycoprotein and other urinary proteins with calcium oxalate crystals. *Urol. Res.* 35, 1-14.

Saavedra, R.A., S.K. Kimbro, D.N. Stern, J. Schnuer, S. Ashkar, M.J. Glimcher, C.I. Ljubetic, 1995. Gene expression and phosphorylation of mouse osteopontin. *Ann N Y Acad Sci* 760, 35-43.

- Sajner, J., 1955. Über die mikroskopischen Veränderungen der Eischale der Vogel im Laufe der Inkubationszeit. *Acta Anat. (Basel)* 25, 141-59.
- Salih E., Ashkar S., Gerstenfeld L.C., Glimcher M.J. 1997. Identification of the phosphorylated sites of metabolically ³²P-labeled osteopontin from cultured chicken osteoblasts. *J Biol Chem* 272:13966-73
- Salih, E., H.Y. Zhou, M.J. Glimcher, 1996. Phosphorylation of purified bovine bone sialoprotein and osteopontin by protein kinases. *J Biol Chem* 271, 16897-905.
- Schlueter, R.J., A. Veis, 1964. The Macromolecular Organization of Dentine Matrix Collagen. II. Periodate Degradation and Carbohydrate Cross-Linking. *Biochemistry* 3, 1657-65.
- Schmidt, W.J., 1960. Polarisationsoptik und bau der kalkschale des huhnereies. *Z. Zellforsch. Mikrosk. Anat.* 68: 874-92.
- Schmidt, W.J., 1965. Morphologie der Kalkresorption an der ausgebruteten Vogel-Eischale. *Z. Zellforsch. Mikrosk. Anat.* 68, 874-92.
- Schuler, D., R.B. Frankel, 1999. Bacterial magnetosomes: microbiology, biomineralization and biotechnological applications. *Applied Microbiology and Biotechnology* 52, 464-73.
- Schumann, D., T.D. Raub, R.E. Kopp, J.L. Guerquin-Kern, T.D. Wu, I. Rouiller, A.V. Smirnov, S.K. Sears, U. Lucken, S.M. Tikoo, R. Hesse, J.L. Kirschvink, H. Vali, 2008. Gigantism in unique biogenic magnetite at the Paleocene-Eocene Thermal Maximum. *Proc. Natl. Acad. Sci. U. S. A.* 105, 17648-53.
- Senger, D.R., C.A. Perruzzi, A. Papadopoulos, 1989a. Elevated expression of secreted phosphoprotein I (osteopontin, 2ar) as a consequence of neoplastic transformation. *Anticancer Res* 9, 1291-9.

- Senger, D.R., C.A. Perruzzi, A. Papadopoulos, D.G. Tenen, 1989b. Purification of a human milk protein closely similar to tumor-secreted phosphoproteins and osteopontin. *Biochim Biophys Acta* 996, 43-8.
- Sethmann, I., A. Putnis, O. Grassmann, P. Lobmann, 2005. Observation of nano-clustered calcite growth via a transient phase mediated by organic polyanions: A close match for biomineralization. *Am. Mineral.* 90, 1213-17.
- Seto, J., Zhang, Y., Hamilton, P., Wilt, F., 2004. The localization of occluded matrix proteins in calcareous spicules of sea urchin larvae. *J. Struct. Biol.* 148: 123-130.
- Sheng, X., T. Jung, J.A. Wesson, M.D. Ward, 2005. Adhesion at calcium oxalate crystal surfaces and the effect of urinary constituents. *Proc. Natl. Acad. Sci. U. S. A.* 102, 267-72.
- Shiraga, H., W. Min, W.J. VanDusen, M.D. Clayman, D. Miner, C.H. Terrell, J.R. Sherbotie, J.W. Foreman, C. Przywiecki, E.G. Neilson, J.R. Hoyer, 1992. Inhibition of calcium oxalate crystal growth in vitro by uropontin: another member of the aspartic acid-rich protein superfamily. *Proc. Natl. Acad. Sci. U. S. A.* 89, 426-30.
- Sibalic, V., X. Fan, J. Loffing, R.P. Wuthrich, 1997. Upregulated renal tubular CD44, hyaluronan, and osteopontin in kdkd mice with interstitial nephritis. *Nephrol Dial Transplant* 12, 1344-53.
- Silyn-Roberts H., Sharp R.M. 1986. Crystal growth and the role of the organic network in eggshell biomineralization. *Proc R Soc London B* 227:303-24
- Simkiss, K., 1961. Calcium metabolism and avian reproduction. *Biol. Rev. Camb. Philos. Soc.* 36, 321-67.
- Simkiss, K., 1967. Acute hypercapnia and eggshell formation. *Nature* 214, 84-6.
- Simkiss, K., 1976. Cellular aspects of calcification, in: Watabe, N, Wilbur, K M, (Eds.), *The*

- mechanisms of mineralization in the invertebrates and plants, Univ. of South Carolina Press, Columbia, SC, Vol. 5, pp. 1-31.
- Simkiss, K., 1986. The processes of biomineralization in lower plants and animals-an overview, in: Leadbeater, B S C, Riding, R, (Eds.), *Biomineralization in lower plants and animals.* , Oxford University Press, Oxford, New York, Vol. 30, pp. 19-37.
- Simkiss, K., 1994. Amorphous minerals in biology. *Bull de l'Institut océanographique (Monaco) No. Spécial 14*, 49–54.
- Simkiss, K., K.M. Wilbur, 1989. *Biomineralization: cell biology and mineral deposition.* Academic Press, San Diego.
- Simons P.C.M., Wiertz G 1963. Notes on the structure of membranes and shell in the hen's egg; an electron microscopic study. *Z Zellforsch Mikrosk Anat* 59:555-67
- Simons, P.C.M. 1971. *Ultrastructure of the hen eggshell and its physiological interpretation.* Centre for Agricultural Publishing and Documentation, Wageningen.
- Singhal, H., D.S. Bautista, K.S. Tonkin, F.P. O'Malley, A.B. Tuck, A.F. Chambers, J.F. Harris, 1997. Elevated plasma osteopontin in metastatic breast cancer associated with increased tumor burden and decreased survival. *Clin Cancer Res* 3, 605-11.
- Sjoberg, E.L., D.T. Rickard, 1984. Temperature-Dependence of Calcite Dissolution Kinetics between 1-Degree-C and 62-Degrees-C at Ph 2.7 to 8.4 in Aqueous-Solutions. *Geochim. Cosmochim. Acta* 48, 485-93.
- Sodek, J., Ganss, B., McKee, M.D., 2000. Osteopontin. *Crit. Rev. Oral Biol. Med.* 11: 279-303.
- Sodek, J., J. Chen, T. Nagata, S. Kasugai, R. Todescan, Jr., I.W. Li, R.H. Kim, 1995. Regulation of osteopontin expression in osteoblasts. *Ann N Y Acad Sci* 760, 223-41.

- Sørensen, E.S., Petersen, T.E., 1993. Purification and characterization of three proteins isolated from the proteose peptone fraction of bovine milk. *J. Dairy Res.* 60: 189-97.
- Stapleton, A.M., R.J. Simpson, R.L. Ryall, 1993a. Crystal matrix protein is related to human prothrombin. *Biochem Biophys Res Commun* 195, 1199-203.
- Stapleton, A.M., A.E. Seymour, J.S. Brennan, I.R. Doyle, V.R. Marshall, R.L. Ryall, 1993b. Immunohistochemical distribution and quantification of crystal matrix protein. *Kidney international* 44, 817-24.
- Stapleton, A.M., C.J. Dawson, P.K. Grover, A. Hohmann, R. Comacchio, V. Boswarva, Y. Tang, R.L. Ryall, 1996. Further evidence linking urolithiasis and blood coagulation: urinary prothrombin fragment 1 is present in stone matrix. *Kidney international* 49, 880-8.
- Stapleton, A.M., R.L. Ryall, 1995. Blood coagulation proteins and urolithiasis are linked: crystal matrix protein is the F1 activation peptide of human prothrombin. *Br J Urol* 75, 712-9.
- Staudt, W., Reeder, R.J., Schoonen, M.A.A., 1994. Surface structural controls on compositional zoning of SO_4^{2-} and SeO_4^{2-} in synthetic calcite single crystals. *Geochim. Cosmochim. Acta* 58: 2087-98.
- Stemberger, B.H., W.J. Mueller, R.M. Leach, 1977. Microscopic study of initial stages of eggshell calcification. *Poultry Science* 56, 53743.
- Stephenson, A.E., J.J. De Yoreo, L. Wu, K.J. Wu, J.R. Hoyer, P.M. Dove, 2008. Peptides enhance magnesium signature in calcite: insights into origins of vital effects. *Science* 322, 724-7.
- Stetler-Stevenson, W.G., A. Veis, 1983. Bovine dentin phosphophoryn: composition and molecular weight. *Biochemistry* 22, 4326-35.
- Stetler-Stevenson, W.G., A. Veis, 1987. Bovine dentin phosphophoryn: calcium ion binding properties

- of a high molecular weight preparation. *Calcif Tissue Int* 40, 97-102.
- Stumm, W., L. Sigg, B. Sulzberger, 1992. *Chemistry of the solid-water interface : processes at the mineral-water and particle-water interface in natural systems*. Wiley, New York.
- Swift, D.M., A.P. Wheeler, 1992. Evidence of an Organic Matrix from Diatom Biosilica. *Journal of Phycology* 28, 202-9.
- Taller, A., B. Grohe, K.A. Rogers, H.A. Goldberg, G.K. Hunter, 2007. Specific adsorption of osteopontin and synthetic polypeptides to calcium oxalate monohydrate crystals. *Biophys. J.* 93, 1768-77.
- Tawada, T., K. Fujita, T. Sakakura, T. Shibutani, T. Nagata, M. Iguchi, K. Kohri, 1999. Distribution of osteopontin and calprotectin as matrix protein in calcium-containing stone. *Urol. Res.* 27, 238-42.
- Tazzoli, V., C. Domeneghetti, 1980. The crystal structures of whewellite and weddellite – re-examination and comparison. *Am. Mineral.* 65, 327-34.
- Tebo, B.M., W.C. Ghiorse, L.G. van Waasbergen, P.L. Siering, R. Caspi, 1997. Bacterially mediated mineral formation: Insights into manganese(II) oxidation from molecular genetic and biochemical studies. *Geomicrobiology: Interactions between Microbes and Minerals* 35, 225-66.
- Temmam, M., Paquette, J., Vali, H., 2000. Mn and Zn incorporation into calcite as a function of chloride aqueous concentration. *Geochim. Cosmochim. Acta* 64: 2417-30.
- Teng, H.H., P.M. Dove, C.A. Orme, J.J. De Yoreo, 1998. Thermodynamics of calcite growth: Baseline for understanding biomineral formation. *Science* 282, 724-727.
- Teng, H.H., P.M. Dove, J.J. De Yoreo, 2000. Kinetics of calcite growth: Surface processes and

- relationships to macroscopic rate laws. *Geochim. Cosmochim. Acta* 64, 2255-66.
- Terepka, A., J. Coleman, H. Armbrecht, T. Gunther, 1976. Transcellular transport of calcium. *Symp. Soc. Exp. Biol.* 30, 117-40.
- Terepka, A.R., 1963a. Organic-inorganic interrelationships in avian egg shell. *Exp. Cell Res.* 30: 183-92.
- Terepka, A.R., 1963b. Structure and calcification in avian egg shell. *Exp Cell Res* 30, 171-82.
- Termine, J.D., A.B. Belcourt, K.M. Conn, H.K. Kleinman, 1981. Mineral and collagen-binding proteins of fetal calf bone. *J Biol Chem* 256, 10403-8.
- Termine, J.D., A.B. Belcourt, P.J. Christner, K.M. Conn, M.U. Nylén, 1980. Properties of dissociatively extracted fetal tooth matrix proteins. I. Principal molecular species in developing bovine enamel. *J Biol Chem* 255, 9760-8.
- Tezuka, K., T. Sato, H. Kamioka, P.J. Nijweide, K. Tanaka, T. Matsuo, M. Ohta, N. Kurihara, Y. Hakeda, M. Kumegawa, 1992. Identification of osteopontin in isolated rabbit osteoclasts. *Biochem Biophys Res Commun* 186, 911-7.
- Thayer, J.M., G.C. Schoenwolf, 1998. Early expression of Osteopontin in the chick is restricted to rhombomeres 5 and 6 and to a subpopulation of neural crest cells that arise from these segments. *Anat Rec* 250, 199-209.
- Thurgood, L.A., P.K. Grover, R.L. Ryall, 2008. High calcium concentration and calcium oxalate crystals cause significant inaccuracies in the measurement of urinary osteopontin by enzyme linked immunosorbent assay. *Urol. Res.* 36, 103-10.
- Touryan, L.A., R.H. Clark, R.W. Gurney, P.S. Stayton, B. Kahr, V. Vogel, 2001. Incorporation of fluorescent molecules and proteins into calcium oxalate monohydrate single. *J. Cryst.*

Growth 233, 380-8.

- Travaille, A.M., J.J.J.M. Donners, J.W. Gerritsen, N.A.J.M. Sommerdijk, R.J.M. Nolte, H. van Kempen, 2002. Aligned growth of calcite crystals on a self-assembled monolayer. *Advanced Materials* 14, 492-95.
- Tsang CPW, Grunder AA, Soares JH, Narbaitz R (1990) Effect of $1\alpha,25$ -dihydroxycholecalciferol on egg shell quality and egg production. *Brit Poultr Sci* 31:241-7
- Tuan, R.S., 1984. Carbonic anhydrase and calcium transport function of the chick embryonic chorioallantoic membrane. *Ann. N. Y. Acad. Sci.* 429, 459-72.
- Tuan, R.S., 1987. Mechanism and regulation of calcium transport by the chick embryonic chorioallantoic membrane. *J Exp Zool Suppl* 1, 1-13.
- Tuan, R.S., J. Zrike, 1978. Functional involvement of carbonic anhydrase in calcium transport of the chick chorioallantoic membrane. *Biochem J* 176, 67-74.
- Tuan, R.S., T. Ono, 1986. Regulation of extraembryonic calcium mobilization by the developing chick embryo. *J. Embryol. Exp. Morphol.* 97, 63-74.
- Tuan, R.S., W.A. Scott, Z.A. Cohn, 1978. Calcium-binding protein of the chick chorioallantoic membrane. I. Immunohistochemical localization. *J Cell Biol* 77, 743-51.
- Tullett, S.G., Lutz, P.L., Board, R.G., 1975. The fine structure of the pores in the shell of the hen's egg. *Br. Poult. Sci.* 16: 93-5.
- Tyler, C., 1958. Studies on egg shells. X. A method for determining variations in characteristics in different parts of the same shell. *J. Sci. Food Agric.* 9, 584-590.
- Tyler, C., 1969. Avian egg shells: Their structure and characteristics, In: Felts, W. J. L. and Harrison, R. J., (Eds.) *International Review of General and Experimental Zoology*, Vol. 4. Academic

- Press, New York, NY, USA, pp. 81-130.
- Tyler, C., K. Simkiss, 1959. Studies on eggshells. XII. Some changes in the shell during incubation. *J. Sci. Food Agric.* 10, 611-15.
- Umekawa, T., K. Kohri, T. Kurita, S. Hirota, S. Nomura, Y. Kitamura, 1995b. Expression of osteopontin messenger RNA in the rat kidney on experimental model of renal stone. *Biochem Mol Biol Int* 35, 223-30.
- Umekawa, T., T. Yamate, N. Amasaki, K. Kohri, T. Kurita, 1995a. Osteopontin mRNA in the kidney on an experimental rat model of renal stone formation without renal failure. *Urol Int* 55, 6-10.
- Urey, H.C., H.A. Lowenstam, S. Epstein, C.R. Mckinney, 1951. Measurement of Paleotemperatures and Temperatures of the Upper Cretaceous of England, Denmark, and the Southeastern United-States. *Geological Society of America Bulletin* 62, 399-416.
- Vali, H., B. Weiss, Y.L. Li, S.K. Sears, S.S. Kim, J.L. Kirschvink, L. Zhang, 2004. Formation of tabular single-domain magnetite induced by *Geobacter metallireducens* GS-15. *Proc. Natl. Acad. Sci. U. S. A.* 101, 16121-26.
- van Enckevort, W.J.P., A.C.J.F. van den Berg, 1998. Impurity blocking of crystal growth: a Monte Carlo study. *J Cryst Growth* 183, 441-55.
- Veis, A., 2003. Mineralization in organic matrix frameworks, in: Dove, P M, J.J. De Yoreo, and S. Weiner, (Eds.), *Biom mineralization*, The Mineralogical Society of America, Washinton, D.C., Vol. 54, pp. 249-89.
- Veis, A., A. Perry, 1967. The phosphoprotein of the dentin matrix. *Biochemistry* 6, 2409-16.
- Veis, A., B. Sabsay, 1982. Bone and tooth formation. Insights into mineralization strategies, in:

- Westbroek, P, de Jong, E W, (Eds.), *Biom mineralization and Biological Metal Accumulation*, Reidel Pub. Co., Dordrecht, Holland, pp. 273-84.
- Veis, A., R.J. Schlueter, 1963. Presence of phosphate-mediated cross-linkages in hard tissue collagens. *Nature* 197, 1204.
- Veis, A., R.J. Schlueter, 1964. The Macromolecular Organization of Dentine Matrix Collagen. I. Characterization of Dentine Collagen. *Biochemistry* 3, 1650-7.
- Verdier, J.M., K.V. Ewart, M. Griffith, C.L. Hew, 1996. An immune response to ice crystals in North Atlantic fishes. *European Journal of Biochemistry* 241, 740-3.
- Verhulst, A., M. Asselman, V.P. Persy, M.S. Schepers, M.F. Helbert, C.F. Verkoelen, M.E. De Broe, 2003. Crystal retention capacity of cells in the human nephron: involvement of CD44 and its ligands hyaluronic acid and osteopontin in the transition of a crystal binding- into a nonadherent epithelium. *J Am Soc Nephrol* 14, 107-15.
- Verkoelen, C.F., B.G. van der Boom, D.J. Kok, J.C. Romijn, 2000. Sialic acid and crystal binding. *Kidney Int.* 57, 1072-82.
- Wang, L., S.R. Qiu, W. Zachowicz, X. Guan, J.J. De Yoreo, G.H. Nancollas, J.R. Hoyer, 2006. Modulation of calcium oxalate crystallization by linear aspartic acid-rich peptides. *Langmuir* 22, 7279-85.
- Wang, L.J., R. Tang, T. Bonstein, P. Bush, G.H. Nancollas, 2006. Enamel demineralization in primary and permanent teeth. *J. Dent. Res.* 85, 359-63.
- Watabe, N., R.J. Kingsley, 1989. Extra-, inter-, and intracellular mineralization in invertebrates and algae, in: Crick, R E, (Ed.), *Origin, Evolution, and Modern Aspects of Biom mineralization in Plants and Animals*, Plenum, New York, pp. 209-23.

- Weber, G.F., H. Cantor, 1996. The immunology of Eta-1/osteopontin. *Cytokine Growth Factor Rev* 7, 241-8.
- Weiner, S., 1979. Aspartic acid-rich proteins: major components of the soluble organic matrix of mollusk shells. *Calcif Tissue Int* 29, 163-7.
- Weiner, S., F. Nudelman, E. Sone, P. Zaslansky, L. Addadi, 2006. Mineralized biological materials: A perspective on interfaces and interphases designed over millions of years. *Biointerphases* 1, P12-P14.
- Weiner, S., P.M. Dove, 2003. An overview of biomineralization processes and the problem of the vital effect, in: Dove, P M, J.J. De Yoreo, and S. Weiner, (Eds.), *Biomineralization*, The Mineralogical Society of America, Washinton, D.C., Vol. 54, pp. 1-29.
- Weiner, S., W. Traub, 1980. X-Ray-Diffraction Study of the Insoluble Organic Matrix of Mollusk Shells. *Febs Letters* 111, 311-6.
- Weiner, S., W. Traub, 1984. Macromolecules in mollusk shells and their functions in biomineralization. *Philosophical Transactions of the Royal Society of London Series B-Biological Sciences* 304, 425-34.
- Weiner, S., W. Traub, H.A. Lowenstam, 1983a. Organic matrix in calcified exoskeletons. , in: Westbroek, P, de Jong, E W, (Eds.), *Biomineralization and Biological Metal Accumulation*, Reidel Publishing Co, Dordrecht, Holland, pp. 205-24.
- Weiner, S., Y. Talmon, W. Traub, 1983b. Electron diffraction of mollusk shell organic matrices and their relationship to the mineral phase. *International Journal of Biological Macromolecules* 5, 325-8.
- Weiner, S., Y. Levi-Kalishman, S. Raz, L. Addadi, 2003. Biologically formed amorphous calcium

- carbonate. *Connect. Tissue Res.* 44, 214-8.
- Weiss, I.M., N. Tuross, L. Addadi, S. Weiner, 2002. Mollusc larval shell formation: amorphous calcium carbonate is a precursor phase for aragonite. *J Exp Zool* 293, 478-91.
- Wellman-Labadie, O., J. Picman, M.T. Hincke, 2008a. Comparative antibacterial activity of avian egg white protein extracts. *British Poultry Science* 49, 125-132.
- Wellman-Labadie, O., J. Picman, M.T. Hincke, 2008b. Antimicrobial activity of the Anseriform outer eggshell and cuticle. *Comparative Biochemistry and Physiology B-Biochemistry & Molecular Biology* 149, 640-9.
- Werness, P.G., J.H. Bergert, L.H. Smith, 1981. Crystalluria. *J. Cryst. Growth* 53, 166-81.
- Wesson, J.A., E.M. Worcester, 1996. Formation of hydrated calcium oxalates in the presence of poly-L-aspartic acid. *Scanning Microsc.* 10, 415-23; 423-4.
- Wesson, J.A., E.M. Worcester, J.H. Wiessner, N.S. Mandel, J.G. Kleinman, 1998. Control of calcium oxalate crystal structure and cell adherence by urinary macromolecules. *Kidney Int.* 53, 952-7.
- Wesson, J.A., M.D. Ward, 2006. Role of crystal surface adhesion in kidney stone disease. *Curr. Opin. Nephrol. Hypertens.* 15, 386-93.
- Wesson, J.A., R.J. Johnson, M. Mazzali, A.M. Beshensky, S. Stietz, C. Giachelli, L. Liaw, C.E. Alpers, W.G. Couser, J.G. Kleinman, J. Hughes, 2003. Osteopontin is a critical inhibitor of calcium oxalate crystal formation and retention in renal tubules. *J. Am. Soc. Nephrol.* 14, 139-47.
- Wiessner, J.H., G.S. Mandel, N.S. Mandel, 1986. Membrane interactions with calcium oxalate crystals: variation in hemolytic potentials with crystal morphology. *J. Urol.* 135, 835-9.
- Williams, A., M. Cusack, 1999. Evolution of a rhythmic lamination in the organophosphatic shells of

- brachiopods. *J Struct Biol* 126, 227-40.
- Williams, E.D., N.C. Bartelt, 1991. Thermodynamics of surface morphology. *Science* 251, 393-400.
- Wilt, F.H., 1999. Matrix and mineral in the sea urchin larval skeleton. *J. Struct. Biol.* 126, 216-26.
- Wilt, F.H., 2002. Biomineralization of the spicules of sea urchin embryos. *Zoolog. Sci.* 19, 253-61.
- Wong, K.K.W., B.J. Brisdon, B.R. Heywood, A.G.W. Hodson, S. Mann, 1994. Polymer-mediated crystallisation of inorganic solids: calcite nucleation on the surfaces of inorganic polymers. *Journal of Materials Chemistry* 4, 1387-1392.
- Wong, M., M.J. Hendrix, K. von der Mark, C. Little, R. Stern, 1984. Collagen in the egg shell membranes of the hen. *Dev Biol* 104, 28-36.
- Worcester, E.M., 1996. Inhibitors of stone formation. *Semin. Nephrol.* 16, 474-86.
- Worcester, E.M., A.M. Beshensky, 1995. Osteopontin inhibits nucleation of calcium oxalate crystals. *Ann N Y Acad Sci* 760, 375-7.
- Worcester, E.M., S.S. Blumenthal, A.M. Beshensky, D.L. Lewand, 1992. The calcium oxalate crystal growth inhibitor protein produced by mouse kidney cortical cells in culture is osteopontin. *J Bone Miner Res* 7, 1029-36.
- Wrana, J.L., Q. Zhang, J. Sodek, 1989. Full length cDNA sequence of porcine secreted phosphoprotein-I (SPP-I, osteopontin). *Nucleic Acids Res* 17, 10119.
- Wyburn, G.M., Johnston, H.S., Draper, M.H., Davidson, M.F., 1973. The ultrastructure of the shell forming region of the oviduct and the development of the shell of *Gallus domesticus*. *Q. J. Exp. Physiol. Cogn. Med. Sci.* 58: 143-51.
- Xie, Y., M. Sakatsume, S. Nishi, I. Narita, M. Arakawa, F. Gejyo, 2001. Expression, roles, receptors, and regulation of osteopontin in the kidney. *Kidney Int.* 60, 1645-57.

- Yamate, T., K. Kohri, T. Umekawa, N. Amasaki, Y. Isikawa, M. Iguchi, T. Kurita, 1996. The effect of osteopontin on the adhesion of calcium oxalate crystals to Madin-Darby canine kidney cells. *Eur Urol* 30, 388-93.
- Yasui, T., K. Fujita, K. Asai, K. Kohri, 2002. Osteopontin regulates adhesion of calcium oxalate crystals to renal epithelial cells. *Int J Urol* 9, 100-8.
- Yasui, T., M. Sato, K. Fujita, K. Tozawa, S. Nomura, K. Kohri, 2001. Effects of citrate on renal stone formation and osteopontin expression in a rat urolithiasis model. *Urol. Res.* 29, 50-6.
- Yokosaki, Y., K. Tanaka, F. Higashikawa, K. Yamashita, A. Eboshida, 2005. Distinct structural requirements for binding of the integrins α v β 6, α v β 3, α v β 5, α 5 β 1 and α 9 β 1 to osteopontin. *Matrix Biol* 24, 418-27.
- Young, J.R., K. Henriksen, 2003. Biomineralization within vesicles: the calcite of coccoliths, in: Dove, P.M., J.J. De Yoreo, and S. Weiner, (Eds.), *Biomineralization*, The Mineralogical Society of America, Washington, D.C., Vol. 54, pp. 189-215.
- Young, M.F., J.M. Kerr, K. Ibaraki, A.M. Heegaard, P.G. Robey, 1992. Structure, expression, and regulation of the major noncollagenous matrix proteins of bone. *Clin Orthop Relat Res*, 275-94.
- Zelenitsky, D.K., Hills L.V., Currie P.J., 1996. Parataxonomic classification of ornithoid eggshell fragments from the Oldman Formation (Judith River Group; Upper Cretaceous), southern Alberta. *Can. J. Earth Sci.* 33, 1655-67.
- Zelenitsky, D.K., Modesto S.P., Currie P.J., 2002. Bird-like characteristics of troodontid theropod eggshell. *Cretac. Res.* 23, 297-305.
- Zhong, S.J., A. Mucci, 1993. Calcite precipitation in seawater using a constant addition technique - a

new overall reaction kinetic expression. *Geochim. Cosmochim. Acta* 57, 1409-17.

Zohar, R., W. Lee, P. Arora, S. Cheifetz, C. McCulloch, J. Sodek, 1997. Single cell analysis of intracellular osteopontin in osteogenic cultures of fetal rat calvarial cells. *J Cell Physiol* 170, 88-100.